Università degli Studi di Palermo

AREA QUALITÀ, PROGRAMMAZIONE E SUPPORTO STRATEGICO
SETTORE STRATEGIA PER LA RICERCA
U. O. DOTTORATI

Dottorato di Ricerca in Energia e Tecnologie dell'Informazione.
Dipartimento di Ingegneria
SSD ING-IND/11 Fisica Tecnica Ambientale

INNOVATIVE PHOTOVOLTAIC-THERMAL HEAT PUMP SOLUTIONS FOR DOMESTIC HOT WATER PRODUCTION

LA DOTTORESSA
FRANCESCA MARTORANA

IL COORDINATORE
PROF. ING MAURIZIO CELLURA

IL TUTOR
PROF. ING. MARCO BECCALI

CICLO XXXIV
2022

Index

Abstract

With the rapid growth of energy consumption in the building sector and the consequent necessity to develop energy efficiency strategies, the application of heat pump systems seems to be a competitive solution to improve energy efficiency.
In particular, air-source heat pump (ASHP) systems assisted by solar energy have drawn great attention, owing to their great feasibility in buildings for space heating/cooling and hot water production purposes. The complementation system between solar and air energy can solve the poor performance of the air source heat pump under low-temperature conditions and can also make up for the shortcoming of the solar collector as an unstable energy source.
Both solar energy technologies and air source heat pumps (ASHP) are widely used renewable energy sources at the moment. The former has the advantages of low utilization cost, simple technology, easy access, and no pollution, while the latter has the advantages of high efficiency, energy-saving, and good environmental benefits.
Among emerging technologies coupled to heat pump systems, PV/T hybrid solar collectors are estimated to have a high potential and a fast-growing market. The PV performance of PV/T collectors increases slightly compared with a panel with PV cells since the operating temperatures of the PV cells are reduced due to the cooling effect of the heat extraction. Solar-assisted heat pump systems for DHW and space heating purposes have been studied by several researchers. Both experimental investigations and numerical studies aimed to assess the potential and performance of various system designs under different climatic boundaries.

The aim of the present thesis is the investigation of the energy performance of systems based on the coupling of air to water heat pumps with PV/T hybrid solar collectors for producing domestic hot water (DHW). The gains from using these two currently promising technologies and the benefits of their integration are investigated by analising different configurations of these integrated systems. Comparisons with more traditional technologies were performed both in terms of thermal and electrical power production and energy savings. In particular, investigations were performed in order to identify the optimal number of modules that make up the solar plant and the most performing technology with the purpose of this thesis among PV, PV/T, and ST collectors. Furthermore, two different integration configurations were analysed depending on the different functions of the thermal contribution of the PV/T string within the entire system. The simulations were performed both for the context of the mainland, considering the climate of Palermo (Italy), both for the context of the minor Mediterranean islands, with particular reference to Lampedusa (Italy). For the latter case, in particular, the impact of the substitution of existing fuel-based technologies with heat pump systems eventually coupled to a photovoltaic (PV), solar thermal plant (ST), and hybrid photovoltaic-thermal (PV/T) systems was analysed.

Introduction

Objectives and working steps

The purpose of this thesis falls within the scope of the project deriving from the MiSE-ENEA Program Agreement on Electricity System Research Three-year Realization Plan 2019-2021, aimed at carrying out a feasibility study of possible solutions for the energy efficiency of users of small islands.
Systems based on the use of HP technology dedicated only to the production of domestic hot water for individual domestic users and combined with solar systems, have proved to be a valid alternative to the use of electric water heaters especially in the context of small Italian islands. However, such a plant system presupposes the availability of a surface on the roof such as to be able to install a sufficient number of photovoltaic panels and/or solar collectors.
Starting from the consideration that this surface is not always available, this work proposes the use of hybrid PV/T technology which combining the PV and ST technologies in a single module can allows the optimisation of the the use of spaces.
In particular, the study of a plant system based on the integration of a hybrid type solar plant to the HP dedicated to DHW production is performed.
The main objective was to reduce the thermal consumption of the system by exploiting solar production, consequently reducing the electricity consumption of the HP and at the same time ensuring coverage of the latter by means of the electricity production of the PV system. Specifically, two main plant solutions were hypothesized, with the aim of pre-dimensioning the main components and verifying the advantages and disadvantages of each of them by introducing appropriate indices
The main objective of the feasibility study presented here is the design of a plant layout to be installed at the joint ENEA/DING laboratory in Casaccia (Rome, Italy). Specifically, this thesis presents the pre-sizing of the experimental plant through simulations in dynamic regime aimed at defining the optimal set-up.
In particular, the study has the main purpose of defining the functional and performance requirements for a system consisting of a heat pump (HP) combined with a photovoltaic (PV), solar or hybrid system to test control logics aimed at optimizing the use of the tank of domestic hot water (DHW) as thermal storage of the energy produced by the Renewable Energy Sources (RES) plant and at the same time allowing participation in aggregation programs promoted by the network operator or by an aggregator.
Since the context of the small islands is the subject of the ENEA/DING project (Report RdS / PTR2019 "Feasibility study of solutions for the energy efficiency of the Minor Islands"), a minor Sicilian island was selected as a relevant case study and simulations were also carried out for this specific climatic context.

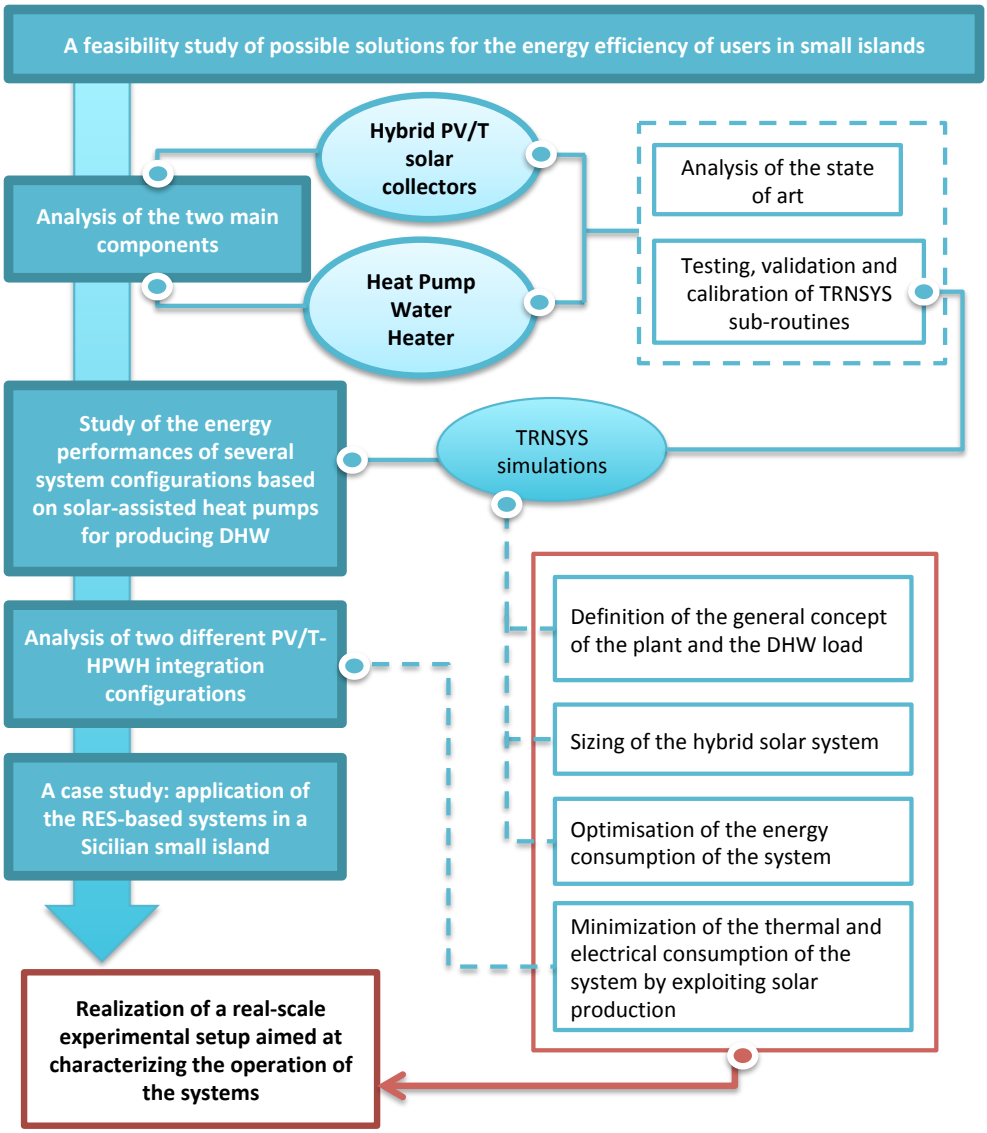

Thesis structure

The present thesis is focused on the investigation of the energy performance of systems based on the coupling of air to water heat pumps with PV/T hybrid solar collectors for producing domestic hot water (DHW).
As a first step, an overview of hybrid PV/T collectors is provided in Chapters 1 and 2.

In **chapter 1** the state of the art of this technology is analysed both as concern the theoretical description of physical functioning and performances of these innovative collectors both as concern the available products on the market. A detailed description of the most spread criteria used in literature for PV/Ts classification is provided. An analysis of the global market is performed reporting a sample of case studies regarding PV/T systems installed, with the most relevant applications, and based on various types

of PV/T collectors. Furthermore, the physical and technical data of some of the main commercial models are reported.

Chapter 2 reports an analysis of the main mathematical models present in the literature on the modeling of PV/T systems. Since the implementation, validation, and parameter identification procedure of the PV/T performance model were performed using the TRNSYS simulation tool, particular attention was paid to the models underlying the main types of TRNSYS that describe the behavior of hybrid solar collectors.
The second part of this chapter gives a specific focus on the main procedures used to test the thermal performance of the PV/T collectors and carry out their characterization, with reference to the relevant technical standards.

Chapter 3 introduces the topic of air to water heat pumps technology applied to systems mainly dedicated to the production of domestic hot water in residential buildings.
After providing a brief description of the functioning of air to water heat pumps, the peculiarities and main critical issues of this technology are discussed.
To overcome the technological limits of heat pumps, solar integration of air-source heat pump systems (ASHP) is proposed as one solution to improve their performance. With solar-assisted ASHP systems, it is possible to achieve improved techno-economic and environmental performances, to meet a higher ratio of the energy demand. These systems can also produce different types of energies, which in the case of hybrid PV/T collectors is not only heating/hot water or cooling but also electricity from PV modules.
An overview is then given of the more diffuse system's solution based on the coupling of the heat pumps with the hybrid PV/T collectors for producing DHW.
Finally, considering their actual tightening development and diffusion in the market a deepening concerning the latest technology of hybrid heat pumps is made. Here in particular, among the different variants that are labeled as “hybrid” solutions, only systems consisting of the coupling of a heat pump and a gas condensing boiler are taken into consideration. In particular, a comprehensive review has been performed on hybrid systems using Heat Pumps (HPs) for HVAC systems and DHW production using case studies from 2016 to 2022. After an explanation of the methodology used to carry out the review, the layouts of the hybrid heat pump systems are described as well as the main control strategies implemented in order to improve their performances.

Chapter4 deals with the study of the energy performances of several system configurations based on solar-assisted heat pumps equipped with photovoltaic (PV) and photovoltaic-thermal (PV/T) panels as well as solar thermal collectors, which is the main subject of this thesis. These studies have been useful for the realization of a real-scale experimental setup aimed at characterizing the operation of the systems under study, in the context of a collaboration project with ENEA (Report RdS / PTR2019 "Feasibility study of solutions for the energy efficiency of the Minor Islands"). The chapter presents, as the first step, the definition of the general concept of the plant. The

loads' definition is then performed by identifying several DHW load profiles. A description of the main components, which were chosen as system equipment for the realization of the experimental setup, is then provided reporting their rated technical and physical characteristics.
A TRNSYS model was developed to reproduce the operation of the overall plant as far as to do preliminary sizing. Before running TRNSYS simulations of the entire plant, each sub-routines were tested separately and, when required, a validation and calibration process was conducted. The validated models allowed exploring the dynamic performance of the systems under different climate and operation conditions. In particular, three different types of panels (PV/T, PV, and ST) and a different number of them (4, 6, and 8, referred to as "configuration_1", "configuration_2", and "configuration_3" respectively) were studied to assess their performances. The main object of study of the first phase was the sizing of the hybrid solar system and specifically the number of panels that allow optimising the energy consumption of the system and the consequent choice of auxiliary components (inverter, storage, etc.).
After the sizing of the systems, two different integration configurations were analysed depending on the different functions of the thermal contribution of the PV/T string within the entire system: configuration A and configuration B. In the former, the water heated by PV/T collectors is used to directly feed the heat pump, in the latter instead the thermal contribution is used to preheat the water feeding the heat pump by using an intermediate solar storage tank.

The results of the dynamic simulations described in chapter 4 are reported and discussed in **chapter 5**. Results were used to identify the best configuration in terms of energy-saving, to well understand the effectiveness of the solar collectors (PV/T, PV, or ST) under different load demands. Several indices are defined and calculated to guide toward correct sizing, to check users' satisfaction, and to assess primary energy savings. To quantify the thermal and electrical contributions of the solar plants to cover the thermal and electrical energy needs of the overall DHW plant, the solar fractions (thermal and electric) were calculated. Furthermore, through primary energy analysis, the degree of interaction with the electricity grid was assessed and opportunities to support demand-response actions for grid electricity management were investigated. Starting from the first results obtained an alternative plant layout was analysed based on the introduction of a preheating water tank between the HPWH and the PV/T system. The main objective was to reduce the thermal consumption of the system by exploiting solar production, consequently reducing the electricity consumption of the HP and at the same time ensuring coverage of the latter using the electricity production of the PV/T system.

Finally, **chapter 6** reports an analysis carried out to test the application of several RES-based systems for producing DHW, including solar plants which were described in chapter 4, on the energy system of the Mediterranean minor islands as a relevant case study. The impact of the substitution of existing electric storage water heaters (ESWH)

with dedicated HPWH, eventually coupled to a photovoltaic (PV) plant, a solar thermal plant (ST), or a solely ST system was analysed. Furthermore, an alternative scenario was examined where the existing ESWH is substituted with the DHW production system described in chapter 4, considering, in particular, the configuration_2 where the HPWH is coupled to 6 PVT panels system. The effectiveness of this retrofit solution is analysed by using the energy and operational indices introduced in chapter 5 adjusted for the context of the minor island of Lampedusa (Sicily, Italy).

Author's original contributions

Publications in scientific papers

- Martorana F, Giardina M, Buffa P, Beccali M, Zammuto C. (2021, September). A new tool to process forecast meteorological data for atmospheric pollution dispersion simulations of accident scenarios: A Sicily-based case study. DOI:10.13044/j.sdewes.d8.0377. In JOURNAL OF SUSTAINABLE DEVELOPMENT OF ENERGY, WATER AND ENVIRONMENT SYSTEMS - ISSN:1848-9257 vol. 9 (3)

- Martorana F, Bonomolo M, Leone G, Monteleone F, Zizzo G, Beccali M, (2021). Solar-assisted heat pumps systems for domestic hot water production in small energy communities. DOI:10.1016/j.solener.2021.01.020. pp.113-133. In SOLAR ENERGY - ISSN:0038-092X vol. 217

- Beccali M, Bonomolo M, Pietra B.D, Leone G, Martorana F. (2020). Solar and heat pump systems for domestic hot water production on a small island: The case study of Lampedusa. DOI:10.3390/app10175968. pp.5968. In APPLIED SCIENCES - ISSN:2076-3417 vol. 10 (17)

- Marco Beccali, Marina Bonomolo, Biagio Di Pietra, Giuliana Leone, Francesca Martorana, Gaetano Zizzo (2020). Efficientamento energetico di utenze domestiche nelle isole minori italiane. DOI:10.36164/AiCARRJ.60.01.04. pp.48-53. In AICARR JOURNAL - ISSN:2038-2723 vol. 60 (1)

- Martorana F, Parlato A, Perrone G, Tomarchio E. (2019). Response Of Gafchromic® Hd-V2 Film Dosimeter In 10-300 Gy Dose Range For Radiation Testing Of Electronic Devices. DOI:10.2298/NTRP180801005M. pp.79-84. In NUCLEAR TECHNOLOGY & RADIATION PROTECTION - ISSN:1451-3994 vol. 34 (1)

Conferences

- Martorana, F., Bonomolo, M., Leone, G., Beccali, M., Di Pietra, B. (2021). Systems layouts with additional heat storages for low-temperature PVT collectors assisting Heat Pumps for DHW production. Proceedings of 52° CONVEGNO INTERNAZIONALE AiCARR "HVAC and Health, Comfort, Environment. Equipment and design for IEQ and sustainability. ISBN 978-88-95620-75-6 (pp. 335-350)

- Martorana, F.; Agnello, G.; Giardina, M.; Buffa, P.; Beccali, M. (2019). A new preprocessing tool of ECMWF data for CALMET forecasting simulations. In

CD PROCEEDINGS-DUBROVNIK CONFERENCE ON SUSTAINABLE DEVELOPMENT OF ENERGY, WATER AND ENVIRONMENT SYSTEMS. In CD PROCEEDINGS-DUBROVNIK CONFERENCE ON SUSTAINABLE DEVELOPMENT OF ENERGY, WATER AND ENVIRONMENT SYSTEMS - ISSN:1847-7178.

Nomenclature

°C degrees Celsius
°CDB degrees Celsius (Dry Bulb)
1M+1L+1XL combination of one M profile, one L profile and one Xl profile
2L+1XL combination of two L profiles and one XL profile
2XL combination of two XL profiles
3L combination of three L profiles
6M combination of six M profiles
A Ampère
a_1 coefficient related to the heat loss
a_2 coefficient related to the temperature dependence of the heat loss
Aa aperture area (m^2)
A_C collector surface (m^2)
AM air mass coefficient
A_{rec} receiver area (m^2)
b bond width (m)
c coefficient describing temperature heat loss
C geometrical concentration ratio
C_b bond conductance (W/mK)
C_{bat} required battery capacity
c_p specific heat capacity (kJ/kgK)
D_i internal tube diameter (m)
E_{AC} the energy delivered to the primary circuit from the HP condenser-absorber
$E_{bin,I}$ the hourly energy loading for each bin
E_E the energy supplied to the evaporator by the heat source
E_{grid} energy supplied by the grid
$E_{grid,ref}$ Electricity from the grid
$E_{HPWH,day}$ average daily HPWH consumption in the most critical month
E_{HPWH} heat pump consumption
E_{loss} energy losses due to the converison and storage system
E_{PV} electric energy supplied by the PV system
$E_{PV/PVT}$ electrical energy contribution from the RES plants
$E_{pump-ST}$ consumption of the solar thermal pump
E_{HPWH}^{RES} energy consumed from the grid by the RES-based plants
E_{HPWH}^{Std} energy consumed from the grid by a conventional HPWH
E_{tot} Total consumed electricity
F fin efficiency (-)
F' collector efficiency factor
F'' collector flow factor
$f_{m,i}$ Monthly correction factor
F_R heat removal factor
$f_{sav.NREN}$ non-renewable energy saving factor
G Irradiance
G'' net solar irradiance

G_c concentrated effective irradiance
G_{hem} hemispherical solar irradiance
G_T total solar radiation (beam + diffuse) incident upon the collector surface (kJ/hr.m^2)
h_{fl} heat transfer coefficient between fluid and tube wall (W/m^{2}K)
h_{IRR} equivalent number of hours of irradiation in a day [h]
h_{outer} the heat transfer coefficient from the PV surface to the ambient air [kJ/hr.m^{2}K]
h_{rad} the radiative heat transfer coefficient from the PV surface to the sky [kJ/hr.m^{2}K]
I solar radiation
I_{br} beam radiation from the reflector
I_{dr} diffuse radiation from the reflector
I_{mp} Current at maximum power
J_c energy cost
J_e primary energy consumption
k conductivity (W/mK)
k_{abs} absorber conductivity (W/mK)
k_b bond thermal conductivity (W/mK)
k_γ module temperature correction factor
k_g low irradiance correction factor
k_θ optical correction factor
$K_{\theta,b,pv}$ beam irradiance IAM for PV conversion process
$K_{\theta,d,pv}$ diffuse irradiance IAM for PV conversion process
k_λ spectrum correction factor
K_m correction factor for the missing radiation from the reflector
$K_{\tau\alpha b}$ incident angle dependence for beam radiation
$K_{\tau\alpha d}$ incident angle dependence for diffuse radiation
m mass (kg)
$\dot{m}$ mass flow rate (kg/h)
m_{DHW} Domestic hot water mass flowrate at 40 °C
N_{aut} number of days of autonomy granted by the battery
P_{abs} absorbed power (W)
p_{gas} price of the gas (€/kWh)
$p_{el,grid,HP}$ set price of the electricity tariff (€/kWh)
$p_{el,PV,sold}$ price of the sale of PV electricity (€/kWh)
P_{el} electrical power (W)
P_{es} standby power input (kW)
$p_{heat,HP}$ predicted heat price
P_{inv} Inverter deliverable power
P_{loss} power losses (W)
P_{mp} Power at maximum power
P_{out} total power output (W)
P_{th} termal power (W)
P_{pv} electrical power generated by PV/T collector
q_e local electrical output
Q thermal energy
Q_C reference annual cooling demand (kWh)
Q_{CE} annual energy consumption for cooling (kWh)
Q_{DHW}: thermal energy for DHW

$Q_{el,ref}$ electrical auxiliary demand
$Q_{el,DE}$ domestic electricity demand
$Q_{HP\text{-}tap}$ useful thermal energy during one single draw-off (kWh)
Q_{HPWH} thermal energy from the heat pump cycle
Q_{HX_DHW} heat released from the thermal storage tank to the DHW
Q_{loss} net of thermal losses
$Q_{loss,ref}$ losses for domestic hot water preparation
Q_{LP} total useful energy content during the whole DHW load profile (kWh)
Q_{TANK} thermal energy of the tank
$Q_{ST/PV}$ thermal energy contribution from the RES plants
Q_u useful energy gain
q'_u useful energy gain per unit of area
q_{urm} heat produced from the reflector
R reflectance
R_T resistance to heat transfer from the PV cells to the absorber plate [hr.m^{2}K/kJ]
S net absorbed solar radiation
S' modified net absorbed solar radiation
T_a air temperature (K)
T_{amb} ambient temperature (K)
T_b base temperature (K)
$T_{f,i}$ inlet fluid temperature (K)
$t_{f,m}$ mean fluid temperature
T_i internal temperature (K)
T^*_m reduced mean temperature [°C]
$t_{pv,m}$ mean PV cell temperature
$t_{pv,r}$ reference PV cell temperature
T_r reflector temperature (K)
T_{sky} sky temperature (K)
T_c takes into account the electrical loads coverage by photovoltaic systems including the electrical capacity of the battery.
T_{cold} Temperature DHW exchanger inlet
T_{DHW} Outlet tank temperature of domestic hot water system
T_{hot} Temperature DHW exchanger outlet
T_{pv} PV cell temperature [°C]
T_{sky} sky temperature for long-wave radiation calculations [°C]
T_{WC} temperature of water from network
T_{WH} temperature of DHW
t_{TTC} load profile time (h)
u air speed (m/s^2)
u' reduced air speed (m/s^2)
Ub bottom loss coefficient
Ue edge loss coefficient
U_L overall heat loss coefficient
U'_L modified overall heat loss coefficient
UNI-A profile from UNI EN 12831
U_{sky} heat losses towards the sky
U_t top loss coefficient

V_{40} max. volume of mixed water at 40 °C (l)
$V_{DHW,max}$ Maximum valued of volume demand of domestic hot water
$V_{DHW,min}$ Minimum valued of volume demand of domestic hot water
V_{mp} Voltage at maximum power
W distance between tubes (m)
$W_{EL\text{-}LP}$ total electrical energy consumption during the whole load DHW profile (kWh)
$W_{EL\text{-}M\_LP}$ total measured electrical energy consumption (kWh)
$X_{CellTemp}$ dependence of the PV efficiency value on the ambient temperature
$X_{Radiation}$ dependence of the PV efficiency value on the incident solar radiation

Subscripts

abs absorber
b beam
d diffuse
e effective
h heating
el electrical
th thermal
v ventilation

Greek letters

α absorptance
$\alpha_{laminate}$ absorptance of the PV/T laminate
β_{pv} MPP cell efficiency tempera\\ture coefficient
γ average bond thickness
$\varepsilon_{NREN,ec}$ primary energy ratio (non-renewable contribution for each energy carrier)
$\varepsilon_{NREN,ec}$ primary energy ratio (non-renewable contribution for each energy carrier)
$\varepsilon_{NREN,grid}$ primary energy ratio (non-renewable from grid)
ε_{REN} primary energy ratio (renewable contribution)
η cell array efficiency
$\eta_{0,b}$ peak collector efficiency based on beam irradiance
$\eta_{0,hem}$ peak collector efficiency based on hemispherical irradiance
η_a PV efficiency at the ambient temperature
η_{CGB} efficiency of the gas condensing boiler
η_G the natural gas combustion efficiency
η_{hs} efficiency of heating system
η_n nominal efficiency
η_{pv} photovoltaic efficiency
$\eta_{pv,r}$ cell reference electrical efficiency
η_r rated efficiency
η_{ref} electric efficiency of a reference system
η_{th} thermal efficiency
$\eta_{th,0}$ thermal conversion factor
θ_{bcr} the incidence angle for beam radiation from reflector

θ_{dcr} the incidence angle for diffuse radiation from reflector
$\theta_{WC}(t)$ cold water temperature at inlet of the domestic water storage
$\theta_{WH}(t)$ hot water temperature at outlet of the domestic water storage
ρ reflectance
ρ_{cover} cover reflectance
ρ_{pv} PV packing factor
ξ_{tot} heating season energy process cost saving potential
τ transmittance
$\tau\alpha$ transmittance-absorptance product for the solar collector
τ_{cover} cover transmittance
τ_G glass cover transmittance

Acronyms

AC air conditioner
AEEF available electric energy efficiency
AHU air handling unit
ASHP air source heat pump
BAC building automation control
BECMS building energy control and management system
BIMAX maximum allowed energy charged for the chosen value of battery index
BImin minimum allowed energy charge value for the chosen value of battery index
BIPV building-integrated photovoltaic
CGB condensing gas boiler
CHP combined heat and power
COP Coefficient of Performance
C-PV/T concentrating photovioltaic thermal collector
CSt Storage capacity
CTA transparent cover
DHW domestic hot water
DI Discomfort index
DSM Demand-side management
EC Energy Communities
EER Energy Efficiency Ratio
EES Electric Energy Saving
EHPA European Heat Pump Association
ERWH Electric Resistance Water Heate
ESI Electric storage index
ESWH Electric Storage Water Heater
FSOCav Average fractional state of charge
GC Grid-connected
GWP global warming potential
HHP hybrid heat pump
HP heat pump
HPWH heat pump water heater
HPWH + grid Heat pump water heater combined with grid supply
HPWH + ST Heat pump water heater combined with solar thermal plant

HX heat exchanger
IAM The incidence angle modifier
IEA International Energy Agency
LOC linear optimal control
MLR Multiple linear regression
MPC model predictive control
MPP maximum power point
NF nanofluid
NMPC non-linear model predictive control
NPV Net present value
nZEB net zero emission building
ODP ozone depletion potential
OC operational cost
OCP optimal control problem
PBT Payback time
PCM phase change material
PDI Potential discomfort index
PEC primary energy consumption
PEE primary energy efficiency
PER Primary Energy Ratio
PEF_{hp} Primary Energy Factor for heat production
PEF_{hp} Primary Energy Factor for heat source
PER_{NREN} Primary Energy Ratio (non-renewable sources)
PER_{NREN} Primary Energy Ratio covered by non-renewable source
$PER_{NREN.ref}$ Primary Energy Ratio for a reference system
PV photovoltaic
PPV PV plant power
PV/T Photovoltaic - Thermal collector
PVT/WHP photovoltaic/thermal acetone wickless heat pipe
QDT quasi dynamic testing
RBC rule-based control
RES renewable energy sources
RH resistance heater
SA Stand-alone
SAASHP solar assisted air source heat pump
SC speficic cost
SCOP seasonal coefficient of performance
SEER seasonal energy efficiency ratio
SF_{el} Solar Fraction considering electric balance
SF_{th} Solar Fraction considering thermal balance
SHC Solar Heating and Cooling programme
SOC_{MAX} Maximum value of the state of charge in the battery
SOC_{min} Minimum value of the state of charge in the battery
SPF seasonal performance factor
SPF_{hhp} seasonal performance factor of the hybrid heat pump
SPI Setpoint index
SPT Simple payback time
SSPV/T spectral splitting photovoltaic-thermal collectors

SST steady state testing
ST Solar Thermal
SWOT Strengths, weaknesses, opportunities, and threats
TES Thermal Energy Storages
VCASHP vapour compression air source heat pump
XL eXtra Large size
WHGB wall-hung gas boiler
WISC wind and/or infrared sensitive collectors

1. Hybrid solar technology: state of the art and peculiarities

The hybrid Photovoltaic/Thermal (PV/T) technology is based on the combination of a photovoltaic (PV) panel with a thermal collector capable of simultaneously producing electricity and heat from the same gross area. The idea, as proposed by Zondag (Zondag, 2008), probably arose from the need to satisfy both thermal and electrical demands, which are often supplementary, with a single device. Starting from the 1970s it was developed the idea of cooling the surfaces of photovoltaic panels to exploit the heat generated from the absorbed solar radiation that is not converted into electricity. In addition to offering the same advantages of photovoltaic and solar thermal technologies, a PV/T collector leads to the maximization of available space for installation, lower installation costs, and higher photovoltaic efficiency.
The combined photovoltaic/thermal (PV/T) technology allows increasing the overall efficiency of a PV module using excess heat, which otherwise, increasing the operating temperature of the solar cells, would reduce the PV output. Therefore, for a better performance, to keep the operating temperature of the solar cells low it is essential to remove the heat produced from the dissipation of the unused radiations of the solar spectrum. For this purpose, a heat transfer fluid flows inside the receiver removing the excess heat from the PV cells. This leads to a double benefit because it helps to reduce the temperature of the PV module and to make the recovered useful heat available for technical applications (i.e., to power a thermal user).
In this chapter the state of the art of this technology is analysed both as concern the theoretical description of physical functioning and performances of these innovative collectors both as concern the available products on the market. A detailed description of the most spread criteria used in literature for PV/Ts classification is provided, such as for example the material used for the PV cells realisation or the heat transfer fluid employed. An analysis of the global market is performed reporting a sample of case studies regarding PV/T systems installed, with the most relevant applications, and based on various types of PV/T collectors. Furthermore, the physical and technical data of some of the main commercial models are reported.

1.1. Technology review and future trend

PV/T collector was mentioned for the first time in 1976 by Martin Wolf (Wolf, 1976), who in his article analyzed the performance of a combined system consisting of a silicon solar array mounted inside a stationary, non-concentrating thermal collector. The study analyzed the combined system of photovoltaic solar panels and solar heating for a single-family residence for a whole year, using hourly meteorological data. Results showed that the system was cost-effective, and the value of the combined energy output was significantly greater than that of each single-purpose system's output alone.

A few years later Raghuraman and Hendrie (Raghuraman and Hendrie, 1980) described numerical methods for predicting the thermal and electrical performances of two typical PV/T collector designs, one using liquid and the other using air as heat transfer fluid. The temperature difference between the photovoltaic cells and the thermal absorber flat plate was analyzed to maximize the total energy extracted from the PV/T collectors.
In 1985, C. H. Cox, III and P. Raghuraman with their work, through simulations of flat-plate PV/T collectors, performed studies on different and potentially useful features regarding the design of hybrid photovoltaic/thermal PV/T collectors to determine their effectiveness and interaction (Cox and Raghuraman, 1985).
Although the studies on PV/T collectors start as early as the 70s, their commercialization has suffered an initial slowdown, also related to the high costs of the technology and the problems related to significant heat losses affecting the top surface.
Therefore, PV/T systems have seen an increase in technological development only starting from the 1990s. The renewed interest in PV/T technology is probably attributable to better exploitation of spaces, where limited, and a better architectural uniformity with the buildings compared to the separate ST and PV technologies. Anyway, as reported in (Chow, 2010), PV/T studies in this period were more related to the collector design improvement and performance evaluation, with more rigorous analyses of the energy and mass transfer phenomena on conventional collectors followed by experimental validation.
A steady-state model was developed in (Garg and Adhikari, 1999) in order to predict the thermal and electric performance of a hybrid PV/T air heating collector coupled with a compound parabolic concentrator (CPC). Through parametric studies, the influence of different parameters (like for example collector length, air mass flow rate, etc.) on the thermal and electrical output of the PV/T systems was analysed.
The thermal and electrical yield of a PV/T panel were investigated also in (Zondag *et al.*, 2000), where a good correspondence was found between the measurements on annual efficiency of a non-optimised PV/T prototype and the results of the simulations.
Chow in (Chow, 2003) developed an explicit dynamic model for a single-glazed flat-plate water-heating PV/T collector. The proposed model resulted suitable for dynamic system simulation applications providing information on the transient performance, including the instantaneous thermal/ electrical gains, their efficiencies, and thermal conditions of various collector components.
Tiwari and Sodha in (Tiwari and Sodha, 2006) have made an attempt to develop a thermal model of an integrated photovoltaic and thermal solar system deriving an analytical expression for the temperature of the PV module and the water.
While on the one hand a great deal of work had been carried out on PV/Ts regarding the technical aspects, in particular relating to the optimization of their performance, on the other hand, the issues of reliability, installation, financing, building integration, and testing guidelines had not yet received the attention they deserve. As also highlighted at the 20th European Conference on Photovoltaic Solar Energy in (Zondag *et al.*, 2005), a series of priority actions were necessary in order to improve the market penetration of

PV/T collectors for the short, medium, and long term. In this regard focus research on the effect of stagnation temperature on photovoltaic cells and on increasing their optical efficiency, detailed market studies, development of methods to integrate PV/T into buildings with respect for aesthetics, development of low-cost financing scheme had become paramount.

The suitability of hybrid PV/T systems for the provision of electricity, hot water, or space heating in the domestic sector was assessed in (Herrando, Markides and Hellgardt, 2014) and in (Herrando and Markides, 2016). In the former a model was developed to estimate the performance of hybrid PV/T systems for the provision of electricity and hot water in the UK domestic sector, with particular focus on a typical terraced house in London. The role of important system parameters was investigated in maximising the supply potential of both electricity and hot water and in maintain, at the same time, simplicity of design, leading to a minimisation of systems costs to the end-user. The latter complements the previous study by considering the economic aspects of PV/T technology, based on which invaluable policy-related conclusions can be drawn concerning the incentives that would need to be in place to accelerate the widespread uptake of such systems.

In the last decade, several research studies have been carried out to optimize the performance of PV/T collectors in order to make them competitive with other types of solar energy converters. In particular, many efforts have been made to propose solutions to the main critical aspects of this technology, mainly related to low performances and high costs. In this regard, Mellor et al. in (Mellor *et al.*, 2018) presented a roadmap of the technological advances required to achieve this goal. Strategies for reducing convective, radiative, and electrical losses at elevated temperatures are discussed, and experimental characterisation of a novel transparent low-emissivity coating for photovoltaic solar cells is presented. In (Kazemian *et al.*, 2018) the effects of using a mixture of water and ethylene glycol in both glazed and unglazed conditions on the performance of a PV/T system are experimentally investigated.

A novel photovoltaic thermal collector was designed and tested in (Rejeb *et al.*, 2020) with the purpose of maximizing the electrical power and minimize the thermal losses of the solar panel. In particular, the innovative PV/T configuration aimed to reduce the optical and thermal losses thanks to an optical anti-reflective and low-emissivity coating, maximize the fluid temperature, and minimize the PV module operating temperature effect.

In the last years, PV/T collectors proved to be a sharp option in several contexts, as highlighted in (Herez et al., 2020), considering that they can deliver thermal and electrical power simultaneously to meet different final uses. The review study reported in (Brahim and Jemni 2017) on the historical and recent trend of PV/T development technology, identifies as the greatest market potential of this hybrid technology that relating to domestic hot water (DHW) applications, possibly combined with space heating.

In (Tsai, 2015) and (Dannemand et al., 2019) the coupling of PV/T collectors with electric heat pumps, and eventually cold buffer and hot storage tanks, for domestic hot

water (DHW) production is proposed and investigated as a promising choice due to the increased flexibility of such devices in managing several energy vectors.

A wide variety of research works focused on solar-assisted air conditioning systems, currently in practice mainly either absorption, adsorption, or desiccant-based cooling systems. In (Farooq *et al.*, 2020), (Y. Wang *et al.*, 2020), (Guo, Bilbao and Sproul, 2020) the performance of solar-based desiccant cooling systems powered by PV/T collectors was analysed. In particular, dynamic simulations and performance analyses were performed to optimize the key design parameters and to quantify the energy-saving potential of these cooling systems, considering different plant configurations and different climatic locations.

Thanks to their peculiarities, PV/Ts could also be appropriate for desalination applications which are an indispensable help to the limited natural supplies in satisfying the freshwater demand, especially in climatic locations with high ambient and operating temperatures where the population is affected by water shortages. In (Alqaed, Mustafa and Almehmadi, 2021), (Ammous and Chaabene, 2015), (Bilton, 2018), (Calise et al., 2019), (Kelley and Dubowsky, 2013), (Lee et al., 2012), (Li et al., 2019), (Manokar et al., 2017), (Modi and Shukla, 2018) the optimization of the integration of PV/T collectors in low energy cost desalination systems are investigated.

Recently, very innovative PV/T systems have been proposed which are essentially based on the exploration of new configuration designs or the use of innovative materials, such as heat pipes, optical filters, nanofluids, phase change materials (PCMs).

Wickless heat pipes are an effective passive heat transfer device that, due to their improved heat transfer capabilities, can enhance photovoltaic system efficiency.

An assessment investigation for a photovoltaic/thermal acetone wickless heat pipe (PV/T-WHP) solar system was conducted in (Brahim and Jemni, 2021). Results about optimal PV/T panel area and optimal number of heat pipes, maximum thermal and electrical efficiency gain compared to conventional PV/T water-based systems are reported. A new heat pipe – PV/T system is proposed in (Kılkış, 2020) which has controls that are embedded to the panel with thermally adjustable heat pipes as cheap solutions such that even small buildings may afford the cost compared to more expensive external controls.

Fluid PV/T collectors based on spectral splitting of the solar radiation are proposed in (Huang *et al.*, 2021) as a promising solution capable of generating high-temperature thermal energy while keeping the PV cell working at a lower temperature. Different ideal fluid filters are assumed and applied to the SSPV/T collector, in order to explore the optimal optical filter and the maximum potential of such fluid-based SSPV/T collectors under different scenarios. The spectral, thermal, and temperature distributions through the collector are also simulated and analysed under different working conditions.

The use of nanofluids in PV/T collectors, providing a higher overall performance because of the greater thermal conductivity of nanoparticles suspended inside a base fluid, is also widely analysed in literature. In (Hemmat Esfe, Kamyab and Valadkhani, 2020) and (Sheikholeslami *et al.*, 2021) review researchers focused on the thermal efficiency improvement of PV/T systems through the utilization of nanomaterial are

presented. In the former the fluid and nanofluid in PV/Ts have been evaluated in single fluid flows, dual fluid flows (air-liquid), phase change materials (PCM), and nanofluid flows. The latest review, focusing on improving the thermal efficiency of PV/T systems, summarizes and numerically, theoretically, and experimentally analyses all common types of nanofluids used within PV/T systems. The integration of phase change materials to regulate PV/T operating temperatures has also attracted the attention of several authors. Experimental analyses were conducted on the innovative design of PV/T-PCM solar systems for the evaluation of the energy performances, for example by assessing the differences between glazed and unglazed collectors (Kazemian *et al.*, 2020) or with the operating of traditional photovoltaic systems (Carmona and Palacio, 2021).
Although is available a large amount of research work and technological solutions in the literature to overcome the main limitations of PV/T collectors, however, before the large-scale implementation of all these innovative systems, further studies are needed to reduce the uncertainties around the advanced technologies they use. Furthermore, their acclaimed advantages and stability still need further validation through experimental analyses.

1.2. Different types of photovoltaic-thermal hybrid systems (PV/T)

A PV/T collector can be considered as a kind of solar thermal collector, which has an absorption plate, a module of PV cells, and a fluid heat extraction unit, in which the heat removal fluid circulates. Besides, a glass cover can be added on the top of PV/T collector to reduce thermal losses, or the collector can be unglazed, to avoid the reduction in electrical output due to reflection optical losses and absorption heat losses from the glazing. The PV/T collector has also thermal insulation at the non-illuminated collector parts, like the way this is applied to a typical solar thermal collector.
Several and different classifications have been proposed by researchers for PV/T collectors. The following paragraphs refer to the most used classification criteria for PV/Ts in the literature, summarized for sake of clarity in the diagram in Figure 1.1.

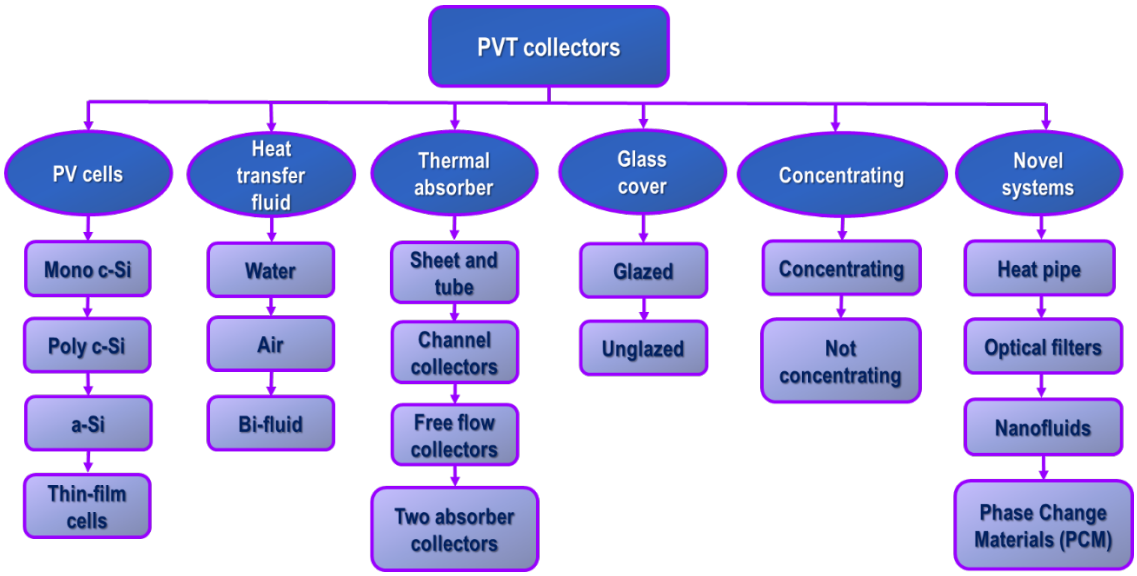

Figure 1.1. Classification of PV/T collectors

1.2.1. PV cells

The PV cells can be classified into two categories: "first-generation" cells, made of monocrystalline silicon (mono c-Si) or polycrystalline silicon (poly c-Si), and "second generation" cells, which include amorphous silicon (a-Si) and thin-film solar cells. The mono-crystalline cells are made of pure silicone with a single crystal structure with almost no defects or impurities. The main advantage of monocrystalline cells is their high efficiency, while a disadvantage of these cells is their high cost due to the complicated manufacturing process. Given their cost, monocrystalline modules are mostly used where the maximum possible power is required from a confined space, such as residential and commercial roofs (Kalogirou, 2014). The polycrystalline cells are also made of silicon, but instead of a single crystal, they are composed of several fragments melted together. In this case, a simpler manufacturing process is required which implies a lower cost (Kalogirou, 2014). Mono-crystalline and poly-crystalline generate the same power when using the same area; however, mono-crystalline has higher efficiency (Cappelletti et al., 2016) than poly-crystalline (about 20% against 15% respectively) due to the grains existing in the poly-crystalline. Nevertheless, mono-crystalline silicon is more expensive than poly-crystalline due to the complex formation of a single crystal.

In the amorphous silicon (a-Si) PV cells the silicon atoms are arranged in a thin homogenous layer. It is possible to have thinner thicknesses thanks to the greater ability of this type of cells to absorb light more effectively than crystalline silicon. Advantages of these cells are their low manufacturing cost and high energy production per rated power capacity (kWh/kWp). Because of their low cost, they are applied in a wide variety of PV systems however, they face increasing competition from other thin-film technologies which allow higher efficiencies.

Within the category of thin-film PV cells, essentially two families can be identified: Cadmium Telluride (CdTe) and Copper Indium Gallium Selenide (CIGS) PV cells. The Cadmium Telluride cells present a combination of low cost, moderate efficiency, and large manufacturing volume, which has favored their wide diffusion on the market relating to industrial-scale solar power plants. Copper Indium Gallium Selenide PV cells are a newer thin-film technology. Thanks to their moderate efficiency, low cost, and lightweight they are ideally suited for rooftop installations, both residential and commercial, and building-integrated photovoltaic (BIPV) products (Kalogirou, 2014).

1.2.2. Heat transfer fluid

A widely used classification criterion of the various types of PV/T collectors is based on the heat transfer fluid used in the PV/T system, mostly water or air. In a water PV/T collector, the heat extraction unit is usually a heat conductive plate with pipes for the circulation of the water, which is in thermal contact with the PV rear side, while in air PV/T collectors it is usually an air duct placed at the rear side of the photovoltaic panel. As obtained by Tripanagnostopoulos et al (Tripanagnostopoulos *et al.*, 2002), the thermal efficiency of the PV/T systems with air heat extraction is lower than that of the corresponding systems with water heat extraction due to the less effective heat exchanging mode of air circulation. As regards instead the electrical efficiency, results showed that the η_{el} of air-cooled systems is almost the same (slightly lower) to that of water-cooled systems, since η_{el} depends mainly on PV temperature.
At locations with low levels of solar radiation and ambient temperatures, as reported in (Chow, 2010), space heating is almost required all the year and air PV/T collectors can be useful and cost effective. At locations with high solar input as well as ambient temperature, water PV/T collectors can be useful for providing year-round water pre-heating services, and on top with intermittent air heat extraction to provide space heating in winter and natural ventilation in summer.
To overcome limitations related to the use of air or water as single coolant, bi-fluid based PV/T collectors have been introduced, which employ both air and water, allowing for more effective heat removal. El Manssouri (Manssouri *et al.*, 2021) presented an energetic analysis devoted to evaluating the performance and the potential field of applications of a novel bi-fluid PV/T collector, investigated through a numerical model which takes into account the energy balance equations, and geometrical and optical features of the different layers that constitute it. In (Lebbi *et al.*, 2021) a new hybrid PV/T Bi-fluid system has been designed, built and tested experimentally under outdoor operating conditions. This new hybrid system was actively cooled from the backside of the PV module by forced air circulation, while its front side was cooled and cleaned by flowing water. The output voltage, electrical current, electrical power output, and electrical efficiency was assessed experimentally as function of operating temperature

and solar radiation intensity. Results proved the design efficacy of the hybrid PV/T Bi-fluids system in terms of yield either electrical and/or thermal energy.

1.2.3. Thermal absorber

One of the most used classifications for water-type PV/T collectors is the one proposed by Zondag (Zondag *et al.*, 2003). The collectors based on the use of water as a heat transfer fluid are classified into four groups based on the type and the mode of heat exchange:

a) Sheet and tube PV/T collectors;
b) Channel PV/T collectors;
c) Free flow PV/T collectors;
d) Two absorber PV/T collectors.

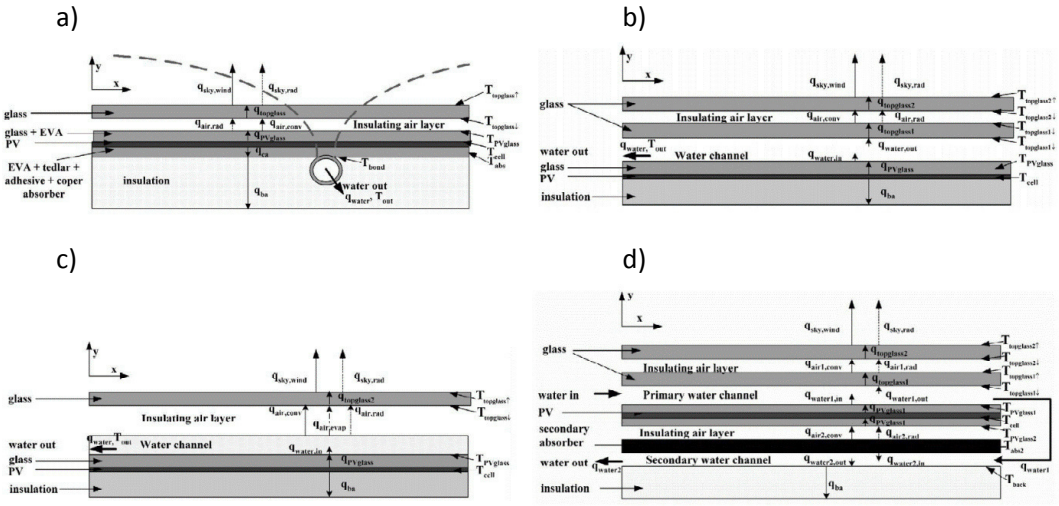

Figure 1.2. Schematic representation of the heat flows for the four typologies of PV/T collectors: sheet and tube PV/T collector (a), channel PV/T collector (b), free flow PV/T collector, and two absorber PV/T collector (d) (Zondag *et al.*, 2003).

In sheet and tube configuration (a), the simplest and the most economical one, the heat produced in the photovoltaic layer is removed by a series of channel located below, inside which the heat transfer fluid flows. In the second typology of collectors (b), a channel is located above the PV cells and the heat transfer fluid flows between the PV layer and a glass cover. Such absorber configuration imposes constraints on the choice of the collector fluid since the absorption spectrum of the fluid should be sufficiently different from the absorption spectrum of the PV in order to allow the PV to receive the incoming radiation. In free-flow PV/T collectors (c), the fluid flows over the PV layer. Compared to the (b) type this design presents one less layer of glass. This reduces the costs of materials and the mechanical fragility of the cover structure. The main disadvantage of this configuration is related to the increased heat losses caused by the

evaporation of the fluid. The two-absorber PV/T panel (d) uses a transparent PV laminate as the primary absorber and a black metal plate as the secondary absorber. The panel contains two water channels on top of each other. The water flows through the upper channel and is returned through the lower channel.

1.2.4. Glazing

The collectors can have one or two covers of glass above the PV module (a higher number brings no further benefit) or be completely devoid of it. The two types of PV/T collectors are called "glazed" and "unglazed" respectively. In the former, a cover of glass with a thickness of 3 ÷ 4 mm is added on the top of a PV/T collector in order to reduce the heat losses increasing the outlet temperature of the heat transfer fluid.
In the latter, the absorber is in direct contact with the environment, which causes significant heat losses, and fluid temperatures are strongly influenced by external parameters (e. g. ambient temperature, wind speed, etc.). These collectors are also called wind and/or infrared sensitive collectors (WISC). In several studies, comparisons were made on the electrical and thermal performance between glazed and unglazed collectors in order to identify the best configuration. In (Aste, Del Pero and Leonforte, 2017) and (Kazemian *et al.*, 2018) it was found that among the two types, the glazed collectors record the highest thermal efficiencies. On the contrary, unglazed collectors have the best electrical performances with higher efficiency values. As a consequence, the former are preferred when high thermal efficiency is required, the latter when a high electrical output is needed.

1.2.5. Concentrating or not

As reported in (Kalogirou, 2014) a non-concentrating collector uses the same area for intercepting and absorbing solar radiation, whereas a concentrating solar collector, which may or may not be equipped with a solar tracking system, usually has concave reflecting surfaces to intercept and focus the sun's beam radiation to a smaller receiving area, to increase the radiation flux. The purpose is to increase energy delivery temperatures by concentrating a large amount of solar radiation on a relatively small collection area, thereby decreasing heat losses. This makes concentrating collectors (C-PV/T) particularly suitable for high-temperature applications. Many researchers developed C-PV/T systems using different solar materials and solar concentrators, such as plane reflecting mirrors, Fresnel lenses, parabolic troughs, (Karathanassis *et al.*, 2019). Among the main advantages of concentrating collectors compared to the non-concentrating ones are the higher temperatures that the working fluid can reach and consequently greater thermodynamic efficiency, greater thermal efficiency thanks to the small area of thermal dispersion compared to the area of the receiver, and a lower cost

per unit area of the solar collector surface since reflective surfaces require less material and are structurally simple. On the other hand, however, the concentrating systems collect little or no diffused radiation depending on the concentration ratio, therefore a tracking system is necessary to allow the collector to follow the sun, solar reflective surfaces can lose their reflectance over time and may require periodic cleaning (Kalogirou, 2014).

1.2.6. Novel PV/T collectors

Among the novel PV/T systems recently proposed four main categories based on innovative systems and materials can be identified: heat pipe, optical filters, nanofluids, and phase change materials (PCMs).
The heat pipe PV/T systems have been developed to provide electrical and thermal energy in a stable way, overcoming the problem of freezing in winter months for systems that use water as the coolant. As reported in (Zhou *et al.*, 2021) the heat pipe PV/T system uses a two-phase boiling heat transfer. High reliability, minimal maintenance requirements, an extensive working life, high heat transfer efficiency, and avoiding freezing in the pipe are indicated as the main advantages that characterize this method. Kılkış in (Kılkış, 2020) proposed the integration of heat pipes into PV/T as a way to replace the pump so to reduce power demand of the system. The new PV/T system with thermoregulated heat pipes was presented as an affordable solution even for small buildings, representing a valid alternative to more expensive external controls. In (Brahim and Jemni, 2021) the advantages of using wickless heat pipes, also known as closed thermosyphon or gravitationally assisted heat pipes, have been analysed. Wickless heat pipes are a two-phase, passive heat transfer system (no external power source) that can transport a large amount of heat and have a high thermal conductivity. In comparison to other PV/T systems, it results that they can preserve a relatively uniform temperature distribution across the panel and provide a fast-thermal response. As compared to wicked heat pipe systems, they have the advantage of being simple to build and maintain.
The optical filters, starting from the consideration that a photovoltaic cell is effective only within a certain spectral range, are aimed to select only the part of the solar spectrum useful for the photovoltaic cell for the generation of electricity. The rest of the spectrum is sent to a thermal absorber for thermal energy generation, thus avoiding the unnecessary heating of the cell. Therefore, SSPV/T collectors are capable of generating high-temperature thermal energy while keeping the PV cell working at a lower temperature. As reported in (Huang *et al.*, 2021), two types of optical filters are currently employed in spectral splitting PV/T (SSPV/T) collectors: selectively reflective film filters and selectively absorptive fluid filters. Film filters direct part of the solar spectrum to the photovoltaic cells, while the rest is reflected on a thermal absorber. These collectors usually require optical concentrators and sunlight tracers. Fluid-based filters, on the other hand, act both as optical filters and as thermal absorbers and heat transfer fluids, usually making fluid-based SSPV/T collectors more compact than

SSPV/T film collectors. An alternative strategy by employing a set of new fluid developed for spectral beam splitting PV/T collectors is offered in (Walshe *et al.*, 2021). The potential of concentrating spectral-splitting PV/T systems is assessed in terms of energetic, economic and environmental metrics in (K. Wang *et al.*, 2020). In (Huang, Wang and Markides, 2021) a method for identifying the efficiency limits of ideal SSPV/T collectors is provided along with guidance for selecting optimal PV materials and spectral-splitting filters under different conditions and in different applications.

A nanofluid (NF) is a special type of fluid characterised by a suspension of nanoparticles in a base fluid. Nanofluids are prepared with a two-step method: the nanoparticles are first prepared in a powder and then suspended in a base fluid, which is usually water (Al-Shamani *et al.*, 2018). These innovative heat transfer fluids have been designed also for PV/T collectors in order to be an alternative solution to standard fluids such as water which have not very high thermal conductivity. The addition of nanoparticles with various properties to pure fluids can improve PV/T performances, thanks their greater thermal conductivity. Mathematical and experimental evaluations were conducted in (Al-Shamani *et al.*, 2018) to evaluate the performance enhancement of the PV/T system under different water based nanofluids (CuO, SiO_2, and ZnO). The theoretical results obtained were validated through experimental tests conducted outdoors in tropical climatic conditions. Significant enhancements in the different performance parameters of the PV/T-NF system were achieved when compared with the PV/T-water system. In particular, electrical, thermal and overall PV/T- NF (SiO_2) efficiencies were enhanced by 12.70%, 64.40% and 77.10%, respectively.

In (Akbar *et al.*, 2021) different cooling fluids, including Ag-H2O, SiO_2-H_2O, water, and air, were used as cooling fluids and the effect of using these fluids on the performance and output power of the analysed system was evaluated. Hissouf et al. (Hissouf *et al.*, 2020) and (Fayaz *et al.*, 2018) developed numerical models to investigate thermal and electrical performances of PV/T systems using nanofluids as working fluids. The thermal, electrical and overall efficiency of the PV/T collectors with the effect of nanofluids have been investigated with varying mass flow rate and considering different climatic conditions. In particular, enhancement achieved for the nanofluids were compared to obtained results of performances relative to pure water.

PCM are among the different strategies developed to improve electrical efficiency of PV/T collectors. Due to their ability to absorbs, store and release huge amount of thermal energy during physical phase transition, PCMs allow to reduce the degradation rate of photovoltaic cells, achieving a lower and stable operating temperature. The phase change materials increase thermal inertia of solar systems, increasing the capacity for capturing thermal energy during transitory periods of reduction or absence of incident solar radiation. In literature PCMs are often grouped into three types of organic, inorganic and eutectic. The most widely used categories are organic paraffin compounds. Kalidasan et al. in their research (Kalidasan *et al.*, 2020) reported the various classifications of PCM and their role in thermal energy storage for performance improvement of solar thermal systems. The numerous PV/T-PCM systems analysed were instead classified, based on temperature of solar systems, in low temperature application system, medium temperature application system and high temperature

application system. In (Carmona and Palacio, 2021) an innovative design is proposed combining the advantages of flat plate PV/T collector and direct contact coil systems with those of flexible PCM containers with finned plates. Design considerations and the results of an experimental evaluation of the energy performance of a PV/T-PCM solar system were compared with a traditional photovoltaic system. The novelty of the simultaneous use of water/EG mixture as a coolant and PCM as coolant media in the glazed and unglazed PV/Ts is analysed in (Kazemian *et al.*, 2020). Furthermore, a thermodynamic analysis is conducted to study the performance of three different systems, i.e. PV unit, glazed and unglazed PV/T/PCM systems, from both energy and exergy viewpoints.

1.3. Analysis and comparison of the main products on the market

According to results published in the 2020th edition of Solar Heat Worldwide (Weiss and Spörk-Dür, 2020), which gives an overall overview of the global solar thermal market development in 2019, it was recorded that by the end of 2018 more than 1 million m^2 of PV/T collectors were installed in over 25 countries. Currently, how it is possible to observe in the below-reported diagram, which is based on reported data about the total capacity in operation, the largest PV/T markets are France, South Korea, China and Germany.

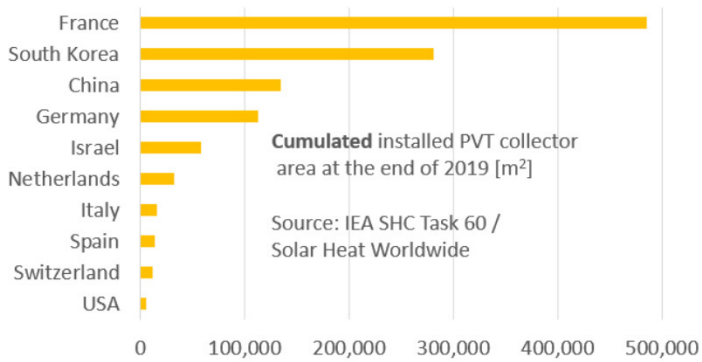

Figure 1.3. Comulated installed PV/T collectror area at the end of 2019 (Solarthermalworld website, 2021)

By the end of 2019, a total installed PV/T collectors' area of 1,166,888 m^2 was recorded with a thermal power of 606 MWth. In 2019, the market grew by about 170 % in Denmark but also expanded in other countries, such as China and Germany, mainly because the technology became more cost competitive. In all, 58 % of global installations at the end of 2019 was located in Europe, the main producers were France, which holds the record with an installed collector area of 484,587 m^2, Germany and Netherlands, followed by Italy, Spain and Switzerland.
In Task 60 of the Solar Heating and Cooling (SHC) program of the International Energy Agency (IEA) the residential sector was identified as the main driver of the recent

development of PV/T market in France, the largest contributor to the total PV/T capacity.
As also reported in (*solarthermalworld website*, 2021) from data collected in (Baggenstos *et al.*, 2020) more than half the installed PV/T capacity is represented by non-covered, water-filled collectors (55 %), followed by air collectors (43 %), while covered, water-driven systems played only a minor role.
Below are reported the technical data of some of the main commercial PV/T models used, also considering the case studies described in (Baggenstos *et al.*, 2020), which provides an overview of the global market and a sample of case studies regarding PV/T systems installed with the most relevant applications and based on various types of PV/T collectors.

1.3.1 POWERTHERM and POWERVOLT

Two type of PV/T modules are produced by Turkish Solimpeks company, one of European biggest solar thermal manufacturers, POWERTHERM and POWERVOLT. The two modules are both glazed but differ, as the name suggests, in their preferred energy yield, thermal or electrical respectively. In table 1.1 and 1.2 data of POWERTHERM and POWERVOLT are reported respectively (*Solarchoice website*, 2021).

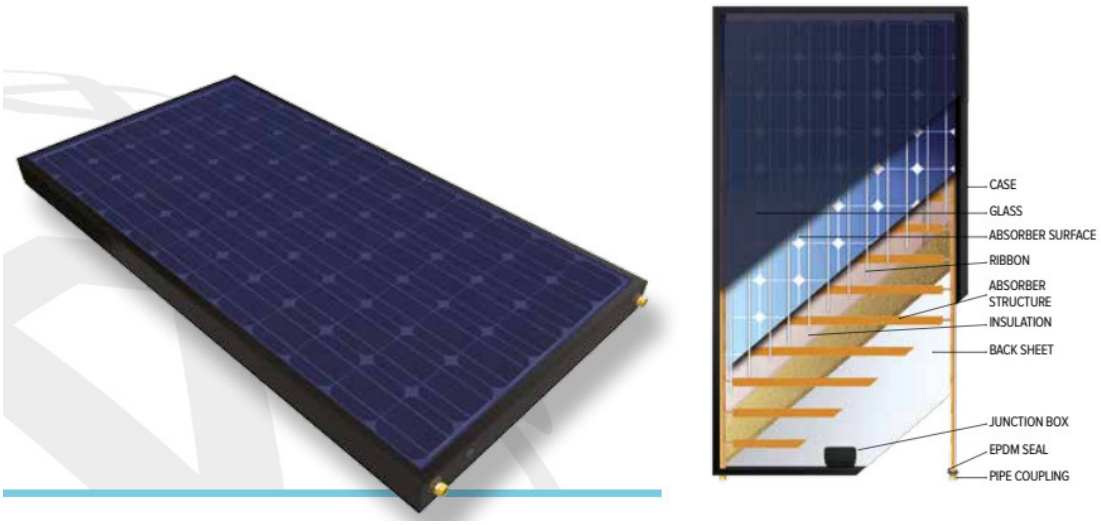

Figure 1.4. PV/T panel by Solimpeks

Table 1.1. Technical data of a glazed POWERTHERM PV/T panel

Physical characteristics		Photovoltaic characteristics		Thermal characteristics	
Length	1640 mm	**Nominal Power**	180 W	**Thermal power**	680 W_{th}/m^2
Width	828 mm	**PV efficiency**	12,9%	**Gross area**	1,474 m^2
Thickness	90 mm	**Rated Voltage**	35,15 V	**Liquid volume**	1,21 L
Weight	34,4 kg	**Rated Current**	5,12 A	**Max operating p**	6 bar
N° of cells	72	**Open circuit V**	43,39 V	**Test Pressure**	13 bar
Cell type	Monoc.	**Short-circuit I**	5,55 A	**Maximum T**	134 °C
Cell dimens.	125x125 mm	**V temp. coeff.**	-0,34 %/K	**Optical efficiency**	48,6%
Connectors	JMTHY/PV-JM601	**I temp. coeff.**	0,06 %/K	**Coefficient a1**	4,028 W/Km^2
Max load	Pa	**P temp. coeff**	-0,45 %/K	**Coefficient a2**	0,067 $W/(m^2K^2)$
Cover glass	Extra low Iron Temperated Glass	**Power Tolerance**	±3%	**Recomm. Flow rate**	65 L/hr

The Powertherm product couples a photovoltaic module with monocrystalline silicon cells to an aluminum sheet and tube plate. The disadvantage of this product is the high temperature coefficient of the photovoltaic cells, which, due to the presence of the cover glass, can reach high temperatures, compromising their electrical performance.
The PV/T module consisting of 72 mono-crystalline silicon (c-Si) cells of 125x125 mm presents a peak electrical power of 180Wp and an electrical efficiency of 12,9%. The thermal power of the PV/T panel is of about 1000 W with an optical efficiency of 48,6%. As for the thermal absorber, it is made of copper with a "sheet and tube" structure in contact with the aluminum rear side of the PV layer.

Table 1.2. Technical data of a glazed POWERVOLT PV/T panel

Physical characteristics		Photovoltaic characteristics		Thermal characteristics	
Length	1601 mm	**Nominal Power**	200 W	**Thermal power**	630 W_{th}/m^2
Width	828 mm	**PV efficiency**	15,08%	**Gross area**	1,370 m^2
Thickness	90 mm	**Rated Voltage**	37,89 V	**Liquid volume**	1,21 L
Weight	24,4 kg	**Rated Current**	5,28 A	**Max operating p**	6 bar
N° of cells	72	**Open circuit V**	45,26 V	**Test Pressure**	13 bar

Cell type	Monoc.	**Short-circuit I**	5,66 A	**Maximum T**	101 °C
Cell dimens.	125x125 mm	**V temp. coeff.**	-0,34 %/K	**Optical efficiency**	47,5%
Connectors	JMTHY/PV-JM601	**I temp. coeff.**	0,06 %/K	**Coefficient a1**	8,37 W/Km^2
Max load	Pa	**P temp. coeff**	-0,45 %/K	**Coefficient a2**	0,586 W/(m^{2}K^2)
Cover glass	PV Glass	**Power Tolerance**	±3%	**Recomm. Flow rate**	65 L/hr

The technical features of POWERVOLT PV/T panel are very similar to those of POWERTHERM module. The main differences are in an increased electrical power and electrical efficiency (15, 08% against 12,9% of POWERTHERM's one) on one side and in a decreased thermal output with a thermal power of 630 W_{th}/m^2 against 680 watts produced by POWERTHERM on the other.

1.3.2 Abora Solar

Another high-efficiency hybrid module is Abora Solar PV/T panel which is based on the "aHTech" technology. This innovation consists of a series of insulating layers whose design and arrangement manage to minimize the thermal losses of the panel and maximize electrical production thanks to the cooling obtained from the photovoltaic cells. Spanish Abora Solar PV/T panels are produced in the two version of 60 photovoltaic cells module (aH60 SK) and 72 photovoltaic cells module (aH72 SK).

Figure 1.5. PV/T panel by Abora Solar

Table 1.3. Technical data of Abora Solar PV/T panel

Physical characteristics		Photovoltaic characteristics		Thermal characteristics	
Length	1650 mm	**Nominal Power**	290 W	**Thermal power**	W_{th}/m^2
Width	995 mm	**PV efficiency**	17,66%	**Gross area**	1,65 m^2
Thickness	85 mm	**Rated Voltage**	32,43 V	**Liquid volume**	1,2 L
Weight	43,0 kg	**Rated Current**	8,62 A	**Max operating p**	10 bar
N° of cells	60	**Open circuit V**	39,49 V	**Stagnation T**	129,9 °C
Cell type	Monoc.	**Short-circuit I**	9,03 A	**Optical efficiency**	67,0%
Cell dimens.	156x156 mm	**V temp. coeff.**	-0,30 %/K	**Coefficient a1**	5,7 W/Km^2
Connectors	Solarlok PV4 / 1m	**I temp. coeff.**	0,09 %/K	**Coefficient a2**	0,004 $W/(m^2K^2)$
Cover thickness	3.2 mm	**P temp. coeff**	-0,38 %/K	**Nominal Flow rate**	50 L/hr
Cover glass	Temperated Glass	**Power Tolerance**	±3%		

1.3.3. ECOMESH

The second generation ECOMESH hybrid solar panels incorporate a front cover system of innovative technology (CTA technology) that maximizes their thermal output. The use of the CTA (Transparent Insulating Cover) incorporates a layer on the front of the panel that captures the sun's rays, reducing losses due to reflection and making them ideal for cold climates. With it, it is possible to significantly improve the thermal performance of the panel, maximizing its production of hot water and making it one of the most competitive on the market. Although the ECOMESH PV/T-2 hybrid solar panel has a smaller surface of just over 1.6 m^2, it shows a very high optical performance than its competitors (67%) (*Endef website*, 2021).

Figure 1.6. ECOMESH hybrid solar panel by Endef.

Table 1.4. Technical data of ECOMESH PV/T panel

Physical characteristics		Photovoltaic characteristics		Thermal characteristics	
Length	1645 mm	**Nominal Power**	260 W	**Thermal power**	680 W_{th}/m^2
Width	978 mm	**PV efficiency**	15,98%	**Gross area**	1,55 m^2
Thickness	93 mm	**Rated Voltage**	31,65 V	**Liquid volume**	1,2 L
Weight	45,8 kg	**Rated Current**	8,06 A	**Max operating p**	10 bar
N° of cells	60	**Open circuit V**	38,58 V	**Pressure drop**	0,04 bar
Cell type	Monoc.	**Short-circuit I**	9,06 A	**Coefficient a1**	4,93 W/Km^2
Cell dimens.	156x156 mm	**V temp. coeff.**	-0,37 %/K	**Coefficient a2**	0,021 $W/(m^2K^2)$
Connectors	IP65/IP67	**I temp. coeff.**	0,06 %/K		
		P temp. coeff	-0,47 %/K		
		Power Tolerance	+4,99 Wp		

1.3.4. Dualsun

As regards the French market a promising module is that made by Dualsun (Brottier, Hugo and Bennacer, 2014). The innovative 1.6 m² PV/T collector with 60 monocrystalline cells and a nominal power of 300 W, is produced by direct lamination. The 3.1mm thick exchanger is made of a specific stainless-steel type to reduce

differential dilatation constraints. The module succeeded in all IEC 61215 tests without any delamination. During thermal and electrical measurements that were carried out in the indoor testing the stagnation temperature of the DualSun PV/T module has been measured at 74.7°C where a standard thermal module stagnates at 137.5°C, and a pure photovoltaic module stagnates at 71.2°C. This means that with this module, even during summer vacation, if inhabitants do not consume any hot water, electrical production will not be affected due to the hybridation aspect (Brottier, Hugo and Bennacer, 2014).

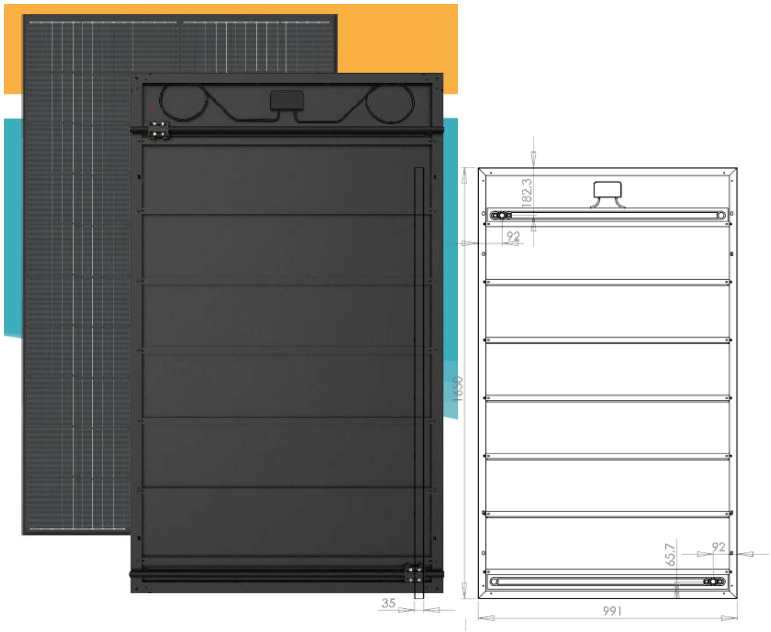

Figure 1.7. SPRING panel by DualSun

Table 1.5. Technical data of a non-insulated DualSun PV/T panel

Physical characteristics		Photovoltaic characteristics		Thermal characteristics	
Length	1650 mm	**Nominal Power**	300 W	**Thermal power**	629 W_{th}/m^2
Width	991 mm	**PV efficiency**	18,3%	**Gross area**	1,635 m^2
Thickness	35 mm	**Rated Voltage**	32,6 V	**Liquid volume**	5 L
Weight	24 kg	**Rated Current**	9,19 A	**Max operating p**	1,5 bar
N° of cells	60	**Open circuit V**	39,9 V	**Pressure drop**	
Cell type	PERC Monoc.	**Short-circuit I**	9,77 A	**Stagnation T**	70°C
Connectors	MC4	**V temp. coeff.**	-0,29 %/K	**Optical efficiency**	58,9%
Cable length	1000 mm	**I temp. coeff.**	0,05 %/K	**Coefficient a1**	16,0 W/Km^2

Max load	5400 Pa	**P temp. coeff**	-0,39 %/K	**Coefficient a2**	0 W/(m^{2}K^2)
Frame	Black	**Max system V**	1000 VDC		
		Max revers I	20 A		
		NMOT	45+/- 2°C		

1.3.5. Solarus

The C-PV/T collector by Swedish Solarus (Saizar and Vila, 2016) is based on an asymmetric Compound Parabolic Collector. The panel consists of a two-sided PV module, a thermal absorber and a compound reflector. The upper PV side of the receiver works like a standard module, while the lower side has concentration thanks to a reflector with a particular geometry called "MaReCo".

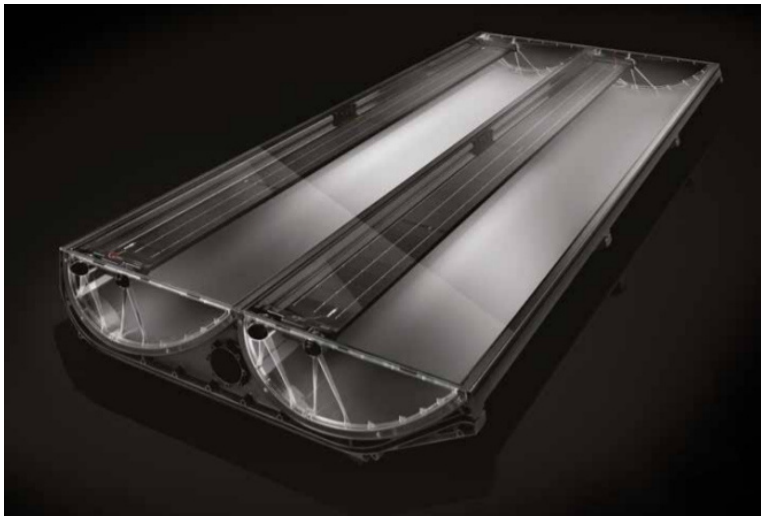

Figure 1.8. Solarus C-PV/T power collector

Table 1.6. Technical data of a Solarus C-PV/T panel

Physical characteristics		**Photovoltaic characteristics**		**Thermal characteristics**	
Length	1054 mm	**Nominal Power**	270 W	**Thermal power**	1350 W
Width	2243 mm	**PV efficiency**	%	**Gross area**	2,57 m^2
Thickness	241 mm	**Rated Voltage**	40 V	**Liquid volume**	1,4 L/module
Weight		**Rated Current**	2,80/3,93 A	**Max operating p**	10 bar

N° of cells	152	**Open circuit V**	48,1 V	**Pressure drop**	
Cell type		**Short-circuit I**	3,12/ 4,48A	**Operating T**	180°C
Connectors		**V temp. coeff.**	%/K	**Optical efficiency**	
Cable length		**I temp. coeff.**	%/K	**Coefficient a1**	
Max load		**P temp. coeff**	%/K	**Coefficient a2**	

1.3.6. Fototherm

Among the available products there is also the PV/T hybrid solar panel by Fototherm. The products offered by the Italian Company from 2006 are classified into two series: CS series and AS series (ex-AL series) based on the different type of photovoltaic cell used and the rated power range. PV/T collector of the FT300AL series was chosen for the PV/T systems analysed in (Martorana *et al.*, 2021). It is an unglazed PV/T panel with a sheet-and-tube thermal absorber using water as heat transfer fluid. It falls into the category of hybrid collectors obtained from photovoltaic modules equipped with a heat exchanger for the exploitation of thermal energy.

Figure 1.9. FT300AL(AS) panel by Fototherm

Table 1.7. Technical data of a Fototherm PV/T panel

Physical characteristics		Photovoltaic characteristics		Thermal characteristics	
Length	1660 mm	**Nominal Power**	300 W	**Thermal power**	921 W
Width	990 mm	**PV efficiency**	18,3%	**Gross area**	1,58 m^2
Thickness	51 mm	**Rated Voltage**	31,2 V	**Liquid volume**	0,96 L
Weight	32 kg	**Rated Current**	9,63 A	**Max operating p**	1,5 bar
N° of cells	60	**Open circuit V**	39,4 V	**Pressure drop**	
Cell type	Monoc. Si	**Short-circuit I**	9,97 A	**Stagnation T**	°C
Connectors	MC4	**V temp. coeff.**	-0,29 %/K	**Optical efficiency**	58,3%
Cable length	1000 mm	**I temp. coeff.**	0,05 %/K	**Coefficient a1**	6,08 W/Km^2
Max load	5400 Pa	**P temp. coeff**	-0,40 %/K	**Coefficient a2**	0 W/(m^2K^2)
Frame	Black	**Max system V**	1000 VDC		
		Max revers I	20 A		

The panel has a rated power of 300 W_p with 60 monocrystalline silicon PV cells, is connected at the rear with a copper-made absorber with polyurethane foam insulation. The entire panel is closed with a pre-painted aluminium sheet (Leonforte, 2014). Its nominal thermal power is 921 W.
The performance of the Fototherm module was experimentally analyzed in the study conducted in (Rizzini, 2015), where a connection of four Fototherm AL series thermal-photovoltaic panels with a "roll bond" heat exchanger is taken as a reference.

1.3.7 Tecom

The Italian “Tecom Energie” produces a hybrid PV/T panel characterized by a thermal power of 900 W thanks to the high efficiency of the aluminum roll bond heat exchanger, with an instantaneous absorber efficiency of 53%. The panel is available in the two versions of 280 and 300 W of electrical power. It is suitable for producing domestic hot water, for the integration of low temperature radiant heating in buildings or for heating swimming pools.

Figure 1.10. PV/T panel by Tecom

Table 1.8. Technical data of Tecom PV/T panel

Physical characteristics		Photovoltaic characteristics		Thermal characteristics	
Length	1649 mm	**Nominal Power**	300 W	**Thermal power**	900 W_{th}/m^2
Width	991 mm	**PV efficiency**	18,4%	**Gross area**	1,63 m^2
Thickness	40 mm	**Rated Voltage**	31,6 V	**Liquid volume**	0,65 L
Weight	28,0 kg	**Rated Current**	9,5 A	**Pressure drop**	100 mbar
N° of cells	60	**Open circuit V**	40,4 V	**Min unit capacity**	4 bar
Cell type	Monoc.	**Short-circuit I**	9,9 A	**Maximum T**	85 °C
Cell dimens.	156x156 mm	**V temp. coeff.**	-0,30 %/K	**Optical efficiency**	53,0%
Cover thickness	3,2 mm	**I temp. coeff.**	0,046 %/K	**Coefficient a1**	9,5 W/Km^2
Cover glass	Temperated Glass	**P temp. coeff**	-0,39 %/K	**Coefficient a2**	0,012 $W/(m^2K^2)$
		Max Allowable Voltage	1000 V	**Recomm. Flow rate**	100 L/hr

References

Akbar, A. *et al.* (2021) 'Performance enhancement of a hybrid photovoltaic-thermal-thermoelectric (PVT-TE) module using nanofluid-based cooling : Indoor experimental tests and multi-objective optimization', *Sustainable Energy Technologies and Assessments*, 46(December 2020), p. 101276. doi: 10.1016/j.seta.2021.101276.

Al-Shamani, A. N. *et al.* (2018) 'Mathematical and experimental evaluation of thermal and electrical efficiency of PV/T collector using different water based nano-fluids', *Energy*, 145, pp. 770–792. doi: https://doi.org/10.1016/j.energy.2017.11.156.

Alqaed, S., Mustafa, J. and Almehmadi, F. A. (2021) 'Design and energy requirements of a photovoltaic-thermal powered water desalination plant for the middle east', *International Journal of Environmental Research and Public Health*, 18(3), pp. 1–16. doi: 10.3390/ijerph18031001.

Aste, N., Del Pero, C. and Leonforte, F. (2017) 'Water PVT Collectors Performance Comparison', *Energy Procedia*, 105, pp. 961–966. doi: 10.1016/j.egypro.2017.03.426.

Baggenstos, A. *et al.* (2020) *Existing PVT systems and solutions Existing PVT systems and solutions*. doi: 10.18777/ieashc-task60-2020-0001.

Brahim, T. and Jemni, A. (2021) 'Parametric study of photovoltaic/thermal wickless heat pipe solar collector', *Energy Conversion and Management*, 239, p. 114236. doi: https://doi.org/10.1016/j.enconman.2021.114236.

Brottier, L., Hugo, J. and Bennacer, R. (2014) 'An innovative PV-T collector : CFD and experimental results', (September), pp. 3–8.

Carmona, M. and Palacio, A. (2021) 'Experimental evaluation of a hybrid photovoltaic and thermal solar energy collector with integrated phase change material (PVT-PCM) in comparison with a traditional photovoltaic (PV) module', 172. doi: 10.1016/j.renene.2021.03.022.

Chow, T. T. (2003) 'Performance analysis of photovoltaic-thermal collector by explicit dynamic model', *Solar Energy*, 75(2), pp. 143–152. doi: 10.1016/j.solener.2003.07.001.

Chow, T. T. (2010) 'A review on photovoltaic/thermal hybrid solar technology', *Applied Energy*, 87(2), pp. 365–379. doi: 10.1016/j.apenergy.2009.06.037.

Cox, C. H. and Raghuraman, P. (1985) 'Design considerations for flat-plate-photovoltaic/thermal collectors', *Solar Energy*, 35(3), pp. 227–241. doi: 10.1016/0038-092X(85)90102-1.

Endef website (2021). Available at: https://endef.com/en/hybrid-solar-panel/ecomesh.

Farooq, A. S. *et al.* (2020) 'Dynamic simulation and parametric analysis of solar assisted desiccant cooling system with three configuration schemes', *Solar Energy*, 197, pp. 22–37. doi: https://doi.org/10.1016/j.solener.2019.12.076.

Fayaz, H. *et al.* (2018) 'Energy and exergy analysis of the PVT system : E ff ect of nano fl uid fl ow rate', 169(April), pp. 217–230. doi: 10.1016/j.solener.2018.05.004.

Garg, H. P. and Adhikari, R. S. (1999) 'Performance analysis of a hybrid photovoltaic/thermal (PV/T) collector with integrated CPC troughs', *International Journal of Energy Research*, 23(15), pp. 1295–1304. doi: 10.1002/(SICI)1099-114X(199912)23:15<1295::AID-ER553>3.0.CO;2-T.

Guo, J., Bilbao, J. I. and Sproul, A. B. (2020) 'A novel solar cooling cycle – A ground coupled PV/T desiccant cooling (GPVTDC) system with low heat source temperatures', *Renewable Energy*, 162, pp. 1273–1284. doi: https://doi.org/10.1016/j.renene.2020.08.050.

Hemmat Esfe, M., Kamyab, M. H. and Valadkhani, M. (2020) 'Application of nanofluids and fluids in photovoltaic thermal system: An updated review', *Solar Energy*, 199(December 2019), pp. 796–818. doi: 10.1016/j.solener.2020.01.015.

Herrando, M. and Markides, C. N. (2016) 'Hybrid PV and solar-thermal systems for domestic heat and power provision in the UK: Techno-economic considerations', *Applied Energy*, 161, pp. 512–532. doi: https://doi.org/10.1016/j.apenergy.2015.09.025.

Herrando, M., Markides, C. N. and Hellgardt, K. (2014) 'A UK-based assessment of hybrid PV and solar-thermal systems for domestic heating and power: System performance', *Applied Energy*, 122, pp. 288–309. doi: https://doi.org/10.1016/j.apenergy.2014.01.061.

Hissouf, M. *et al.* (2020) 'Numerical study of a covered Photovoltaic-Thermal Collector (PVT) enhancement using nano fl uids', *Solar Energy*, 199(August 2019), pp. 115–127. doi: 10.1016/j.solener.2020.01.083.

https://www.solarthermalworld.org/news/pv-thermal-major-markets-and-most-sought-after-technologies (2021).

Huang, G. *et al.* (2021) 'On the performance of concentrating fluid-based spectral-splitting hybrid PV-thermal (PV-T) solar collectors', *Renewable Energy*, 174, pp. 590–605. doi: 10.1016/j.renene.2021.04.070.

Huang, G., Wang, K. and Markides, C. N. (2021) 'Efficiency limits of concentrating spectral-splitting hybrid photovoltaic-thermal (PV-T) solar collectors and systems', *Light: Science & Applications*, 10(1), p. 28. doi: 10.1038/s41377-021-00465-1.

Kalidasan, B. *et al.* (2020) 'Phase change materials integrated solar thermal energy systems: Global trends and current practices in experimental approaches', *Journal of Energy Storage*, 27, p. 101118. doi: https://doi.org/10.1016/j.est.2019.101118.

Kalogirou, A. S. (2014) *Solar Energy Engineering Processes and Systems*. Second.

Karathanassis, I. K. *et al.* (2019) 'Dynamic simulation and exergetic optimization of a Concentrating Photovoltaic/ Thermal (CPVT) system', *Renewable Energy*, 135, pp. 1035–1047. doi: 10.1016/j.renene.2018.12.085.

Kazemian, A. *et al.* (2018) 'Effect of glass cover and working fluid on the performance of photovoltaic thermal (PVT) system: An experimental study', *Solar Energy*, 173(July), pp. 1002–1010. doi: 10.1016/j.solener.2018.07.051.

Kazemian, A. *et al.* (2020) 'Energy, exergy and environmental analysis of glazed and

unglazed PVT system integrated with phase change material: An experimental approach', *Solar Energy*, 201(May 2019), pp. 178–189. doi: 10.1016/j.solener.2020.02.096.

Kılkış, B. (2020) 'Development of a composite PVT panel with PCM embodiment, TEG modules, flat-plate solar collector, and thermally pulsing heat pipes', *Solar Energy*, 200, pp. 89–107. doi: https://doi.org/10.1016/j.solener.2019.10.075.

Lebbi, M. *et al.* (2021) 'Energy performance improvement of a new hybrid PV/T Bi-fluid system using active cooling and self-cleaning: Experimental study', *Applied Thermal Engineering*, 182, p. 116033. doi: https://doi.org/10.1016/j.applthermaleng.2020.116033.

Leonforte, F. (Politecnico di M. (2014) *Messa a punto e analisi prestazionale di un collettore ibrido fotovoltaico termico a fluido termovettore acqua.* Politecnico di Milano.

Manssouri, O. El *et al.* (2021) 'Electrical and Thermal Performances of Bi-Fluid PV / Thermal Collectors'.

Martorana, F. *et al.* (2021) 'Solar-assisted heat pumps systems for domestic hot water production in small energy communities', *Solar Energy*, 217(November 2020), pp. 113–133. doi: 10.1016/j.solener.2021.01.020.

Mellor, A. *et al.* (2018) 'Roadmap for the next-generation of hybrid photovoltaic-thermal solar energy collectors', *Solar Energy*, 174(September), pp. 386–398. doi: 10.1016/j.solener.2018.09.004.

Raghuraman, P. and Hendrie, S. D. (1980) 'Analytical Predictions of Liquid and Air Photovoltaic/Thermal Flat-Plate Collector Performance'.

Rejeb, O. *et al.* (2020) 'Novel solar PV/Thermal collector design for the enhancement of thermal and electrical performances', *Renewable Energy*, 146, pp. 610–627. doi: 10.1016/j.renene.2019.06.158.

Rizzini, M. (2015) 'Analisi sperimentale di pannelli fotovoltaici termici innovativi presso il SolarTech Lab', p. 101.

Saizar, X. and Vila, G. (2016) 'Analysis of the Solarus C-PVT solar collector and design of a new prototype Market review and'. Available at: http://hig.diva-portal.org/smash/record.jsf?pid=diva2%3A938925&dswid=-3747.

Sheikholeslami, M. *et al.* (2021) 'Recent progress on flat plate solar collectors and photovoltaic systems in the presence of nanofluid: A review', *Journal of Cleaner Production*, 293, p. 126119. doi: 10.1016/j.jclepro.2021.126119.

Solarchoice website (2021). Available at: https://www.solarchoice.net.au/wp-content/uploads/Solimpeks-Data-Sheet-PowerVolt-PowerTherm.pdf.

Tiwari, A. and Sodha, M. S. (2006) 'Performance evaluation of solar PV/T system: An experimental validation', *Solar Energy*, 80(7), pp. 751–759. doi: 10.1016/j.solener.2005.07.006.

Tripanagnostopoulos, Y. *et al.* (2002) 'Hybrid photovoltaic/thermal solar systems',

Solar Energy, 72(3), pp. 217–234. doi: 10.1016/S0038-092X(01)00096-2.

Walshe, J. *et al.* (2021) 'Organic luminescent down-shifting liquid beam splitters for hybrid photovoltaic-thermal (PVT) applications', *Solar Energy Materials and Solar Cells*, 219, p. 110818. doi: https://doi.org/10.1016/j.solmat.2020.110818.

Wang, K. *et al.* (2020) 'Spectral-splitting hybrid PV-thermal (PVT) systems for combined heat and power provision to dairy farms', *Renewable Energy*, 159, pp. 1047–1065. doi: https://doi.org/10.1016/j.renene.2020.05.120.

Wang, Y. *et al.* (2020) 'Optimization of the areas of solar collectors and photovoltaic panels in liquid desiccant air-conditioning systems using solar energy in isolated low-latitude islands', *Energy*, 198, p. 117324. doi: https://doi.org/10.1016/j.energy.2020.117324.

Weiss, W. and Spörk-Dür, M. (no date) *Solar Heat Worldwide - 2020 Edition*. 8200 Gleisdorf, Austria.

Wolf, M. (1976) 'Performance analyses of combined heating and photovoltaic power systems for residences', *Energy Conversion*, 16(1–2), pp. 79–90. doi: 10.1016/0013-7480(76)90018-8.

Zhou, J. *et al.* (2021) 'A Review on the Heat Pipe Photovoltaic/Thermal (PV/T) System', *Journal of Thermal Science*. doi: 10.1007/s11630-021-1434-3.

Zondag, H. A. *et al.* (2000) 'Thermal and Electrical Yield of a Combi-Panel', *1999 ISES Solar World Congress*, 3(1999), pp. 96–101. doi: 10.1016/b978-008043895-5/50188-0.

Zondag, H. A. *et al.* (2003) 'The yield of different combined PV-thermal collector designs', *Solar Energy*, 74(3), pp. 253–269. doi: 10.1016/S0038-092X(03)00121-X.

Zondag, H. A. *et al.* (2005) 'A roadmap for the development and market introduction of PVT technology', *15 Symposium Thermische Solarenergie, Bad Staffelstein, Germany, 27-29 April 2005*, (April), pp. 1–5.

Zondag, H. A. (2008) 'Flat-plate PV-Thermal collectors and systems: A review', *Renewable and Sustainable Energy Reviews*, 12(4), pp. 891–959. doi: 10.1016/j.rser.2005.12.012.

2. Modeling and testing of PV/T collectors

For the planning and design of PV/T installations, it is of great importance to be able to predict and reproduce their performance accurately both in terms of electrical and thermal power output. The development of validated and standardized PV/T collector models is an important task to allow for the effective comparison of products based on energetic and economic performance indicators. Furthermore, it is necessary to have a performance model based on standardized parameters. Prerequisite for predictions, as also highlighted in (Helmers and Kramer, 2013), is a performance model that on the one hand covers the relevant physical processes with a high degree of accuracy and on the other hand is based only on accessible input data, i.e. standard measurement data.

The study of modeling PV/T systems started in the middle of the 1970s when Martin Wolf investigated the performance of a PV/T prototype for residential heating (Wolf, 1976). Results showed the technical feasibility and cost-effectiveness of the combined photovoltaic-thermal system.

This pioneering study was further developed by Florschuetz (Florschuetz, 1979), who built a mathematical model modifying the well-known Hottel and Whillier thermal model. Over the years, several models have been suggested in order to develop an explicit PV/T model capable to assess the suitability of various design parameters in any ambient conditions, which can consequently lead to improving the performance of the panel. Models of various configurations of PV/T collectors and for different climatic conditions have been found in the literature. The latter are mainly aimed at analysing the influence on their performance of multiple parameters such as optical, geometrical and, thermo-physical properties, type of fluid, wind speed and direction, solar radiation, and ambient temperature. Most of these models have the same theoretical background, consisting of the classical numerical model developed by Florschuetz (1979), based on the Hottel–Whillier–Bliss equations with various improvements. In particular, the methodology of calculating the temperatures in the PV/T layers is based on the assessment of the energy exchange between the layers and with the environment (Barbu, Siroux and Darie, 2021).

The use of a physical collector model is very often made difficult by the unavailability of collector data, which is required for the consistent comparison of different types of collectors, how also stated in (Lammle, 2018). Therefore, the simulation of annual yields of PV/T systems requires a PV/T collector performance model, which is based on standard performance parameters but at the same time considers the interdependence of simultaneous electrical and thermal operation.

In this chapter, an analysis of the main mathematical models present in the literature on the modeling of PV/T systems is reported. Since the implementation, validation, and parameter identification procedure of the PV/T performance model were performed using the TRNSYS simulation tool (reported in more detail in Chapter 4), particular

attention was paid to the models underlying the main types of TRNSYS that describe the behavior of hybrid solar collectors.
The second part of this chapter gives a specific focus on the main procedures used to test the thermal performance of the PV/T collectors and carry out their characterization, with particular reference to the relevant technical standards. Currently, the thermal performance of solar thermal and PV/T collectors is tested according to the international standard ISO 9806 and the electrical performance of PV modules according to different IEC standards. As also highlighted in IEA SHC Task 60 (Kramer, 2020), only by establishing functioning standards it is possible to achieve reliability of product quality, which is a key factor for sustainable PV/T market development.

2.1. Mathematical PV/T models

Being a hybrid technology, the PV/T collectors are modeled considering models already developed separately for solar thermal and photovoltaic technologies and then making the appropriate corrections.
Based on the heat transfer analysis of a solar collector, empirically validated mathematical models are available giving a good description of the collector performances as a function of environmental and operating conditions.
In the current state of the art, and also according to (*UNI EN 12975-2*, 2006) and (*UNI EN ISO 9806*, 2017), two approaches are followed, which through an easily accessible adaptation of the measurement data, provide a series of parameters that fully describe the performance of the collector.
The first method, also known as the "steady-state" method, is based on a quadratic model. Here, steady-state measurements under stable environmental conditions are used to obtain the parameters of the thermal efficiency curve. In addition to this, a more complete evaluation method is given by the quasi-dynamic characterization, such as in (Perers, 1997) which considers the different environmental conditions due to the introduction of additional parameters. Due to multi-linear regression, therefore, the relevant collector parameters are determined. Finally, after the determination of the collector parameters, both approaches can be used to conduct gross collector energy output calculations based on hour-by-hour climate data using appropriate software.
The main PV/T models found in the literature are reported below. Among the many available, particular attention has been paid to the ones developed by Hottel and Whillier and Duffie and Beckman for the thermal performance, and Florscheutz. The model developed by the latter is the basis of the TRNSYS types of PV/T collectors (Specialists, 2017).

2.1.1. Hottel and Whillier

As concerns the solar thermal collectors, the model derived by Hottel-Whillier-Bliss is the most used/spread and represents a guide for the design, development, and testing of

flat-plate solar collectors. It is a simplified theoretical description that evaluates the efficiency of solar thermal panels as a function of various environmental and operational conditions (Pressiani, 2016).
A method was proposed for experimentally determining the three factors that define collector efficiency in the Hottel-Whillier equation:

$$Q_u = F_R A_c \left[(\tau\alpha)_e I - U_L \left(T_{f,i} - T_a \right) \right] \quad (2.1)$$

The factors involved in equation (2.1) represent in order: the collector heat removal factor (F_R), the useful surface of the collector (A_c), the effective transmittance-absorptance product $(\tau\alpha)_e$, and the overall heat loss coefficient (U_L). Finally, $T_{f,i}$ and T_a are the fluid temperature at the collector inlet and the air temperature respectively.
The equation (1) equals the useful heat collected by the solar collector per unit area to the difference between solar energy absorbed by the absorber, $(\tau\alpha)_e I$, and the heat loss, $U_L(T_{f,i} - T_a)$, multiplied by a factor that takes into account the effectiveness of transferring the heat absorbed by the absorber to the heat removal fluid, F_R.
The effective transmittance-absorptance product, $(\tau\alpha)_e$ represents the complex interaction of optical properties in the solar radiation wavelengths. It is influenced by factors like cover transmittance, number of covers, and absorptance of the absorber plate.
The heat removal factor, F_R, is influenced by the heat transfer resistance between the absorber surface, heated by the solar irradiation, and the collector fluid, the type of heat transfer fluid and its flow rate inside the collector. It is therefore necessary to pay attention to the design of the absorber plate and the properties of the collector fluid.
The heat loss coefficient, U_L, is influenced by the number and spacing of covers, by the longwave radiative properties of the absorber, and wind speed.
In this model, it is also highlighted how these three factors influence the total efficiency of the collector and how they can be addressed independently. The three factors can be used to identify features that would enhance the thermal performance of the PV/T collector with the highest cost-benefit.

2.1.2. Duffie and Beckman

Duffie and Beckman faced the complicated problem to carry out the detailed analysis of a solar collector providing a simplified model capable to yield very useful data. The results of this relatively simple analysis show the relationship between the main variables and how they affect the performance of a solar collector (Duffie and Beckman, 2013).
The main assumptions under this two-dimensions steady-state model are:

- The thermal gradient across through the thickness of the panel is neglected and the sky is a black body for long-wavelength radiation at an equivalent sky temperature.

- The covers are considered opaque to infrared radiation and does not absorb solar radiation.
- Temperature gradients in the flow direction and between tubes can be treated independently, while temperature gradients around tubes can be neglected.
- Finally, properties of the materials are independent of temperature, dust, dirt, and shading on the collector can be neglected.

The model was developed based on a glazed solar collector with a sheet and tube absorber. In figure 2.1 it is possible to see the representation of the collector section under study and the various layers that compose it:

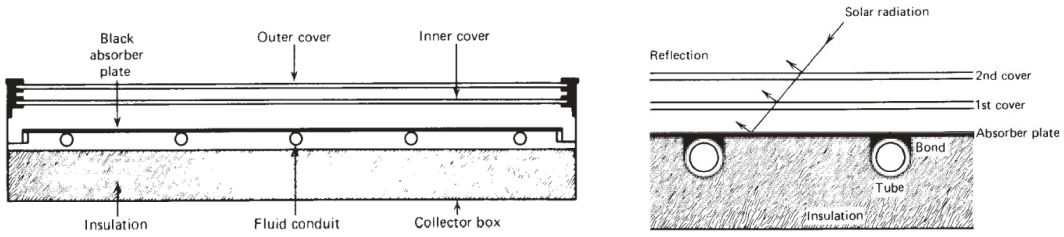

Figure 2.1. Sections of the collector under study (Duffie and Beckman, 2013)

It was developed the concept of an overall thermal loss coefficient for a solar collector in order to simplify the mathematics and have a general parameter representative of all the different types of collectors available. The energy S absorbed by the plate is distributed to thermal losses through the top and bottom and to useful energy gain. In figure 2.2 the schematic of all heat transfers (conduction, convection, and radiation) affecting the various layers of the collector is illustrated:

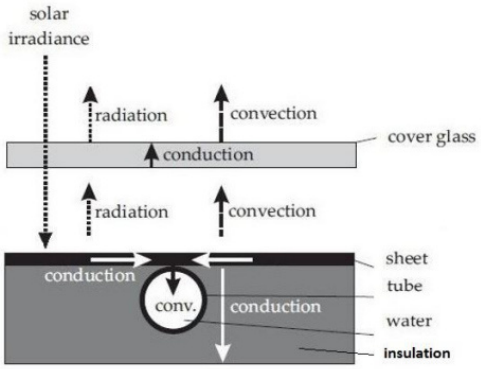

Figure 2.2. Schematic of the heat transfers terms affecting the PV/T layers (Pressiani, 2016)

All the contributions related to the heat losses affecting the different layers of a solar thermal collector are calculated using the electrical analogy (schematically reported in figure 2.3). In particular, the example referred to a solar thermal collector with two glass covers is analysed.

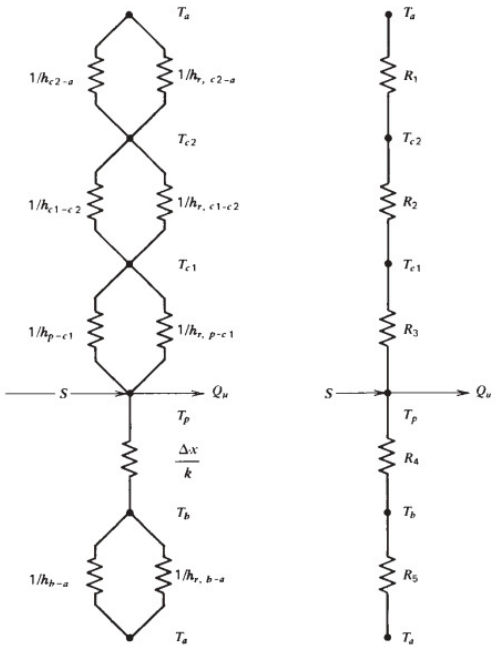

Figure 2.3. Schematic of electrical analogy used for thermal losses calculation

The temperature distribution between two tubes has been derived for the sheet-tube configuration assuming the temperature gradient in the flow direction is negligible. Because the sheet material is a good conductor, the temperature gradient through the sheet has been neglected and the sheet above the bond has been assumed at some local base temperature T_b. The region between the centreline separating the tubes and the tube base has been considered as a classical fin problem.

The useful energy gain q'_u per unit of the area collected by the PV/T collector is evaluated with the equation (2.2):

$$q'_u = WF'\left[S - U_L\left(T_f - T_a\right)\right] \tag{2.2}$$

where S is equal to the incident solar radiation reduced by optical losses. If it is assumed that all losses occur to a common sink temperature T_a, the collector overall loss coefficient U_L is the sum of the bottom (U_b), edge (U_e), and top (U_t) loss coefficients and represents how much energy is lost to the environment:

$$U_L = U_b + U_e + U_t \tag{2.3}$$

F' is interpreted as the ratio between the heat transfer resistance from the fluid to the ambient air and the heat transfer resistance from the absorber plate to the ambient air:

$$F' = \frac{1/U_L}{W\left[\frac{1}{U_L\left[D+(W-D)F\right]} + \frac{1}{C_b} + \frac{1}{\pi D_i h_{fi}}\right]} \tag{2.4}$$

In equation (above) W is the distance between tubes (m), D is the external tube diameter (m), D_i is the internal tube diameter (m), and h_{fl} the heat transfer coefficient between the fluid and the tube wall (W/m^{2}K). C_b is the bond conductance (W/mK) and is evaluated as:

$$C_b = \frac{k_b b}{\gamma} \tag{2.5}$$

Where k_b is the bond thermal conductivity, γ is the average bond thickness, and b is the bond width.
F is the fin efficiency, a constant for any collector design and fluid flow rate:

$$F = \frac{\tanh\left(m\frac{(W-D)}{2}\right)}{m\frac{(W-D)}{2}} \tag{2.6}$$

Where the coefficient m is defined as:

$$m = \sqrt{\frac{U_L}{k_{abs}\delta_{abs}}} \tag{2.7}$$

k_{abs} is the conductivity of the absorber (W/mK) and δ_{abs} is the thickness (m).
Even if F' is a function of U_L and h_{fi}, each of which has some temperature dependence, it is not a strong function of temperature.
It is convenient to define a quantity that relates the actual useful energy gain of a collector to the useful gain if the whole collector surface were at the fluid inlet temperature. This quantity is called the collector heat removal factor F_R (Duffie and Beckman, 2013) and it is calculated as:

$$F_R = \frac{\dot{m}C_p}{A_c U_L}\left[1-\exp\left(-\frac{A_c U_L F'}{\dot{m}C_p}\right)\right] \tag{2.8}$$

Then the collector flow factor F'' is introduced as the ratio of F_R to F':

$$F'' = \frac{F_R}{F'} = \frac{\dot{m}C_p}{A_c U_L}\left[1-\exp\left(-\frac{A_c U_L F'}{\dot{m}C_p}\right)\right] \tag{2.9}$$

The quantity F_R is assessed like the effectiveness of a conventional heat exchanger, which is defined as the ratio of the actual heat transfer to the maximum possible heat transfer. The maximum possible useful energy gain (heat transfer) in a solar collector occurs when the whole collector is at the inlet fluid temperature; heat losses to the surroundings are then at a minimum. The collector heat removal factor times this

maximum possible useful energy gain is equal to the actual useful energy gain Q_u (Duffie and Beckman, 2013):

$$Q_u = A_c F_R \left[S - U_L \left(T_i - T_a \right) \right] \tag{2.10}$$

Finally, the thermal efficiency η_{th} is introduced and defined as:

$$\eta_{th} = F_R \left[(\tau\alpha) - U_L \frac{T_{fi} - T_{amb}}{G_T} \right] \tag{2.11}$$

Where, $(\tau\alpha)$ is the average transmittance-absorptance product of the cover and absorber. Since the expressions for U_L were derived assuming that the glazing did not absorb solar radiation an effective transmittance-absorptance product $(\tau\alpha)_e$ has been introduced in order to account for the reduced thermal losses due to absorption of solar radiation by the glass. It has been stated that the solar radiation that is absorbed by a cover system is not entirely lost since this absorbed energy tends to increase the cover temperature and consequently reduce the thermal losses from the plate.

2.1.3. Florschuetz

One of the first studies about the extension of the Hottel-Whillier model for thermal analysis of flat-plate solar collectors to the analysis of combined photovoltaic/thermal collectors was conducted by Florschuetz in (Florschuetz, 1979).
The extension has been carried out in such a way that the thermal performance of the combined collector may be assessed using the same methodology as for a pure thermal collector, with the only foresight of replacing U_L and S, wherever they appear in the relevant equations, with their modified values U'_L and S'.
It is only necessary to assume that the local electrical conversion efficiency of the solar cell array (absorber) can be represented as a linearly decreasing function of the local absorber temperature over its operating temperature range.

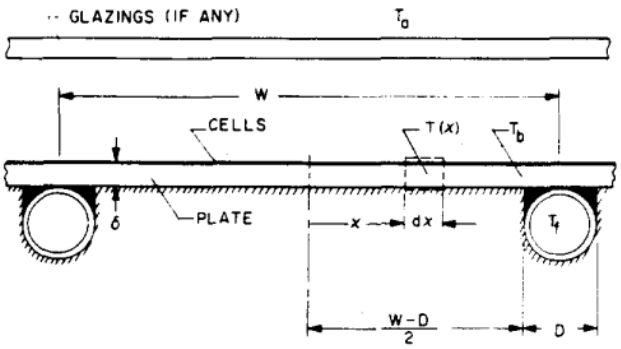

Figure 2.4. Cross-section of sheet and tube configuration for illustration of combined collector analysis

In particular, the modifications done to the model depend on two cell parameters, one of which specifies the cell array reference efficiency while the other specifies the decrease of cell efficiency with temperature. The steady state energy balance results in:

$$\frac{d^2T}{dx^2} = \frac{1}{k\delta}[U_L(T - T_a) - S + q_e] \tag{2.12}$$

Setting q_e equal to 0 the equation (2.12) is reduced to that for a conventional thermal collector without a photovoltaic module.
The term q_e is the local electrical output and may be written as:

$$q_e = \eta \frac{S}{\alpha} \tag{2.13}$$

In this equation, η represents the cell array efficiency and it is assumed to decrease linearly with absorber temperature, which is described with the following equation:

$$\eta = \eta_r[1 - \beta_r(T - T_r)] \tag{2.14}$$

By utilising eqns (2.13) and (2.14) to replace q, in eqn (2.12) it results in:

$$\frac{d^2T}{dx^2} = \frac{1}{k\delta}[\tilde{U}_L(T - T_a) - \tilde{S} + q_e] \tag{2.15}$$

Where were set:

$$\tilde{U}_L = U_L - \frac{S}{\alpha}\eta_r\beta_r \tag{2.16}$$

and

$$\tilde{S} = S\left(1 - \frac{\eta_a}{\alpha}\right) \tag{2.17}$$

Where η_a represents the efficiency of the PV cells at the ambient temperature T_a.
It is possible to see that equation (2.15) for the combined photovoltaic/thermal collector is identical in form to equation (2.12) for the pure thermal collector. Consequently, replacing U_L and S with $\tilde{U}_L$ and $\tilde{S}$ respectively, as defined by equations (2.16) and (2.17), solutions and results based on equation (2.12) also apply for the combined PV/T collector.

2.1.4. Perers

The model developed by Perers was aimed to find a practical and accurate enough connection between measured collector performance data and collector efficiency parameters that can be used in standard simulation programs for long-term performance prediction based on 1 h time steps. As reported in (Magalhães, 2018), in Perers model

the various heat transfer processes and dependencies are calculated through individual terms consisting of linear functions of key parameters. As a consequence, the parameter estimation via multi-linear regression (MLR) results particularly convenient (Perers, 1997).

The collector model used was based on the Hottel Whillier Bliss equation with improvements made to consider thermal capacitance effects, incidence angle effects and the temperature, and wind and sky temperature dependence of the heat loss coefficient.

The proposed model is derived by mixing already existing and validated models for the complex instantaneous thermal and optical behavior of a solar collector. The model, reported in equation (2.18), is referred to a glazed PV/T collector and it is valid only for the instantaneous steady-state collector performance:

$$Q = F'(\tau\alpha)_{en} G - c_1(t_m - t_a) - c_2(t_m - t_a)^2 \tag{2.18}$$

where c_1 and c_2 terms describe the temperature-dependent heat losses.

With the addition of the one-node capacitance term $(mC)_e$ to the equation (2.18), the integrated effect of thermal capacitance within the time step is taken care of, and the instantaneous model can be used also for mean values up to one hour:

$$\begin{aligned} q_u = {} & F'(\tau\alpha)_e K_{\tau\alpha b}(\vartheta) I_b + F'(\tau\alpha)_e K_{\tau\alpha d} I_d - F'U_0 \Delta T - F'U_1 (\Delta T)^2 + \\ & - F'U_w \Delta T w - F'U_{sky} \Delta T_{sky} - (mC)_e \frac{dT_f}{dt} - U_p \Delta T \end{aligned} \tag{2.19}$$

The incidence angle dependence $K_{\tau\alpha b}(\theta)$ for beam radiation is described through standard b_0 equation:

$$K_{\tau\alpha b}(\vartheta) = 1 - b_0(1/\cos(\vartheta) - 1) \tag{2.20}$$

This equation is sufficient for describing the incidence angle dependence for most flat-plate collectors. The equation also shows a characteristic cut-off angle before 90 degrees, representing the shadow effects from the glazing frames and the side of the collector.

The mean fluid temperature T can only be accurately determined as long as there is a mass flow in the collector loop. Therefore, only data with a continuous flow during the time step can be used as input data for the parameter identification.

The derived collector parameters can be used directly in most detailed simulation programs, such as TRNSYS, WATSUN, MINSUN (Perers, 1993).

An extension of this model is provided in (Perers, 1997) in order to be able to modeling also the behaviour of unglazed collectors.

A complete model was suggested for glazed, unglazed, evacuated tube and concentrating collectors:

$$q_u = F'(\tau\alpha)_e K_{\tau\alpha b}(\vartheta) I_b + F'(\tau\alpha)_e K_{\tau\alpha d} I_d - B_w I_{tot} w - F'U_0 \Delta T + \\ -F'U_1(\Delta T)^2 - F'U_w \Delta T w - F'U_{sky} \Delta T_{sky} - (mC)_e \frac{dT_f}{dt} - U_p \Delta T \quad (2.21)$$

where $B_w I_{tot} w$ is added correction term, for wind and sky temperature dependence, necessary for describing an unglazed collector.
The collector model proposed here has also been used to model concentrating collectors with good results. If an external booster reflector is introduced two terms have to be added to the right-hand side of eqn (2.21) for the additional beam and diffuse radiation from the reflector. The additional contribution to the heat production from the reflector is given:

$$q_{urm}(R) = F'(\tau\alpha)_e K_{\tau\alpha b}(\theta_{bcr}) K_m I_{br} + F'(\tau\alpha)_e K_{\tau\alpha d}(\theta_{dcr}) I_{dr} \quad (2.22)$$

In equation (2.22) $q_{urm(R)}$ represents the additional collector output caused by a booster reflector characterized by a reflectance R, I_{br} and I_{dr} are the beam and diffuse radiation from the reflector respectively, θ_{bcr} and θ_{dcr} are the incidence angle for beam and diffuse radiation from the reflector, and K_m is a correction factor for missing radiation from the reflector at finite reflector length.
The proposed collector model with parameters given by a special MLR-method is shown to be able to simulate measured performance even on a very short time resolution. The instantaneous response of the outlet temperature to gradients in the inlet temperature and the heat capacity effects of the insulation with a long-time constant give rise to small deviations between model and measurements (Perers, 1997).

2.1.5. Chow T.T.

The thermal models yet (so far) analysed in previous studies about the performance of hybrid photovoltaic-thermal (PV/T) collectors were mostly steady-state models for predicting the annual yields. However, as the operation of a PV/T collector is inherently dynamic, Chow in (Chow, 2003) highlighted the necessity to develop a dynamic model suitable for predicting working temperatures of the PV module and the heat-removal fluid during periods of fluctuating irradiance or intermittent fluid flow.
An explicit dynamic model was developed for a flat-plate water-heating PV/T collector with a single glass cover which is suitable for dynamic system simulation applications. It allows detailed analysis of the transient energy flow across various collector components and is able to provide information on the transient performance, including the instantaneous thermal/electrical gains, efficiencies, and thermal state of various collector components (Chow, 2003).

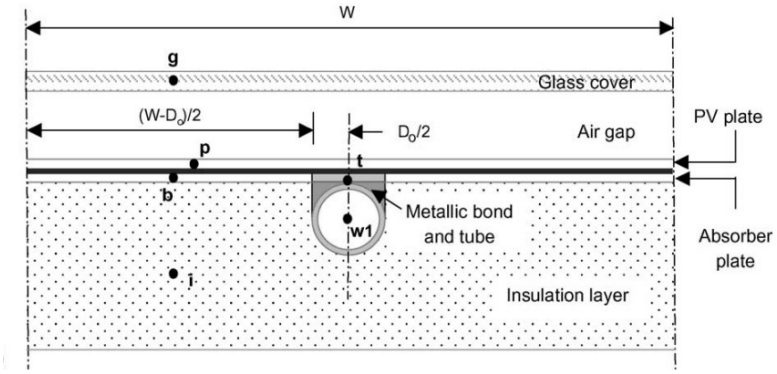

Figure 2.5. Section view (across one water tube) of the PV/T collector analysed

The PV/T collector, whose section view is reported in figure 2.5, is represented by seven nodes, and mathematically, by a matrix equation set derived from the instantaneous energy and mass flow balance at these nodes. Each node is representative of a specific component of the PV/T collector, from the glass cover (g) to the insulation layer (i).

As reported in (Chow, 2003) the seven-node model can provide information about the transient performance, the instantaneous thermal and electrical gains, and thermal conditions of various collector components. It allows detailed analysis of the transient energy flow across various collector components and captures the instantaneous energy outputs. This is often required when the flow velocity is low, or the simulation time step is small. Because of the relatively short simulation time required, the model is also suitable for hourly analysis of equipment energy performance.

2.1.6. Helmers – Kramer

Despite the existing literature on the theoretical modeling of PV/Ts, the performance model for hybrid collectors, which allows electrical and thermal efficiency predictions based exclusively on standard measurement data, is only available in a simplified form (compare Perers et al. (2012)). Therefore, in the work of Helmers-Kramer (Helmers and Kramer, 2013) a performance model of a hybrid (C)PV/T collector has been derived such that it can be applied both to non-concentrating and concentrating collectors. The model proposed only with standard measurement quantities about ambient conditions and thermal and electrical operation is able to determine the relevant parameters. In this way it is possible to give an accurate collector performance prediction in the same manner as for the quasi-dynamic model. The Helmers and Kramer model is based on considerations concerning the energy balance, the heat transfer, and the dependence of the photovoltaic efficiency on the absorber temperature. As for the quasi-dynamic model for thermal collectors, linear parameterizations are derived for both electrical and thermal power outputs.

First, the general energy balance illustrated in Figure 2.6 is presented and used to derive an expression for the absorber temperature.

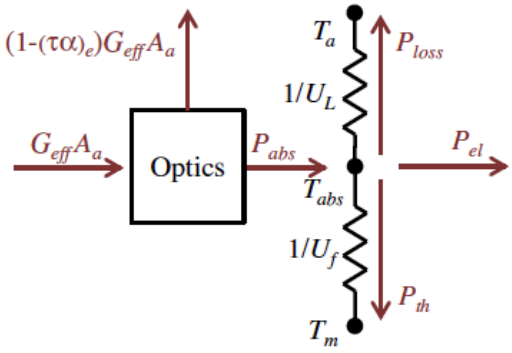

Figure 2.6. Schematic representation of the basic energy balance of a (C)PV/T collector

The product of effective irradiance G_{eff} and aperture area A_a defines the incident radiation power, which is then reduced by optical losses. P_{abs} denotes the power absorbed at the solar receiver (at absorber temperature T_{abs}) after optical losses. This latter is divided among the two usable output power defined by the thermal power that is transferred to the fluid P_{th} (at mean temperature $T_m = (T_{in} + T_{out})/2$) and the electrical power output P_{el}. A part of the absorbed power P_{abs} is lost to the environment (P_{loss}). at ambient temperature T_a.

Then, an equation is derived that expresses the temperature dependence of the electric power. Based on this derivation, finally, a formalism based only on linear coefficients is presented which allows a complete description of the interacting electrical and thermal power of the collector (C) PV/T.

The basic energy balance is evaluated, with reference to figure 2.6, as follows:

$$P_{abs} - P_{el} = P_{th} + P_{loss} = U_f (T_{abs} - T_m) + U_L (T_{abs} - T_a) \tag{2.23}$$

where effective heat transfer coefficients U_f and U_L from the absorber to the fluid and environment, respectively, have been introduced.

The expression for the absorber temperature T_{abs} is obtained solving equation (2.23):

$$T_{abs} = F' T_m + (1 - F') T_a + F' \frac{P_{abs} - P_{el}}{U_f} \tag{2.24}$$

As concern the hybrid model, the total power output of a (C)PV/T collector, $P_{out} = P_{th} + P_{el}$, is assumed to follow a similar description given by Perers in (Perers 1997) with the addition of the appropriate adjustments to also consider the contribution of the solar radiation concentration:

$$\frac{P_{th} + P_{el}}{A_{rec}} = a_0 G_c - a_1 \Delta T - a_2 (\Delta T)^2 - a_3 \Delta T v - a_4 \Delta T_{sky} - a_5 \frac{dT_m}{dt} - a_6 G_c v \tag{2.25}$$

G_c represents the concentrated effective irradiance given by the product of G_{eff} and the geometrical concentration ratio C calculated as:

$$C = A_a / A_{rec} \tag{2.26}$$

Where A_a is the effective aperture area and A_{rec} is the receiver area.
The results obtained demonstrate how the thermal power is affected by the increase in wind speed due to the increase in convection losses. Furthermore, a good forecasting and metering agreement for electricity emerges. At present, existing standards for performance testing lack explicit coverage of (C)PV/T collectors, as highlighted in (Helmers and Kramer, 2013). Therefore, the presented model is proposed as a candidate for an extension of existing standards to such technology.

2.1.7. Aste et al.

A new design of an experimental PV/T collector and a new dynamic model for the simulation of flat plate PV/T water collectors are presented in (Aste, Leonforte and Pero, 2015). The new PV/T collector, based on the integration of a silicon thin film double junction sandwich characterized by a low temperature coefficient, was proposed in order to reduce temperature power losses, overcoming the well-known temperature effect on the characterization of the electrical performance of a PV/T module.
The model is aimed to calculate the electrical and thermal performance of a PV/T collector coupled to a storage tank, as the climatic and operating conditions vary. It takes into account the influence of various parameters on the performance of hybrid collectors, such as the spectral efficiency, the losses due to temperature, the real angle of incidence of the solar radiation on the surface and the thermal inertia of the collector.
Also in this case the simulation model is based on energy balances applied to each of the different components of the PV/T collector (glass cover, PV cells, air gap and absorber plate) and organized in a numerical matrix. Two additional equations related to the storage tank and 5 equations for the dynamic calculation of convective and radiative coefficients are also considered.
Particularly worth to note are considerations made about of the efficiency of the PV. Considering that the nominal efficiency of PV cells is measured referring to Standard Test Conditions (STC) (cells temperature at 25 °C and normal irradiance of 1000 W/m^2) and the real operating conditions can be remarkably different from those of reference, it the necessity to calculate the value of real efficiency (η_a). This latter takes into account variations of operative temperature of the cells, incident angle of solar irradiance and solar spectrum, and it is assessed as in equation proposed in (Aste and Del Pero, 2006):

$$\eta_a = \eta_n \times k_\gamma \times k_\theta \times k_\lambda \times k_g \tag{2.27}$$

In equation (2.27) the real efficiency (η_a) is calculated multiplying the nominal efficiency of the PV module (η_n) for four correction factors $k_\gamma, k_\theta, k_\lambda,$ and k_g.
k_γ is the module temperature correction factor and is given by:

$$k_\gamma = \left[1 - \gamma_{PV} \times (T_{PV} - 298.15)\right] \tag{2.28}$$

k_θ is the optical correction factor and is given by the ratio between the solar transmittance at specific angle of incidence on the front cover surface (τ_G) and the corresponding value at normal incidence (τ_n):

$$k_\theta = \frac{\tau_G}{\tau_n} \tag{2.29}$$

k_λ is the spectrum correction factor and is calculated using an empiric formula which relates the changes of incident solar light spectrum to air mass coefficient (AM) proposed in (Riordan and Hulstron, 1990) to characterize the influence of spectral variation on the production of the PV sandwich (Heckttheuer, 2001):

$$k_\lambda = 1.0547 - 0.0214 \times \mathrm{AM} - 0.0075 \times \mathrm{AM}^2 + 0.0004 \times \mathrm{AM}^3 \tag{2.30}$$

Finally, k_g is the low irradiance correction factor in order to take into account the power losses due to low irradiance behavior of PV modules.
The model validation was carried out using measured data in an experimental analysis. It resulted that the numerical model has been able to give accurate simulation of the daily thermal and electric performances also in days with different climatic conditions.

2.1.8. Lammle et al.

In their work, Lammle et al. focused their studies on PV/T collectors equipped with spectrally selective but transparent low-emissivity (low-e) coatings which are, as already discussed in chapter 1, an innovative and suitable measure to reduce thermal losses (Lammle *et al.*, 2016).
A numerical model of the high-efficiency PV/T collectors is presented that describes the interaction between the optical properties of "low-e" (low emissivity) coatings, overall heat losses, and *F'*. The approach is divided into two phases: in the first phase, the characteristic coefficients of performance are calculated from optical and thermal design parameters using a PV/T collector model. In the second step, these coefficients of performance are used in a system simulation environment to calculate annual energy returns for typical applications. This integral modeling approach helps to understand the interaction between design parameters and to develop technically and economically optimized PV/T collectors (Lammle *et al.*, 2016). The thermal energy flows are modelled using multiple nodes connected with temperature-dependent thermal resistances analogous to an electrical circuit. Mean temperature values are employed at every node. Since performance measurements are carried out under steady-state conditions, dynamic effects are neglected. All energy flows occurring inside the collector are described numerically and solved iteratively until convergence. The

diagram reported in figure 2.7 illustrates the nodal model according to Helmers and Kramer (Helmers and Kramer, 2013)

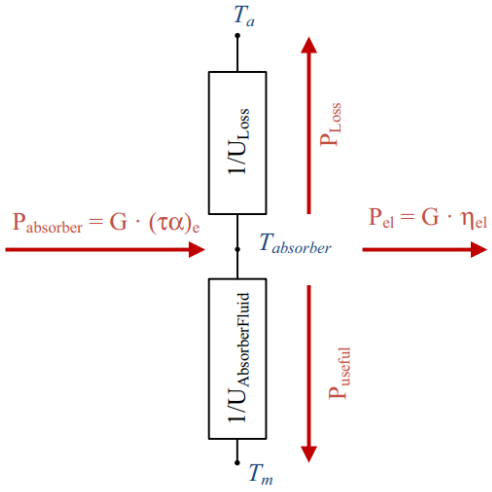

Figure 2.7. Diagram illustrating the nodal model adopted according to (Helmers and Kramer, 2013).

How is possible to see, the incident irradiation G is first reduced by the effective optical losses $(\tau\alpha)_e$, the absorbed radiation P_{abs} is then divided into electricity produced P_{el}, useful thermal energy P_{useful}, and thermal losses P_{loss}.
$(\tau\alpha)_e$ is the effective transmittance–absorptance product and represents the total share of solar irradiance being absorbed under normal incidence conditions. It is calculated according to Duffie and Beckman (2013) through the equation (2.31):

$$(\tau\alpha)_e = \tau_{\text{cover}}\alpha_{\text{laminate}}\sum_{n=0}^{\infty}\left[\rho_{\text{cover}}\left(1-\alpha_{\text{laminate}}\right)\right]^n = \frac{\tau_{\text{cover}}\alpha_{\text{laminate}}}{1-\rho_{\text{cover}}\left(1-\alpha_{\text{laminate}}\right)} \qquad (2.31)$$

In particular, the transmittance of the cover τ_{cover}, absorptance of the PV/T laminate $\alpha_{laminate}$ are considered, and the multiple reflections between cover and PV/T laminate are taken into account.
A good agreement was found between the simulation results obtained with the numerical model of the PV / T collector and the experimental data. Furthermore, this model resulted able to assess the effect of low-e coatings on thermal and electrical performance. However, due to idealized assumptions, the numerical model tends to overestimate the thermal efficiency.

2.1.9. Perers model extension

UNI EN ISO 9806, which represents the main international standard for tests on solar thermal collectors, indicates stationary and quasi-dynamic test methods based on the Perers model.

However this latter, how is reported in (Magalhães, 2018), seems no to differentiate between hybrid and non-hybrid (when no electricity generation occurs) operation of PV/T collectors. Furthermore, despite 9806 standard's latest version requires the tests to be conducted in maximum power point (MPP) mode, the Perers model does not explicitly account for the thermal performance reduction caused by electricity generation.

An extension of this latter is proposed by Magalhães in (Magalhães, 2018) with the main objective to provide a more accurate thermal performance model of PV/T collectors under hybrid MPP operation. The extended version is identical to the Perers model, but it also explicitly takes into account the effective reduction of the absorption factor caused by electricity generation in PV/T collectors which operate at maximum power point (MPP). Furthermore, it discusses its suitability for parameter estimation using multi-linear regression (MLR).

The specific heat flow rate can be divided in the sum of two terms, as reported in equation (2.32):

$$\frac{\dot{Q}(\eta_{pv})}{A_a} = \frac{\dot{Q}(\eta_{pv}=0)}{A_a} - \frac{\dot{q}_{pv}}{A_a} \tag{2.32}$$

The first term represents the specific heat flow rate without electricity generation, while the second one is the specific heat flow rate loss prompted by PV electricity generation. Considering equation (2.32) the collector efficiency factor (F') can be written, assuming the local position is the one where the mean fluid temperature ($t_{f,m}$) can be sensed ($t_x = t_{f,m}$), as in equation (2.33):

$$F' = \frac{\dot{Q}}{\dot{Q}(t_p = t_x)} = \frac{\dot{Q}}{\dot{Q}(t_p = t_{f,m}, \eta_{pv} = 0) - \dot{q}_{pv}(t_p = t_{f,m})} \tag{2.33}$$

Making in equation (2.33) $\dot{Q}$ explicit and dividing each term by the aperture area of the collector (A_a) equation (2.34) it was obtained:

$$\frac{\dot{Q}}{A_a} = F' \frac{\dot{Q}(t_p = t_{f,m},\ \eta_{pv} = 0)}{A_a} - F' \frac{\dot{q}_{pv}(t_p = t_{f,m})}{A_a} \tag{2.34}$$

In equation (2.34) the first term on the right represents the Perers model, while the second is the product between F' and the specific electrical power generated assuming the absorber plate and the cells are at the mean fluid temperature.

The photovoltaic efficiency η_{pv} is evaluated as:

$$\eta_{pv} = \eta_{pv,r}[1 + \beta_{pv}(t_{pv,m} - t_{pv,r})] \tag{2.35}$$

Where $\eta_{pv,r}$ is the cells' reference electrical efficiency, $t_{pv,r}$ is the reference cell temperature, $t_{pv,m}$, is the mean cell temperature, and β_{pv} is the MPP cell efficiency temperature coefficient.

The resulting bulk electrical power generated (P_{pv}) by the PV/T collector is given by:

$$P_{pv} = A_a \tau_c \rho_{pv} \eta_{pv} (\mathrm{K}_{\theta,b,pv}\, G_b - K_{\theta,d,pv}\, \mathrm{G}_d) \tag{2.36}$$

where ρ_{pv} is the PV packing factor, τ_c is the front cover transmittance (if there is one, otherwise τ_c equals 1), $K_{\theta,d,pv}$ and $K_{\theta,b,pv}$ are the diffuse and beam irradiance IAMs for the PV conversion process.
Substituting (2.35) in (2.36), and replacing the result in (2.34) yields (2.37), the expanded form of $\dot{q_{pv}}/A_a$ before considering specific incidence angle effects:

$$\begin{aligned} \frac{\dot{q}_{pv}}{A_a} &= F'\tau_c\rho_{pv}\eta_{pv,r}\left[1+\beta_{pv}\left(t_{f,m}-t_{pv,r}\right)\right]K_{\theta,b,pv}G_b + \\ &+F'\tau_c\rho_{pv}\eta_{pv,r}\left[1+\beta_{pv}\left(t_{f,m}-t_{pv,r}\right)\right]K_{\theta,\mathrm{d},pv}G_d \end{aligned} \tag{2.37}$$

Replacing (2.32) and (2.37) in (2.34) leads to an expanded form of the extended model, (2.33), from which a close variant of the Florschuetz model can be obtained by neglecting a few terms (θ=0°, c_2 = 0 W/m^{2}K^2, c_4 = 0, c_5 = 0 J/m^2 K, c_6 = 0 s/m), assuming F' is equal to Florschuetz' modified collector efficiency factor and rearranging:

$$\begin{aligned} \frac{\dot{Q}}{A_a} &= \eta_{0,b}K_{\theta,b}G_b + \eta_{0,b}K_{\theta,\mathrm{d}}G_d - F'\tau_c\rho_{pv}\eta_{pv,r}\left[1+\beta_{pv}\left(t_{f,m}-t_{pv,r}\right)\right]K_{\theta,b,pv}G_b + \\ &-F'\tau_c\rho_{pv}\eta_{pv,r}\left[1+\beta_{pv}\left(t_{f,m}-t_{pv,r}\right)\right]K_{\theta,\mathrm{d},pv}G_d - c_1\left(t_{f,m}-t_a\right) - c_2\left(t_{f,m}-t_a\right)^2 + \\ &-c_3u\left(t_{f,m}-t_a\right) + c_4\left(E_L-\sigma T_a^4\right) - c_5\frac{dt_{f,m}}{d\tau} - c_6uG_{hem} \end{aligned} \tag{2.38}$$

2.2. Regulations for testing PV/T performances

Currently, there is no "ad hoc" regulation for PV/T hybrid solar collectors; therefore, reference is made to the regulations in force relating to solar thermal collectors and photovoltaic panels separately.
The main quality label for solar thermal collectors is the Solar Keymark, a voluntary third-party certification mark for solar thermal products, demonstrating to end-users that a product conforms to the relevant European standards and fulfills additional requirements (*Keymark website*, 2018).
The testing procedure aims to ensure the effective compliance of the components of a solar thermal system with European standards, as well as their quality, safety, and functionality. It is also a binding condition for obtaining the incentives provided for the installation of a solar thermal system following the provisions of the New Thermal Account 2.0.

As reported also in (*Guide to Standard ISO 9806 : 2017*, 2018) due to legal requirements, a Solar Keymark Certificate can only be issued if tests are performed according to a European Standard. For this reason, the tests and measurements must be performed according to UNI EN ISO 9806, which defines the testing requirements, replacing EN 12975-2.
Nowadays the certification of collectors and solar thermal systems is carried out according to UNI EN 12975 (section 1), UNI EN ISO 9806 [formerly UNI EN 12975 (part 2)], and UNI EN 12976 (section 1 and 2).
In Report B1 of SHC Task 60 (Kramer, 2020) the Status Quo of PV/T characterization is reported in order to support PV/T technology in its further development and applications.

2.2.1. ISO 9806

ISO 9806 "Solar energy - Solar thermal collectors - Test methods", the international standard for testing solar thermal collectors, was first published in 1994. As there have been major advances in hybrid PV/T technology since that time, and especially in recent decades, the need to update the standard has emerged. Thus, to keep up with technological developments and with the growing market demand an update of this standard was done in 2013, while the most recent one was completed in 2017.
With the introduction of the UNI EN ISO 9806 several supplements and changes have been made with respect to the replaced EN 12975-2 standard, in (*Guide to Standard ISO 9806 : 2017*, 2018) the main ones are summarized as follows:

- Extension of the applicability of the standard to concentrating and tracking collectors, air collectors, and PV/T collectors.
- Definition of the gross area as a reference for thermal performance.
- Definition of climatic classes for durability and reliability tests.
- Change in general conditions for test exposure: the total incident radiation as a relevant parameter has been substituted for the number of days with radiation of at least 14 MJ/(m²d). This leads to shorter test periods and also allows for measurements during the winter.
- Modification of the rain penetration test about carrying out the test and detecting the penetration of water.
- Minimum pressure and tensile loads during the high mechanical load test from 1,000 Pa to 2,400 Pa.

While EN 12975-2, like the specifying standard test methods, has been incorporated into the new EN ISO 9806, the general requirements for solar collectors defined in EN 12975-1 remain valid.
ISO 9806 was published to provide a common method for testing the durability and the performances of the most common solar heating collectors, reproducing the most probable extreme conditions that a collector would be subjected to during its lifetime.

All the tests required by ISO 9806 for solar heating collectors are listed in Table 1:

Table. 2.1. List summarizing all tests covered by ISO 9806

Clause	Test
Clause 6	Internal Pressure Test for Fluid Channels
Clause 7	Air Leakage Rate Determination
Clause 8	Rupture and Collapse Test
Clause 9	Standard Stagnation Temperature Determination
Clause 10	Exposure Test
Clause 11	External Thermal Shock Test
Clause 12	Internal Thermal Shock Test
Clause 13	Rain Penetration Test
Clause 14	Freeze Resistance Test
Clause 15	Mechanical Load Test
Clause 16	Impact Resistance Test
Clause 17	Final Inspection
Clause 19-26	Thermal Performance Test
Clause 27	Pressure Drop Measurement

According to EN ISO 9806, PV/T collectors must be tested like any other solar thermal collector in compliance with durability and thermal efficiency. All thermal efficiency tests must be conducted under maximum electrical power generation conditions. For all durability tests, the electrical power generator must not be connected to any load (open circuit) to avoid cooling the collector and simulate the worst operating conditions.
The electric power generator must be described in detail in the test report. Furthermore, the electrical operating mode must be reported for all tests (*UNI EN ISO 9806*, 2017). In the following figure (figure 2.8) an example of schematic test configuration for liquid heating collectors is shown:

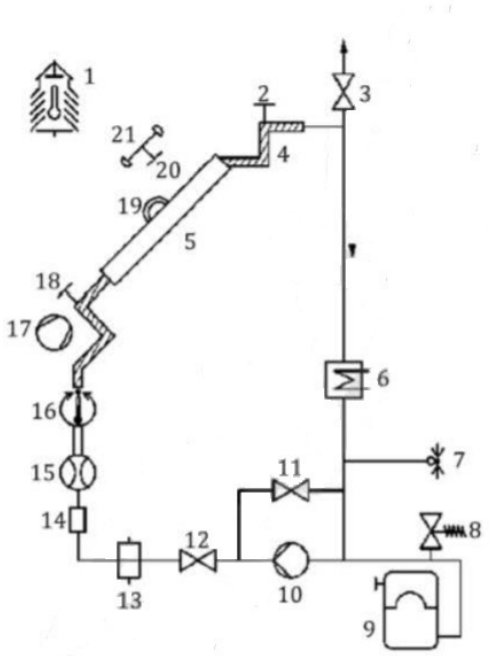

Figure.2.8. The example of a closed test loop reported in UNI EN ISO 9806. It includes an ambient temperature sensor (1), a temperature sensor for tout(2), an air vent (3), an insulated pipe (4), the solar collector to be tested (5), heater/cooler for primary temperature control (6), pressure gauge (7), safety valve (8), expansion tank (9), a pump (10), a bypass valve (11), a flow control valve (12), a filter (13), a sight glass (14), a flow meter (15), a secondary temperature regulator (16), an artificial wind generator (17), a temperature sensor for tin(18), a pyrgeometer (19), a pyranometer (20), and an anemometer (21).

The normative indicates specific mounting requirements since the way in which a collector is mounted will influence the results of thermal performance tests. In particular, the collector has to be positioned considering that its lower edge has to be at a height not less than 0,5 meters from the floor (*UNI EN ISO 9806*, 2017), and oriented towards the south with a tilt angle of 45 °. Indications are given also regarding the quality and the technical characteristics of the instrumentation shall be used as well as their mounting. As an example, for measuring the temperature of the heat transfer liquid the sensors shall be mounted at a distance lower than 200 mm from the inlet and the outlet of the collector.

For the purpose of the central object of this thesis, the attention was mainly paid to the procedures and indications related to thermal performance testing.

As reported in Section 19 of the European Standard, performance testing includes the assessment of the thermal power output delivered by the collector considering various operating conditions. This is achieved by determining collector parameters like conversion factor, incident angle modifier, heat capacity and time constant. Furthermore, the influence the incidence angle of the solar irradiation on the collector has on the thermal performance and the heat capacity of the collector have to be measured. The aim of Thermal Performance Testing is to provide a procedure capable

of making comparisons between different collectors and collector technologies with each other in a fair and transparent way.
Two performance test methods, Steady State Testing (SST) and Quasi Dynamic Testing (QDT), are reported in the standard. Furthermore, two different procedures for water heating collectors and air heating collectors are reported.
The two methods are equivalent but only the QDT model includes the differentiation between diffuse and direct radiation. This method is more applicable for collector technologies whose thermal performance is sensible to the diffuse fraction (e.g. concentrating collectors). The entire procedure, from the analysis of the manufacturer's technical data to the evaluation of the final data evaluation, is illustrated According to (*Guide to Standard ISO 9806 : 2017*, 2018) in Figure 2.9, both for SST and QDT testing method.

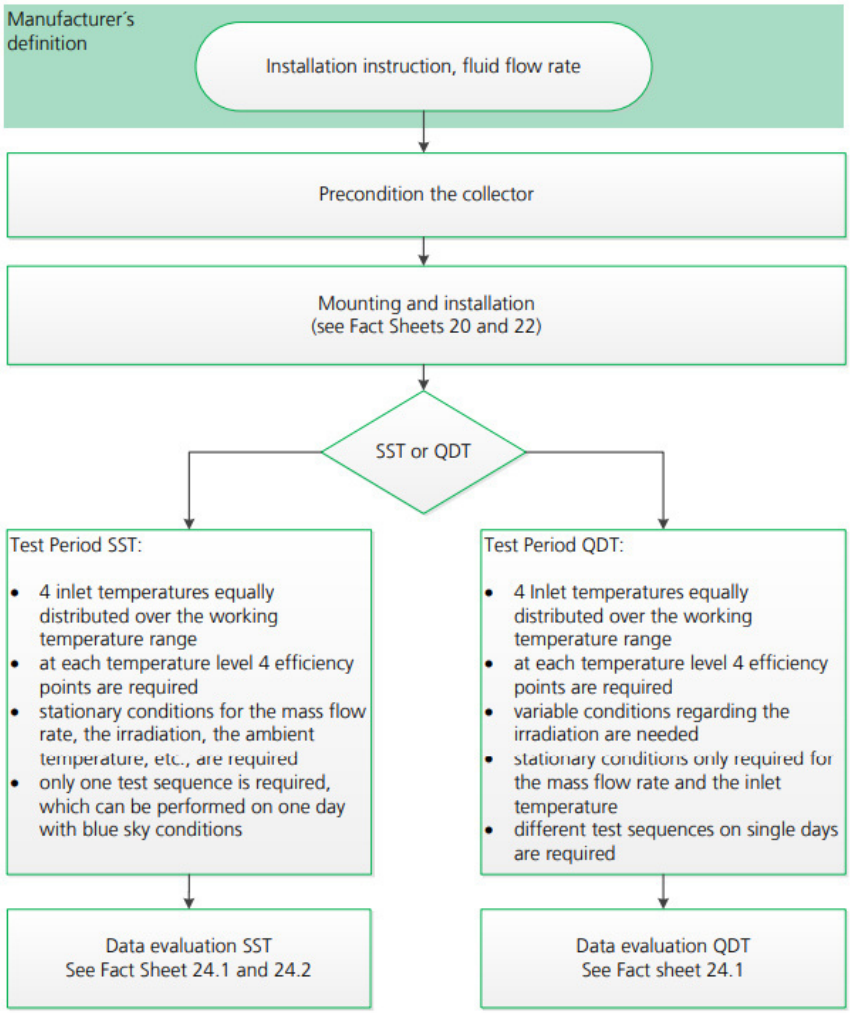

Figure 2.9. Schematic of the thermal performance test procedures according to UNI EN 9806 (*Guide to Standard ISO 9806 : 2017*, 2018) for SST and QDT methods.

Thermal performance tests can be performed both on indoor or outdoor test rigs. For the indoor testing, solar irradiance simulator has to be used as well as a wind simulator, both with specific requirements on physical and technological characteristics. Alternatively, ISO 9806 allows outdoor testing under natural weather conditions with the steady-state (SST) or the quasi-dynamic test method (QDT) (Lammle, 2018).
The equation of the thermal efficiency curve of solar thermal collectors in its simplest form, as reported in (ISO 9806 2013), is given by:

$$\eta_{th} = \eta_{th,o} - c_1 \frac{(T_m - T_a)}{G} - c_2 \frac{(T_m - T_a)^2}{G} \tag{2.43}$$

where $\eta_{th,0}$ is the thermal conversion factor and c_1 and c_2 are the linear and quadratic heat loss coefficients. The temperature difference between mean fluid temperature T_m and ambient temperature T_a divided by the normal irradiance G is often also noted shortly as the reduced temperature $\Delta T/G$.
The equations for assessing the extracted thermal power $\dot{Q}_{th}$ [W] according to ISO 9806:2013, and then according to ISO 9806:2017 are summarized in (Kramer, 2020) and are reported below.

1) In ISO 9806:2013 two equations for steady state test method, one specific for glazed liquid collectors and one for unglazed liquid collectors, and one equation for quasi dynamic test method are indicated.
The equation of steady-state test (SST) method for glazed liquid heating collectors is:

$$\dot{Q}_{th} = A_G G\left[\eta_{0,\text{hem}} - a_1((\vartheta_m - \vartheta_a)/G) - a_2\,\mathrm{G}((\vartheta_m - \vartheta_a)/G)^2\right] \tag{2.44}$$

The equation of steady-state test method for unglazed liquid heating collectors is:

$$\dot{Q}_{th} = A_G G''\left[\eta_{0,\text{hem}}(1 - \mathrm{b}_u \mathrm{u}) - (\mathrm{b}_1 + b_2\,\mathrm{u})((\vartheta_m - \vartheta_a)/G'')\right] \tag{2.45}$$

Under quasi dynamic test (QDT) method the equation has to be considered:

$$\dot{Q}_{th} = A_G \left[\begin{array}{l} \eta_{0,\mathrm{b}} K_b(\theta_L, \theta_T)\,\mathrm{G}_b + \eta_{0,\mathrm{b}} K_d\,\mathrm{G}_d - a_1(\vartheta_m - \vartheta_a) - a_2(\vartheta_m - \vartheta_a)^2 - \\ a_3 u(\vartheta_m - \vartheta_a) + a_4(E_L - \sigma T_a^4) - a_5(d\vartheta_m/dt) - a_6 uG \end{array}\right] \tag{2.46}$$

How it is possible to see while for the steady-state method the peak collector efficiency based on hemispherical irradiance ($\eta_{0,hem}$) is considered, in equation (2.46) the peak collector efficiency based on beam irradiance ($\eta_{0,b}$) is used. With respect to the steady-state one, the quasi-dynamic test method offers a much more complete characterization of the collector, and a much wider range of collectors can be tested within the same method. Furthermore, as reported in (Fischer and Drück, 2014) less restrictions in the test requirements makes it easier to find periods for outdoor testing.

2) According to ISO 9806:2017 standard for liquid heating collectors the extracted thermal power $\dot{Q}_{th}$ [W] is modelled as follows:

if steady-state test method is considered:

$$\dot{Q} = A_G \begin{bmatrix} \eta_{0,hem} G_{hem} - a_1(\vartheta_m - \vartheta_a) - a_2(\vartheta_m - \vartheta_a)^2 - a_3 u'(\vartheta_m - \vartheta_a) + \\ a_4(E_L - \sigma T_a^4) - a_6 u' G_{hem} - a_7 u'(E_L - \sigma T_a^4) - a_8(\vartheta_m - \vartheta_a)^4 \end{bmatrix} \quad (2.47)$$

if quasi dynamic test method is considered:

$$\dot{Q} = A_G \begin{bmatrix} \eta_{0,b} K_b(\theta_L, \theta_T) \mathrm{G}_b + \eta_{0,b} K_d \, \mathrm{G}_d - a_1(\vartheta_m - \vartheta_a) - a_2(\vartheta_m - \vartheta_a)^2 - \\ a_3 u'(\vartheta_m - \vartheta_a) + a_4(E_L - \sigma T_a^4) - a_5(d\vartheta_m / dt) - a_6 u' G - \\ a_7 u'(E_L - \sigma T_a^4) - a_8(\vartheta_m - \vartheta_a)^4 \end{bmatrix} \quad (2.48)$$

The thermal performance coefficients for the thermal power output calculation of the PV/T collectors should be determined in MPP mode since the electrical mode of operation has a significant impact on the thermal efficiency (Lämmle *et al.*, 2017). It is worth to note that in the 2017 version of the ISO 9806, the two steady state equations are combined to only one equation which can be used for both glazed and unglazed PV/T collectors. From a comparison between ISO 9806: 2013 and ISO 9806: 2017 it is possible to see that while the equation of steady-state test method for unglazed collectors (2.45) uses the net solar irradiance (*G"*), in the 2017 version (equation 2.47) the hemispherical solar irradiance is considered (G_{hem}). Furthermore, the surrounding air speed (u) is replaced by the reduced surrounding air speed (u'), which is equal to $u' = u$ - 3 m/s (Kramer, 2020).

REFERENCES

Aste, N., Leonforte, F. and Pero, C. Del (2015) 'Design, modeling and performance monitoring of a photovoltaic – thermal (PVT) water collector', 112, pp. 85–99. doi: 10.1016/j.solener.2014.11.025.

Barbu, M., Siroux, M. and Darie, G. (2021) 'Numerical model and parametric analysis of a liquid based hybrid photovoltaic thermal ({PVT}) collector', *Energy Reports*. doi: 10.1016/j.egyr.2021.07.058.

Chow, T. T. (2003) 'Performance analysis of photovoltaic-thermal collector by explicit dynamic model', *Solar Energy*, 75(2), pp. 143–152. doi: 10.1016/j.solener.2003.07.001.

Duffie, J. A. and Beckman, W. A. (2013) *Solar engineering of thermal processes*. Fourth Edi. John Wiley & Sons. doi: 10.1016/0142-694x(82)90016-3.

Fischer, S. and Drück, H. (2014) 'Standards and Certification Schemes for Solar Thermal Collectors, Stores and Systems — An Overview about the Latest Developments', *Energy Procedia*, 57, pp. 2867–2871. doi: https://doi.org/10.1016/j.egypro.2014.10.320.

Florschuetz, L. W. (1979) 'Extension of the Hottel-Whillier model to the analysis of combined photovoltaic/thermal flat plate collectors', *Solar Energy*, 22(4), pp. 361–366. doi: 10.1016/0038-092X(79)90190-7.

Guide to Standard ISO 9806 : 2017 (2018). doi: 10.13140/RG.2.2.27725.08168.

Helmers, H. and Kramer, K. (2013) 'Multi-linear performance model for hybrid (C)PVT solar collectors', *Solar Energy*, 92, pp. 313–322. doi: 10.1016/j.solener.2013.03.003.

Keymark website (2018). Available at: https://keymark.eu/en/.

Kramer, K. (2020) *Status Quo of PVT Characterization*. doi: 10.18777/ieashc-task60-2020-0004.

Lammle, M. *et al.* (2016) 'Development and modelling of highly-efficient PVT collectors with low-emissivity coatings', *Solar Energy*, 130, pp. 161–173. doi: 10.1016/j.solener.2016.02.007.

Lammle, M. (2018) *Thermal management of PVT collectors : development and modelling of highly efficient glazed, flat plate PVT collectors with low emissivity coatings and overheating protection*.

Lämmle, M. *et al.* (2017) 'PVT collector technologies in solar thermal systems: A systematic assessment of electrical and thermal yields with the novel characteristic temperature approach', *Solar Energy*, 155, pp. 867–879. doi: https://doi.org/10.1016/j.solener.2017.07.015.

Magalhães, P. L. (2018) 'Extension of the Perers model for photovoltaic-thermal (PV-T) collectors', *Solar Energy*, 174(May), pp. 455–462. doi: 10.1016/j.solener.2018.09.012.

Perers, B. (1993) 'Dynamic Method for Solar Collector Array Testing a N D Evaluation

With Standard', *Solar Energy*, 50(6), pp. 517–526.

Perers, B. (1997) 'An improved dynamic solar collector test method for determination of non-linear optical and thermal characteristics with multiple regression', *Solar Energy*, 59(4-6–6 pt 4), pp. 163–178. doi: 10.1016/S0038-092X(97)00147-3.

Pressiani, M. (2016) *Photovoltaic / thermal hybrid solar collectors . trnsys analysis and possible improvements*. POLITECNICO DI MILANO.

Specialists, T. – T. E. S. (2017) 'TESSLibs 17 HVAC - Component Libraries for the TRNSYS Simulation Environment - Electrical Library Mathematical Reference TESS'. Madison, Wisconsin, USA, pp. 1–40.

UNI EN 12975-2 (2006) Thermal solar systems and components – Solar collectors – Part 1: General requirements, Part 2: Test methods.

UNI EN ISO 9806 (2017) Energia solare - Collettori solari termici - Metodi di prova.

Wolf, M. (1976) 'Performance analyses of combined heating and photovoltaic power systems for residences', *Energy Conversion*, 16(1–2), pp. 79–90. doi: 10.1016/0013-7480(76)90018-8.

3. Air to water heat pumps for DHW production

Electrification of water heating systems has recently gained ground more and more as a prime option for achieving a low-carbon building sector.
Buildings are responsible for a huge share of energy, electricity, and water consumption across the globe. Analysing the statistical data of the European Heat Pump Association (EHPA) (ehpa website, 2021), it emerges that buildings account for 36% of EU CO_2 emissions and approximately 40% of final energy consumption. Consequently, the building sector has a great potential to deliver significant cuts in energy consumptions. Furthermore, the replacing of old and inefficient water heating devices across Europe would have an enormously positive effect to accelerate the transition to the carbon-neutrality goals set for building by 2050 (*Heating Market Report 2020*, 2021).
With the rapid growth of energy consumption in the building sector and the consequent necessity to develop energy efficiency strategies, the application of heat pump systems seems to be a competitive solution to improve energy efficiency, as also reported in (Lun and Tung, 2020).
In (Gaur, Fitiwi and Curtis, 2021) is highlighted that heat pumps have an important role in the decarbonisation of the heating sector as they can be a source of flexibility in the power system and can upgrade waste heat to provide low-cost heating in district heating networks.
EHPA statistics showed that European heat pump sales grew by 7.4% in 2020, with 1.62 million units sold across Europe (ehpa website, 2021). In particular, three main factors have been identified that led to the growth of the heat pumps market:

1. Compared to a decade ago, heat pumps operate efficiently over a wider temperature range, allowing them to be used in a much larger share of buildings (they still operate at -25 °C and increasingly often provide hot water at a temperature of 65 °C).

2. As building standards mandate the integration of renewable energies and favour smart buildings, the need to accelerate the energy transition also in the heating and cooling sector moved heat pumps to the centre of attention of policy makers.

3. Heat pumps are particularly suitable for combined systems with photovoltaic panels which, thanks to the sharp decrease in production costs of PV technology, provide a very low-cost energy source for buildings (ehpa website, 2021).

Heat pumps are an effective means of energy production in several fields of modern technology. Different criteria are used for their classification. Depending on the type of their thermodynamic cycle and therefore in nature of fluids they use as well as the form of energy used to run them. Based on this latter they can be distinguished, for example, into vapor-compression (mechanically-driven) or absorption (thermally-driven) heat pumps. The former follows a traditional inverse thermodynamic cycle and uses a compressor usually electrically driven. Absorption heat pumps do not have a

mechanical compressor and their functioning is based on the use of a mixture of two fluids with a different vapor pressure as a refrigerant. The most common mixtures are water and lithium-bromide and water and ammonia. Another common criterion for differentiating heat pumps is based on the type/nature of thermal source their heat exchangers interact with.

The final fluid to be heated or cooled is the indoor air in most of the residential uses. The fluid flowing in heating, or cooling, devices can be the refrigerant itself, which is the case of direct expansion systems, or water exchanging heat with the refrigerant in the heat pump heat exchangers. As regards the outdoor heat source air has been and is, in general, the most diffused so far, but also geothermal and hydrothermal sources are often used. Lastly, heat pumps can be classified based on their final use which can be sanitary water production only or to both heating and sanitary water production. Finally, heat pumps can fully cover the thermal energy needs of buildings or be used in combination with a backup device in well-known "hybrid systems" (Grassi, 2018).

Although heat pumps are environmentally friendly and provide a viable path for decarbonising the heating sector, there are still economic, regulatory, structural, and infrastructural barriers that can hinder the rate of integration of the heat pump. The potential of heat pumps to abate emissions, as also reported in (Gaur, Fitiwi and Curtis, 2021), is highly dependent on the type of technology, location, and electricity mix.

To overcome their operating limits, heat pumps are very often coupled to other technologies, especially solar ones (Huang, Fan and Furbo, 2020) (Heinz and Rieberer, 2021) (Saini *et al.*, 2021) (Pena-Bello *et al.*, 2021), which are able to improve their performances and reduce energy consumptions. Compared to other alternative energy sources, solar energy is considered cheap, readily available, and nonpolluting which can be used in domestic or industrial low-temperature thermal applications (Hawlader, Chou and Ullah, 2001).

Among emerging technologies coupled to heat pump systems, PV/T hybrid solar collectors are estimated to have a high potential and a fast-growing market. The PV performance of PV/T collectors increases slightly compared with a panel with PV cells since the operating temperatures of the PV cells are reduced due to the cooling effect of the heat extraction. In combination with a heat pump, solar collectors may be operated below the temperature of the ambient air and its dew point (Hadorn, 2015).

There are many cases studies available in the literature on integrated heat pump systems and PV/T solar collectors. A solar hybrid photovoltaic-thermal heat pump system for the simultaneous provision of space heating and electricity to residential homes is investigated in (Obalanlege *et al.*, 2020). In particular, the variation of key parameters that allow controlling the performance of a hybrid system, including solar irradiance, water flow rate in the PV/T, and storage tank size, was analysed. It emerged that optimisation of the water flow rate into the PV/T panel of the system was necessary in order to maximise the total efficiency of the system.

The coupling of heat pumps with PV/T collectors has also proved to be a promising retrofit solution to improve the comprehensive economic performance (up to 49%)

efficiency and the hot water production (up to 80%) for a public bath in China (Mi, Ma and Zhang, 2020a).
The implementation of a PV/T collector to an existing heat pump (HP) heating system was simulated in (Hengel *et al.*, 2020) for a single-family house located in Graz (Austria). Improvements in terms in the seasonal performance factor (SPF) and electrical energy savings were assessed and comparisons with a standard HP heating system were made.
The present thesis is focused on the investigation of the energy performance of systems based on the coupling of air to water heat pumps with PV/T hybrid solar collectors for producing domestic hot water (DHW). The gains from using these two currently promising technologies and the benefits of their integration are investigated by analising different configurations of these integrated systems. Comparisons with more traditional technologies were performed both in terms of thermal and electrical power production and energy savings.
This chapter deals with air to water heat pumps technology applied to systems mainly dedicated to the production of domestic hot water in residential buildings.
After providing a brief description of the functioning of air to water heat pumps, the peculiarities and main critical issues of this technology are discussed.
To overcome the technological limits of heat pumps, solar integration of ASHP systems is proposed as one solution to improve their performance. With solar-assisted ASHP systems, it is possible to achieve improved techno-economic and environmental performances, to meet a higher ratio of the energy demand. These systems can also produce different types of energies, which in the case of hybrid PV/T collectors is not only heating/hot water or cooling but also electricity from PV modules.
An overview is then given of the more diffuse system's solution based on the coupling of the heat pumps with the hybrid PV/T collectors for producing DHW.
Finally, considering their actual tightening development and diffusion in the market a deepening concerning the latest technology of hybrid heat pumps is made. Here in particular, among the different variants that are labeled as “hybrid” solutions, only systems consisting of the coupling of a heat pump and a gas condensing boiler are taken into consideration.

3.1. Air to water heat pump technology

Air Source Heat Pumps (ASHPs) are the most common form of heat pump in Europe. Among the different classifications of heat pumps, the most commonly used one is based on the heat source and the distribution means of thermal energy. According to this criterion, the basic types of heat pumps are air-to-water heat pumps, water-to-water heat pumps, and air-to-air heat pumps.
Among the main factors that have favored the popularity of the air source heat pumps the following are worthy of mention:
- the use of air as the primary heat source, which is free and always available;

- there is no necessity to provide fuel storage;
- air source heat pumps are easy to install as most of them are packaged units;
- their simple structure and low initial cost (Zhang *et al.*, 2018).

However, there are also limitations in using heat pumps, especially when installations are located in cold regions because the efficiency of heat pumps is significantly affected by outdoor conditions, especially low air temperatures of the winter season. Furthermore, as winter coincides with the higher heat demand supplementary or backup heat may be required to provide indoor comfort of buildings when the outdoor temperature is extremely low (Ricardo Energy & Environment, 2020).
In the coldest climates, it is essential to take into account, when sizing the heat pump system, the possibility of a switch to reverse operation to defrost the coils. Each defrost cycle causes a decrease in the DHW temperature as well as a loss of approximately 10% of energy and energy efficiency. Furthermore, the heat pumps system takes a longer time to respond to the change in demand. It may not fully meet the quick response demand for indoor comfort. All these factors need to be considered when designing the heat pump system (Lun and Tung, 2020).
Despite these operational limitations, in the building sector Air-Source Heat Pump (ASHP) water heater is considered one of the main technological solutions to produce domestic hot water effectively (Guo, Bilbao and Sproul, 2020), as well as a more sustainable alternative to traditional electric boilers.
Although heat pump water heaters have been around for over three decades, this technology has only matured in recent years, in part because of improved systems and infrastructure as well as emerging energy conservation standards on water heating (Willem, Lin and Lekov, 2017).
A fast increase in using heat pumps for sanitary water production is taking place both as stand-alone units, where heat pumps are integrated units with built-in water storage tanks, or as heat pumps with separate storage tanks (Grassi, 2018).
The current generation of heat pump water heaters (HPWHs) reportedly offers efficiencies that are at least twice that of conventional electric water heaters in the U.S. (Shapiro and Puttagunta, 2016). Correspondingly, the electrical demand of currently available HPWHs is typically one-half that of conventional electric water heaters (NEEA, 2015). Another benefit of HPWHs is that the application of a heat pump system also reduces environmental impact by lowering carbon emissions compared to conventional electric water heaters (NEEA, 2015) (Willem, Lin and Lekov, 2017).

3.1.1 Peculiarities and functioning

Vapor compression air source heat pump (VCASHP) is generally defined as an electrically driven machine that employs a relatively small amount of external energy transfers heat extracted from a low-temperature heat source to a high-temperature heat sink. Inside the heat pump, the refrigerant flows in a closed circuit and is continuously compressed and expanded. At each cycle, a certain amount of heat is absorbed from the

air and is transferred to water in the tank, which can be integrated or not inside the heat pump storage. Accordingly, heat pumps can use renewable energy to generate cooling and heating in order to ensure the indoor comfort climate of buildings or for industrial applications. The main components involved in a compression heat pump are, how is also shown in figure (3.1), an evaporator, a compressor, a condenser, and an expansion valve.

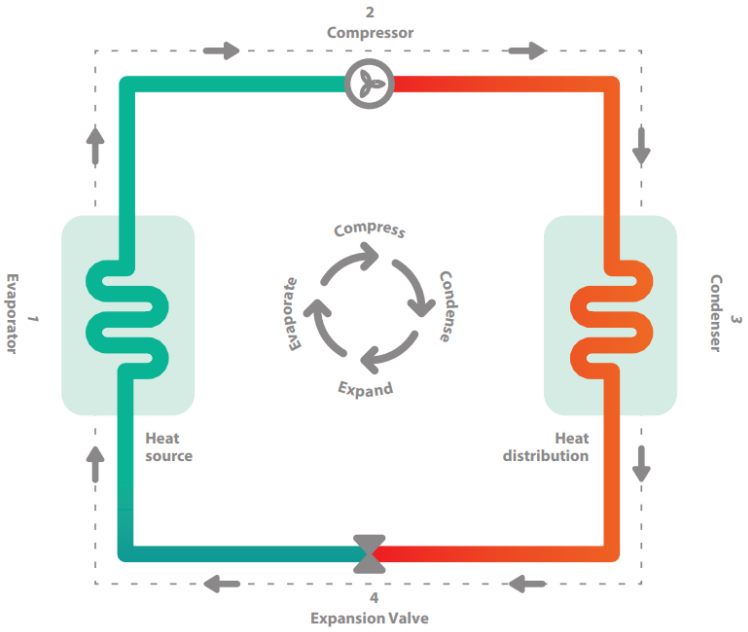

Figure 3.1. Vapour-compression refrigeration cycle (Ricardo Energy & Environment, 2020)

As already mentioned before, even if there are many renewable natural energy sources for heat pumps, which can be aerothermal, geothermal, hydrothermal heat, or non-natural processed wasted heat, air source heat pump is the most popular system used in sustainable buildings and industrial applications (Lun and Tung, 2020).
Although manufacturers have improved over the years their products with a more flexible and user-friendly control system, as pointed out in (Willem, Lin and Lekov, 2017), the currently available HPWH have not drastically evolved since the early 2000s.
Air source heat pumps can have the mono-bloc or the split system configuration, depending on whether they are made up of compact or separate units. The former can be installed entirely inside or outside the house, the latter usually have one unit inside the building and one outside. Heat is commonly distributed inside the house by a hydronic distribution system (*Market Report 2021*, no date).
HPWHs are primarily designed as replacements for traditional electric resistance water heaters (ERWHs) and can achieve higher efficiencies by using the vapor-compression heat pump cycle.
The air-to-water heat pump absorbs heat from outside cold air using the evaporator to heat water and can be used for space heating or domestic hot water supply in a cold climate and, if it can operate reversely, it can also generate chilled water for space

cooling. An example of building application of an HPWH, which has been investigated in (Lun and Tung, 2020), is illustrated in figure 3.2, as well as the vapour-compression cycle envolved.

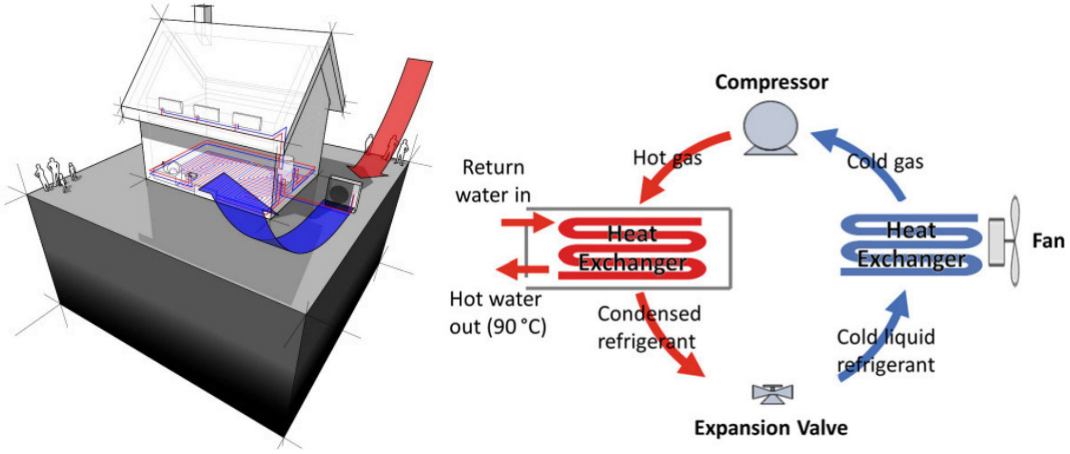

Figure 3.2. Air-to-water heat pump and vapour compression cycle (Lun and Tung, 2020)(Ricardo Energy & Environment, 2020).

The system was aimed to absorb heat from outside to inside a building to supply domestic hot water and provide space heating. In a hot climate, the reversible operations for outside heat rejection are possible to provide indoor space cooling.

Most HPWHs are hybrid devices that combine a heat pump, backup electric resistance element(s), and a storage tank (Figure 3.3). Although the heat pumps in these hybrid water heaters can heat water at high efficiencies, their recovery rate is significantly slower than traditional electric resistance heating mechanisms. Auxiliary electric resistance elements are thus also installed in HPWHs for increased reliability and quicker hot water production recovery. Most HPWHs use the heat pump whenever possible, but built-in controls switch to conventional resistance heating during times of high hot water demand (Shapiro and Puttagunta, 2016).

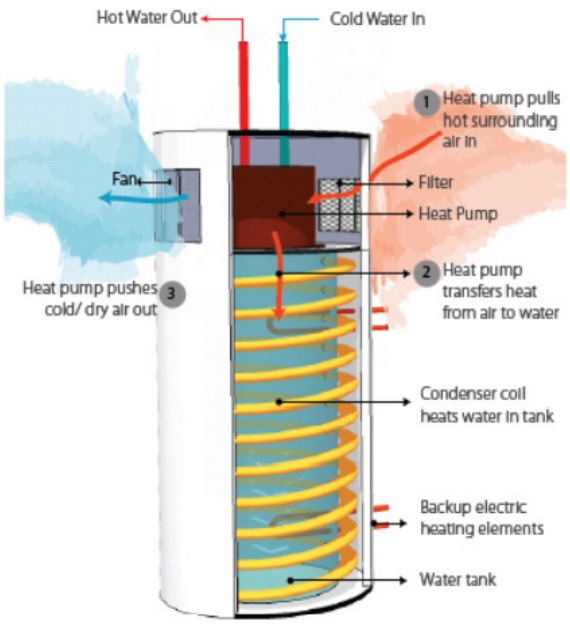

Figure 3.3. Internal view and operation of an HPWH.

Despite the various advantages deriving from the use of heat pumps in DHW systems, various factors influenced HPWHs performance. The decline of outdoor temperature, as well known, significantly affects their capacity and efficiency which may be insufficient with respect to the consumer's requirement. Furthermore, low outdoor temperatures bring the additional problem of frost build-up on the surface of the outdoor coil. This latter increasing the thermal resistance and the pressure drop across the heat exchanger, restricts air flow and reduces heat transfer across the evaporator (Willem, Lin and Lekov, 2017). Different methods can be used for the defrosting procedure. It can be done both by using a reversing valve to temporarily deliver hot gas to the outdoor coil or by diverting some discharge gas to the evaporator using a hot gas bypass valve. The duration of very low outside air temperature conditions may be relatively short, but their occurrence usually coincides with the most acute need for heating. Consequently, it is often necessary a backup heating system (Hundy, 2016).

The additional backup electric elements are designed only to operate when the tank is nearly depleted of hot water, the minimum ambient conditions are not met, or the heat pump system fails (Willem, Lin and Lekov, 2017).

Another critical issue affecting heat pump systems concerns the typology of refrigerant to be used. The choice of refrigerant plays a key role in vapor compression heat pumps. The properties of the refrigerant not only determine the performance of the vapor compression heat pump but also affect its environmental impact. Currently, refrigerant selection principles prioritize the global warming potential (GWP) and ozone depletion potential (ODP) of the refrigerant to protect the environment, with a preferred ODP value of zero and a preferred GWP less than 150 (*European Commission Regulation (EU) No 517/2014 of the European parliament*, 2014), (*EC Regulation No 842/2006 of*

the Council of 16 april 2014 on fluorinated greenhouse gases and repealing regulation, 2014).

The traditional working fluids used in heat pumps, in fact, generally have a high GWP and produce a significant greenhouse effect when leaked. Therefore, low-GWP refrigerants have recently become a topic of widespread research interest for the continuing development of vapor compression heat pumps. Much research has examined the performance, characteristics, and application potential of low-GWP refrigerants in heat pumps. Wu et al. (Wu, Hu and Wang, 2021) provide a review where analysed the use of 17 different pure low-GWP refrigerants, including natural refrigerants (R717, R718, and R744), hydrocarbons (R290, R600, R600a, R601, and R1270), hydrofluorocarbons (R152a and R161), hydrofluoroolefins (R1234yf, R1234ze(E), R1234ze(Z), R1336mzz(Z), and R1336mzz(E)), and hydrochlorofluorolefins (R1233zd(E) and R1224yd(Z)), for use in vapor compression heat pumps.

Besides Kim et al. in (Kim *et al.*, 2020) highlighted the necessity of investigating the performance improvements of HPWHs employing alternative refrigerants with low GWPs, in order to satisfy the Kyoto Protocol regulations. They presented a study aimed to evaluate the performance improvements of optimized HPWHs employing low-GWP refrigerants against the performance of a conventional R-410A HPWH. The optimization of the design parameters of the evaporator, such as the number of paths and tube diameter, and condenser was conducted for each low-GWP refrigerant analysed. The comparative performance improvements of optimized heat pump water heaters (HPWHs) employing low-global warming potential (GWP) refrigerants were evaluated against the conventional R-410A HPWH performance through simulations.

The systematic review reported in (Wu, Hu and Wang, 2021) has looked at systems using pure low-GWP refrigerants and their applications. In particular, guidelines have been developed for the use of low-GWP heat pumps in different areas of application with different output temperatures.

In (Al-Sayyab, Navarro-Esbrí and Mota-Babiloni, 2021) the effect of several low global warming (GWP) refrigerants on the proposed system is investigated and compared with R134a. The study compares eleven lower global warming potential (GWP) refrigerants from different ASHRAE safety groups (R450A, R513A, R515A, R515B, R516A, R152a, R444A, R1234ze(E), R1234yf, R290, and R1243zf) with the hydrofluorocarbon (HFC) R134a for a novel compound PV/T waste heat driven ejector-heat pump system for simultaneous data center cooling and waste heat recovery for district heating networks. For all investigated refrigerants, the novel system arrangement shows an overall system performance enhancement.

Shen et al. (Shen, Nawaz and Elatar, 2021) developed a hardware-based design model to evaluate refrigerants having lower global warming potentials to replace R-134a, including R-1234yf, R-1234ze, R-290, R-513A and R-450A, when effects of compressor size, the refrigerant charge on 24-hour uniform energy factor (UEF) and first-hour rating (FHR) were investigated for an HPWH system.

The “cradle to grave” climate impact of low-GWP refrigerants is assessed by Yang et al. (C. Yang *et al.*, 2021). In gauging the climate impact of low-GWP refrigerants comprehensively, they developed the LCCP evaluation of a domestic heat pump system using various next-generation refrigerants. The LCCP of six types of refrigerants, including HFC32, the binary blends of HFC32/HFO1234yf with different mass compositions (0.42/0.58, 0.28/0.72, 0.22/0.78) with the target GWP of 300, 200 and 150, and the blends of HFC32/HFO1234ze(E) with 0.42/0.58 and 0.28/0.72 for the respective GWP of 300 and 200, are discussed.

3.1.2 Measures of efficiency

The most important step in the design and installation of a heat pump system is the correct sizing of the heat pump. An oversized heat pump will not be efficient in generating heat and an undersized heat pump installation will never be able to meet the energy needs of the building for which it is installed.
The design of a heat pump system has to be done accurately and following the current regulations and guidance documents published by the relevant bodies. Furthermore, to justify the installation costs of a heat pump, which can be prohibitive, it is necessary to ensure that the new heat source will work efficiently and will be suitable for the type of application (Ricardo Energy & Environment, 2020).
There are various ways of estimating heat pump systems' performance. The main parameters that have to be calculated are the Coefficient of Performance (COP), the Energy Efficiency Ratio (EER), and the Seasonal Performance Factor (SPF).
When the heat pump operates in heating mode the performance efficiency is measured by the coefficient of performance. The COP is generally defined as the ratio of heat output to electricity input at a specified set of operating temperatures:

$$\text{Coefficient of performance} = \frac{\text{Rate of heat delivered (kWth)}}{\text{Power input (kWe)}} \tag{3.1}$$

When the heat pump operates in cooling mode, the performance of heat pump systems is typically evaluated through the Energy Efficiency Ratio (EER), which is defined as:

$$\text{Energy Efficiency Ratio} = \frac{\text{Total cooling capacity } (kW_{th})}{\text{Power input } (kW_e)} \tag{3.2}$$

Finally, the seasonal performance factor (SPF), defined as the ratio of the units of heat delivered in kWh over one full year to the units of electricity consumed over that same period, is a measure of the heat pump system’s operational performance (Ricardo Energy & Environment, 2020):

$$\text{SPF} = \frac{\text{Annual heat supply}}{\text{Annual electricity supply}} \tag{3.3}$$

The heat pump performance is rated accordingly to European Standard EN 14511, which specifies the laboratory conditions that must be respected during the tests.
This latter indicates the test methods for the rating and performance of air conditioners, liquid chilling packages, and heat pumps using either air, water, or brine as heat transfer media, with electrically driven compressors when used for space heating and cooling (UNI EN 14511-1, 2018).
Standard EN 14825:2019 (UNI EN 14825, 2019) instead provides temperatures and part load conditions and calculation methods for determining additional performance parameters, such as seasonal energy performance coefficients (SEER and SEER on), seasonal performance coefficients (SCOP, SCOP on and SCOP net) and efficiency.
The seasonal coefficient of performance SCOP is an average coefficient of performance of the unit in active mode for the designated heating season, determined from the part load, supplementary heating capacity (where required) and bin-specific coefficients of performance ($COP_{bin}(T_j)$) and weighted by the bin hours where the bin condition occurs:

$$SCOP = \frac{Q_H}{Q_{HE}} \tag{3.4}$$

In particular, the SCOP is a measure of the seasonal efficiency of a heat pump that takes into account how well the whole heating system works over a period of time. It is a weighted average of the COP over a full heating season at a specified boundary of the heating system. As indicated in (Chesser *et al.*, 2021), this allows a meaningful energy label to be defined for ecodesign.
The equivalent seasonal parameter for EER is the seasonal energy efficiency ratio SEER, which represents the average energy efficiency ratio of the unit in active mode for the cooling function, determined from part load and bin-specific energy efficiency ratios ($EER_{bin}(T_j)$) and weighted by the bin hours where the bin condition occurs. It is given by equation (3.5):

$$SEER = \frac{Q_C}{Q_{CE}} \tag{3.5}$$

where Q_C is the reference annual cooling demand expressed in kWh and Q_{CE} is the annual energy consumption for cooling expressed in kWh.
Further performance parameters are introduced by UNI EN 16147:2017 that is specifically dedicated to testing, performance rating, and requirements for making domestic hot water units (UNI EN 16147, 2017).
In order to assess the heat pump performance of DHW production the useful thermal energy $Q_{HP\text{-}tap}$ (kWh) during one single draw-off has to be assessed by using equation (3.6):

$$Q_{HP-tap} = \frac{1}{60 \times 1000 \times 3600} \int_0^{t_{tap}} c_p \times \rho(T) \times f(T) \times (\theta_{WH}(t) - \theta_{WC}(t)) dt \qquad (3.6)$$

where $\theta_{WH}(t)$ - $\theta_{WC}(t)$ is the temperature difference between hot water temperature at the outlet and cold water at the inlet of domestic hot water storage in K, $f(t)$ is the useful water flow rate, expressed in l/min, t_{tap} is the time duration of a draw-off of useful water in s, c_p is the specific heat capacity of water in kJ/kg K, and $\rho(T)$ is the density of the hot water at the flow meter in kg/m^3.

The associated total electrical energy consumption W_{EL-LP} is obtained from the total measured electrical energy consumption W_{EL-M_LP} (kWh) of the appliance during the measurement period of the load profile t_{TTC} following the equation (3.7):

$$W_{EL-LP} = W_{EL-M-LP} - W_{EL-Corr} + (24 - t_{TTC}) \times P_{es} + Q_{EL\_LP} + W_{EL-OFF} \qquad (3.7)$$

where W_{EL_LP} is the total electrical energy consumption during the whole load profile in kWh, t_{TTC} is the load profile time in h, and P_{es} is the standby power input in kW.

A coefficient of performance COP_{DHW} specific for the DHW production for the whole load profile is calculated using the following equation:

$$COP_{DHW} = \frac{Q_{LP}}{W_{EL-LP}} \qquad (3.8)$$

where Q_{LP} is the total useful energy content during the whole load profile expressed in kWh and W_{EL-LP} is the total electrical energy consumption during the whole load profile in kWh.

In EN 16147:2017 it is reported that the $SCOP_{DHW}$ is to be considered equal to the COP_{DHW} when determined in test condition and average climate for outdoor air units, and with the maximum load profile declared by the manufacturer.

Finally, another important parameter worth to be assessed is the maximum volume of mixed water at 40 °C in liters in a single draw-off:

$$V_{40} = \frac{1}{(40-10) \times 60} \int_0^{t_{40}} f_{\max}(t) \times \left[\theta_{WH}(t) - \theta_{WC}(t)\right] dt \qquad (3.9)$$

Where $\theta_{WH}(t) - \theta_{WC}(t)$ is the temperature difference between hot water temperature at the outlet and cold water at the inlet of domestic hot water storage in K, t_{40} is the time from starting the draw-off until $\theta_{WH}(t)$ is less than 40 °C in s, and $f_{max}(t)$ is the flow rate of hot water during draw-off in l/min.

V_{40} is calculated considering the hot water energy during the draw-off and measuring the hot water flow rate f_{max} together with the temperatures of the incoming cold water θ_{WC} and the outgoing hot water θ_{WH} are measured during the draw-off at least each 10 s.

3.2 PV/T collector-driven heat pumps

With the increase of energy consumption for a building's heating the air source heat pump (ASHP) systems assisted by solar energy have drawn great attention, owing to their great feasibility in buildings for space heating/cooling and hot water production purposes (X. Wang *et al.*, 2020).

Both solar energy technologies and air source heat pumps (ASHP) are widely used renewable energy sources at the moment. The former have the advantages of low utilization cost, simple technology, easy access, and no pollution, while the latter has the advantages of high efficiency, energy-saving, and good environmental benefits (Long *et al.*, 2021).

The coupling between thermal collectors and a heat pump can increase the overall performance of the system, as it can provide the increase of the temperature of the cold side of the heat pump. Furthermore, the heat generated by the solar panels leads to a decrease in the electrical energy consumption of the heat pump. The coupling of PV/T collectors and heat pump presents an additional advantage since the net electrical consumption of energy of the heat pump can be provided by the PV electrical production (Del Amo *et al.*, 2020).

The integration of PV/T collectors and HPs improves the performance of both sub-systems, increasing solar energy exploitation and HP efficiency while reducing defrosting cycles in air-source HPs and bore-hole depletion in ground-source HPs.

As also indicated in (Long *et al.*, 2021) the complementation system between solar and air energy can solve the poor performance of air source heat pumps under low-temperature conditions and can also make up for the shortcoming of a solar collector as an unstable energy source.

Heat pumps operate as complementary energy device of PV/T collectors since solar energy resource is intermittent and has a low energy density. At the same time, solar integration improves the heat pump functioning when the outdoor air temperature is low and its heating capacity and COP tend to decrease.

In order to improve the utilization efficiency of solar energy and air energy, a solar-assisted air source heat pump system has become an important research content.

As yet discussed in Chapter 1, PV/T collectors are the combination of photovoltaic and solar thermal technologies and present higher overall efficiency with respect to that of independent photovoltaic (PV) and thermal collectors. Besides their capability to produce electricity and thermal energy simultaneously, another attractive feature of PV/T collectors is the compactness of their structure which makes them really attractive to the residential sector (Del Amo *et al.*, 2020), where there is limited space on the roof of the buildings.

In (Miglioli *et al.*, 2021) is highlighted that PV/T-ASHP systems represent a very interesting solution also in the context of the nZEB design, being able to cover all the building thermal needs with a high share of RES.

Solar-assisted heat pump systems for DHW and space heating purposes have been studied by several researchers. Both experimental investigations and numerical studies aimed to assess the potential and performance of various system designs under different climatic boundaries. A large number of publications were made within the IEA Task 44 on solar and heat pump systems between 2010 and 2013 (Hadorn, 2012).

Hengel in his paper (Hengel *et al.*, 2020) demonstrated an implementation of a PV/T-collector to an existing heat pump (HP) heating system making a comparison to that of a standard HP heating system for a low energy single-family house consisting of four persons located in Graz, Austria. The PV/T collector provided thermal energy to increase the inlet temperature of the evaporator and to raise the ground temperature level to obtain higher COP, and hence higher seasonal performance factors. By use of the PV/T system, a proper control strategy was defined for the investigations. On the sink side of the HP, a thermal energy storage tank was used to provide energy for domestic hot water and space heating, whereas else for the latter, the heat is provided to a floor heating system (Hengel *et al.*, 2020).

Dupeyrat et al. (Dupeyrat, Ménézo and Fortuin, 2014) characterized a prototype PV/T collector and simulated the performance of a solar hot water system. They concluded that the combined PV/T panel had many advantages compared to separated PV and solar thermal collectors. The performance of an experimental hybrid collector being part of a solar thermal system in a building was determined and compared to that of systems operating with standard solar devices through simulations using TRNSYS. Comparisons according to various evaluation criteria were made assuming the same surface area and under the same climatic conditions. TRNSYS simulations were carried out that showed that the integrated PV/T technology on a limited roof area not only provides for higher total PV and exergy output but also higher primary energy-saving (and consequent potential reduction of emissions) than side-by-side installations with conventional ST and PV components.

However, even if solar thermal energy is an optimal way to integrate heat pumps systems for producing energy in building sectors, some drawbacks have been found related to the solar energy availability during the day and throughout the year. There is in fact a gap between the daily demand and the solar energy production, as the highest energy demand in a day occurs in the last hours of the day when solar radiation does not fall on the solar collectors. This mismatch occurs also with the seasonal demand if we consider that the highest space heating and DHW demand takes place during the coolest months when the solar radiation is less powerful. This critical issue was analysed by Del Amo et al. (Del Amo *et al.*, 2020) that investigated the effectiveness to compensate the daily gap with the use of water storage tanks.

Del Amo et al. (Del Amo *et al.*, 2020), in particular, showed the technical and economic feasibility of an energy system in a building at the University of Zaragoza (Spain), where a SAHP was integrated with a PV/T collector and seasonal storage and validated a simulation model with the measured data.

Thermal Energy Storages (TES) are used to balance the energy demand and supply. In (L. W. Yang *et al.*, 2021) was highlighted that they are essential for SAASHPs to mitigate solar energy discontinuity and to increase the COP and SPF of the system. TES can be connected either to the solar collector and the evaporator of the heat pump or to the condenser and the end-use. The TES can also work as a buffer to reduce the noise and voltage shocks caused by the frequent start-up and shutdown of HP.

In (Dannemand, Perers and Furbo, 2019) the results of an experimental study about a solar PV/T assisted - heat pump system with a cold buffer storage tank on the source side of the heat pump and a hot storage tank for domestic hot water preparation was presented. Measurements were performed and analysed over nine months, including a full winter season, was presented on the system subjected to real weather conditions and hot water withdrawals. In particular, the implementation of buffer storage has been assessed as a potential improvement of the system's seasonal performance.

By implementing storage between the collector and the heat pump, it was possible to store heat from a sunny period when the heat pump was not in operation to periods without solar radiation and colder air temperatures in which the heat pump needed to operate. The proposed solution resulted able to can give the heat pump better operating conditions and led to better system performance, increasing the instantaneous COP of the heat pump (Dannemand, Perers and Furbo, 2019).

The introduction of a novel hot water supply system with multi-heat-source based on PV/T (photovoltaic and thermal) heat pump and water source heat pump was studied in (Mi, Ma and Zhang, 2020b) to improve the comprehensive energy efficiency and the supply capacity of the hot water supply system for the public bath in Dalian University of Technology in China. In particular, the integration of the hot water supply system according to the characteristics of heat sources was studied and optimized to improve the comprehensive energy efficiency and the hot water production of the system. This was made both by enhancing the utilization efficiency of solar energy and by decreasing the proportion of electric boiler and other high energy consumption and low energy efficiency heat sources in the system. As result, the comprehensive COP of the system increased from 3.0 to 7.1 while the energy consumption of system operation decreased from 15.2 kWh/t to 6.0 kWh/t, the energy-saving ratio of the novel system is over 60%. Thanks to the retrofit solution an 80% increase in the plant's daily production of hot water and an improvement in the overall economic performance of 49% were achieved (Mi, Ma and Zhang, 2020a).

Besides the great amount of research about integrated PV/T and HP systems, they are quite recent technology, therefore there are many other aspects, such as economics, environmental issues, which need to be discussed and some improvements are still necessary. A focus on the main potentials and the necessary future research developments about PV/T-SAHP systems is provided in (L. W. Yang *et al.*, 2021), where a comprehensive and complete overview of these systems is performed. Further studies are for example needed to improve the defrosting process both at component and in system level. At the component level, the material or the structure of the air source

evaporator can be optimised to prevent or reduce the freezing process. At the system level, optimisation on system configuration is also a potential approach for dual-source IX-SAASHP and hybrid SAASHP. Currently, refrigerants (e.g. R22, R134a, R410A and R407C) are widely used in HP systems due to their good thermodynamic and thermophysical properties. R32 is a more environmentally friendly alternative refrigerant for R410A in ASHP. However, it is classified as a flammable refrigerant A2L and therefore some countries are researching other retrofits, such as R454B. Therefore, future studies should concentrate more on the applications of environmentally friendly refrigerants in SAASHPs responding to global restrictions. (L. W. Yang *et al.*, 2021).
A deeper investigation about storage solutions coupled to concentrating PV/T panels could be able to cover a longer heating period with the heat pump in a very cold climate such as Milan and Krakow are suggested in (Colucci *et al.*, 2019).
In (X. Wang *et al.*, 2020) further researches are recommended also regarding the following main aspects:

- optimization of the PV/T-ASHP systems, including structure, control, and operation to improve performance of the system;
- combine two or more system concepts, which may have a prospective development, e.g. combination of the heat recovery system and solar ASHP system, which can avoid the disadvantages in a single system and provide more solutions to buildings energy systems;
- Standard indicators: common standards and official certifications can help users to make better choices and comparisons among different solar-assisted ASHP systems.

3.3 Hybrid heat pumps

As already discussed above, the main performance limits of heat pumps (poor coefficient of performance and a reduced heating capacity at low evaporation temperatures in cold climates, and limitations of delivering heat at high temperatures, such as for DHW purposes) can be overcome by coupling the HPs with other devices using alternative energy sources. Different types of poly-generation systems based on HPs systems assisted by one or more other forms of technology are available in the literature, especially suitable for the residential sector. The term “hybrid heat pump” is used to indicate the most varied technological solutions involving heat pumps systems that combine at least two different energy sources and whose operation is managed by one control logic.
The most common product is the hybrid heat pump based on the combination of an electric heat pump with a gas condensing boiler (*Heating Market Report 2020*, 2021).
In the final report of Annex 45 (Friedel *et al.*, 2019) hybrid heat pumps (HHP) are intended as the combination of fossil-fired boilers and heat pumps employed in space heating and domestic hot water systems of residential and light commercial buildings.

In particular, the following definition given by the International Energy Agency is reported: “a hybrid heat pump is the combination of an electric heat pump and a fossil-fueled boiler or furnace under a single optimized control strategy”.
Another official definition was found in standard UNI EN14825:2018 (UNI EN 14825, 2019), which states that the term “hybrid heat pumps” indicates “encased assembly or assemblies as a unit consisting of an air/water(brine)/DX-yo-water(brine) electrically-driven heat pump with a second heat generator using fossil fuel, and managed by a common controller providing an optimized operation of the heat generators for space heating”.
Consequently, this paragraph is only focused on hybrid heat pumps designed to combine gas boiler heating and ASHP heating systems, both of which can contribute to domestic heating and hot water demands.
The main components of a hybrid system, heat pump, and gas boiler are well known and have already been developed into mature market products. The novelty of the hybrid concept rather lies in the optimized and integrated control strategy that can be used to maximize the performance of both components and minimize operation costs (Friedel *et al.*, 2019).
The coupling of the HPs with other devices using alternative energy sources can overcome the issues related to the poor COP recorded in cold climates, combined with a reduced heating capacity at low evaporation temperatures.
Many researchers presented heat pumps assisted by one or more other forms of technology, showing different types of poly-generation systems especially suitable for the residential sector. Different types of HPs (Fitzpatrick *et al.*, 2020) can be used equipped with gas boilers, solar collectors, or micro-CHP systems (Palomba *et al.*, 2018), (Calise, Dentice d’Accadia, *et al.*, 2017) in compact “all-in-one” devices. Experience in the design and installation of these combi-systems, especially on a small-medium scale such as in residential or small tertiary applications, is still limited, and much more effort is needed (Kalogirou and Florides, 2016). What is attractive is the dual-fuel capability of Hybrid Heat Pumps (HHP) is that they can switch between fuel sources, meaning they can use the HP, the boiler, or both to meet the heat demand. The choice of operating mode can be made depending on different parameters relating to the efficiency of the system under current circumstances, such as outdoor temperature, flow temperature, or prices of gas/electricity to name a few. Furthermore, another advantage of HHP for the user is that the rating of HPs (which is the more expensive component) can be lower because the gas boiler can be used to integrate the heat production (Sun *et al.*, 2019). In this way, as Kozarcani et al. (Kozarcanin *et al.*, 2020) reminded gas heating could have a role as a bridging technology to low carbon heating through the use of these systems.
As demonstrated by some researchers, the efficiency of the systems can be increased by using renewable sources e.g. solar panels (Lazzarin, 2020)(Palomba *et al.*, 2021)(Miglani, Orehounig and Carmeliet, 2017), or a geothermal plant (Wang *et al.*,

2017). The performance is always heavily influenced by climatic conditions and by installation conditions (Carroll, Chesser and Lyons, 2020).

The operation of hybrid heat pumps can be managed by an electronic control system that determines the heat requirements and optimises the operation of the two sources to minimise the running cost. The compressor is usually speed controlled, and the water flows and can be regulated. These constitute outputs from the control logic along with heated water temperature.

"Based on pre-set preferences chosen by users (e.g. minimise CO_2 emissions or running costs), the hybrid's control will select the most appropriate operation mode for the heater in a given building, climate zone, and current energy prices. This reliance on two technologies makes hybrid heat pumps very efficient: in well-insulated buildings, the heater will operate mostly as a heat pump during spring and autumn. It will then use the condensing boiler during the coldest days of the year or in old, less insulated buildings. Moreover, they can be installed without any prior adaptation of the building envelope and they facilitate staged renovation, i.e. to progressively add insulation. To cut CO_2 even further, they can be used with decarbonised and renewable fuels and electricity" (*Heating Market Report 2020*, 2021).

Many barriers exist to large-scale uptake of heat pumps, however hybrid heat pump technology can help to mitigate some of the traditional barriers. Hybrid add-on heat pumps have the benefit of being cheaper than standard electric heat pumps due to the smaller size requirements. They may reduce customer resistance to heat pumps as consumers are used to gas-powered heating. They can also be used to deliver a high-temperature heating output (using the boiler for backup) and domestic hot water. Furthermore, experience in the design and installation of these combi-systems, especially on a small-medium scale such as in residential or small tertiary applications, is still limited, and much more effort is needed. They are new to the market and there is a lack of trial information, and so the cost benefits and performance are unproven. Hybrid heat pumps also suffer from other commonly quoted barriers to heat pumps, such as concerns over the performance of earlier heat pump installations, and the need for additional space. (BEIS, 2016).

A comprehensive review has been performed on hybrid systems using Heat Pumps (HPs) for HVAC systems and DHW production using case studies from 2016 to 2022. After an explanation of the methodology used to carry out the review, the layouts of the systems are described, including the type and size of the components as well as the type of devices utilised. This work focuses in particular on studies that investigated systems with HPs assisted by a gas boiler. Some studies that considered the exploitation of renewable energy sources, but not as a whole substitute for fossil sources, have also been considered.

Furthermore, advances in numerical analysis methods for HP control are investigated by distinguishing the type of method applied: rule-based control methods or predictive control methods. In the case of the former, the review considers control methods based on predefined threshold values of trigger parameters (such as energy price, load, power,

time), which are constantly monitored. When a threshold is reached, it triggers a control action on the HP (such as start/stop or change in set-point among others). In the case of the predictive control method, the studies are analysed based on a black or grey box model of the process used to estimate a future control signal. These models can forecast a parameter and/or behaviour of the system or the load and send an input to correct the operation of the plant (i.e. controls based on machine learning). Finally, the review also analyses the performance of the systems in terms of energy and economic aspects, according to their location and the respective climate. Concerning energy, the location can influence performance in terms of the specific energy carrier and the availability of energy sources. Regarding economic issues, the different revised installations can vary according to specific political actions. Several key performance indices (KPI) are described and commented on.

3.3.1 Layouts of Hybrid Heat Pump systems

The search performed allowed identifying different layout applications. In general, the HP represents the main central part of the system with air-water HPs being the most commonly used. The systems used to produce DHW are equipped with a storage tank. The boiler is used to produce heating (when it is the best option according to the control strategies) and to provide additional heating if the energy produced by the HP is not enough. The heat transfer system temperature is set relatively low during most of the heating season, even if it is not strictly set up for 'low-temperature heating'. Only during winter or in very cold conditions can the boiler component outperform the HP regarding primary energy, CO_2, or running costs. Thus, an HP retrofit is useful if the transfer system is suitable for low-temperature heating during an important part of the heating season. The system can be sold as an integrated system or as separate components. In the latter case, the HP does not need to be from the same manufacturer as the boiler. Indeed, it could be installed in addition to an existing boiler that was installed at an earlier time.

In Annex 45 studies (Friedel *et al.*, 2019), a few European countries and the Canadian market have been analysed in the context of domestic housing. The authors found two main examples of typologies: an integrated package and an add-on package with a ventilation exhaust source. Regarding the first, the HP represents an added system to the boiler. Consequently, the gas boiler and HP do not need to be produced by the same manufacturer. This solution enables the retrofit of existing boilers as hybrid systems. Furthermore, since there is no need to physically integrate the HP and the boiler, the two components can be installed in separate rooms. On the other hand, the integrated package solution foresees that the boiler and the HP are sold together, most often delivered by the manufacturer in a single physical box.

It was recorded that integrated hybrid packages are by far the most commonly available solution. Because the HP and boiler have been designed to work together, there is

minimal risk of problems involving placement or controls. Only where boilers installed at an earlier time are already a fairly widespread technology for heating buildings, as in the case of the Dutch market, is the "add-on" solution advantageous for energy retrofit. For the most common hybrid packages, there is only a limited number of configurations, mainly based on the presence or not of storage for hot water production, which is basically determined by typical local preferences. If a storage tank is present, it is only natural to use the HP to deliver the hot water demand, while, if not, hot water will be produced by the boiler.

Add-on systems are very prevalent in some countries (e.g. in the Netherlands) where high-quality condensing boilers cover most of the share of the heat demand of houses. In such contexts, in fact, add-on systems represent an easy retrofit solution allowing the customers to enhance their existing boiler by adding an HP with very few operational risks.

From the analysis of the studies in the literature, it emerged that the schemes of the systems based on HPs are essentially based on the same structure. Small variations are found with regard to possible additional components and control logics.

In general, the operation of the entire system and the distribution of loads between the two heating devices are managed in such a way as to meet the minimum total cost of the energy process. Beyond the different control logics proposed, discussed in detail in paragraph 3.3.2, particular attention was paid to the main critical issues encountered in the design and sizing of HP systems. In recent years, several efforts have been made to pursue the best system configuration in terms of component sizing and load profile, as these are factors that greatly influence the performance of the HP.

The heating system investigated in (Li, 2018) presents a base structure consisting of a gas-fired water heater coupled with an air-source heat pump (ASHP) characterised by a rated capacity of 25 kW (Figure 3.4). A parallel hybrid heating system was designed to investigate the water flow rate distribution for two different types of space heating (underfloor heating and internal radiators). The study proposed a parallel loop configuration for the space heating of a residential building in cold climate conditions.

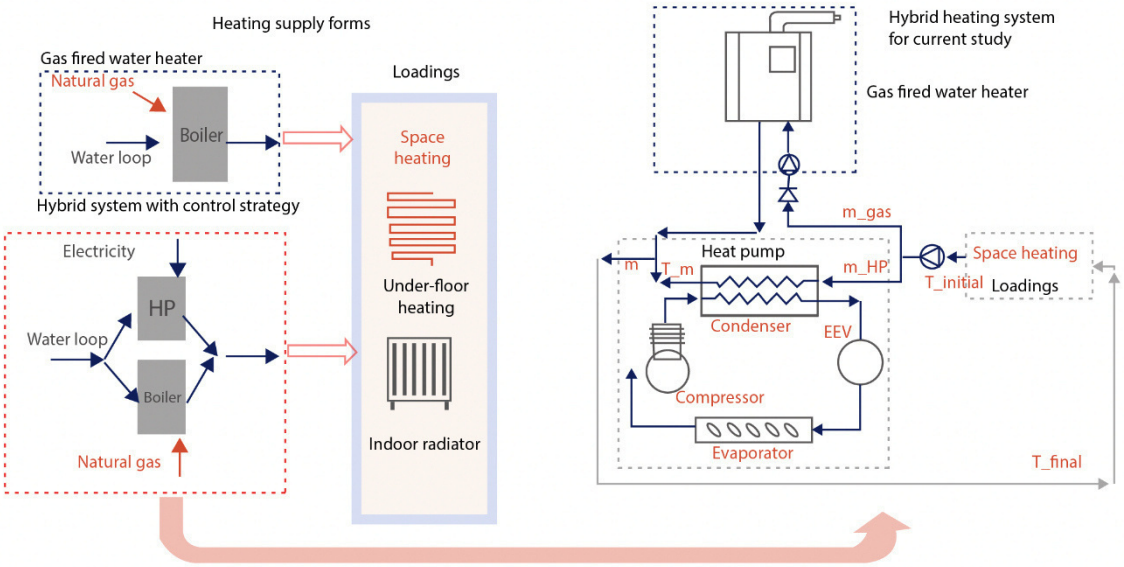

Figure 3.4. Schematics of HP and gas fired water heater system (Li, 2018).

The gas heater was dedicated to the underfloor heating system, while the hybrid system gas boiler – ASHP – provided space heating through the inner radiator system. The mainstream water flow rate, adjusted with a multistage centrifugal water pump, was divided into two circuits, one for the gas boiler and the other for the HP. Finally, the two streams were mixed together to reach the desired final temperature.

The aim of Keogh et al. (Keogh *et al.*, 2019) was to study the suitability of a compact hybrid electric-gas heat pump system as a retrofit measure for an Irish residential dormer bungalow built in 1999 with a floor area of 160 m^2 with an easterly facing aspect and retrofitted from a condensing gas boiler system to a hybrid heat pump system. The system (Figure 3.5) was a commercially available air source hybrid heat pump system and it was composed of a split system consisting of an outdoor unit (electric air-to-water heat pump) and an indoor unit containing a condensing natural gas boiler and heat exchanger. The heat pump had a nominal output of 8 kW and the gas boiler 33 kW.

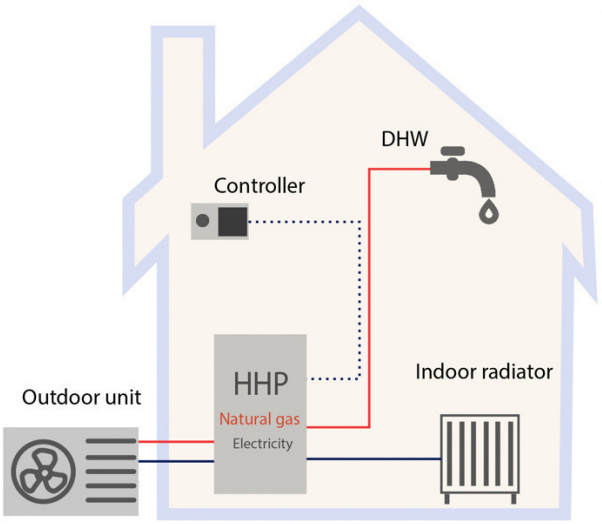

Figure 3.5. HHP system schematic (Keogh *et al.*, 2019).

Actually, in most of the research analysed there is also a buffer tank or a thermal energy storage system. Jarre et al.'s (Jarre *et al.*, 2017) study compared different thermal energy generation technologies to provide space heating to three existing buildings located in Turin, Italy: an electric resistance (ER), a traditional natural gas boiler (NGB), a heat pump + backup electric resistance (HP+ER), and a hybrid natural gas boiler and heat pump + backup electric resistance (NGB+HP+ER). They found that the adoption of a hybrid system (heat pump and natural gas boiler working alternately) provides advantages in terms of reduced primary energy consumption only if the required supply water temperature is high. In some cases (mainly in more recent ones), the system HP-gas boiler is compact, such as in the system presented by Bennet et al. (Bennett *et al.*, 2021), who studied and mapped the boundaries of how CoCo hybrid heating can impact the home heating sector in comparison to both the incumbent technology (gas boilers) and the leading low carbon technology (heat pumps) in UK scenarios. To do this, they simulated five heating system scenarios in the model to convert the building heating load into gas and/or electricity demand. The first scenario represented the current status quo of near universal use of gas boilers for heating. Another scenario considered the use of air source heat pumps (ASHP), and the other 3 scenarios analysed a CoCo (compact combination) hybrid consisting of a 28kW heat output gas boiler plus 4kW heat output ASHP with three different control scenarios.
In the hybrid heating system analysed in (Dongellini, Naldi and Morini, 2021), for example, which is based on an air-to-water HP coupled to a gas boiler working as a backup device, a small water buffer tank of 79 L is added. The considered thermal storage allowed an increase in the system's thermal inertia and the limitation of the frequency of the HP on-off cycles. The heat generators in this configuration were connected in series, in order to improve the HP energy performance according to a lower sink temperature (Figure 3.6).

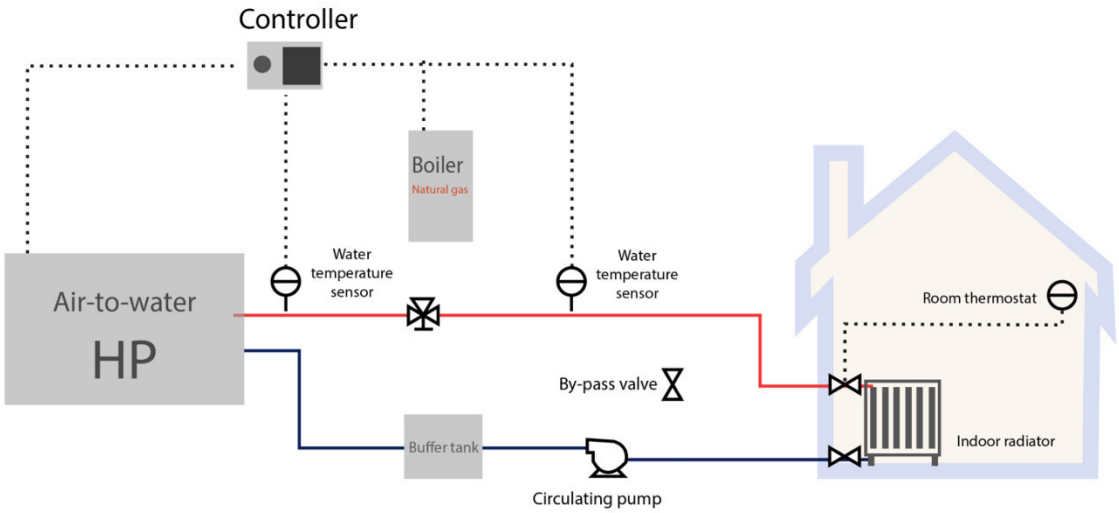

Figure 3.6. Layout of HHP system based on air-to-water heat pump and condensing gas boiler (Dongellini, Naldi and Morini, 2021).

Each thermal zone was heated by low-temperature radiators, each one equipped with a thermostatic valve. The design supply temperature was set to 55□ and the design water flow rate was calculated for each radiator by considering a temperature difference of 10 K. Moreover, the set-point temperature of the supply of hot water to the emitters was variable based on the outdoor air temperature. The boiler used in these simulations was a condensing gas-fired unit. Both heaters were activated in parallel during the whole heating season with priority on the HP, considered the main heater of the system.

Several studies have also been conducted on HP systems coupled with thermal storage tanks. It has been proven that these devices can increase the system performance, as their presence allows the operation of the HP to be shifted to the most profitable periods, minimising both the operating cost and the consumption of primary energy. For instance, the effect of the presence of a thermal storage tank on the operation of an HP was analysed in (D'Ettorre, Conti, *et al.*, 2019). A hybrid generator composed of an air-to-water electrically-driven HP coupled with a gas boiler was considered in order to analyse the cost-optimal sizing and hourly control strategy of an HP system for heating applications. The two generators operated in parallel mode, making this the most widespread solution in existing applications. Two cases were analysed: a baseline layout without thermal energy storage (represented in black in the scheme below) and the effective layout in which the storage is inserted (represented in red). In the latter, the thermal storage tank was connected in parallel to the hybrid generator, with the purpose of decoupling energy generation from energy distribution, taking advantage of the best possible working conditions for the HP.

For this study, an experimental apparatus was set up in order to characterise the HP behaviour. This included a primary hydraulic circuit consisting of an 8 kW HP and a hydraulic separator, from which a secondary hydraulic circuit was derived to connect the hydraulic separator to a cold-water storage tank. The HP operation was investigated under different working conditions in a climatic chamber. The flow rate in the primary

circuit was kept constant, while in the secondary circuit the flow rate can be varied according to the building thermal load to be simulated. Part of the ongoing flow from the manifold was then sent to the water storage tank, which was kept at a constant temperature using a chiller, while the other part of the flow bypassed storage through a three-way valve. Subsequently, the water leaving the storage tank was mixed with the by-passed flow to reach the desired return temperature to the manifold and, therefore, to the HP. Furthermore, to emulate different outdoor temperature conditions, the temperature inside the climatic chamber was varied employing an air handling unit.

In the HP system analysed in (Mehrfeld *et al.*, 2020) a combi-tank was considered, which integrated both thermal energy storage (TES) and the system controller. The calibration of a hybrid system consisting of an air source HP, a condensing gas boiler, a thermal energy storage, and a system controller was performed. The experimental setup used to collect the data necessary for the calibration process is reported in Figure 8, with details of the sensors for monitoring the operation of the system. The hybrid system consisted of an air source HP, a condensing gas boiler, and a combi tank as thermal energy storage.

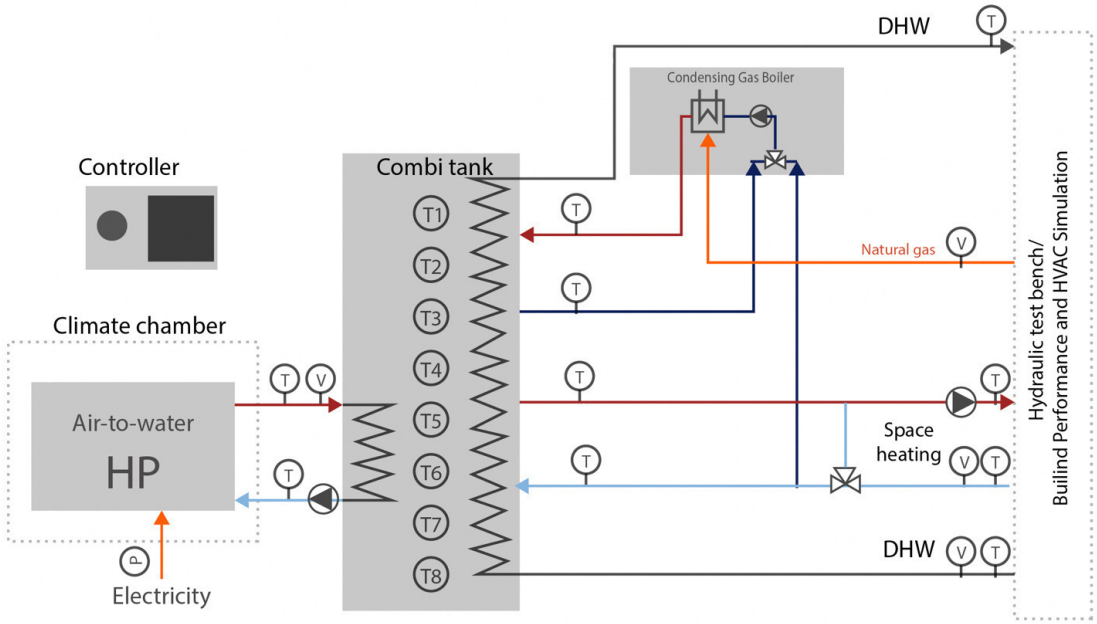

Figure 3.7. Experimental setup for data acquisition (Mehrfeld *et al.*, 2020).

The HP is an on/off controlled monoblock unit located in the outdoor surroundings. Furthermore, the integration of the system with a photovoltaic system was also considered. Three scenarios were simulated to analyse the performance of the system as the final use of electricity produced by the PV varies.

In d'Ettorre et al. (D'Ettorre, De Rosa, *et al.*, 2019) a comparison between a system with a tank and one without a tank was reported. As regards the impact of the tank, the authors demonstrated its cost-effectiveness. Indeed, it allowed the operation of the HP by taking advantage of periods during which low electricity tariffs apply. So, it allowed

load-shifting throughout the day, by limiting the use of the boiler to periods when the COP was lower than the COP of economic equivalence. The authors calculated a cost-saving of up to 8% and a reduction of primary energy consumption (and consequently of CO_2 emissions) of up to 13% compared to the configuration without a tank.

As stated in the introduction, some studies considered the integration of renewable sources such as PV panels in addition to the thermal storage system, in order to exploit the electricity locally produced. In this way the coverage rate of the electricity needed to power the HP further increases. In the research work of Fitzpatrick (Fitzpatrick *et al.*, 2020), a three-storey residential building located in Wüstenrot, Stuttgart, Germany was studied. In this case, the heating system consisted of an air-water HP (HP) equipped with thermal energy storage (TES) and a gas boiler.

During operating hours, the thermal demand requested by the building can be met by the boiler, the HP, and/or the tank. This switching was managed by an implemented control strategy aimed at minimising the energy bill. The compact hybrid heating system with a water tank as thermal energy storage presented by Zanetti et al. (Zanetti *et al.*, 2020) was assisted by photovoltaic panels as well. In their work, they implemented the model in a MatLab environment of the system in order to investigate the energy cost savings and the optimal control strategies together with a baseline rule-based controller (RBC).

The GSHP application has seen a rapid increase during the past years, mainly in heating-dominant climate zones where the advantages over other heat pump or boiler-based heating systems are particularly high (You *et al.*, 2021).

As mentioned in the introduction, other researchers presented studies about systems that combine a gas boiler and ground-source HPs. In this case, by considering the initial investment of GSHP, fossil fuels can be integrated with the GSHP system to supplement the peak heating load and mitigate soil thermal imbalance (Wang *et al.*, 2017). In most cases, the GSHP system operates as the main heat source and the boiler runs as a supplementary one. This kind of integrated system can take advantage of the boiler for its low initial investment and in GSHP systems for its energy-saving (Xu *et al.*, 2021) (Rivoire *et al.*, 2018).

It should be noted that this can depend on the characteristics of specific case studies, such as in (Allaerts *et al.*, 2016). The authors presented an HHP installed in a school building both heated and cooled by a combination of floor heating, fan coils and a central air handling unit. In this case, for the whole building, the heat was provided by a single HP, which worked at a temperature regime of 45/35 °C. The gas-fired boiler provided back-up heating, but it was used as a primary heat source for the older buildings in the school complex.

Of course, these hybrid systems are preferred over unitary systems due to higher efficiency (Soni, Pandey and Bartaria, 2016). In some cases, the hybrid systems (or better the gas boiler components) are assisted not only by the ground source, but also by a solar thermal collector. While, Zhou et al. (Zhou *et al.*, 2017) investigated a hybrid experimental space heating system that comprised the novel mini-channel solar thermal

and PV/T panels, many other studies are based on HHP assisted by ground sources for different end-uses and in different climate conditions. Menberg (Menberg *et al.*, 2017) investigated a thermodynamic model for each subsystem in a hybrid heating and cooling system of an existing building, the architecture studio building of the University of Cambridge, by using the concept of cool and warm exergy. Liu e Xu (Liu *et al.*, 2017) focused their attention on the feasibility and performance of HGSHP in Shenyang, located in a cold area, in a typical office building with seven layers. Between the different configurations for different end-uses of ground source HP, Picard (Picard, 2017) evaluated the performance of an HHP (ground source HP and gas boiler) for a school. Ikeda et al. (Ikeda, Choi and Ooka, 2017) modelised a simple system configuration composed by an air source HP, a ground source HP for cooling, a ground source HP for hot water, an auxiliary boiler, a pump for circulating fluid of BHE loop, and a pump for heat sources. Their aim was to develop an efficient optimisation method to determine optimal operations of the hybrid ground source HP system used to handle the cooling load and hot water demand.

Aditya (Aditya and Narsilio, 2020) adopted a multi-objective optimisation method to study the economic and environmental performance of hybrid ground source HP systems in seven Australian cities. In particular, they investigated two hybrid systems, one composed of a GSHP system and a reverse cycle air conditioner system, and one composed of a gas boiler, a reverse cycle air conditioner system for cooling and a GSHP system. To find the best solution set, they used a Pareto optimal approach. The results of the study (Aditya and Narsilio, 2020) showed that the systems are affected by the efficiency of the components, climatic conditions, energy price ratio between gas and electricity, and the emission factor ratio between electricity and gas.

Some studies considered the combination of an HP and an auxiliary gas boiler for polygeneration systems. In Calise et al. (Calise *et al.*, 2016), they presented a dynamic simulation model and a thermo-economic analysis of a system aimed at providing space cooling and space heating and domestic hot water (DHW) all year long. In this case, the main elements were the solar collectors used to cover the electrical demand of the users and supply energy to the electrical grid.

The same authors (Calise *et al.*, 2016) presented a similar study, but in (Calise, Macaluso, *et al.*, 2017) they included the electrical energy storage and the bidirectional connection with the national grid. The layout was composed of PV/T panels, three thermal storage systems, a solar loop heat exchanger, an auxiliary boiler, a storage system used to store the eventual solar heat in excess, a reversible water to water HP, an adsorption chiller, a cold water surface aquifer well, which provided cooling water to the condenser of the HP (when operating as an auxiliary device) or to the cooling side of the adsorption system, an inertial hot/chilled water regulation tank, a hydronic fan-coil system that supplied thermal energy for space heating and cooling, a regulator/inverter for the electrical energy fluxes of the solar field, user demand, battery and grid, a lead acid battery system that stored the electrical energy and mixers.

In addition to the standard air-to-water type, which seems to be the most widespread one, other types of HPs have also been proposed in the literature within hybrid configuration systems, such as split-type air conditioners. In this regard, Wang et al. in (J. Wang *et al.*, 2020) studied and modelled a smart home with a novel hybrid heating system, which consisted of a wall-hung gas boiler (WHGB) that was connected to a water tank with an auxiliary electric resistance heater (RH) and auxiliary split air conditioners (ACs). The WHGB was aimed at both space and water heating, while RH was only for water heating and ACs for space heating. Besides the hybrid heating system, the smart home was also equipped with an onsite photovoltaic (PV) system, a battery energy storage system, an electric vehicle, and various types of flexible loads (Figure 3.8). As shown in the scheme "below", the wall-mounted gas boiler had two separate circuits for space and water heating.

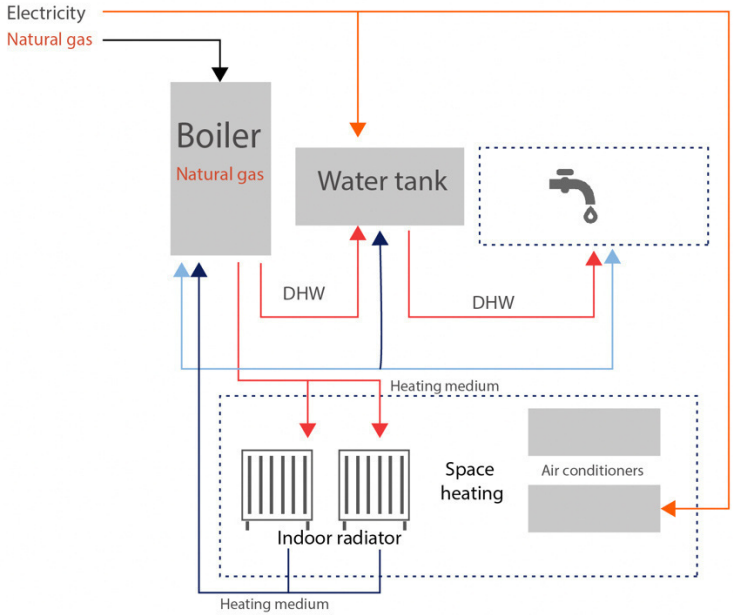

Figure 3.8. The structure of the hybrid heating system (J. Wang *et al.*, 2020).

In the water heating circuit, the boiler after heating the cold water sends it to a storage tank equipped with a resistance heater. In the space heating circuit, the hot water leaving the boiler feeds several radiators to heat the room and then returns to the boiler. Furthermore, the possible installation of air conditioners is foreseen to favour the heating of the rooms in winter and their cooling in summer.

3.3.2 Control strategies

The control strategies of the plants can widely influence the performances of them. In the case of the hybrid system control the time when the HP or the boiler will provide heat dynamically.

The 'best' strategy cannot be standardised because it depends on different parameters related to local conditions on external or internal signals processing and the performance metric, such as CO_2-emission, price (running costs) and primary energy. Some of input/parameters are:

- External preference signal (e.g. congestion tariff from grid operator)
- Internal optimization (e.g. avoid switching the HP or boiler on/off too often)
- Forced shutdown of HP (e.g. operating outside temperature too low, heat demand temperature too high)

The control strategy can be implemented as a fixed or flexible switching between HP and boiler operation. So, in the first case, the above-listed parameters can be fixed. It is possible to use a specific value or the outside temperature as the cut-off point for HP operation. Below this temperature, the HP is turned off. If the hybrid system has not an active defrost control system, the HP is turned off at quite high outdoor temperature (around 4°C) to avoid frosting or the HP. In other cases, the HP works until it frosts, but it is switched off for "natural/passive" defrosting with the help of the boiler.
This approach will not give the theoretically best performance (it ignores factors like wind-chill, solar irradiation, internal heat contribution from occupants, etc.) and, for this reason, it is very easy to set up. In addition to the lower performance, there is the disadvantage that, using a completely fixed strategy, over time, values for the underlying parameters will change (e.g. lower CO_2-emissions for electricity production, higher costs for a particular fuel, changes in tax regimes, etc.). Thus, the values should be constantly checked in order to control if they are adequate or if some of them have to be changed. This action cannot be conducted by the occupants themselves and sometimes they are helped by some app to optimize the system settings.
More advanced hybrid systems can be integrated into the smart grid. In this case, the control strategy is based on real-time input parameters (e.g. commercial parameters) and so the strategy is "flexible" (Halvgaard *et al.*, 2012).
It is important to underline that, it is very advantageous, because, having the hybrids always a fueled backup boiler available, the dependency from the electricity can be managed with more freedom. As well in this case, the parameters on which the strategy could be based on, are determined by the efficiencies of the HP and the boiler, and on the external circumstances, such as grid congestion, peak demand (i.e. peak shaving or demand response), accommodating renewable electricity production, variable pricing or CO2-emission factors.
Comparing the hybrid systems with the all-electric HP, it is necessary to highlight that there is an important difference. Indeed, in this second case the heating demand can be shifted in the time, for instance by using thermal storage. However, at another time the heating has to be provided by the HP. So, in this case, the electricity demand decreases at a certain point, but increases in a second time. By using a hybrid system it is possible to use the electricity or the gas in a certain moment.

So, it will not be necessary to increase the electricity in a second moment because the energy demand will be supplied by fossil fuel.
Moreover, it is possible to classify the control strategy based on rule control methods and control strategy based on the predictive control ones.
While the first kind of control strategies, as said, are rule-based. In this case, the system can be controlled, as well, according to predictive control methods.
In summary, in the first case, the control methods are based on predefined threshold values of trigger parameters (e.g. energy price, load, power, time) that are constantly monitored. When the threshold is reached, it triggers a control action on the heat pump (start/stop or change in set-point among others). In the case of a predictive control method, the system control is based on a model of the process developed and used to estimate a future control signal. These models are able to forecast a parameter and/or behaviour and to send an input to correct the operating of the plant (i.e. controls based on machine learning). So, the main advantage of this second kind of control strategy is due to the fact that the smart hybrid heat pumps can switch between gas and electricity by applying a fully-optimized control technology with predictive demand-side management to automatically use, e.g., the most cost-effective heating mode across time (Sun *et al.*, 2019) (Zhang *et al.*, 2021). Following some strategies applied in cases study present in literature are shown.

Hybrid heat pump controlled by rule-based controls methods

The control of some samples of HHP can be based on very simple components and parameters. In (Counsell, Khalid and Stewart, 2017), the HHP was controlled by using two thermostats and charge controllers. A thermostat controlled the HP to maintain 55°C water temperature in the hot water tank. The second thermostat controlled the quantum boiler for reheating water supply to 55°C during the on peak period (considered to be around 4-8 pm) when the HP was off to maintain the required zone temperature set-point at 21°C.
Even if the RB control strategy is in general less complex, it can be based on many variables. In another study, Zanetti (Zanetti *et al.*, 2020) et al. developed a strategy based on a large number of states and control variables and, for this reason, the optimal control problem was converted to the nonlinear parameter optimisation problem. Mehrfeld et al. (Mehrfeld *et al.*, 2020) calibrated an energy conversion system consisting of an air source HP, a condensing gas boiler (CGB), a thermal energy storage, as well as the system controller. To do this, the authors used monitored data from a hardware-in-the-loop experiment. Regarding the control strategies, three scenarios of building performance simulations of one year simulation time each were developed. In one scenario, the signal of the PV electricity production was utilised by an enhanced energy manager that took into account the virtually lowered electricity price; in the remaining two scenarios, the PV electricity was sold. The three scenarios are listed below:

- Scenario 1: CGB, no HP, no PV self-consumption
- Scenario 2: CGB, HP, no PV self-consumption
- Scenario 3: CGB, HP, PV self-consumption

If there is no PV self-consumption, all the electricity produced by the PV cells is sold (fed to the grid). On the contrary, Scenario 3 considers the advanced controller. It uses the current PV as a signal to switch off the HP and increase the HP's thermal coverage rate of the whole hybrid system. If the electricity exceeds ($P_{PV,curr} - P_{el,HP,actual} > 0$ W), it is also sold to the grid as in Scenarios 1 and 2. The authors analysed a typical basic control approach and advanced ones by implementing the controller algorithm according to that given by most expert manuals. They identified the hystereses trigger temperatures suiting 8 installed sensors and used the temperature information for the controller model.

The "basic control" is based on economical (by considering price ratio of electric energy and gas) and ecological aspects (McNeil *et al.*, 2016) (by considering the ratio of primary energy factors for electricity mix and gas). All 4 values can be defined in the hybrid system's controller. The second control strategy is explained in a further subsection of this paper.

In the study proposed by Gang Li, Yuqing Du (Li and Du, 2018), two different control strategies were tested. The hybrid system with two control strategies was presented as an alternative option for domestic hot water supply and space heating with the aim of revealing its economic benefits. According to the first strategy, the HP and gas boiler can be switched, either in HP mode or in gas heater mode. According to the second one, the two heating sources can be handled with the proper arrangement for the loading share. Moreover, the system was tested in different climate conditions, with different water initial temperature and final temperature.

Keogh (Keogh *et al.*, 2019) presented a system that can allow the configuration to work as a hybrid system or as a single component. The boiler provided the entirety of the domestic hot water. The control strategy was based on the outdoor temperature and it can be regulated by mode (electricity to gas) switching (cut-off) temperature based on the external ambient temperature. When the outdoor temperatures were low, the gas boiler (more economical) provided the complete load. So, in this case, the system worked in tandem when it is more efficient to produce higher flow temperatures by using the boiler. The HP provided the full load at higher ambient temperatures which led to better efficiencies (i.e. higher coefficient of performance).

Gang Li (Li, 2018) developed and applied an economic-based new control strategy for the hybrid system to investigate the system thermal performance and reveal the economic benefits for residential space heating applications. Figure 3.9 shows the decision process diagram of the control strategy.

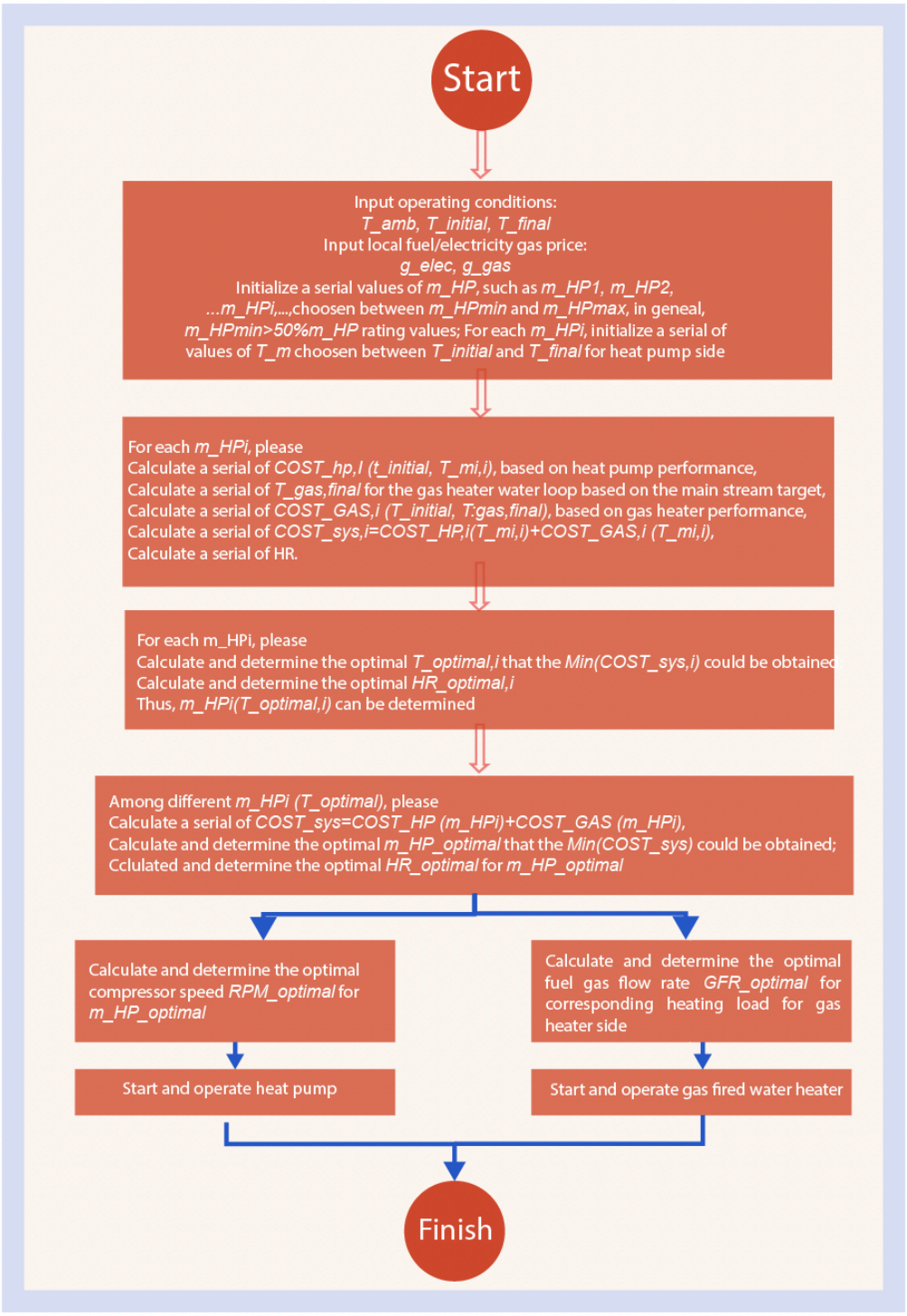

Figure 3.9. Flow chart of hybrid system control strategy (Li, 2018).

Based on the setting of several parameters (e.g. water return temperatures from loadings, various climate conditions, price ratios of electricity to gas), the two heating sources can be arranged for each loop.

Calise et al. (Calise, Macaluso, *et al.*, 2017) described in detail the control strategy applied in their work.

During winter, PV/T solar thermal energy was supplied to the first tank. If the tank was thermally loaded, the PV/T collectors supplied the second tank in order to produce DHW. The thermal energy stored in the first tank was supplied to the evaporator of the reversible HP. The latter was supplied by the thermal energy exchanged with the condenser to the hydronic system of the building (for space heating). Then the HP can be activated in order to ensure the third tank top temperature (within the fixed range of 45–48 C). This third tank supplied the fan-coil system in the rooms. During summer, the heat produced by the PV/T and stored in the first tank, was supplied to the generator side of the adsorption chiller. It supplied space cooling by using the thermally driven cooling effect. The fan coil hydronic system, supplied by the chilled water stored in the third tank (12–14 C), maintained the indoor temperature ranges between 25 and 27° C. The auxiliary boiler was activated to match DHW demand when the second tank top temperature was below the set point.

Bagarella et al. (Bagarella, Lazzarin and Noro, 2016) simulated a dynamic model of an HHP for both a cold-humid and a mild-dry climate. They considered a typical European family house built in the 1970s with the usual energetic renovation upgrades. The aim was to study how the choice of cut-off temperature can influence the annual efficiency of the system. Moreover, they wanted to study the best cut-off temperature, from an energy perspective, according to different climate conditions and HP sizing. For clarity, they reported the definition of the bivalent temperature (BT), which is according to (UNI EN 14825, 2019) the outdoor temperature declared by the manufacturer for heating. In particular, and said that it may be defined as the temperature at which the thermal capacity of the HP equals the building thermal load. Their results showed that there might be no benefits to setting a Tcut-off lower than BT. On the other hand, with a low size HP, a bivalent parallel system can lead to appreciable (up to 5% in the cold-humid climate and up to 8% in the mild-dry climate when BT = 6 °C) energy savings compared to a bivalent alternative plant. In addition, for the lower sizes of HP, the best Tcut-off shifted towards lower values. The main economic advantages of an HHP, with respect to the monovalent heat-pump plant, come from the lower annual electric and gas energy needs. Anyway, an appreciable advantage can be achieved (up to 10.5%) as well as the initial investment of the lower size HP costing less.

Hybrid heat pump controlled by predictive controls methods

In (De Coninck and Helsen, 2016) a model predictive control (MPC) was implemented in a medium-sized office building in Brussels, Belgium. They presented the implementation of the controller and the measured performance in comparison with the default, rule-based control (RBC). The building had two floors and a total size of 960m^2. The controllable system was the hybrid heat production consisting of two air/water HPs and a condensing gas boiler. The practical situation did not allow the control of end-units in different zones of the building. The MPC made use of a Modelica grey-box control model resulting from a system identification with

monitoring data. The paper covers the monitoring, model identification, forecasting of disturbances, state estimation, formulation and solving of the optimal control problem (OCP) and transmission of the control signals. The performance was evaluated on a daily basis based on analysis of heating degree days, thermal comfort, energy costs and primary energy consumption. The results show that the model predictive controller is able to provide a similar or better thermal comfort than the reference control while reducing the energy costs by more than 30%. This is due, among other things, to a better use of the HPs and an adapted hot water supply temperature. They compared the measured performance with the existing one. In this case, the fan coil units were controlled by the users, while the building energy control and management system (BECMS) controlled the hot water supply temperature and influenced the heat consumption indirectly. The supply temperature was managed based on the heating curve of the ambient temperature (with indoor temperature compensation). A proportional-integral controller followed this heating curve and controlled the total thermal power to be produced. A particular cascade controller spread the set point power on three different units of production based on regulations and weights that determine the priority (e.g. a weight for being off, a weight in case of a disturbance on the unit, a weight based on the unit temperature, a weight based on the minimum modulation degree of the unit, ensuring that small units get started first) This gave priority to the HPs when the total heat demand was low. Furthermore, in order to ensure the priority of the gas boiler, avoiding the operation of the HPs at low efficiency, other specific weights were used in particular circumstances (requested supply water temperature $T_{Sup} \geq 45 \circ C$ and $T_{Amb} \leq 3 \circ C$). The air handling unit (AHU) and the hot water circulation pump were switched on and off simply based on a weekly schedule. The implementation of MPC as a high-level control made use of the BECMS for low level control.

So, by using the BECMS, it was possible to set and control variables directly by a file transfer protocol and to use an MPC to control the thermal power of both the HPs and the gas boiler.

Lyden (Lyden and Tuohy, 2022) applied their research on a residential district space, but the presented PyLESA can be applied as well for smaller cases. It is an open-source planning-level modelling tool authors used it to demonstrate the benefits at the planning-level, and to do this they investigated model predictive control vs fixed order control, existing and future wind-influenced electricity tariffs, and optimal cost size combinations of HP and hot water tanks. For the fixed order control, introduced in this study just as a representation of a commonly employed control, they used a predefined set of rules and used them to order the dispatch of supply and to determine the use of storage. In this case, it was possible to rearrange this set of rules at the start of the simulation but it was not possible to change the order of dynamic system variables during the simulation period.

The software PyLESA uses a predictive control (MPC) based on the influences of energy systems and optimises the performance of the components as a supervisory

control strategy. In particular, it uses an economic model predictive control (EMPC) to optimise the economic performance by ranging control variables and, consequently, to minimise costs over a receding prediction horizon. In order to develop the model, authors used many data as input for this tool, such as local resources, electrical demand, district heating demand, presence of electrical production technologies, data about components (HPs, auxiliary heat units, hot water tank), electricity tariff data based on a flat rate, day and night schedules, time-of-use, and wind data (a combination of day and night base tariff adjusted by wind pricing structures).

Chen et al. (Chen *et al.*, 2021) focused their attention on the battery used by a system as an auxiliary power source to achieve efficient engine operation. The frequent changes in external load can cause frequent charge/discharge of the battery. Consequently, it adversely affects energy conversion efficiency. In order to realise power distribution between the gas engine and the electric motor, they proposed a dynamic energy control strategy based on the engine, the economic terms, and battery status.

D'Ettorre et al. (D'Ettorre, Conti, *et al.*, 2019) analysed the cost-optimal sizing and hourly control strategy of an HP system for a heating application. The system was composed of an electrically-driven air source HP and a gas boiler. They investigated the optimal control problem by means of mixed-integer linear programming by considering an ideal forecast of external temperature and thermal load on given horizon periods (the model predictive control). Achievable cost savings with respect to a traditional rule-based control strategy with no storage were studied as a function of both prediction horizon and storage capacity in a dimensionless form. The authors found a relation between prediction horizon length and optimal storage capacity. D'Ettorre et al. in (D'Ettorre, Conti, *et al.*, 2019) reported that by applying a model predictive control to an air-source HP coupled with a water thermal storage system, the tank allows the controller to operate load-shifting throughout the day. As mentioned in section 3.3.1, the controller limits the use of the boiler to meet the load demand when it cannot be met by the HP. They observed a reduction in the specific costs associated with different DR actions between 45% and 75% (0.5 m^3 volume of tank) and between 50% and 78% (0.75 m^3 volume tank). The results of this last study showed that the energy flexibility depends on the storage capacity and operations are affected by the generator sizing. According to the study (Fischer *et al.*, 2017), flexibility applied to the HP control is strongly dependent on ambient temperature and time of day.

As mentioned above, in the work of Mehrfeld et al. (Mehrfeld *et al.*, 2020), an advanced control strategy was studied. Such an advanced controller was able to take a potential current PV production into account and decide on self-consumption instead of selling the generated electricity. It is conceivable to use such a smart controller within a home energy management system. In order to enable the HP only when it was preferable compared to the CGB, heat prices for both energy conversion units were calculated dynamically. Such a heat price quantifies the cost in € for 1 kWh_{th}. Regarding the CGB control, the price of heat can be calculated by dividing the price of the gas p_{gas} = 0,06€/kWh by the efficiency of the boiler ηCGB. On the contrary, the price of heat for

the HP depended on the power provided by the PV ($P_{PV,curr}$). Furthermore, the algorithm worked by using the set price electricity tariff $p_{el,grid,HP}$ = 0.21€/kWh as input and the proceeds from the sale of PV electricity $p_{el,PV,sold}$= −0.12 €/kWh. The max {} function in the following equation limits the predicted heat price $p_{heat,HP}$ to 0 in case of $P_{PV,curr} > P_{el,HP,pred}$.

$$p_{heat,CGB} = \frac{p_{gas}}{\eta_{CGB}} \tag{3.10}$$

$$p_{heat,\mathrm{HP}} = \max\left\{ p_{el,grid,HP} \frac{p_{el,HP,pred} - p_{PV,curr}}{p_{el,HP,pred} \cdot COP_{pred}}, 0 \right\} \tag{3.11}$$

To reduce the $p_{heat,HP}$ to the baseline scenario, its control algorithm, $P_{PV,curr}$ can be set to 0.

Dongellini et al. (Dongellini, Naldi and Morini, 2021) carried out a series of simulations to calculate the seasonal performance of hybrid systems based on an air-to-water HP and to assess the optimal configuration of the system. They found that the energy performance of these systems depends on several parameters, such as the back-up device typology, the HP sizing, and the control algorithm used for the activation of the heat generators.

Wang et al. (J. Wang *et al.*, 2020) also conducted a study based on a simulation in order to study a smart home with a novel hybrid heating system, consisting of a wall-hung gas boiler (for both space and water heating) connected to a water tank with an auxiliary electric resistance heater (for water heating), and auxiliary split air conditioners (for space heating). They implemented a multi-objective optimisation to optimise the gas operation and electricity consumption. They considered different parameters such as the minimisation of operating energy cost (including both electricity and gas payment) and the maximisation of thermal comfort. Furthermore, in their sensitivity analysis the authors considered various levels of electricity/gas prices, onsite PV capacity, battery capacity and outdoor air temperature.

In their study, Fitzpatrick et al. (Fitzpatrick *et al.*, 2020) focused their attention on the influence of electricity tariffs on energy flexibility in buildings and associated energy costs by developing and testing a model predictive control algorithm. It was based on several DR programs by adopting different metrics capable of describing the flexibility of the system. To do this, they analysed a residential building located in Stuttgart, Germany, equipped with an HP coupled with a thermal energy storage unit and a gas boiler and included several tariff structures: real-time pricing, two-level day-night tariffs and critical-peak pricing with both fixed and variable feed-in price components.

Heinen (Heinen, Burke and O'Malley, 2016), in the work cited above, developed a model to assess the system value of deploying hybrid technologies. In particular, besides developing algorithms to minimise the total system costs, they considered the endogenous determination of the control variables such as capacity C (MW) and energy generated E (MWh) for each power and heat technology. Moreover, the function included total annualised investment, fuel and carbon expenditure for both power generation and residential heat, based on specific investment cost, fuel prices, energy demand, carbon emission factors, carbon price, annuity factors and the number of residential households with the selected heating technology.
Atam et al. (Atam *et al.*, 2015) presented a prediction-based dynamic programming (DP) control approach, a nonlinear model predictive control (NMPC) approach, and a linear optimal control (LOC) approach to analyse the minimisation of the total energy use of a hybrid ground-coupled HP system. DP was used as a reference for performance assessment. As in most studies, given that electricity and gas costs denote the time-dependent electricity and gas price per kilowatt hour, in order to solve the optimal control problem, they used a cost function for an HyGCHP system operation over a time period. The developed algorithms were used to control heating–cooling systems of three types of buildings: a heating dominated building, a cooling dominated building, and a thermally balanced one. They included and analysed the effects of constraining thermal decrease of the ground, the variable electricity prices, the thermal comfort conditions, and the performance of the different controllers applied. The parameters related to the systems such as the COP were fitted to TRNSYS data.
It is important to underline that the best performance can be achieved only if a detailed sizing of the system and a heating demand analysis are considered (Renaldi, Kiprakis and Friedrich, 2017).

3.3.3. Energy performance and economic issues

As described in the previous sections, many studies presented in the literature have analysed case studies and presented the energy performance of HP systems. In some of them, the HHPs are compared with traditional systems and the percentages of the achievable energy savings are reported. Other studies include the presentation and the calculation of key performance indicators (KPI) (Martorana *et al.*, 2021). Previous studies introduced KPI for other energy conversion processes and for the assessment of the plant performance, mainly if it is necessary to account for both heat and electrical renewable and non-renewable contributions to the system.
The primary energy factor (PEF) describes the efficiency of converting energy from primary sources (Poredoš *et al.*, 2017). It can be defined as the ratio of primary energy to secondary energy for a specific energy vector. It can be useful to consider the primary energy efficiency of the heat source that is being studied (Keogh *et al.*, 2019) (Poredos

et al., 2017) reported the following equation used to calculate PEFs for heat production in the case of heating systems with oil and natural gas boilers:

$$PEF_{hp} = \frac{PEF_{hs}}{\eta_{hs}} \tag{3.12}$$

where PEF_{hp} is the primary energy factor for heat production, PEF_{hs} is the primary energy factor of heat source, and η_{hs} is the efficiency of the heating system.

In case of air-source HP heating system, the PEF for heat production was calculated as:

$$PEF_{hp} = \frac{PEF_{el}}{SPF} \tag{3.13}$$

where PEF_{el} is the primary energy factor of electricity, and SPF is the seasonal performance factor of the HP. The SPF of the HP is calculated using following equation:

$$SPF = \frac{Q_{hp}}{W_{el}} \tag{3.14}$$

where Q_{hp} is the annual produced heat, and W_{el} is the annual electricity consumption of the HP system.
Given that it is not useful to use the COP of a conventional electric HP for the HHP system, it should be necessary to use a formula that include both the efficiency of the boiler and the COP of the HP. To define the hybrid air-source HP/gas boiler system performance factor, the methodology of Stafford (Stafford, 2017) was used, which can be calculated using following equation:

$$SPF_{hhp} = \frac{W_{uh}}{Q_{fuel}} \tag{3.15}$$

where SPF_{hhp} is the HHP performance factor, W_{uh} is the sum of the net useful heating effect, and Q_{fuel} is the total fuel energy input into both systems.
The PEF of the hybrid heating system can be calculated using Equation (3.16):

$$PEF_{hhp} = \left[\left(\frac{PEF_{hs}}{\eta_{bs}} \right) \cdot R_{gas} + \left(\frac{PEF_{el}}{SPF} \right) \cdot R_{el} \right] \tag{3.16}$$

where R_{gas} is the ratio of space heating provided by gas boiler, R_{el} is the ratio of space heating provided by HP, and SPF is the seasonal performance factor of the HP. With knowledge of the PEF_{hs} of all heating systems, the primary energy savings (PES) can be calculated using Equation (3.17). In the study (Poredos *et al.*, 2017), the reference *PEF*

of renewable electricity generation was set equal to 1.0, and used to calculate *PES* (Lazzarin, 2020).

$$PES = (1 - PEF) \cdot 100\% \tag{3.17}$$

Furthermore, they calculated the annual carbon intensity as:

$$\varepsilon = \frac{Q \cdot EF}{1000} \tag{3.18}$$

where ε is the carbon intensity in tonnes of CO_2 per year, Q is the energy use in kWh, and EF is the emissions factor for each fuel vector. It is noted that in the case of the hybrid HP system (Scenario (c)), the emissions of both the natural gas and the electricity fuel vectors are summed.

As Neyer (Neyer, 2018) states, Non-Renewable Primary Energy Ratio (PER_{NRE}) was introduced to avoid problems related to partly valid key performance indicators on system efficiency. The energy ratio is based on the entire/total useful heating and cooling energy ($Q_{CD} + Q_{DC} + Q_{HD} + Q_{WD} + Q_{DH} + Q_{el.DE}$) and is compared to the non-renewable primary energy effort of the system. Electricity ($Q_{el,\ grid}$ (GD) and PV) and other thermal inputs (energy carrier, Q_{EC}) are converted to non-renewable primary energy units with a (country specific) primary energy factor (ε_{el}, ε_{EC}). This primary energy factor can be calculated by using the coefficient obtained according to useful energy in the form of electricity produced by specific power plants and supplied through the National Power Grid to final users (E_{grid}).

$$PER_{NRE} = \frac{Q_{CD} + Q_{DC} + Q_{HD} + Q_{WD} + Q_{DH} + Q_{el.DE}}{\frac{Q_{EC}}{\varepsilon_{EC}} + Q_{el}\left(\frac{\%GD_{el}}{\varepsilon_{el}} + \frac{\%PV_{el}}{\varepsilon_{PV,el}}\right)} \quad \left[\frac{kWh_{use}}{kWh_{prim}}\right] \tag{3.19}$$

This PER_{NRE} is calculated for the entire renewable/solar based system and for the standardised reference system. The heat demand is summed ($Q_{HD} + Q_{WD} + Q_{DH}$) and includes losses for domestic hot water preparation ($Q_{loss.ref}$). The conversion to end energy use is achieved by the reference efficiency of the natural gas boiler and the conversion to primary energy effort by the corresponding primary energy conversion factor (ε_{EC}). In a similar way, cold demands are summed ($Q_{CD} + Q_{DC}$) and converted using the entire/total efficiencies of the air-cooled vapor compression chiller ($SPF_{C.ref}$) and corresponding primary energy factor (ε_{el}). The electrical auxiliary demand ($Q_{el.ref}$) and the domestic electricity demand ($Q_{el.DE}$) are converted with ε_{el} accordingly.

$$PER_{NRE.ref} = \frac{Q_{CD} + Q_{DC} + Q_{HD} + Q_{WD} + Q_{DH} + Q_{el.DE}}{\frac{Q_{HD} + Q_{WD} + Q_{DH} + Q_{loss.ref}}{\varepsilon_{EC.ref} \cdot \eta_{HB.ref}} + \frac{Q_{CD} + Q_{DC}}{SPF_{C.ref} \cdot \varepsilon_{el}} + \frac{Q_{el.ref} + Q_{el.DE}}{\varepsilon_{el}}} \quad \left[\frac{kWh_{use}}{kWh_{prim}}\right] \quad (3.20)$$

As stated before, the performance of the system depends on the flexibility of the control and of the grid. Fitzpatrick et al. (Fitzpatrick *et al.*, 2020) underlined that, right now, there is not a common, standardised assessment procedure to evaluate DR programs and the energy flexibility in buildings.
Lazzarin and Noro 2018 (Bagarella, Lazzarin and Noro, 2016) calculated the primary energy ratio (PER) for the whole HVAC plant and also separated the two sections (heating and ventilation) as:

$$PER_{tot} = \frac{E_{h,Boiler} + E_{h,HP3+HP4} E_{h,Solar} E_{h,Boiler} E_{h,HP1+HP2} E_{\mathrm{v},Static\_rec}}{E_{p,h,Boiler} + E_{p,\mathrm{v},Boiler} + E_{\mathrm{p},HP1+HP2} + E_{\mathrm{p},HP3+HP4}} \quad \left[\frac{kWh_{use}}{kWh_{prim}}\right] \quad (3.21)$$

$$PER_h = \frac{E_{h,Boiler} + E_{h,HP3+HP4} E_{h,Solar}}{E_{p,h,Boiler} + E_{\mathrm{p},HP3+HP4}} \quad (3.22)$$

$$PER_v = \frac{E_{\mathrm{v},Boiler} + E_{\mathrm{v},HP1+HP2} E_{h,Static\_rec}}{E_{p,\mathrm{v},Boiler} + E_{\mathrm{p},HP1+HP2}} \quad (3.23)$$

where E is the useful thermal energy produced and if it is subscript with "h" refers to the heating, with "v" to the ventilation, and with p to the energy consumed.
Furthermore, in their analysis they considered the gas utilisation efficiency (GUE) for the HPs (UNI EN 12309-1, 2002) calculated as:

$$GUE = \frac{E_{AC}}{E_{AC} + E_E} \cdot \eta_G \quad (3.24)$$

Where E_{AC} is the energy delivered to the primary circuit from the HP condenser-absorber, E_E is the energy supplied to the evaporator by the heat source and η_G is the natural gas combustion efficiency.

De Conick et al. (De Coninck and Helsen, 2016) compared the performance of the conventional rule-based control (RBC) with the model predictive control on a daily basis, for working days only. In order to do this, they defined three key performance

indicators (KPI) and one normalisation variable. The first KPI, the energy cost J_c is as follows:

$$J_c = \int_0^{th} \left(c_g \dot{P}_g + c_e \dot{P}_e \right) dt \tag{3.25}$$

The second KPI, the primary energy consumption J_e, is obtained from

$$J_e = \int_{t_i}^{t_e} \left(2.5 \dot{P}_e + \dot{P}_g \right) dt \tag{3.26}$$

They used a primary energy factor of 2.5 for electricity and 1.0 for natural gas. The values of ti and te will be given below. As J_c is part of the objective function and J_e is not, it is logical to judge the merits of the MPC on J_c.

In order to make fair comparisons between days, authors implemented a time shift prior to the computation of all metrics according to the beginning of the low electricity tariff period and the occupation period. Furthermore, to cover accidental or unforeseen heating at the weekend, they added the energy use and costs of the weekend to the KPIs for Monday. The third KPI regarded the thermal discomfort.

For each work day, the time of discomfort was calculated. The discomfort condition was considered with a PPD>6%. Taking into account a clothing factor of 1.0 and a metabolism rate of 1.2, the temperature boundaries corresponding to PPD=6% were 21.0□ and 23.0□.

In addition, Fitzpatrick et al. (Fitzpatrick *et al.*, 2020) selected 3 indicators to analyse the building flexibility potential from an energy, economic and technical performance point of view. The first one was called available electric energy flexibility (AEEF). It was useful to evaluate the variation of the building electrical energy consumption due to the activation of DR programs over a specific period. Defining P_{DR} and P_b as the electric power consumption profiles with and without DR actions respectively, the *AEEF* can be expressed as follows:

$$AEEF^{(\tau)} = \int_0^{\tau} \left[P_{DR} - P_b \right] \cdot dt = \int_0^{\tau} \left[\alpha_{DR} - 1 \right] \cdot P_b \cdot dt \tag{3.27}$$

The second indicator is the primary energy efficiency (*PEE*) and it is the ratio between the primary energy consumption (*PEC*) with and without DR actions. Since the activation of DR actions typically leads to higher primary energy consumption, *PEE* values lower than 1 can be expected. So, the *PEE* can be important in order to have quantitative information on the energy cost of the DR action.

$$PEE^{(\tau)} = \left(\frac{PEC_b}{PEC_{DR}} \right)_{\tau} \tag{3.28}$$

The third one is the specific (marginal) costs (*SC*). The cost (*C*) associated with a specific DR program can be obtained by comparing the system operational costs (*OC*) with and without the activation of the DR actions. The specific cost (*SC*) is determined by the ratio between the total DR cost (C_{DR}) and the available energy flexibility provided (AEEF):

$$SC_{DR}^{(\tau)} = \left(\frac{C_{DR}}{AEEF} \right)_{\tau} = \left(\frac{OC_{DR} - OC_b}{AEEF} \right)_{\tau} \tag{3.29}$$

The results of this study show that it is possible to achieve up to 1370 kWh_e of energy flexibility over the heating season with an average specific (marginal) cost of between €0.024–0.035 per kWh_e. The DR programs lead to higher utilisation of thermal energy storage along with increased boiler consumption by up to 17.1% and 12.1% respectively in the case of maximum DR intensity. Consequently, this leads to a higher overall primary energy consumption (between 1.6% and 9.1%). Furthermore, real-time pricing is the most favourable tariff structure, capable of offering the greatest energy flexibility with lowest associated electricity costs.

The analysis conducted by Dongellini et al. (Dongellini, Naldi and Morini, 2021) demonstrated that the overall seasonal efficiency can be increased by up to 6% and 22%, if compared to monovalent systems based on an HP or a gas boiler, but only if the heaters are activated following an alternate operating mode, with a cut-off temperature selected between the design and the bivalent temperature. On the other hand, if the back-up device of the hybrid system is an electric resistance heater, the heaters have to work in parallel during the whole heating season and the only achievable advantage is that the HP can be slightly under-sized with respect to the nominal building load.

Interesting results were found as well in terms of CO_2 emissions. Lin et al. (Lin *et al.*, 2021) carried out a life cycle assessment analysis, by comparing a condensing gas boiler and a hybrid heating pump for a common type of existing house in the UK. The results show that the HP provided emission reduction (from 13% to 48%). It was calculated comparing it to the condensing gas boiler in terrestrial acidification, photochemical oxidant formation, particulate matter formation and fossil depletion.

Sevindik and Catalina Spataru (Sevindik and Spataru, 2020) also used a life cycle approach to analyse the environmental impacts of domestic HPs with gas boilers. The study analysed three scenarios (transport (SK), 50% hybrid and 75% hybrid) to compare their results with a baseline model.

The study conducted by Mehrfeld et al. (Mehrfeld *et al.*, 2020) and described in the previous section analysed three scenarios and two control strategies. The results presented in this study in terms of energy and economic issues demonstrated that Scenario 3, controlled by the advanced control strategy, showed a higher operational time of the HP. As a positive effect, the coverage of HP can increase from 13% to 16% and the energy use increases, too.

Moreover, considering purely the CGB, the operating and investment costs should be lower. In addition, the analysis of internal temperatures shows that Scenario 1 did not provide discomfort conditions compared with the other scenarios. Thus, the CGB as a single heat generator can cover the heat demand and achieve good comfort conditions. Scenario 3 with advanced control strategy needs higher operating costs than Scenario 2, where the electricity produced by the PV system can be fully sold (it is not auto-consumed).

In conclusion, based on their simulation outputs, the authors demonstrated that the scenarios without HP achieved better performances. Indeed, the outlet temperature in the condenser quickly increased, overcoming the supply temperature. Thus, the actual momentary COP was worse than the predicted COP. However, the lower yearly operational costs of a condensing gas boiler, in comparison to a HP system, was due to neglecting dynamic effects e.g. losses during start-up and shut-off phases or heat losses in the components, especially the thermal energy storage, and relying on an ideal COP from the characteristic field.

Gang Li (Li, 2018) reported the effect of the control applied strategy in terms of energy and costs. He tracked and found "optimal points tracking" of the optimal HP water outlet temperature for one water flow rate for the HP (50 L/min, i.e. 0.83 kg/s). Results show that in hybrid function it is possible to extend the optimal HP water outlet temperature to both high and low regions. By fixing the main stream water flow rate, increasing the water flow rate for the HP side can improve the system efficiency, especially in hot climates. For space heating applications for −12 °C to 20 °C ambient, the control strategy can lead to ~10% to ~60% system operating economic benefits. If the price ratio increases, the optimal outlet water temperature and HR can decrease, especially for higher final water target temperatures. If the price ratio decreases, the energy process saving potential (% gas heater heating mode baseline) can be greatly enhanced. In order to investigate the economic benefits of the applied control strategy, Gang Li carried out an analysis conducted for several typical cities in China. The cost for the heating season energy process used an hourly resolution and was based on the bin method (Claridge *et al.*, 1987). $E_{bin,i}$ is the hourly energy loading for each bin, which can be summed to obtain total energy loadings for the heating season as follows:

$$E_{tot} = \sum_{i=1}^{n} E_{bin,1} \tag{3.20}$$

n is the total number of bins. The total energy process cost for the heating season can be calculated as:

$$COST_{tot,season} = \sum_{i=1}^{n} COST_{bin,1} = \sum_{i=1}^{n} f(E_{bin,1}) \tag{3.21}$$

For each bin, the corresponding hourly energy cost can be obtained from $E_{bin,i}$ according to the applied control strategy. Then all sub-costs can be summed in order to calculate the total energy cost $COST_{tot,season}$. The heating season energy process cost saving

potential compared with gas heating only can be calculated by using the following equation:

$$\xi_{tot} = \left(\frac{COST_{tot,season} - \frac{Y_{gas} E_{tot}}{\eta_{gas}}}{\frac{Y_{gas} E_{tot}}{\eta_{gas}}} \right) \cdot 100 \tag{3.22}$$

He found that there is an increasing share of electricity use, from the colder regions to hotter ones, since the HP is more efficient in hot climates. In addition, all cities can achieve energy cost savings when the gas heating only mode is chosen as the baseline. The warm areas share ~12% or even less; while the cold areas have more than 70% of the total operating cost for natural gas. The hybrid system can produce even more $CO_{2\text{-}eq.}$ emissions than the gas heating only mode, especially for the cold areas. Obviously, the use of lower emission fuel sources for power generation can decrease the emission factor for electricity generation toward a sustainable target.

Cho et al. (Cho *et al.*, 2016) investigated a combined heat and power system integrated with a residential HP. The proposed model consisted of a power generation unit driving an HP and a heat recovery system used to offset the HP heating load and the DHW demand. The authors considered a single-family residential building in ten different U.S. locations representing different climate zones. The performance of the proposed system was then compared to the performance of conventional systems in the same locations. They used the electrical power ratio ($PR_{elec.}$) and the electricity to fuel cost ratio (EFCR), to analyse the effect of the electricity consumed by the auxiliary heater and energy prices on the CHP-HP operation. Results showed that the system can be effective in cold climate zones by supplementing the auxiliary gas boiler energy consumption with the recovered waste heat from the power generation unit.

In order to evaluate the energy and economic performances, they presented the mathematical description used to model a conventional HP and used to model the CHP-HP systems. The total cost to operate the CHP-HP system included the fuel cost of the PGU and the boiler, as well as the electricity cost of the auxiliary heater. The annual maintenance cost of the PGU ($Cost_{PGUmaint}$) was also considered in the calculation.

$$\begin{aligned} Cost_{CHP-HP} &= Cost_{PGU} + Cost_{boiler} + Cost_{aux} + Cost_{PGU_{\text{maint}}} \\ &= Cost_f (F_{PGU} + F_{boiler}) + Cost_e E_{aux} + Cost_{PGU_{\text{maint}}} \end{aligned} \tag{3.23}$$

The cost saving, if any, using the proposed CHP-HP system can be determined as the difference between the operational cost of the conventional and CHP_HP systems:

$$Cost_{saving} = Cost_{conv} - Cost_{CHP-HP} \tag{3.24}$$

Then the percent cost saving can be determined as:

$$\%Saving = \frac{Cost_{conv} - Cost_{CHP-HP}}{Cost_{conv}} \cdot 100\% \quad (3.25)$$

The calculation of energy and economic performances changes depending on the components of the hybrid system. An interesting sample is presented in Nguyen (Nguyen *et al.*, 2016), where the economic effects of choosing an entering fluid temperature for a hybrid ground-source HP were investigated. In particular, they used a computational approach to size hybrid GSHP systems published in (Alavy *et al.*, 2021).
Of course, in some studies the performance was evaluated by monitoring data.
Taler (Taler, Pitry and Taler, 2019) monitored a ground source HHP assisted by solar collectors. The system provided heat for space heating and ventilation and to supply domestic hot water. Results showed that the thermal energy generated depended considerably on the device operating time within the system and was not proportional to the rated output of the device that produced it. For instance, the percentage share of the annual thermal energy produced by gas boiler production was 51.11% even though the installed power was 186 kW. While, for the 81.1 kW ground HP, the percentage share of the overall annual thermal energy generation was 43.02%.
Stafford monitored a commercially available (Daikin Altherma) hybrid system (nominal output of 5kW) installed in the North of England and another (nominal output of 8 kW) installed in Southern Scotland. The aim was to evaluate the systems' potential for energy flexibility. The systems studied operated frequently in hybrid mode during the heating season (unless there was no call for space-heating), with the gas-boiler element providing both domestic hot water (DHW) and additional space-heating not covered by the heat-pump element. The HP provided space-heating only, while the gas boiler provided instantaneous DHW (no storage tank) together with additional space-heating as required. They were controlled by a proprietary smart logic system that considered external temperatures, internal space-heating and DHW demand and the relative cost of gas and electricity given the owners' input energy tariffs. Each monitoring system consisted of two Siemens WFN21.E131 heat metres, of measurement accuracy class 3 to EN 143419 to measure the total heat output to space-heating and heat-pump heat output. Then they measured the electrical energy consumption of the HP (including controls, displays, etc.) and the gas boiler (including fan), the gas and DHW volume, and the outdoor and indoor temperatures. The boiler output to space heating was, therefore, calculated as the difference between these two heat metre readings. From these measurements, it was possible to calculate the performance of each sub-system on a daily or monthly basis, the overall energy consumption and energy efficiency being defined as:

(space-heating output + DHW output)/gas energy input + electrical energy input)

all measured in kilowatt hours.

Amirkhizi and Jensen (Amirkhizi and Jensen, 2020) presented a cost optimisation model of an HHP and compared the levelised cost of heat of this system with other individual heating systems. They investigated the changes in the operation schedule of the system and focused their attention both on socio-and
a private-economic perspectives. Thus, they analysed how certain technological and economic framework conditions influence their operation schedule. Results showed that the end-consumer's optimal operation schedule uses the gas boiler component of the system 24% of the time. Results showed that, by comparing the levelised cost of heat with other heating alternatives, the HHP setup was the most cost-efficient individual heating alternative.

3.3.4. Discussion and conclusions

The present review investigated studies on hybrid systems using heat pumps (HP) for HVAC systems and DHW production carried out during the period 2016-2022. As outlined in Table 1, most of the papers were published in 2019. In 8 case studies, HHPs were used for SH, in 3 cases for DHW, and in 2 cases for heating systems. Furthermore, in some cases the system was supported by renewable sources. Regarding the control strategies, 3 of the analysed case studies applied RB control strategies, while 6 applied MPC strategies. The first typology has the advantage that it is easy to implement; the second typology is more complex and costly to integrate, but it provides better results.
In all cases, it was demonstrated that the application of HHP can achieve significant energy savings. Unfortunately, authors of the reviewed papers reported the energy savings in different terms (e.g. economic terms, in terms of energy process, in terms of primary energy), so, it is not possible to make a comparison in a direct, simple or immediate way. The low number of case studies shows that this technology is currently not so common.

Table 3.1. Comparison of the analysed papers.

Authors	Year	Country	Renewable sources	Control strategies (RB-PC)	Savings	Heating load (DHW-SH)	Storage system
Aditya & Narsilio	2020	Adelaide, Brisbane, Cairns, Hobart, Melbourne, Perth and Sydney	Ground	PC	The lowest net present cost (NPC) for the 20-year lifespan of the system is approximately A$40,000 with a lifetime GHG emissions (LGE) of 52 ton CO2e. If the system is designed to minimise the LGE,	SH	Ground

					the optimum design has an NPC of approximately A$44,000 but with an LGE of 44 ton CO2e. This 8 ton CO2e savings seems low, but this value represents 15% of the total emissions (8/52).		
Allaerts et al.	2017	Veurne, Belgium	Ground	RB	The total reduction of primary energy consumption that can be realised amounts to 10.7% in the hybrid ground source heat pump systems configuration, respectively 11% in combination with passive cooling during summer holidays.	SH	Ground
Amirkhizi & Jensen	2020	Denmark	-	PC-RB	-	SH-DHW	Water tank
Antonov	2016		Ground	PC		SH-DHW	Ground
Bagarella et al.	2016	Milan, Italy	-	RB	Economic advantages up to 10.5%)	SH	Thermal energy storage
Bennet et al.	2021	United Kingdom	-	RB	From 16% to 76%	SH	Water storage tank
Calise et al.	2016	Naples, Palermo, and Milano, Italy	PV/T	RB	the utilization of the produced solar thermal energy is up to 83%. The space heating demand is entirely supplied with the solar assisted heat pump, and the cooling demand is supplied by higher than 70% by the adsorption chiller for the base case study	SH-DHW	Water storage tank
Cho et al.	2016	10 different U.S.	-	RB	CHP-HP system can potentially achieve annual energy consumption reduction for the auxiliary heater and	DHW and SH	Heat Recove

					boiler as high as 87.7–91.5%, when compared to the conventional system performance. Yearly cost savings were found more than 40% in New York, NY, Detroit, MI, Duluth, MN, and Milwau-kee, WI.		ry System
Counsell et al.	2017	United Kingdom	-	RB	9.3%	SH-DHW	Heating storage tank
Deng et al.	2022	Changsha, China	Ground	PC	Compared with the traditional model (MI), the typical start- factor model (MII) has advantages in all aspects, especially the FTL operation strategy (energy saving reached 23.10%; the total annual cost reduction reached 22.80%; the annual carbon dioxide emission reduction reached 22.33%)	SH	Thermal storage tank
Francesco D'Ettorre et al.	2019	Pisa, (Italy)	-	PC	cost savings of up to 8%.	SH	Water storage tank
Francesco D'Ettorre et al.	2019	Pisa, (Italy); Dublin, (Ireland)	-	PC	cost-saving and a reduction in seasonal primary energy consumption of up to 8% and 13.5%,	SH	Space heating water tank
Gang Li	2018	Shanghai, (China)	-	RB	Nearly 80% energy process cost saving	SH	-
Heinen et al.	2016	Ireland	Wind	PC	On a per household basis, the annual net savings (i. e. difference between savings and cost) are 46–159 € for HP-B (heat pump-gas boiler)	SH-DHW	Water storage tank
Ikeda et al.	2017	Tokyo, Japan	Ground	PC	The simplified optimization strategy that determined only	DHW-SH	Thermal storage

					the start and stop times of the GSHP operation could reduce the operating costs compared to the empirical operation for a single day and 7 days by 3.78% and 9.59%, respectively. The detailed optimization strategy that determined the load rates of all the components in each time step could reduce the operating costs compared to the empirical operation for a single day and 7 days by 6.81% and 12.56%, respectively.		tank
Jarre et al.	2017	northern Italy climates	-	RB	Up to 60% compared with a single HP Up to 30% compared with a gas boiler	SH	-
Jidong Wang, et al.	2020	Tianjin, (China); Cardiff, (UK)	PV	PC	22.8% and 21.0% operating energy costs	DHW and SH	Water storage tank with resistance heater; Electric energy storage
Keogh et al.	2019	Belturbet, Co. Cavan, Ireland.	-	RB	442 €/year	DHW-SH	-
Lazzarin and Noro	2018	Agordo, Italy	Ground-ST	RB	with respect to the previous 15/16 season, the thermal need increased by 10%, while the NG consumption decreased by nearly 4%. -	SH	-
Li & Du	2018	China	-	RB	The control strategies can lead to a ~20% to ~65% economic benefits for hot water supply.	SH-DHW	Water storage tank

					• Control strategy II achieves a ~10% to ~23% energy cost saving than strategy I for hot water supply. • Control strategy II leads to a 6–70% cost saving from gas heater above −15 °C ambient for hourly space heating		
Lin et al.	2021	London, (UK)	-	PC	30% emissions compared to the condensing gas boiler; 13% to 48% emission reduction compared to the condensing gas boiler in terrestrial acidification, photochemical oxidant formation, particulate matter formation and fossil depletion.	SH	-
Liu & Xu	2017	China	Ground	PC	Up to 70% compared with a traditional gas boiler	DHW-SH	Ground
Lyden et al.	2022	Glasgow, United Kingdom	PV-Wind	PC	model predictive control benefits over fixed order control with levelized heat costs reducing 41 %, and heat demand met by renewables increasing 18 %	SH-DHW	Water storage tank
Matteo Dongellini et al.	2021	Bologna, (Italy)	-	RB	primary energy savings (up to 6% and to 22% with respect to AWHP and cond. boiler monovalent configurations)	SH	Water buffer tank
Menberg et al.	2017	Cambridge, United Kingdom	Ground	RB?		SH	Ground
Miglani et al.	2017	Zurich, Switzerland	St+Ground	PC	-	SH-DHW	Storage tank
Mingyang Sun et al.	2019	London, (UK)	-	PC	The main savings are in reduced opex and capex of low-carbon	Heating	-

					generation. In the 100 gCO2/kWh cases, the benefits are between 1.8 and 2.4 £ bn/year. -		
Nguyen et al.	2016	Toronto, Ontario	Ground	RB	By varying cooling and heating entering fluid temperature for a heat pump, savings ranging from 0.47% to 3.6% can be achieved compared to using a fixed entering fluid temperature pair for a heat pump	SH	Ground
Peter Fitzpatrick et al.	2020	Dublin, (Ireland); Stuttgart, (Germany); Montréal, (Canada)	-	PC	-	DHW and SH	Two buffer storage tanks (1000 litres for space heating and 400 litres for DHW).
Philipp Mehrfeld et al.	2019	Aachen, (Germany)	PV	RB	A positive effect is that the HP coverage rate can be increased from 13 % to 16 %. As a consequence, the advanced control strategy also raises the consumption of renewable energy -	DHW and SH	Thermal energy storage
Picard	2017	Brugge, Belgium	Ground	RB-PC	Savings between 30% to 50% for the energy cost and between 28 and 53% for the energy	DHW-SH	Thermal energy storage
Rainaldi et al.	2017	United Kingdom	-	PC	By considering an underfloor heating the cost and emission savings are 37% relative to a conventional gas boiler system	SH	thermal energy storage
Roccatello et al.	2021	Belluno and	-	RB	Energy savings (comparing to a heat	DHW-SH	Thermal

		Reggio Emilia, Italy			pump only solution and provided with radiators, range from 24% to 30%)		energy storage
Stafford	2017	North of England and southern Scotland.	-	PC	-	DHW-SH	-
Taler et al.	2019	Oswiecim, Poland	Ground	RB	The use of ground and air-source heat pumps and solar collectors reduced the consumption of natural gas during the year by 21,621 m3. As a consequence of the reduced natural gas consumption, the carbon dioxide emissions decreased during the year by 13.32 Mg.	SH-DHW	Buffer tank
You et al.	2017	Harbin, China	Ground	RB	With the coupled HCUT-GCHP system saving 13% of the initial investment and 4% of the operation costs are achieved relative to the non-coupled HCUT-GCHP system. When compared to the Boiler-GCHP system, the annual cost savings will be 16 thousand USD.	SH	Ground
Zanetti	2020	Milan (Italy)	PV	RB	20% of the energy consumption cost when compared to state of the art RBC and increased photovoltaic self-consumption by 30%.	SH	Storage tank
Zhou et al.	2017	Lvliang City, China	ST+PV/T panels	RB	-	SH	Heat and water storage

							tanks

Nevertheless, the diffusion of HHP systems is growing increasingly due to their promising advantages and, in this context, they are promising technologies for the future. The layouts are in all cases composed of an HP and a gas boiler. Each case study completed the layout with additional components by making each configuration different from the other. For instance, in 6 cases, water storage tanks were added. It is interesting to see that as many cases were tested in Italy as were in China.

The systems used to produce DHW are equipped with a storage tank. The boiler is used to produce heating (when it is the best option according to the control strategies) and to provide additional heating if the energy produced by the HP is not enough. The HP systems coupled with thermal storage tanks can increase the system performance, as their presence allows the operation of the HP to be shifted to the most profitable periods, minimising both the operating costs and the consumption of primary energy.

Most of the research works analysed the buffer tank or a thermal energy storage system to increase the system's thermal inertia and limit the frequency of the HP on-off cycles.

Regarding the two main typologies of control strategy, the 'best' strategy to be applied depends on different parameters related to local conditions, on external or internal signal processing and on the performance metric, such as CO_2 emissions, price (running costs) and primary energy.

The control strategy implemented with fixed parameters can have some disadvantages. For example, setting the outside temperature as the cut-off point for HP operation to avoid the frosting of the HP can have performance issues because it ignores factors like wind-chill, solar irradiation, and internal heat contribution from occupants. Nevertheless, it has the advantage that it is easy to set up. Another disadvantage is that, over time, values for the underlying parameters will change (e.g. lower CO_2-emissions for electricity production, higher costs for a particular fuel, changes in tax regimes). Thus, the values should be constantly checked in order to control whether they are adequate or if some of them should be changed i.e. by the occupants. The flexible control strategy can avoid these issues because it is based on real-time input parameters (e.g. commercial parameters).

The hybrid systems are very advantageous because, by always having a fuelled backup boiler available, the dependency on electricity can be managed with more freedom.

Moreover, it is possible to classify the control strategy based on rule control methods and on predictive control methods. The main advantage of this second kind of control strategy is due to the fact that the smart HPs can switch between gas and electricity by applying a fully-optimised control technology with predictive demand side management to automatically use the most cost-effective heating mode across time. The main disadvantages of flexible strategy systems are based on predictive strategy, in that the design, the implementation, and the use of both software and hardware parts are more

expensive and less easy to operate. Being more complex, it could be necessary to employ very expert technicians for their maintenance.

REFERENCES

Aditya, G. R. and Narsilio, G. A. (2020) 'Environmental assessment of hybrid ground source heat pump systems', *Geothermics*, 87, p. 101868. doi: https://doi.org/10.1016/j.geothermics.2020.101868.

Al-Sayyab, A. K. S., Navarro-Esbrí, J. and Mota-Babiloni, A. (2021) 'Energy, exergy, and environmental (3E) analysis of a compound ejector-heat pump with low GWP refrigerants for simultaneous data center cooling and district heating', *International Journal of Refrigeration*. doi: https://doi.org/10.1016/j.ijrefrig.2021.09.036.

Alavy, M. *et al.* (2021) 'Assessment of a novel phase change material-based thermal caisson for geothermal heating and cooling', *Energy Conversion and Management*, 234, p. 113928. doi: https://doi.org/10.1016/j.enconman.2021.113928.

Allaerts, K. *et al.* (2016) 'Improving the energy efficiency of ground-source heat pump systems in heating dominated school buildings: A case study in Belgium', *Energy and Buildings*, 138. doi: 10.1016/j.enbuild.2016.09.046.

Amirkhizi, T. S. and Jensen, I. G. (2020) 'Cost comparison and optimization of gas electric hybrid heat pumps', *WIREs Energy and Environment*, 9(3), p. e370. doi: https://doi.org/10.1002/wene.370.

Del Amo, A. *et al.* (2020) 'Analysis and optimization of a heat pump system coupled to an installation of PVT panels and a seasonal storage tank on an educational building', *Energy and Buildings*, 226, p. 110373. doi: https://doi.org/10.1016/j.enbuild.2020.110373.

Atam, E. *et al.* (2015) 'Optimal Control Approaches for Analysis of Energy Use Minimization of Hybrid Ground-Coupled Heat Pump Systems', *IEEE Transactions on Control Systems Technology*, p. 1. doi: 10.1109/TCST.2015.2445851.

Bagarella, G., Lazzarin, R. and Noro, M. (2016) 'Sizing strategy of on–off and modulating heat pump systems based on annual energy analysis', *International Journal of Refrigeration*, 65, pp. 183–193. doi: https://doi.org/10.1016/j.ijrefrig.2016.02.015.

BEIS (2016) *Evidence Gathering – Low Carbon Heating Technologies*.

Bennett, G. *et al.* (2021) 'Domestic Heating with Compact Combination Hybrids (Gas Boiler and Heat Pump) : A simple English stock model of different heating system scenarios Authors: Corresponding Author'.

Calise, F. *et al.* (2016) 'A novel solar-geothermal trigeneration system integrating water desalination: Design, dynamic simulation and economic assessment', *Energy*, 115, pp. 1533–1547. doi: https://doi.org/10.1016/j.energy.2016.07.103.

Calise, F., Macaluso, A., *et al.* (2017) 'A novel hybrid polygeneration system supplying energy and desalinated water by renewable sources in Pantelleria Island', *Energy*, 137, pp. 1086–1106. doi: https://doi.org/10.1016/j.energy.2017.03.165.

Calise, F., Dentice d'Accadia, M., *et al.* (2017) 'Optimal operating strategies of combined cooling, heating and power systems: A case study for an engine manufacturing facility', *Energy Conversion and Management*, 149, pp. 1066–1084. doi: https://doi.org/10.1016/j.enconman.2017.06.028.

Carroll, P., Chesser, M. and Lyons, P. (2020) 'Air Source Heat Pumps field studies: A systematic literature review', *Renewable and Sustainable Energy Reviews*, 134, p. 110275. doi: https://doi.org/10.1016/j.rser.2020.110275.

Chen, T. *et al.* (2021) 'Experimental research and energy consumption analysis on the economic performance of a hybrid-power gas engine heat pump with LiFePO4 battery', *Energy*, 214, p. 118913. doi: https://doi.org/10.1016/j.energy.2020.118913.

Chesser, M. *et al.* (2021) 'Air source heat pump in-situ performance', *Energy and Buildings*, 251, p. 111365. doi: https://doi.org/10.1016/j.enbuild.2021.111365.

Cho, H. *et al.* (2016) 'Design and feasibility study of combined heat and power systems integrated with heat pump', *Applied Thermal Engineering*, 93, pp. 155–165. doi: 10.1016/j.applthermaleng.2015.09.027.

Claridge, D. E. *et al.* (1987) 'A validation study of variable-base degree-day heating calculations, ASHRAE Trans. 93', pp. 57–89.

Colucci, C. *et al.* (2019) 'Energy analysis of a thermal system composed by a heat pump coupled with a PVT solar collector', 174, pp. 91–96. doi: 10.1016/j.energy.2019.02.152.

De Coninck, R. and Helsen, L. (2016) 'Practical implementation and evaluation of model predictive control for an office building in Brussels', *Energy and Buildings*, 111, pp. 290–298. doi: https://doi.org/10.1016/j.enbuild.2015.11.014.

Counsell, J. M., Khalid, Y. and Stewart, M. (2017) 'Hybrid Heat Pump for Micro Heat Network', *World Academy of Science, Engineering and Technology, International Science Index 127, International Journal of Electrical, Computer, Energetic, Electronic and Communication Engineering*. doi: doi.org/10.5281/zenodo.1132659.

D'Ettorre, F., De Rosa, M., *et al.* (2019) 'Mapping the energy flexibility potential of single buildings equipped with optimally-controlled heat pump, gas boilers and thermal storage', *Sustainable Cities and Society*, 50. doi: 10.1016/j.scs.2019.101689.

D'Ettorre, F., Conti, P., *et al.* (2019) 'Model predictive control of a hybrid heat pump system and impact of the prediction horizon on cost-saving potential and optimal storage capacity', *Applied Thermal Engineering*, 148, pp. 524–535. doi: https://doi.org/10.1016/j.applthermaleng.2018.11.063.

Dannemand, M., Perers, B. and Furbo, S. (2019) 'Performance of a demonstration solar PVT assisted heat pump system with cold buffer storage and domestic hot water storage tanks', *Energy and Buildings*, 188–189, pp. 46–57. doi: https://doi.org/10.1016/j.enbuild.2018.12.042.

Dongellini, M., Naldi, C. and Morini, G. (2021) 'Influence of sizing strategy and control rules on the energy saving potential of heat pump hybrid systems in a residential building', *Energy Conversion and Management*, 235, p. 114022. doi: 10.1016/j.enconman.2021.114022.

Dupeyrat, P., Ménézo, C. and Fortuin, S. (2014) 'Study of the thermal and electrical performances of PVT solar hot water system', *Energy and Buildings*, 68, pp. 751–755. doi: https://doi.org/10.1016/j.enbuild.2012.09.032.

EC Regulation No 842/2006 of the Council of 16 april 2014 on fluorinated greenhouse gases and repealing regulation (2014).

ehpa website (2021) *Market Report 2021*. Available at: https://www.ehpa.org/market-data/market-report-2021/.

European Commission Regulation (EU) No 517/2014 of the European parliament (2014).

Fischer, D. *et al.* (2017) 'Model-based flexibility assessment of a residential heat pump pool', *Energy*, 118, pp. 853–864. doi: https://doi.org/10.1016/j.energy.2016.10.111.

Fitzpatrick, P. *et al.* (2020) 'Influence of electricity prices on energy flexibility of integrated hybrid heat pump and thermal storage systems in a residential building', *Energy and Buildings*, 223, p. 110142. doi: https://doi.org/10.1016/j.enbuild.2020.110142.

Friedel, P. *et al.* (2019) *Annex 45 Hybrid Heat Pumps - Technology Collaboration Programme on Heat Pumping Technologies (HPT TCP)*. Available at: https://heatpumpingtechnologies.org/publications/hybrid-heat-pumps-final-report/.

Gaur, A. S., Fitiwi, D. Z. and Curtis, J. (2021) 'Heat pumps and our low-carbon future: A comprehensive review', *Energy Research & Social Science*, 71, p. 101764. doi: https://doi.org/10.1016/j.erss.2020.101764.

Grassi, W. (2018) *Heat Pumps Fundamentals and Applications*. Pisa: Springer International Publishing.

Guo, J., Bilbao, J. I. and Sproul, A. B. (2020) 'A novel solar cooling cycle – A ground coupled PV/T desiccant cooling (GPVTDC) system with low heat source temperatures', *Renewable Energy*, 162, pp. 1273–1284. doi: https://doi.org/10.1016/j.renene.2020.08.050.

Hadorn, J.-C. (2012) *IEA Solar and Heat Pump Systems Solar Heating and Cooling Task 44 & Heat Pump Programme Annex 38*, *Energy Procedia*. doi: 10.1016/j.egypro.2012.11.016.

Hadorn, J.-C. (2015) *Solar and Heat Pump Systems for Residential Buildings*. Edited by J.-C. Hadorn. Wiley.

Halvgaard, R. *et al.* (2012) 'Economic Model Predictive Control for Building Climate

Control in a Smart Grid', in *Innovative Smart Grid Technologies (ISGT), 2012 IEEE PES*, p. 6175631. doi: 10.1109/ISGT.2012.6175631.

Hawlader, M. N. A., Chou, S. K. and Ullah, M. Z. (2001) 'The performance of a solar assisted heat pump water heating system', *Applied Thermal Engineering*, 21(10), pp. 1049–1065. doi: https://doi.org/10.1016/S1359-4311(00)00105-8.

Heating Market Report 2020 (2021). Available at: http://www.ehi.eu/heating-market-report/heating-market-report-2020/.

Heinen, S., Burke, D. and O'Malley, M. (2016) 'Electricity, gas, heat integration via residential hybrid heating technologies – An investment model assessment', *Energy*, 109(C), pp. 906–919. Available at: https://econpapers.repec.org/RePEc:eee:energy:v:109:y:2016:i:c:p:906-919.

Heinz, A. and Rieberer, R. (2021) 'Energetic and economic analysis of a PV-assisted air-to-water heat pump system for renovated residential buildings with high-temperature heat emission system', *Applied Energy*, 293, p. 116953. doi: https://doi.org/10.1016/j.apenergy.2021.116953.

Hengel, F. *et al.* (2020) 'System efficiency of pvt collector-driven heat pumps', *International Journal of Thermofluids*, 5–6, p. 100034. doi: 10.1016/j.ijft.2020.100034.

Huang, J., Fan, J. and Furbo, S. (2020) 'Demonstration and optimization of a solar district heating system with ground source heat pumps', *Solar Energy*, 202, pp. 171–189. doi: https://doi.org/10.1016/j.solener.2020.03.097.

Hundy, G. F. (2016) *Refrugeration, Air Conditioning and Heat Pumps*. Fifth Edit. Edited by Elsevier. Cambridge: McGraw-Hill Book Company.

Ikeda, S., Choi, W. and Ooka, R. (2017) 'Optimization method for multiple heat source operation including ground source heat pump considering dynamic variation in ground temperature', *Applied Energy*, 193, pp. 466–478. doi: 10.1016/j.apenergy.2017.02.047.

Jarre, M. *et al.* (2017) 'Opportunities for heat pumps adoption in existing buildings: real-data analysis and numerical simulation', *Energy Procedia*, 134, pp. 499–507. doi: https://doi.org/10.1016/j.egypro.2017.09.608.

Kalogirou, S. and Florides, G. (2016) 'Solar Space Heating and Cooling Systems', in *Reference Module in Earth Systems and Environmental Sciences*. doi: 10.1016/B978-0-12-409548-9.09701-3.

Keogh, D. *et al.* (2019) 'Energy assessment of hybrid heat pump systems as a retrofit measure in residential housing stock', *E3S Web of Conferences*, 111, p. 1064. doi: 10.1051/e3sconf/201911101064.

Kim, B. *et al.* (2020) 'Performance assessment of optimized heat pump water heaters using low-GWP refrigerants for high- and low-temperature applications', *Applied Thermal Engineering*, 181, p. 115954. doi: https://doi.org/10.1016/j.applthermaleng.2020.115954.

Kozarcanin, S. *et al.* (2020) 'Impact of climate change on the cost-optimal mix of decentralised heat pump and gas boiler technologies in Europe', *Energy Policy*, 140, p. 111386. doi: https://doi.org/10.1016/j.enpol.2020.111386.

Lazzarin, R. (2020) 'Heat pumps and solar energy: A review with some insights in the future', *International Journal of Refrigeration*, 116, pp. 146–160. doi: https://doi.org/10.1016/j.ijrefrig.2020.03.031.

Li, G. (2018) 'Parallel loop configuration for hybrid heat pump–gas fired water heater system with smart control strategy', *Applied Thermal Engineering*, 138, pp. 807–818. doi: 10.1016/j.applthermaleng.2018.04.087.

Li, G. and Du, Y. (2018) 'Performance investigation and economic benefits of new control strategies for heat pump-gas fired water heater hybrid system', *Applied Energy*, 232, pp. 101–118. doi: https://doi.org/10.1016/j.apenergy.2018.09.065.

Lin, H. *et al.* (2021) 'Environmental life cycle assessment of heating systems in the UK: Comparative assessment of hybrid heat pumps vs. condensing gas boilers', *Energy and Buildings*, 240, p. 110865. doi: 10.1016/j.enbuild.2021.110865.

Liu, Z. *et al.* (2017) 'Feasibility and performance study of the hybrid ground-source heat pump system for one office building in Chinese heating dominated areas', *Renewable Energy*, 101, pp. 1131–1140. doi: https://doi.org/10.1016/j.renene.2016.10.006.

Long, J. *et al.* (2021) 'Study on energy-saving operation of a combined heating system of solar hot water and air source heat pump', *Energy Conversion and Management*, 229(December 2020), p. 113624. doi: 10.1016/j.enconman.2020.113624.

Lun, Y. H. V. and Tung, S. L. D. (2020) *Heat Pumps for Sustainable Heating and Cooling*. Springer.

Lyden, A. and Tuohy, P. G. (2022) 'Planning level sizing of heat pumps and hot water tanks incorporating model predictive control and future electricity tariffs', *Energy*, 238, p. 121731. doi: https://doi.org/10.1016/j.energy.2021.121731.

Market Report 2021 (no date). Available at: https://www.ehpa.org/market-data/market-report-2021/.

Martorana, F. *et al.* (2021) 'Solar-assisted heat pumps systems for domestic hot water production in small energy communities', *Solar Energy*, 217(November 2020), pp. 113–133. doi: 10.1016/j.solener.2021.01.020.

McNeil, M. A. *et al.* (2016) 'Energy efficiency outlook in China's urban buildings sector through 2030', *Energy Policy*, 97, pp. 532–539. doi: https://doi.org/10.1016/j.enpol.2016.07.033.

Mehrfeld, P. *et al.* (2020) 'Calibration of a Hybrid Heat Pump System and Application of an Energy Manager in Building Performance Simulations', in. doi: 10.26868/25222708.2019.210350.

Menberg, K. *et al.* (2017) 'Exergy analysis of a hybrid ground-source heat pump system', *Applied Energy*, 204, pp. 31–46. doi: https://doi.org/10.1016/j.apenergy.2017.06.076.

Mi, P., Ma, L. and Zhang, J. (2020a) 'Integrated optimization study of hot water supply system with multi-heat-source for the public bath based on PVT heat pump and water source heat pump', *Applied Thermal Engineering*, 176(February), p. 115146. doi: 10.1016/j.applthermaleng.2020.115146.

Mi, P., Ma, L. and Zhang, J. (2020b) 'Integrated optimization study of hot water supply system with multi-heat-source for the public bath based on PVT heat pump and water source heat pump', *Applied Thermal Engineering*, 176, p. 115146. doi: https://doi.org/10.1016/j.applthermaleng.2020.115146.

Miglani, S., Orehounig, K. and Carmeliet, J. (2017) 'Design and optimization of a hybrid solar ground source heat pump with seasonal regeneration', *Energy Procedia*, 122, pp. 1015–1020. doi: 10.1016/j.egypro.2017.07.468.

Miglioli, A. *et al.* (2021) 'Photovoltaic-thermal solar-assisted heat pump systems for building applications: Integration and design methods', *Energy and Built Environment*. doi: https://doi.org/10.1016/j.enbenv.2021.07.002.

NEEA (2015) *HEAT PUMP WATER HEATER MODEL VALIDATION*. Seattle, WA 98105.

Neyer, D. D. (2018) *New Generation Solar Heating and Cooling - Assessment and Technology Development*.

Nguyen, H. *et al.* (2016) 'A techno-economic analysis of heat-pump entering fluid temperatures, and CO2 emissions for hybrid ground-source heat pump systems', *Geothermics*, 61, pp. 24–34. doi: 10.1016/j.geothermics.2016.01.013.

'No Title' (no date). Available at: http://www.stats.ehpa.org/hp_sales/country_cards/.

Obalanlege, M. A. *et al.* (2020) 'Performance assessment of a hybrid photovoltaic-thermal and heat pump system for solar heating and electricity', *Renewable Energy*, 148, pp. 558–572. doi: https://doi.org/10.1016/j.renene.2019.10.061.

Palomba, V. *et al.* (2018) 'Experimental and numerical analysis of a SOFC-CHP system with adsorption and hybrid chillers for telecommunication applications', *Applied Energy*, 216, pp. 620–633. doi: https://doi.org/10.1016/j.apenergy.2018.02.063.

Palomba, V. *et al.* (2021) 'Hybrid Cascade Heat Pump and Thermal-Electric Energy Storage System for Residential Buildings: Experimental Testing and Performance Analysis', *Energies*, 14(9). doi: 10.3390/en14092580.

Pena-Bello, A. *et al.* (2021) 'Decarbonizing heat with PV-coupled heat pumps supported by electricity and heat storage: Impacts and trade-offs for prosumers and the grid', *Energy Conversion and Management*, 240, p. 114220. doi: https://doi.org/10.1016/j.enconman.2021.114220.

Picard, D. (2017) 'Modeling, Optimal Control and HVAC Design of Large Buildings using Ground Source Heat Pump Systems'. Available at: [freely.

Poredos, P. *et al.* (2017) 'Eligibility of a Heat Pump Based on the Primary Energy Factor', in.

Poredoš, P. *et al.* (2017) 'Thermo-economic and primary-energy-factor assessment based on the field test of an air-to-water heat pump', *International Journal of Refrigeration*, 76, pp. 19–28. doi: https://doi.org/10.1016/j.ijrefrig.2017.02.003.

Renaldi, R., Kiprakis, A. and Friedrich, D. (2017) 'An optimisation framework for thermal energy storage integration in a residential heat pump heating system', *Applied Energy*, 186, pp. 520–529. doi: https://doi.org/10.1016/j.apenergy.2016.02.067.

Ricardo Energy & Environment (2020) *Heat Pumps - Technology Guide*.

Rivoire, M. *et al.* (2018) 'Dynamic simulation of Ground-Coupled Heat Pumps (GCHPs): insights on the economic convenience and on the environmental benefits', in *EGU General Assembly Conference Abstracts*. (EGU General Assembly Conference Abstracts), p. 1656.

Saini, P. *et al.* (2021) 'Techno-economic analysis of an exhaust air heat pump system assisted by unglazed transpired solar collectors in a Swedish residential cluster', *Solar Energy*, 224, pp. 966–983. doi: https://doi.org/10.1016/j.solener.2021.06.026.

Sevindik, S. and Spataru, C. (2020) 'Life Cycle Assessment of Domestic Heat Pumps with Gas Boilers and Hybrid Scenario Analysis in the UK', in.

Shapiro, C. and Puttagunta, S. (2016) *Field Performance of Heat Pump Water Heaters in the Northeast*. Norwalk, CT.

Shen, B., Nawaz, K. and Elatar, A. (2021) 'Parametric Studies of Heat Pump Water Heater Using Low GWP Refrigerants', *International Journal of Refrigeration*. doi: https://doi.org/10.1016/j.ijrefrig.2021.07.015.

Soni, S. K., Pandey, M. and Bartaria, V. N. (2016) 'Hybrid ground coupled heat exchanger systems for space heating/cooling applications: A review', *Renewable and Sustainable Energy Reviews*, 60, pp. 724–738. doi: https://doi.org/10.1016/j.rser.2016.01.125.

Stafford, A. (2017) 'An exploration of load-shifting potential in real in-situ heat-pump/gas-boiler hybrid systems', *Building Services Engineering Research and Technology*, 38(4), pp. 450–460. doi: 10.1177/0143624416688727.

Sun, M. *et al.* (2019) 'Benefits of smart control of hybrid heat pumps: An analysis of field trial data', *Applied Energy*, 247, pp. 525–536. doi: 10.1016/j.apenergy.2019.04.068.

Taler, D., Pitry, R. and Taler, J. (2019) 'Operation assessment of hybrid heat source for heating the building and preparation of hot water in the fire brigade building', *Journal*

of Cleaner Production, 214, pp. 962–974. doi: https://doi.org/10.1016/j.jclepro.2018.12.259.

UNI EN 12309-1 (2002) *Gas-fired absorption and adsorption air-conditioning and/or heat pump appliances with a net heat input not exceeding 70kW, UNI (IT).*

UNI EN 14511-1 (2018) *Condizionatori, refrigeratori di liquido e pompe di calore con compressore elettrico per il riscaldamento e il raffrescamento degli ambienti e refrigeratori per cicli di processo con compressore elettrico - Parte 1: Termini e definizioni*.

UNI EN 14825 (2019) 'Condizionatori d'aria, refrigeratori di liquido e pompe di calore, con compressore elettrico, per il riscaldamento e il raffrescamento degli ambienti - Metodi di prova e valutazione a carico parziale e calcolo del rendimento stagionale'.

UNI EN 16147 (2017) *Pompe di calore con compressore elettrico - Prove, valutazione delle prestazioni e requisiti per la marcatura delle apparecchiature per acqua calda sanitaria*.

Wang, J. *et al.* (2020) 'Optimal scheduling of gas and electricity consumption in a smart home with a hybrid gas boiler and electric heating system', *Energy*, 204, p. 117951. doi: 10.1016/j.energy.2020.117951.

Wang, X. *et al.* (2017) 'Optimal Design methods and experimental validation for hybrid ground source heat pump system with gas boiler', *Procedia Engineering*, 205, pp. 4149–4156. doi: 10.1016/j.proeng.2017.10.159.

Wang, X. *et al.* (2020) 'A systematic review of recent air source heat pump (ASHP) systems assisted by solar thermal, photovoltaic and photovoltaic/thermal sources', *Renewable Energy*, 146, pp. 2472–2487. doi: https://doi.org/10.1016/j.renene.2019.08.096.

Willem, H., Lin, Y. and Lekov, A. (2017) 'Review of energy efficiency and system performance of residential heat pump water heaters', *Energy and Buildings*, 143, pp. 191–201. doi: https://doi.org/10.1016/j.enbuild.2017.02.023.

Wu, D., Hu, B. and Wang, R. Z. (2021) 'Vapor compression heat pumps with pure Low-GWP refrigerants', *Renewable and Sustainable Energy Reviews*, 138, p. 110571. doi: https://doi.org/10.1016/j.rser.2020.110571.

Xu, L. *et al.* (2021) 'Hybrid ground source heat pump system for overcoming soil thermal imbalance: A review', *Sustainable Energy Technologies and Assessments*, 44, p. 101098. doi: https://doi.org/10.1016/j.seta.2021.101098.

Yang, C. *et al.* (2021) 'The life cycle climate performance evaluation of low-GWP refrigerants for domestic heat pumps', *International Journal of Refrigeration*, 121, pp. 33–42. doi: https://doi.org/10.1016/j.ijrefrig.2020.09.020.

Yang, L. W. *et al.* (2021) 'Review of the advances in solar-assisted air source heat pumps for the domestic sector', *Energy Conversion and Management*, 247, p. 114710.

doi: https://doi.org/10.1016/j.enconman.2021.114710.

You, T. *et al.* (2021) 'Hybrid photovoltaic/thermal and ground source heat pump: Review and perspective', *Renewable and Sustainable Energy Reviews*, 151, p. 111569. doi: https://doi.org/10.1016/j.rser.2021.111569.

Zanetti, E. *et al.* (2020) 'Energy saving potentials of a photovoltaic assisted heat pump for hybrid building heating system via optimal control', *Journal of Building Engineering*, 27, p. 100854. doi: https://doi.org/10.1016/j.jobe.2019.100854.

Zhang, L. *et al.* (2018) 'Advances in vapor compression air source heat pump system in cold regions: A review', *Renewable and Sustainable Energy Reviews*, 81, pp. 353–365. doi: https://doi.org/10.1016/j.rser.2017.08.009.

Zhang, L. *et al.* (2021) 'A review of machine learning in building load prediction', *Applied Energy*, 285, p. 116452. doi: https://doi.org/10.1016/j.apenergy.2021.116452.

Zhou, J. *et al.* (2017) 'Clear-days operational performance of a hybrid experimental space heating system employing the novel mini-channel solar thermal \& PV/T panels and a heat pump', *Solar Energy*, 155, pp. 464–477.

4. Design and performance analysis of the systems'setup

The main subject of this thesis is the study of the energy performances of several system configurations based on solar-assisted heat pumps equipped with photovoltaic (PV) and photovoltaic-thermal (PV/T) panels as well as solar thermal collectors.
After having introduced, in chapter 3, the concept of systems based on the coupling of hybrid PV/T collectors and HPWH aimed at producing DHW and having highlighted the main energy benefits given by this integrated solution, this section presents the analysis and dynamic modeling of their functioning. The modeling of the systems and the simulation studies were fundamental to test the behaviour and the performances of the main components involved in configuration systems.
The behaviour of the systems has been simulated using Transient System Simulation (TRNSYS) tool. TRNSYS simulations allowed assessing the dynamic performance of the main system devices, such as PV/T collectors, HPWH, thermal and electrical storages, based on the datasheet provided by the manufacture and experimental data found in the literature (Rizzini, 2015). The systems under analysis were compared with equivalent plant configurations based exclusively on solar thermal collectors or exclusively on photovoltaic panels. The aim is to underline the additional benefits given by the hybrid combination of the two technologies compared to the separate electrical and thermal contributions from PV and ST collectors respectively.
The systems are sized to serve small aggregates of users assumed as micro-energy communities in low housing density context in the South of Italy. Electricity storage is also considered to smooth the interaction with the electric grid.
These studies have been finalized to the realization of a real-scale experimental setup aimed at characterizing the operation of the systems under study, in the context of a collaboration project with ENEA (Report RdS / PTR2019 "Feasibility study of solutions for the energy efficiency of the Minor Islands"). The goal of the project is to create an experimental setup that allows monitoring and verifying, on the one hand, the thermal and electrical performance of the PV/T collectors as the environmental and operating conditions vary, and on the other to monitor the performance of heat pumps electrically powered by the solar system for different user profiles. The experimental set-up was designed and sized according to the indications of the regulations currently in force in the area.
Considering that there is currently no "ad hoc" regulation for PVT hybrid solar collectors to refer to for quality and performance tests, the regulations relating to solar thermal collectors and photovoltaic panels are used.
Following the indications of these regulations, the layout of the hydraulic and electrical circuits of the system have been defined. After having dimensioned the main components, the experimental apparatus necessary for the realization of the experimental set-up of the manifold and to be able to carry out the necessary measurements for the various tests required by the regulations was identified.

After a phase of managing the purchases of all the necessary components, the experimental analyses to be performed on the system in an external environment were defined. The plant is currently being assembled at the dedicated site, identified at the Casaccia ENEA Research Center in Rome (Italy). After commissioning and testing of the main components, it will be possible to proceed with the planned experimental analyzes and the data collection and analysis campaign.

This chapter reports the criteria used for dimensioning of the main components of the system and definition of the experimental set-up configuration, which is currently being built up at the Casaccia Research Centre of the Italian National Board for New Technology, Energy and the Environment (Ente per le Nuove Tecnologie l'Energia e l'Ambiente, ENEA), located in Rome (Italy).

At a preliminary stage, the dynamic modelling and simulations have been aimed at optimising the size of system components for better supporting a power-to-heat approach. All the criteria used to design and size the components of the systems are adopted according to the European Standard UNI EN ISO 9806 (UNI EN ISO 9806, 2017a) as well as the required features of the devices and the sensors to be included for monitoring the experimental setup.

The general approach of the study is depicted step-by-step as a graphical workflow in Figure 4.1.

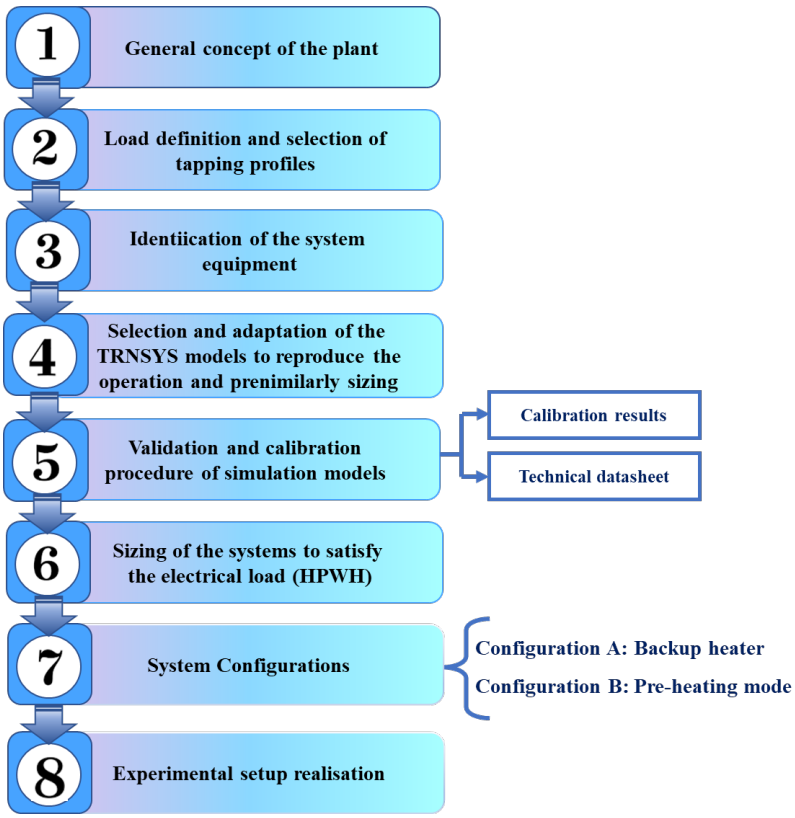

Figure 4.1. Step-by-step workflow of the approach adopted

As the first step, the general concept of the plant was defined. The loads' definition is then performed identifying several DHW load profiles. These were selected among the standard profiles (M, L, XL, UNI-A) defined by Regulations (EU) No 814/ 2013 and UNI EN 12831 (step 2). A description of the main components, which were chosen as system equipment for the realization of the experimental setup, is then provided in step 3 reporting their rated technical and physical characteristics. By changing the typology of some components, several possible variants can be settled. Several types of equipment are present in all the plant configurations, such as thermal storage, heat pump, pipes, circulators, valves, and other auxiliary components.
The study is based on the results of detailed dynamic simulations, so a general TRNSYS model was developed to reproduce the operation of the overall plant as far as to do preliminary sizing. Each component and device was associated with a specific TRNSYS type (step 4). Before running TRNSYS simulations of the entire plant, each sub-routines were tested separately and, when required, a validation and calibration process was conducted (step 5). The validated models allowed exploring the dynamic performance of the systems under different climate and operation conditions.
In particular, three different types of panels (PV/T, PV, and ST) and a different number of them (4, 6, and 8) were studied to assess their performances.
The main object of study of the first phase was the sizing of the hybrid solar system and specifically the number of panels that allow optimising the energy consumption of the system and the consequent choice of auxiliary components (inverter, storage, etc.). Moreover, comparisons between the proposed technology and traditional systems in which the HP is combined with a solar photovoltaic or solar thermal system were made. Having established the size of the PV system, it was hypothesized to introduce a thermal storage tank that was used as a pre-heating system for domestic water from the aqueduct employing the thermal energy produced by the RES system. In the latter case, the size of the aforementioned accumulation was analysed. As the sixth step, the solar plants were sized to match the electrical and thermal loads.
After the sizing of the systems, two different integration configurations were analysed depending on the different functions of the thermal contribution of the PV/T string within the entire system: configuration A and configuration B (step 7). In the former, the water heated by PV/T collectors is used to directly feed the heat pump, in the latter instead the thermal contribution is used to preheat the water feeding the heat pump by using an intermediate solar storage tank. The results of the simulation here described will be reported and discussed in Chapter 5.

4.1 The general concept of the plants

The present study investigates different kinds of plants for DHW production, which use the HPWH technology coupled with solar collectors/panels (i.e., which can be PV, PV/T, or ST). In particular, a split equipment as HPWH was chosen. Its internal unit

includes an integrated service water tank embedding three different heat exchangers. The first one is dedicated to the fast production of DHW, while the second is the condenser of the heat pump cycle. A supplementary heat exchanger enables the connection with auxiliary heating devices. In this case, this heat exchanger is used to couple the storage with the solar thermal loop when ST or PV/T collectors are considered. Figure 4.2 describes the common scheme that can be adapted to define several variants according to the solar components' typology and the size of the components.

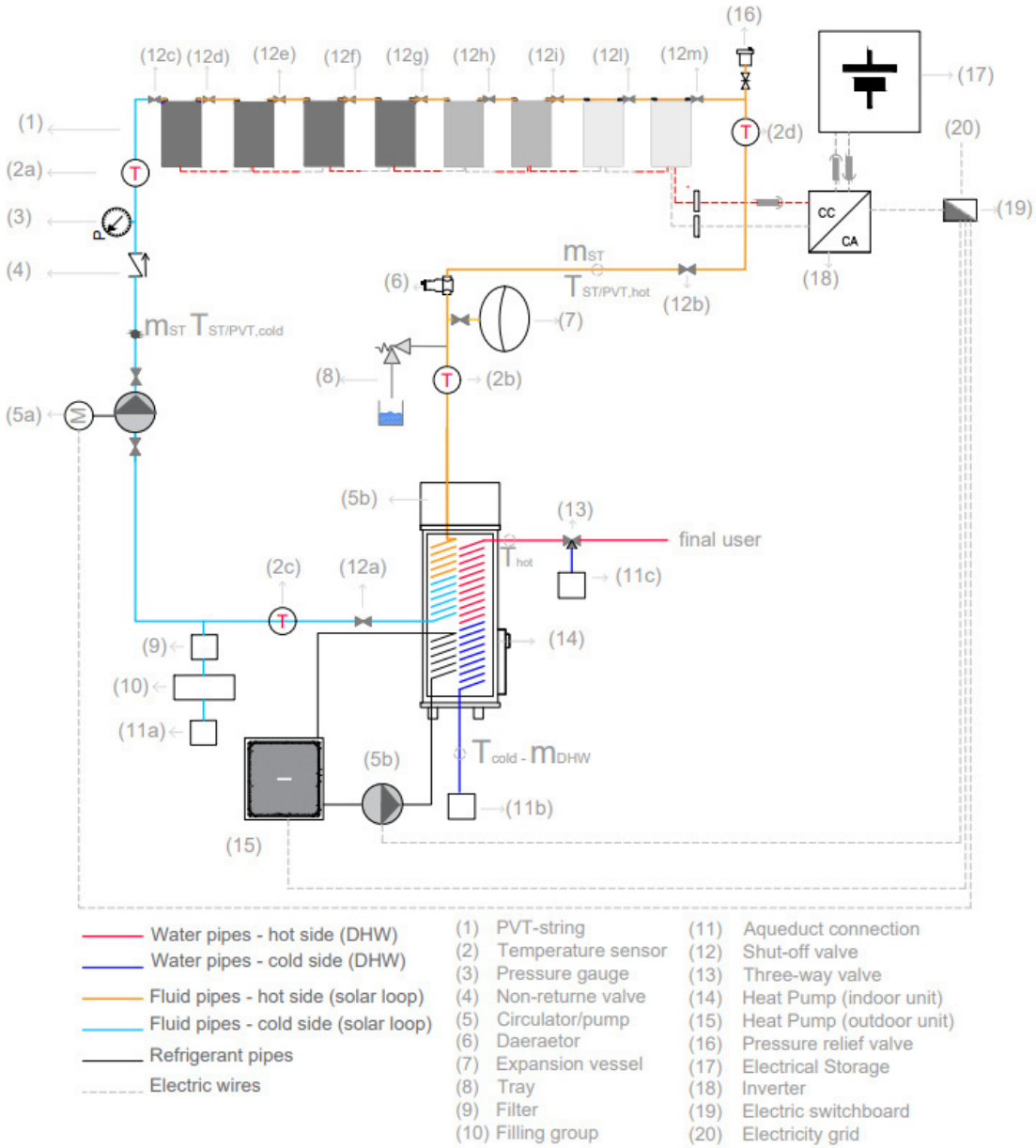

Figure 4.2. General layout of the plant

The study aims to understand how each plant variant can cover the assigned load with the minimum requirement of energy, by using solar contribution through the optimization of the storages and reducing interaction with external energy sources. A focus was also dedicated to the flexibility of the systems in terms of suitability to operate in demand-response mode. To do this, a TRNSYS model was developed, and a set of hourly tapping profiles were built to check for differences in system performances while changing solar components and the number of panels.
The components which were used as the basis for the design of the plant dedicated to the production of DHW are described in detail in section 4.2. The main objective was to reduce the thermal consumption of the system by exploiting solar production, consequently reducing the electricity consumption of the HP and at the same time ensuring coverage of the latter by means of the electricity production of the PV system.
Specifically, two main plant solutions have been hypothesized, with the aim of pre-dimensioning the main components and verifying the advantages and disadvantages of each of them.
Beyond the detailed solutions reported and commented in chapter 5, in the first phase it was assumed that the solar thermal system circuit was directly connected to the HP; while, in a subsequent phase, the presence of a thermal pre-storage tank was assumed.

4.1.1. Load definition and selection of tapping profiles

For the sizing of DHW production it is necessary to consider three main aspects:

- determination of the maximum simultaneous flow rate and period of time in which it can be maintained;
- determination of the maximum energy consumption in a given period of time and the load profiles that can occur;
- determination of the charging time of the thermal storage.

Once a specific HPWH was selected, a set of hourly fractional tapping profiles for multiple users was defined to simulate the demand of micro-energy communities. The hourly demand of hot water is then calculated by multiplying these factors for the daily deliverable volume. Seven combinations of three standard profiles (M, L, XL) defined by Regulation (EU) No 814/2013 (*COMMISSION REGULATION (EU) No 814/2013 of 2 August 2013-Implementing Directive 2009/125/EC of the European Parliament and of the Council with regard to ecodesign requirements for water heaters and hot water storage tanks*, 2013) and by UNI EN 12831 (UNI-A) were built (Fig. 4.3 and Table 4.1).

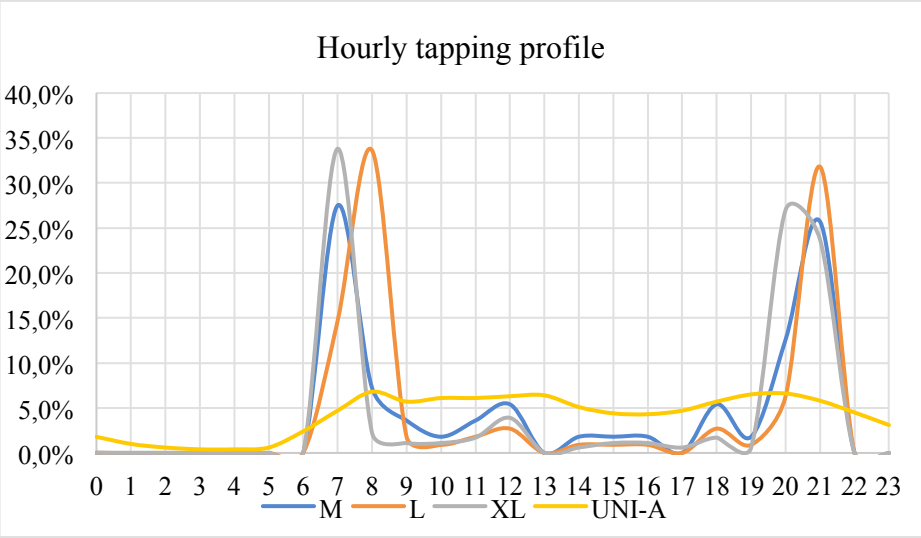

Figure 4.3. Different hourly tapping profiles according to Regulation (EU) No 814/2013 and UNI EN 12831

Once different hourly distributions were chosen, the maximum amount of deliverable DHW at the temperature of 40 ◦C using HPWH was a matter of research. Simulations were then run by increasing the daily DHW volume until the delivered DHW temperature dropped below a critical value (T_{tap} < 40 ◦C) for the first time. The result is a maximum value of 720 L per day. The above-mentioned tapping profiles associated with the maximum water volume that can be heated per day without impinging the users' comfort are listed in Table 4.1.

Table 4.1. Combination of profiles for the analysed scenarios

Tapping 1	Tapping 2	Tapping 3	Tapping 4	Tapping 5	Tapping 6	Tapping 7
2XL	3L	6M	1M+ 1L + 1XL	2L + 1XL	3M + 1XL	UNI-A

In the nomenclature section, these combinations are reported and further explained.

4.2 Identification of main components of the system

All the experimental analyses to be performed on the hybrid collector will be carried out in an external environment, at the laboratories of Casaccia Research Centre of ENEA and are aimed at investigating the effectiveness of innovative solutions for the energy efficiency of users in small islands. The experimental apparatus relating to the thermal part of the system mainly consists of the PV/T string, an air-to-water heat pump, a circulation pump, and a flow meter, while the electrical side presents an hybrid storage inverter and the photovoltaic modules of the PV/T collectors.
Systems based on the use of HPs combined with solar systems, have resulted to be a valid alternative solely dedicated to the DHW production, especially in the context of small Italian islands where the latter is entrusted to electric water heaters. However, a

plant system created in this way presupposes the availability of a surface on the roof such as to be able to install a sufficient number of photovoltaic panels and / or solar collectors, surfaces not always available. Starting from the latter consideration this work proposes, with regard to production systems from solar sources, the use of hybrid PV/T technology. As already highlighted in chapter 1, these collectors are a valid solution for the optimisation of the the use of spaces. As regards the PV/T plant, the hybrid module of the Fototherm FT300AL series was chosen (figure 4.4).

Figure 4.4. Uncovered PV/T panel by Fototherm

It is an uncovered PV/T panel with a sheet-and-tube thermal absorber using water as heat transfer fluid. It falls into the category of hybrid collectors obtained by equipping photovoltaic modules with a heat exchanger for the exploitation of thermal energy.
The panel has a rated power of 300 W_p with a module of 60 monocrystalline silicon PV cells and is connected at the rear with a copper-made absorber with polyurethane foam insulation. The entire panel is closed with a pre-painted aluminium sheet (Leonforte, 2014). Its nominal thermal power is 921 W.

Table 4.2 PV/T technical features.

Parameter	Value	Unit
Dimensions	1660x990x51	mm
Aperture area	1.58	m^2
Number of cells	60	-
Rated power	300	Wp
Electrical efficiency η	18.3	%
Thermal efficiency η_0	58.3	%
Nominal thermal power	921	W
Fluid volume	0.96	l
Coefficient α1	6.08	$W(m^2K)^{-1}$
Coefficient α2	0	$W(m^2K^2)^{-1}$
IAM K0 at 50° C	96.0	%

It must be underlined that the considered PV panels have the same characteristics as the electrical part of the PV/T panels. Indeed, the panels share the same PV equipment, but

not the same system to remove the heat. The technical features of the ST collectors are reported in table 4.3.

Table 4.3. ST collectors' technical features.

Parameter	Value	Unit
Area	1.8	m^2
Efficiency η_0	0.78	-
Coefficient a_1	3.5	$W(m^2K)^{-1}$
Coefficient a_2	0.015	$W(m^2K^2)^{-1}$
Incidence Angle Modifier (IAM)	0.94	-

For the thermal performance test, the collectors will be positioned on a steel support structure, at a height of about one meter from the floor (*UNI EN ISO 9806*, 2017b), and oriented towards the south with a tilt angle of 45°. The support structure is however made in such a way as to allow to vary the angle of inclination of the collector surface (tilt angle).

The project is based on the hypothesis of being able to exploit a hybrid solar system for the production of domestic hot water (DHW). To achieve this, it was decided to couple the hybrid manifold to a heat pump employing a hot water tank with an internal heat exchanger.

The HP, chosen for the study, is an air to water heat pump characterised by a nominal electric power of 700 W, a COP = 4.3 for an external temperature of 7 °C, and a 500 litres service-water tank equipped with a dedicated heat exchanger for DWH production.

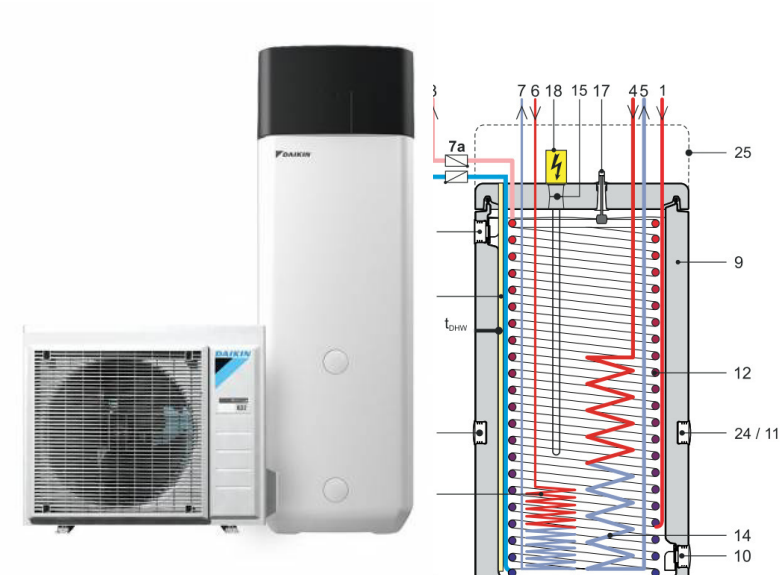

Figure 4.5. The selected HPWH and its inner structure: (1) solar feed, (2) cold water connection, (3) hot water outlet, (4) feed solar, (5) return solar, (6) connection for refrigerant gas line, (7) connection for refrigerant liquid line, (7a) circulation stop valves, (9) storage tank, (10) filling and draining connection or return for solar integration, (11/24) mount for solar controller or handle, (12) heat exchanger for DHW

heating, (13) heat exchanger for storage tank charging by condenser, (14) heat exchanger for storage tank charging by pressurised solar heat generator, (15) connection for integrated electrical Booster-Heater, (17) fill level indicator, (18) integrated electrical Booster-Heater, (19) sensor pocket for tank temperature sensor, (20) pressure-free storage tank water, (23) safety overflow connection, (25) cover hood.

Its internal unit includes a technical water tank embedding three different heat exchangers. The first one is dedicated to the fast production of DHW, while the second is the condenser of the heat pump cycle. A supplementary heat exchanger enables the connection with auxiliary heating devices. In this case, this heat exchanger is used to couple the storage with the solar thermal loop of the PV/T collectors. The heat exchanger can deliver an average of 2790 W/K of specific thermal power and its heat losses at maximum storage temperature are 1.4 kWh/day. The main technical data of the HP are reported in Table 4.4.

Table 4.4. HPWH technical datasheet

PARAMETERS	**Value**	**Unit**
Declared tapping profile	XL	-
COP	4,30	-
Parameter Internal Unit	Value	Unit
Tank water volume	477	l
Max. water temperature (tank)	85	°C
Operating range (DHW) Min.~Max.		
External Temperature	2~35	°CDB
Water side	5~55	°C
Refrigerant type	R-410A	-
Parameter external unit	Value	Unit
Operating range (DHW) Min.~Max.	-15~35	°CDB
Rated compressor power	700	W

The basic idea is to be able to exploit the thermal power produced by the hybrid collector to preheat the water for the hot water tank while increasing efficiency.
In the branch of connection between the manifold and the tank, it is thought to insert a diverter valve controlled by a differential solenoid valve. The latter serves to ensure that the fluid leaving the collector has a higher temperature than that of the fluid contained in the lower part of the tank. If this does not occur, the fluid would instead be diverted towards the by-pass branch and sent back inside the manifold to undergo further heating.
Should there be an overproduction of electrical energy in the PV part, this, in addition to being used to power the heat pump, would be accumulated inside the electric batteries to delay the availability of the system's electricity over time.
The inverter used is a HYD 3000 ES hybrid device, which is combined with a 5 kWh lithium storage system (Figure 4.6).

With the inverter it is possible to manage the battery charge/discharge mode according to programs that can be customized and set remotely by the user, ensuring a good degree of flexibility.
The electrical storage was sized to ensure one day of system autonomy, according to winter averagely consumption by the heat pump. However, their main characteristics are summarized in tables 4.5 and 4.6:

Figure 4.6. ZCS Hybrid storage inverter by AZZURRO

Table 4.5. Storage battery technical features

Parameter	Value	Unit
Battery type	Li-on	-
Rated voltage	48	V
Rated capacity	4.95	kWh
Charging efficiency	0.95	-
Suggested charge current	60-70	A

Table 4.6. Inverter technical features.

Parameter	Value	Unit
Rated power	3000	W
Max input voltage	600	V
Activating voltage	120	V
AC nominal voltage range	180-276	V
Inverter efficiency	0.97	-
Regulator efficiency	0.84	-
Type	MPPT	
Connection	grid-on	
output voltage	230	V
output frequency	50	Hz

The water from the aqueduct is introduced into the heat pump. A check valve has been installed to prevent fluid flow reversals downstream of the circulator. Additional valves have been inserted in the hydraulic circuit to isolate the main components of the system

if maintenance or replacement interventions are necessary. A flowmeter was selected to determine the flow rate.

The UNI EN ISO 9806 standard for thermal efficiency measurements requires three temperature data: the temperature of the fluid at the inlet of the collector, the temperature of the fluid at the outlet of the collector, and the temperature of the ambient air. The temperature values of the absorbent plate and the photovoltaic laminate are detected using contact PT100 probes. For the measurements relating to the temperature of the hydraulic circuit, immersion Pt100 sensors were installed in correspondence with the inputs and outputs of the collector and the boiler and three Pt100 immersion sensors inside the boiler itself. The temperature sensors of the heat transfer fluid must be positioned at a distance from the inlet and outlet of the collector that does not exceed 200 mm (UNI EN ISO 9806, 2017a).

Regarding the UNI EN 12976 standard, the layout has been designed in such a way that the total length of the pipeline respects the maximum limit of 20 meters (10 m outgoing and 10 m returning). It was decided to use insulated annealed copper pipes to be able to use Cu thermocouples, avoiding wells, to measure the temperatures of the fluid in the fundamental points of the circuit.

The computometric data of all the components necessary for the realization of the setup, both hydraulic and electrical ones, are reported with more detail in Appendix A.

4.3 TRNSYS models of analysed systems

Once defined the general task, the first steps of the work were related to planning the simulation study by using the TRNSYS tool. Most common components such as solar thermal collector, inverter, electrical storage, and other auxiliary devices were simulated by using the types shown in Table 4.7 (TRNSYS library).

Table 4.7. TRNSYS *types* with the related modelled components

Component	TRNSYS Type
Heat Pump Water Heater	938 (TESS)
Thermal Storage Tank	1237 (TESS)
Water Heater Energy Supply	1226 (TESS)
PVT/PV Panel	560 (TESS)
Solar Thermal Collector	1b
Circulator	3
Regulator Charge/Inverter	48b
Electrical Storage Battery	47a
Weather Data Processor	15

The two main (and less conventional) investigated devices are the PV/T collector and the HPWH. Consequently, a search on available TRNSYS routines and the correlated types was conducted. In particular, Type 560 (Ruoping *et al.*, 2020)(Specialists, 2017) was chosen for simulating the behaviour of the PV/T collector. Since no TRNSYS type is available for simulating the described air-to-water heat pump, a specific model was

set up for the heat pump operation. It was based on the combined simulation was performed through the Type 938 (heat pump) coupled with Type 1237 (water tank) (TESS Specialists, 2017) (Beccali *et al.*, 2020). After the first test simulations, some critical issues concerning both HPWH and PV/T sub-routines' reliability for the specific case studies arose. In order to obtain consistent results from the two sub-routines, they were tested separately. Moreover, the two sub-routines were used for the first time under nominal operating conditions according to the European standards for labelling: UNI EN 16147:2017 for the HPWH (UNI EN 16147, 2017) and UNI EN ISO 9806 (UNI EN ISO 9806, 2017) for the PV/T collector. Specifically, both documents define the way tests have to be performed to obtain the target values to be declared in the datasheet. Several simulations were run at nominal conditions while changing sensible parameter values. The output from the TRNSYS model was then compared to the declared features in the datasheet in order to match a relative error between official data and simulation results below ± 5%. The detailed work done for PV/T and HPWH models' validation and calibration is discussed in sections 4.3.1.1. and 4.3.1.2. respectively. After the calibration procedure, the sub-routine models for heat pump and hybrid solar panels were integrated into the simulation model. The latter included other most common types to simulate the overall detected plant including inverter, electric storage, and control system. Type 1b is used for ST panels while in order to calculate the electricity production of PV panels the electric model of Type 560 is used. It means that the solar thermal contribution was neglected (the mass of the fluid was set equal to zero) and the cells operated as in an ordinary PV panel. Time distribution of water withdrawal is set in the model according to the hourly DHW demand tapping profile through a specifically dedicated macro. According to this hourly input, the domestic water passes through the wrap-around heat exchanger (Type 31) where it is warmed up. Specifically, the tank temperature is maintained at the desired setpoint temperature using the heat delivered by the heat pump thanks to a thermostat controller ("Aquastat" Type 2). A differential controller is implemented to manage the operation mode of the solar thermal or PV/T collectors. In particular, the solar water loop is activated only when the difference between the fluid temperature measured at the outlet of the last collector and the one at the top of the storage tank is positive and greater than a threshold value.

The heat balance of the water storage is evaluated as the sum of the following contributions:

$$Q_{TANK} = Q_{HPWH} - Q_{HX\_DHW} + Q_{ST} \tag{4.1}$$

where Q_{HPWH} is the thermal contribution from the HPWH to the tank, Q_{ST} is the thermal contribution from solar thermal/PV/T to the tank, Q_{HX_DHW} is the heat released from the thermal storage tank to the DHW. The PV/T collectors' type is also connected to an inverter/charge regulator subroutine and then to an electric storage type. This device contributes to the electrical operation of the system, ensuring a definite period of

autonomy for the system thanks to the production of photovoltaic electricity. The HPWH electrical consumption, the electricity production from PV, the electrical fluxes to/from the battery and to the load, the electricity yield to the grid due to battery full-of-charge status, and the solar thermal contribution to the system were studied by simulations.

4.3.1. Description of the TRNSYS model adopted for the PV/T collector.

In order to simulate the operation of the selected PV/T module in the TRNSYS software environment, among the different types available in the TRNSYS Library tool, Type 560 was used.
The component in question is intended to model the behaviour of a combined PV/T solar collector without a glass cover ("unglazed"), illustrated in figure 4.7, which has the dual purpose of producing power from the built-in photovoltaic cells and supplying heat to a fluid flowing through the tubes belonging to an absorber plate located below the PV cells (TESS Specialists, 2017).
This model is based on linear factors relating the efficiency of the PV cells to the cell temperature and also, the incident solar radiation. The cells are assumed to be operating at their maximum power point condition. The thermal model of this collector relies on algorithms presented in the “Solar Engineering of Thermal Processes” textbook by Duffie and Beckman (Duffie and Beckman, 2013). The optical properties are not constant but vary according to the angle of incidence of solar radiation. Furthermore, the convective heat exchange with the environment is not predetermined (TRNSYS website, 2020).

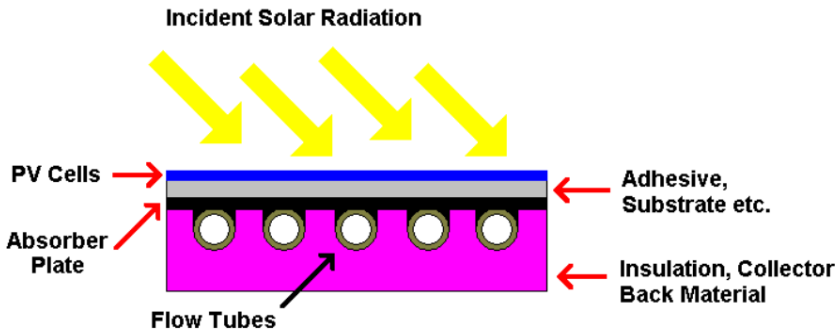

Figure 4.7. Schematic representation of the PV/T collector (TRNSYS website, 2020).

The entire model is based on three equations that describe the 3 layers that make up the PV/T collector (PV layer, absorber layer, fluid layer). Type 560 describes the PV and the absorber layer separately, unlike other basic types of TRNSYS, such as Type 50.

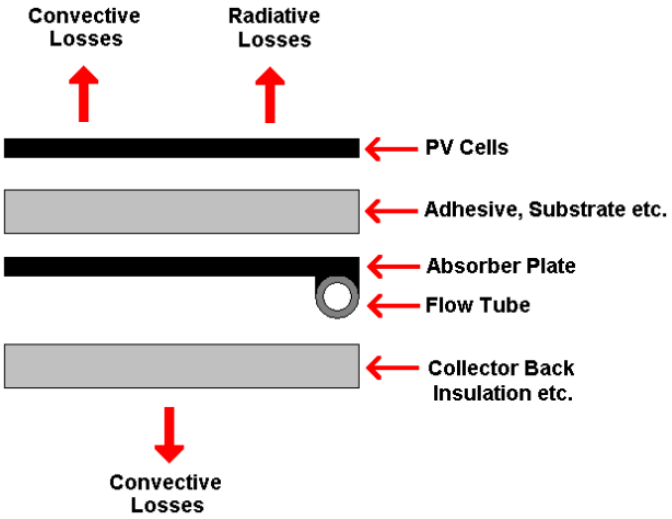

Figure 4.8. Schematic representation of PV/T layers [MathRef_TRNSYS lib]

The energy balance for the PV cells layer is assessed neglecting the conduction phenomena along the surface through the equation (4.2):

$$0 = S - h_{outer}(T_{PV} - T_{amb}) - h_{rad}(T_{PV} - T_{sky}) - \frac{T_{PV} - T_{abs}}{R_T} \quad (4.2)$$

Where h_{outer} is the heat transfer coefficient from the top surface of the collector to the ambient air, h_{rad} is the radiative heat transfer coefficient from the top surface of the collector to the sky, R_T is the resistance to heat transfer from the PV cells to the absorber plate. T_{PV}, T_{amb}, T_{sky}, and T_{abs} are, in order, the PV cell temperature, the ambient temperature, the sky temperature, and the absorber plate temperature.
In particular, h_{rad} is calculated as in Equation (4.3):

$$h_{rad} = \varepsilon\sigma(T_{PV} + T_{sky})(T_{PV}^2 + T_{sky}^2) \quad (4.3)$$

T_{sky}, necessary for computing this parameter, is calculated by the type 15 (Weather Data Processor), inserted as introduced in the previous paragraph in the TRNSYS model. The latter, in addition to reading weather data, such as dry bulb temperatures, from the file given as input, calculates many other parameters including the effective sky temperature.
S is given by the solar radiation absorbed from the collector surface minus the electrical power produced by the photovoltaic module and it can be calculated as in equation (4.4):

$$S = (\tau\alpha)_n \, IAM \, G_T (1 - \eta_{PV}) \quad (4.4)$$

$(\tau\alpha)_n$ is the transmittance-absorptance product at normal incidence, *IAM* is the incidence angle modifier and G_T is the total solar radiation (beam+diffuse) incident upon the collector surface.

The photovoltaic efficiency of the PV cells η_{PV} is evaluated as a function of the cell temperature and the incident solar radiation using a new type of formula that cannot be found elsewhere

$$\eta_{PV} = \eta_{nominal} X_{CellTemp} X_{Radiation} \tag{4.5}$$

In equation (4.5) used to calculate the efficiency of the PV cells (η_{PV}) two correction coefficients appear that consider the dependence of the efficiency value on the ambient temperature ($X_{CellTemp}$) and incident solar radiation ($X_{Radiation}$). $X_{CellTemp}$ and $X_{Radiation}$ are given by equation (4.6) and (4.7) respectively:

$$X_{CellTemp} = 1 + Eff_T (T_{PV} - T_{PV,ref}) \tag{4.6}$$

$$X_{Radiation} = 1 + Eff_G (G_T - G_{T,ref}) \tag{4.7}$$

$X_{CellTemp}$ is the temperature correction coefficient whereas Eff_T (1/°C) is the γ temperature coefficient of the PV panel. Eff_G (m^2/W) instead considers the dependence of the electrical efficiency on the total incident radiation. It is a coefficient that cannot be found on a data sheet provided by the manufacturer.

The energy balance on the collector surface and on the entire collector are implemented in the Type 560 model using the equations (4.8) and (4.9) respectively:

$$Q_{absorbed} = Q_{loss,top,conv} + Q_{loss,top,rad} + Q_{PV \to plate} \tag{4.8}$$

$$Q_{absorbed} = Q_{loss,top,conv} + Q_{loss,top,rad} + Q_u + Q_{loss,\text{back}} \tag{4.9}$$

$Q_{absorbed}$ is the net rate at which energy is absorbed by the collector plate, $Q_{loss,top,conv}$ is the rate at which energy is lost to the ambient through convection off the top of the collector, $Q_{loss,top,rad}$ is the rate at which energy is lost to the sky through radiation off the top of the collector, $Q_{PV->plate}$ is, Q_u is the rate at which energy is added to the flow stream by the collector, and $Q_{loss,back}$ is the rate at which energy is lost to the ambient through the backside of the collector.

The heat transfer terms introduced in equations (4.8) and (4.9) are expressed in (kJ/hr) and are calculated as following reported in equations from (4.10) to (4.17):

$$Q_{loss,top,conv} = h_{outer} Area \left(\bar{T}_{PV} - T_{amb} \right) \tag{4.10}$$

$$Q_{loss,top,rad} = h_{rad} Area \left(\bar{T}_{PV} - T_{sky} \right) \tag{4.11}$$

$$Q_{loss,back} = Area \frac{\left(\bar{T}_{abs} - T_{back}\right)}{R_B} \tag{4.12}$$

$$Q_{\mathrm{PV}\rightarrow\mathrm{plate}} = Area \left(\frac{\bar{T}_{PV} - \bar{T}_{abs}}{R_T} \right) \tag{4.13}$$

$$Q_{absorbed} = Area \left(\tau\alpha\right)_n IAM\, G_T \left(1 - \eta_{PV}\right) \tag{4.14}$$

Where R_B is the resistance to heat transfer from the absorber through the backside of the collector and $\bar{T}_{PV}$ and $\bar{T}_{abs}$ are the mean temperatures of the PV cells and the absorber respectively.

4.3.2 Validation of simulation models of the main plant components

Before the definition of the simulation model of the entire plant, it was necessary to validate/calibrate the simulation models of the plant components introduced in the previous paragraph (Heat Pump and PV/T panel) concerning known reference conditions (Figure 4.9). The simulations were carried out in the TRNSYS environment using the types available in combination with each other. In both cases, the inputs used are those deriving from UNI standards relating to laboratory tests for product labelling. The outputs deriving from the simulation model were then compared to the main characteristics of the products reported in the technical data sheets until percentage errors of less than 10% were obtained.

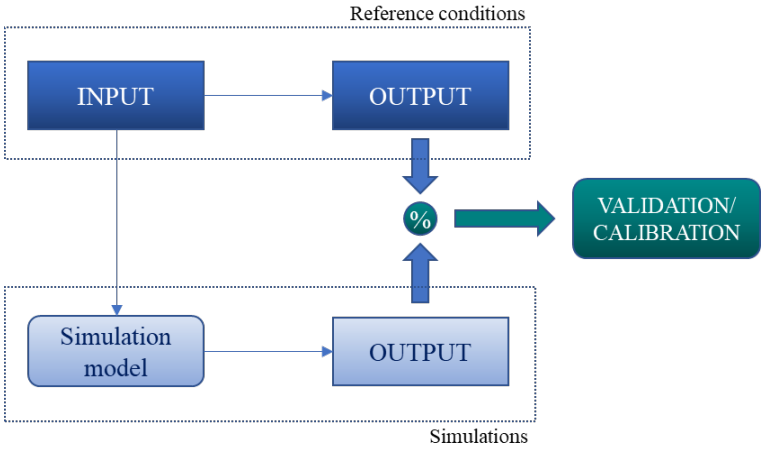

Figure 4.9. Schematic of the validation procedure of simulation model.

4.3.2.1. PVT model validation

After identifying the TRNSYS type most suitable for modeling the selected PV/T Fototherm module, a model calibration procedure was performed to adjust the main parameters. Subsequently, the calibrated model was validated based on the indications provided by current legislation to verify its reliability in reproducing the real operation of the system. This analysis was based in particular on the values indicated by the UNI EN ISO 9806 standard concerning the test methods necessary to test the thermal performance of solar collectors with fluid heating. To simulate the operation of the hybrid solar collector, Type 560 was selected, which reproduces the behavior of an unglazed water-based PV solar collector with a "sheet and tube" heat exchanger.
The calculation of PV energy production is based on the Hottel-Whillier model modified by Florschuets (Florschuetz, 1979) and involves a cycle of 10 iteratively solved analytical equations.
The total radiation absorbed is calculated through an energy balance of the collector, equating it to the sum of the heat transferred by conduction, convection, and radiation. The amount of useful heat produced was calculated from the absorbed net radiation density S captured by the absorber plate:

$$S = G_T \tau\alpha_{eff}(1-\eta_{PV}) \tag{4.15}$$

where G_T is the solar irradiation incident on the collector surface, $\tau\alpha_{eff}$ represents the effective transmittance-absorbance product of the collector, and η_{PV} is the photovoltaic efficiency of the collector.
The thermal model of Type 560 essentially consists of three equations that describe the thermal behavior of the three layers of the PV/T collector: the photovoltaic layer, the absorbent layer, and the fluid layer. The instantaneous thermal efficiency was analyzed with the TRNSYS software as a function of the inlet temperature of the fluid Tin, using the equation proposed by (Duffie and Beckman, 2013):

$$\eta = \frac{Q_u}{A_C I_{sun}} = \frac{mc_p(T_{out}-T_{in)}}{A_C I_{sun}} = F_R(\tau\alpha) - \frac{F_R U_L(T_{in}-T_{amb})}{I_{sun}} \tag{4.16}$$

In the expression (4.16) Q_u represents the useful energy gain, A_c the surface of the collector, m the mass of the fluid, T_{out} the fluid temperature at the collector outlet, T_{in} the temperature of the fluid at the inlet of the collector, I_{sun} solar irradiation, F_R the heat removal factor, $\tau\alpha$ the product between the transmission and absorption coefficient of the collection surface, U_L the thermal transmittance of the solar collector and T_{amb} the ambient temperature. Looking at the equation (above-reported), it can be seen the dependence of the thermal efficiency on $F_R(\tau\alpha)$ and the $F_R U_L$ product, parameters that describe the collector's ability to exploit solar energy. In particular, the $F_R(\tau\alpha)$ product indicates how the energy is absorbed while $F_R U_L$ indicates how it is dissipated (Duffie and Beckman, 2013).

The procedure for validating and calibrating the model relating to the PV/T collector was performed starting from expression (4.16) and as already mentioned, referring to the UNI EN ISO 9806 standard.
The performance test reported in this regulatory reference includes the assessment of the thermal efficiency of the collector, or the conversion efficiency of incident solar radiation into useful heat, as operating conditions vary. The first validation test was carried out between the results of the TRNSYS simulations, and the data reported in the technical sheet of the PV/T Fototherm panel under the standard conditions defined by UNI EN ISO 9806. To calibrate the model, a sensitivity analysis was conducted on the parameters that most influence the efficiency of the solar thermal collector. As a result, the model is significantly influenced by the convective heat exchange coefficient relating to the heat transfer fluid (h_{fluid}) and by that relating to the layer of air in contact with the surface of the collector (h_{outer}). However, as reported in several research papers (Aste, Leonforte and Pero, 2015), the performance of the collector was deduced starting from these parameters, most often empirically evaluated. Consequently, to calibrate the TRNSYS model of the PV/T system, several parametric simulations were performed to evaluate the influence that these coefficients have on the thermal efficiency of the collector and identify the most reliable values of these parameters. Subsequently, the TRNSYS simulations were performed using as reference values both experimental data available in the literature and values reported in the product datasheet. In the first case, the data were obtained from measurements conducted in previous experimental studies reported in (Rizzini, 2015) (simulation indicated as mode 1), in the second the data provided in the technical data sheet (simulation indicated as mode 2) were considered. The reference data indicated above were compared with the simulation results obtained. Specifically, the results of the validation procedure for the thermal efficiency of the PV/T collector were graphically represented through characteristic curves of thermal efficiency as a function of the reduced temperature T^*_m defined as follows:

$$T_m^* = \frac{t_m - t_{amb}}{I_{sun}} \tag{4.17}$$

where t_m is the mean fluid temperature, t_{amb} is the ambient temperature e I_{sun} is the solar radiation.
The results of the validation procedure for the thermal efficiency of the PV/T collector are shown in Figure 4.10. As described, the respective characteristic curves are compared as a function of the reduced temperature T^*_m (see equation 4.17).

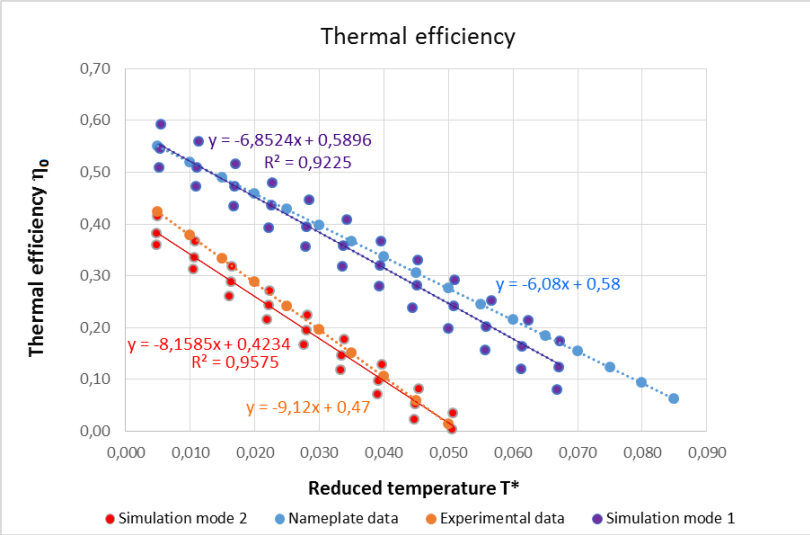

Figure 4.10. Characteristic curves of thermal efficiency

The scenarios in "mode 1" and "mode 2" were simulated in a parametric mode for different average monthly temperatures (ambient temperature, sky, and average water), by varying the value of h_{fluid} from 100 to 2000 and the value of h_{outer} from 0.1 to 20.
As mentioned before, the validation of the results was carried out by comparing the values η_0 and a_1 obtained from the simulation with the values reported in the technical data sheet and evaluating the relative error between the values η_0 and a_1 obtained from the simulation and the experimental values from (Rizzini, 2015). Assuming h_{fluid} =100 and h_{outer} =20 the results show that the relative error is less than 10%.

4.3.2.2. HPWH model validation

The selected air-to-water heat pump with water storage was simulated by using a combination of types to assess its performance at different operating conditions concerning the amount of deliverable DHW at 40 °C and to the tank heat losses.
According to the state of the art, Type 938 was selected to simulate a stand-alone heat pump and Type 1237 for the cylindrical sensible heat storage which is integrated into the condenser side (Specialists, 2017) (Beccali *et al.*, 2020). The mixing valve, which allows delivering water at 40 °C mixing water from the public network and the tank, was modelled by combining "tee-piece" and "diverter" types (Beccali *et al.*, 2020). The DHW heat exchanger (HX) embedded in the tank was simulated by the "pipe" subroutine (Type 31). Selected tapping profiles were used as input for building the mass flow rate and inlet temperature profiles.
The first tests were performed to evaluate tank thermal behaviour with regards to heat losses and wrap-around heat exchanger length and efficiency. In this case, the heat pump was set in OFF mode. The initial values of the tank and ambient temperatures were assumed respectively at 55 °C and 20 °C according to European legislation. Heat

loss coefficient values for the edge, bottom, and top surfaces were considered identical and were a matter of calibration. In order to define the pipe length and the U-value, an iterative process was performed. This latter was conducted by varying both the parameters until a relative error below 5% was found (Table 4.8). In particular, this error was achieved by setting a pipe length of 19 meters and a U-value of 1.8 kJ (h $m^2K)^{-1}$. It is worth noting that 0% relative error was obtained for the delivered volume ad 40 °C.

Table 4.8. HPWH validation results (tank heat losses and HX length).

		Datasheet	Simulation	Err%
Heat losses at 60°C	[kWh/day]	1.60	1.58	2%
Volume of mixed water at 40 °C	[liters]	300	300	0%

A second test was conducted to select the appropriate input data for Type 31 (pipe length and loss coefficient) in order to simulate the DHW heat exchanger capacity within a given time step. According to EN 16147:2017 standard, this test starts at a tank temperature equal to T_{set} (55 °C). It was aimed to measure the deliverable volume of DHW at 40 °C in the assumption of a constant draw-off event at a fixed flow rate (f_{max}= 0.2 kg/s). This volume was calculated as:

$$V_{40} = \left(\frac{1}{\Delta T} \right) \int_0^{t_{40}} f_{\max}(t)[T_{WH}(t) - T_{WC}(t)]\,dt \tag{4.18}$$

where t_{40} is the time of starting the draw-off until hot water temperature (T_{WH}) drops below 40 °C. ΔT is the difference between the reference tapping temperature (40 °C) and the cold-water temperature (T_{WC}) from the water network, fixed at 10 °C.
To achieve a lower relative error between simulations results and technical datasheet figures, different simulations were carried out by varying pipe length while pipe thermal conductivity was set at 400 W $(mK)^{-1}$.
A specific test regarded the calculation of the heat pump efficiency. It was aimed to validate the calculated COP values at the reference ambient and operating conditions according to UNI EN 16147:2017. Type 938 refers to the external data file for considering COP dependency on tank temperature, ambient temperature, and relative humidity. On the other hand, COP values of the datasheet refer to tests performed at steady-state conditions (according to EN 16147:2017), which are quite different from real operating ones. For this reason, the model was at first run in steady-state test conditions until COP results matched the values declared by the manufactures with a relative error below 5%.

Table 4.9. COP Validation results for standard test conditions

Water temperature	Tw=45 °C	Tw=55°C

Ambient conditions	Datasheet	Simulation	Err%	Datasheet	Simulation	Err%
T_{env}=2 °C – ($T_{wetbulb}$ = 1 °C)	3.3	3.27	-1%	3.1	3.14	+1%
T_{env}=7 °C – ($T_{wetbulb}$ = 6 °C)	4.7	4.65	-1%	4.1	4.22	+3%
T_{env}=14 °C – ($T_{wetbulb}$ = 13 °C)	6.1	6.00	-2%	5.2	5.36	+3%

Since operating conditions for standardized tests are very different from real operating conditions in a warm climate such as the one of Palermo (Italy), some adjustment was necessary. Thus, a quadratic regression law between ambient air (for two given test conditions) and COP was introduced. In this way, the air temperature was extended to 25 °C, which is better suited to the real operating conditions in the summer months of Palermo (Figure 4.11). Sufficiently reliable average monthly COP values, according to average air temperature in the month, were found.

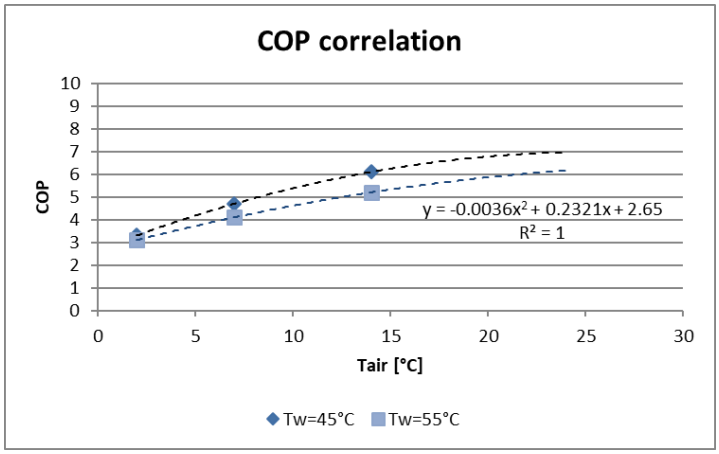

Figure 4.11. COP linear dependence with respect to air temperature

It is worth noting that COP monthly average values vary from 4.4 in January-February to 5.8 in the summer months. It corresponded respectively to 12 °C and 25 °C average air temperature (T_{air_av}), perfectly comparable to COP figures reported in the manufacturer's datasheet.

Once the model was validated, electrical consumption by HPWH was assessed at real operating conditions in the Palermo climate. Input data in simulations correspond to the XL hourly tapping profile and 360 litres DHW at 40 °C per day withdrawal at 55 °C fixed tank temperature set-point. Daily electrical consumption was less than the declared one in the datasheet. Yearly consumption data set as 690 kWh, while average daily consumption varied from 1.5 to 2.4 kWh, as represented in Figure 4.12.

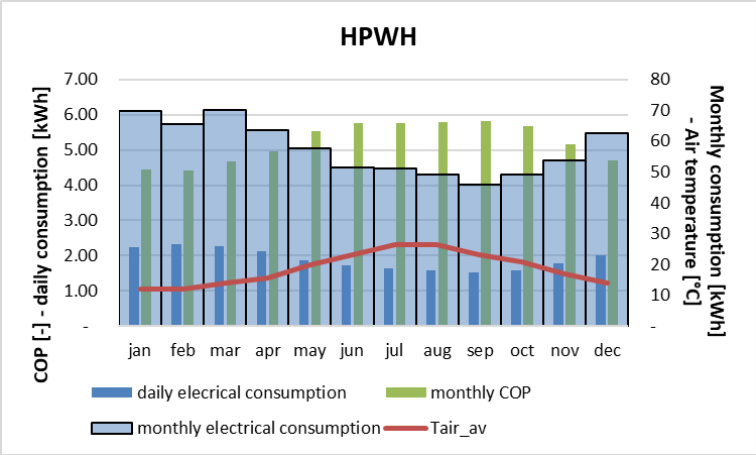

Figure 4.12. HPWH monthly electrical consumption and COP values in real operating conditions.

4.4 System configurations

After having sized the main devices of the systems, different types of plants for Domestic Hot Water (DHW) production, which use the Heat Pump Water Heater (HPWH) technology coupled with solar collectors/panels (i.e., which can be PV, PV/T, or ST) have been investigated.

In particular, investigations were performed in order to identify the optimal number of modules that make up the solar plant and the most performing technology for the purpose of this thesis among PV, PV/T and ST collectors. These analyses led to the definition of the plant configuration defined as "A".

Furthermore, by focusing analyses on the use of the thermal energy produced by the solar thermal collectors within the entire plant, an alternative system configuration was examined (configuration B). The improved energy performances of this latter were analysed by making comparisons with configuration A.

In configuration A (figure 4.13) the PV/T string is thermally connected directly to the heat pump the solar system to be used as a backup heating system with respect to the heat pump, while in configuration B (figure 4.14) the thermal output is used to preheat the water taken from the aqueduct and delivered to the HPWH.

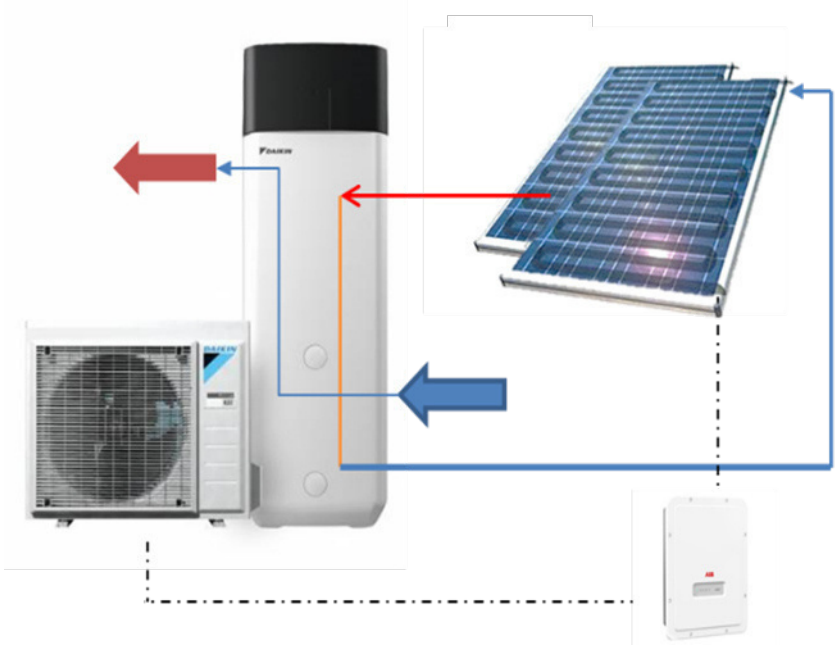

Figure 4.13. Configuration A

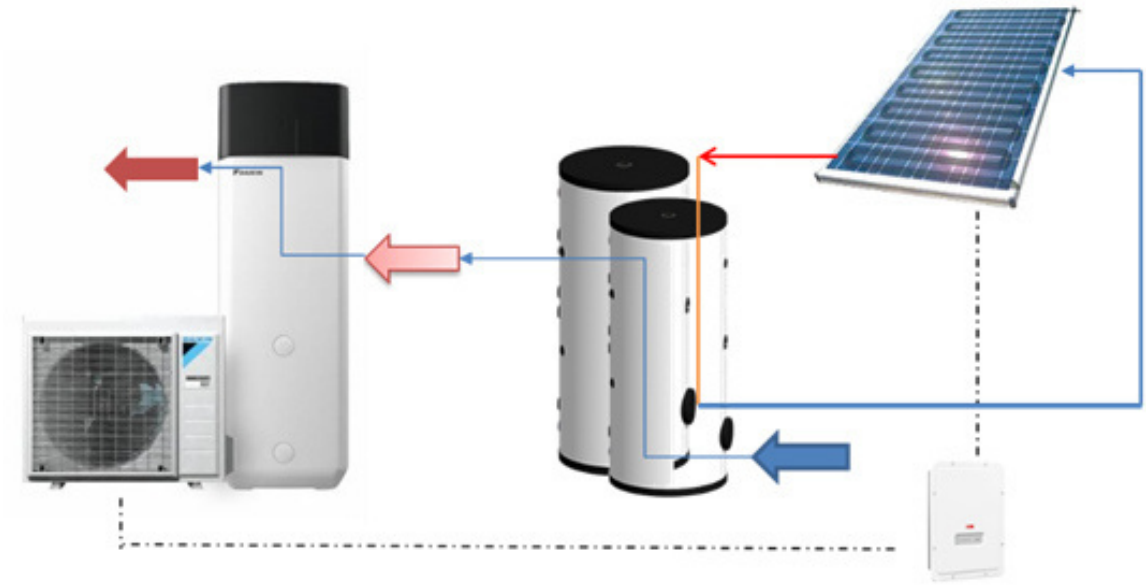

Figure 4.14. Configuration B

The same basic components, already described above in section 4.2, have been kept for both layouts.

4.4.1 Configuration A – Backup heater

A set of different plants was defined to make comparisons on the performance of the different technologies analysed. Figure 4.15 quickly depicts the plant variants. Basically, plants were differentiated using different solar collectors (PVT, PV, and ST)

coupled in all cases with the heat pump. The number of solar collectors/panels has also been varied as well as the profile and demand of users.

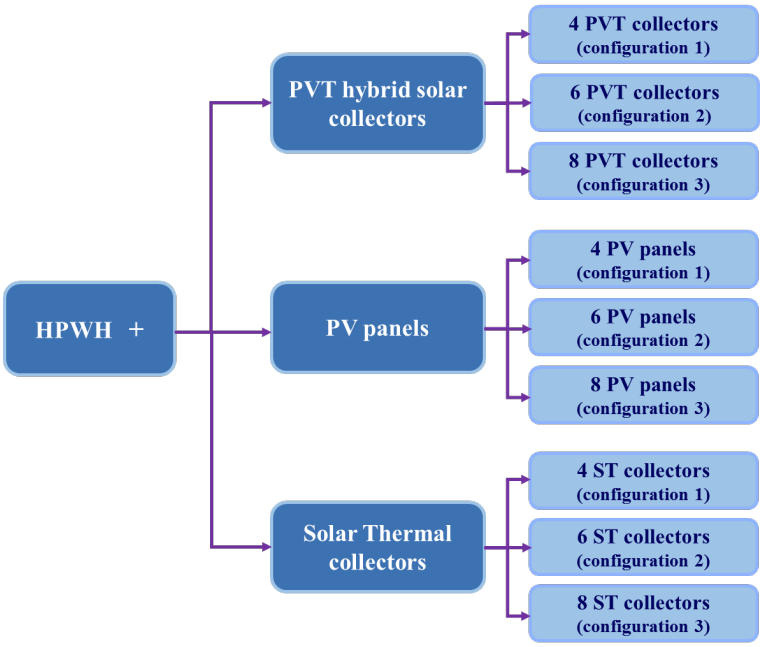

Figure 4.15. Systems simulated with the TRNSYS software.

To size the systems and to define the optimal number of collectors, further evaluations were carried out. Three scenarios with 4, 6, and 8 collectors were analysed. The number of collectors was selected to avoid under and over-sizing. PV and PV/T panels were sized to satisfy the electrical loads of the system, consisting of the HPWH and auxiliary pumps.
The following assumptions were made:

- the electric storage size was fixed to ensure one day of autonomy for the solely HPWH operating in the chosen weather data conditions (the most critical average monthly daily consumption was chosen for this goal);
- PV and PV/T systems were sized to cover the HPWH and auxiliaries' electrical consumption in the heaviest monthly average day;
- PV/T systems were sized only according to the electric demand so their contributions to the heat balance are consequent;
- PV and PV/T panels are always connected in series to form a single string;
- PV/T panels are connected in series also concerning the hydraulic loop;
- ST collectors are connected in series of two and then in parallel;
- the solar thermal plant is aimed to cover at least 50% of DHW yearly demand;
- all systems were simulated for different tapping profiles according to section 4.1.1.

The plant set-up is based on the integration of an air to water heat pump (HPWH) aimed at DHW production with a plant of 6 PV/T hybrid solar collectors. The HPWH has a rated power of 700 W and a 500 liters storage tank, while each PV/T module has a peak power of 300 W_{el}.

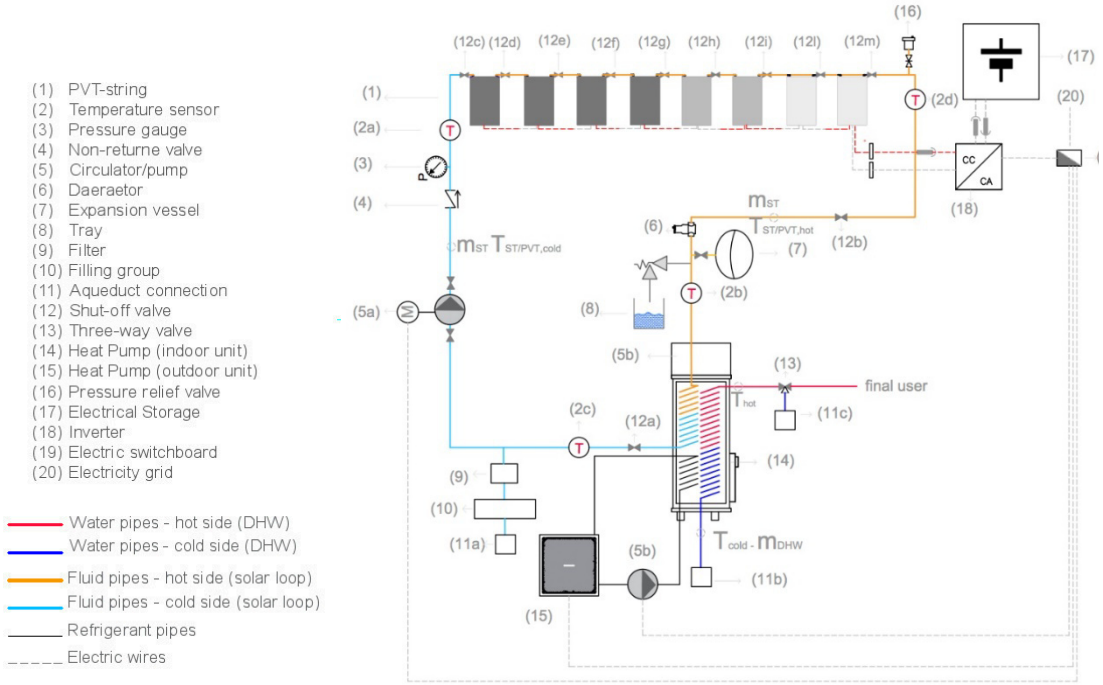

Figure 4.16. Configuration A of the experimental set-up

In this first configuration, the solar thermal system circuit was assumed to be directly connected to the supplementary heat exchanger of the HP designed to enable the connection with auxiliary heating devices. The main purpose was to size the solar system in order to ensure the best performance in terms of energy savings. Furthermore, the performance of the HP integrated in the PVT system was compared with those that would be obtained in the case of installation of a traditional RES system (PV or ST). The comparison between hybrid and traditional technologies was carried out by considering the same plant power. Figure 4.16 describes the common scheme that can be adapted to define several variants according to the solar components' typology and the size of the components.

4.4.2. Configuration B - pre-heating mode

Results for system configuration A showed that the integration of the heat pump with hybrid solar panels allows limited advantages on the thermal performances, how it will be showed in Chapter 5 where results about two configurations A and B are compared and analysed in detail.

In fact, the temperature of the water leaving the collectors rarely exceeds the average temperature of the thermal storage tank of the system, therefore the thermal output of the PV/Ts in A system configuration often fails to make a useful thermal contribution to the system (especially in winter months).

Starting from the results obtained, a variation of the plant set-up was therefore proposed. In order to maximize the exploitation of the low-temperature contribution provided by the PV/Ts, the new configuration provides for the introduction of an additional solar water pre-heating storage to the one normally integrated into the HP. The additional storage tank has the function of preheating the water coming from the aqueduct employing the solar thermal system. The main goal is to improve the thermal performance of the hybrid solar system while simultaneously reducing the need for the heat pump and, consequently, its electricity consumption. In support of this, the results obtained by Brottier and Bennacer in (Brottier and Bennacer, 2020) show that PV/T technology is particularly relevant to domestic hot water preheating. The results also confirm the robustness of the unglazed collector as the highest stagnation temperature recorded is quite below the safe threshold value. The study reported in (Zenhäusern *et al.*, 2017) shoes that in Switzerland in almost 50 % of the systems the PV/T heat serves the (pre-)heating of domestic hot water (DHW), and in more than 40 % of the systems, the collectors are combined with heat pumps.

The plant under analysis includes six PV/T panels (for technical features see table 4.2) and an air-to-water heat pump (table 4.4) dedicated to the production of DHW, as for configuration A. The novelty of configuration B is the introduction in the system of a pre-accumulation tank of domestic water. It is characterized by a volume equal to the technical water tank integrated into the HPWH inside the hydraulic circuit (Figure 4.17).

This tank is located downstream of the aqueduct (water inlet point). It is connected to the solar thermal circuit with the aim of pre-heating the domestic water in a dedicated storage tank. According to the DHW demand, the water is then sent to the secondary side of the heat exchanger inside the HPWH tank to reach the setpoint temperature.

Thanks to a system of three-way valves, the tank can be bypassed.

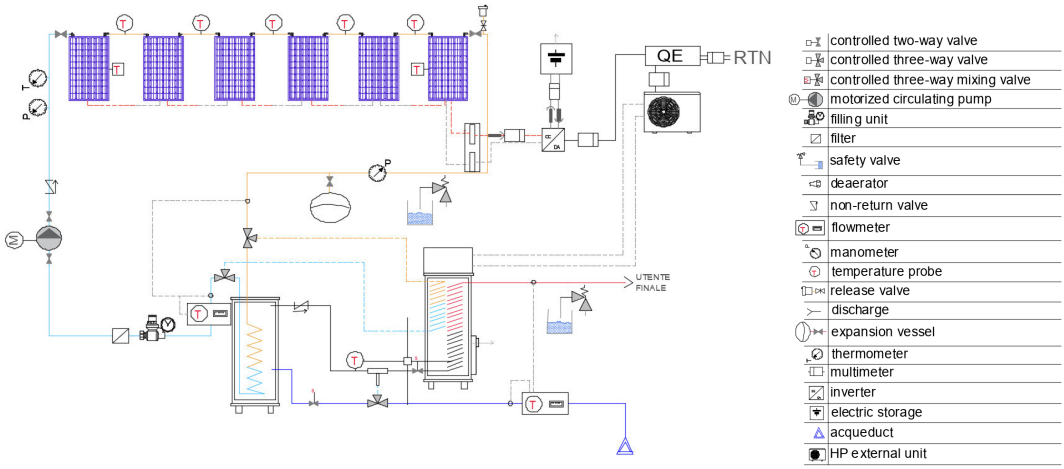

Figure 4.17. Configuration B of the experimental set-up.

For a given setpoint of the water temperature delivered to the end-user (Tset), two operating modes have been tested:

1. ST-standard mode: when the temperature reached inside the pre-storage tank is higher than the temperature inside the heat pump storage ($T_{solar} > T_{HPWH}$) and higher than the setpoint temperature (T_{set}). The heat pump is bypassed and the entire system works like a traditional solar thermal system;

2. ST-preheating mode: when the temperature reached inside the pre-storage tank is lower than the temperature inside the heat pump storage ($T_{solar} < T_{HPWH}$) and lower than Tset. The water is drawn to the HP circuit until it reaches the useful temperature for supplying the DHW at T_{set} (usually 40° C).

It is necessary to underline that, in the above-described case, the cycle of the HP starts whenever the temperature of the storage tank is lower than the setpoint temperature (T_{set}).
In this new configuration of the system, the difference between the temperature of the fluid leaving the collectors and the temperature of the aqueduct water is such as to allow for an added thermal contribution to the system. In general, this leads to a reduction in the DHW demand at 40 °C, with a consequent reduction in the electricity consumption of the HPWH.
The dynamic TRNSYS model developed for configuration B of the system of the proposed system it's basically the same as that used for configuration A. The same Type 1237 (already validated) was used to simulate the thermal behaviour of the pre-heating tank.
Regarding the DHW hourly withdrawal profile, it was considered the standard XL profile (Regulation (EU) No 814/2013) (UNI EN 12831) by setting a daily consumption at 40° C (equal to 720 litres/day). This input data was simulated by using Types 11a and 11b. At the same time, Type 48b was added to the model. It simulates a 3000 W inverter system with an efficiency of 0.97 and a regulation efficiency of 0.84. Similarly,

Type 47a simulates the behaviour of a 10 kWh electric storage system and an efficiency of 0.95 with a charge limit between 10% and 90% of the nominal value.

Table 4.10. TRNSYS Types (TESS Library)

Component	TRNSYS Type
Heat Pump Water Heater	938 (TESS)
Thermal Storage Tank	1237 (TESS)
Water Heater Energy Supply	1226 (TESS)
PV/T Panel	560 (TESS)
Pump	3
Regulator Charge/Inverter	48b
Electrical Storage Battery	47a
Weather Data Processor	15
Differential controller	1669
Thermostat	2
Tempering Valve	11a
Diverter	11b

Finally, the types 1669, 2, and 11a were used to replicate the operating logics described in Figure 4.18.

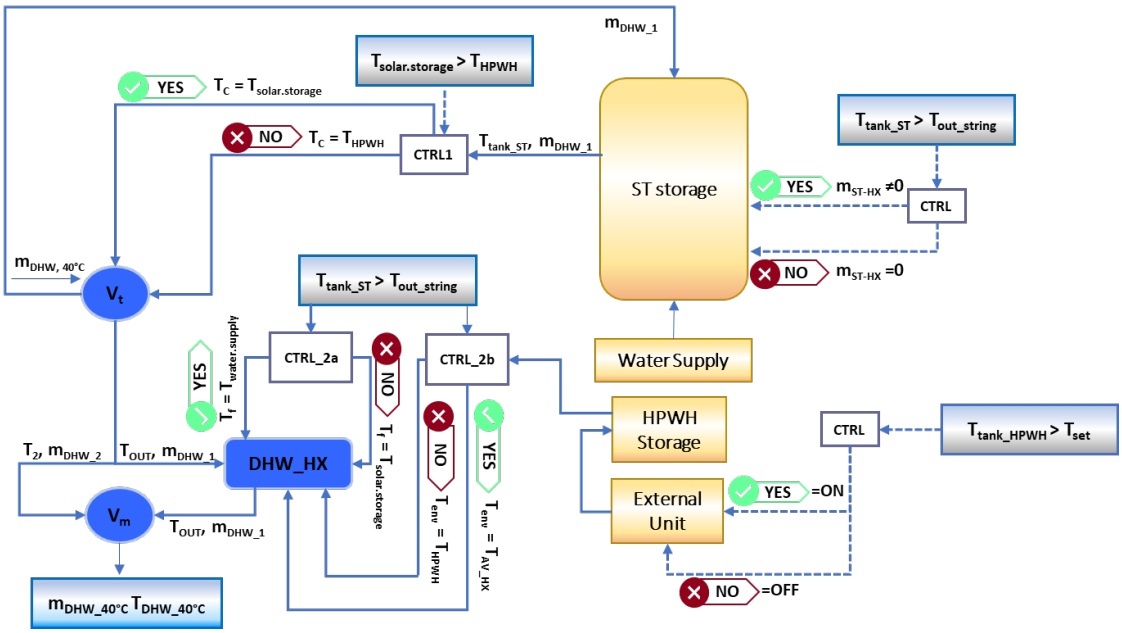

Figure 4.18. Schematic of operating logics of TRNSYS model

4.5 Experimental setup realisation

In order to predict accurately the performance of solar energy systems providing thermal energy or electricity with solar-thermal or hybrid photovoltaic thermal collectors, the components have to be characterized in terms of their steady-state and dynamic performances. By comparison, agreed standards for testing specifically PV/T collectors are not available, the PV/T market is relatively small at present and test data that can be used for developing and validating predictive models for these collectors is scarce. Generally, the experimental investigations on PV/T collectors are performed in order to evaluate the effect that various design parameters have on the thermal and electrical efficiencies with the aim to identify the potential for improvements (Guarracino, 2017).
For the realization of the experimental set-up and the tests to be carried out on the solar collector, reference was made to the UNI EN ISO 9806 and UNI EN 12977, which are the relevant standards for the evaluation of the performance of the system as a whole.
The tests to be carried out are essentially aimed at:

- Determine the thermal and electrical efficiency of the PV/T collector;
- Evaluate the main parameters of the collector;
- Determine the heat losses through the collector;
- Determine "storage" indices capable of evaluating how electrical and thermal energy is used in the system;
- Determine comfort indices related to the DHW capable of evaluating how the system meets the residential demand for hot water with different tapping loads.

As it was mentioned earlier, these studies have been finalized to the realization of a real-scale experimental setup with the main goal of monitoring and verifying, on the one hand, the thermal and electrical performance of the PV/T collectors as the environmental and operating conditions vary, and on the other to monitor the performance of heat pumps electrically powered by the solar system for different user profiles. The experimental set-up was designed and sized by referring to the indications of the regulations currently in force in the area. The project relies on the context of a collaboration project with ENEA, which has developed the executive project and is overseeing the construction of the plant itself (Report ENEA, 2020).
The general layout of the system consists of a thermal section and an electrical section. Inside the thermal section of the plant, it is possible to distinguish two separate circuits: the first is a "closed" circuit in which technical water circulates allowing the thermal energy produced by the PV/T modules to be transferred to the storage unit of the HPWH. This is possible thanks to a heat exchanger integrated into the storage integrated into the HPWH itself. The second hydraulic circuit is the one relating to the DHW path. Specifically, the cold water is drawn from a tank of about 2,000 L instead of being drawn from the aqueduct; in this way, as in the other laboratories, the thermal capacity of the tank is exploited in order not to cause a waste of water during the tests and in any case to have a faithful reproducibility of real conditions. After that, the cold

water is sent to the HPWH where it circulates inside a heat exchanger finally, the DHW produced before being poured into the tank can be cooled in a dry cooler (DC) already present on the installation site to pour colder water into the tank and thus improve the reproducibility of the water draw.
The electrical section will consist of the PV/T modules, the electrical storage, and a "grid-connected" inverter which will power the HPWH as a privileged load and which at the same time will allow, in the event of a power surplus, to enter additional loads into the grid. On the contrary, in the event of a power deficit in production, to withdraw energy from the grid to power the HPWH. The two sections are described in detail in the following paragraphs. Figure 4.19 below shows the general plan of the research center and the photo of the installation site.

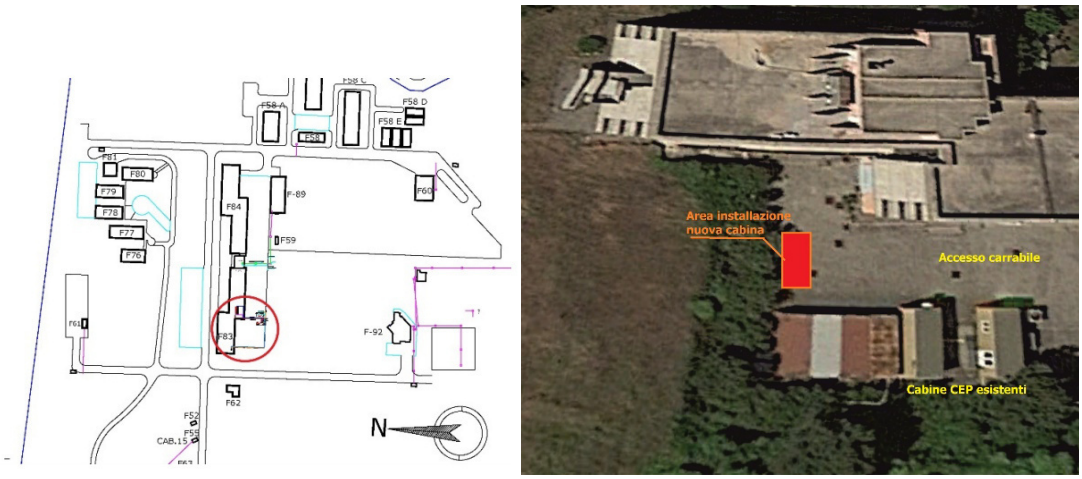

Figure 4.19. Extract of the floor plan and photo of the installation site of the ENEA research center

How it is possible to see, the laboratory will be built in the F83 building (circled in red) of the ENEA national research center in Casaccia. Specifically, the thermophotovoltaic modules will be placed on the roof of the building from which, both the electrical cables and the hydraulic pipes will be placed in a special channel that will descend on the external facade of the building and subsequently be buried to reach the lower tank of cabin 2 in front, which is already present on the installation site. From the latter, the solar cables will reach cabin 1, where the electrical section of the experimental setup (electrical panel, inverter, electrical storage). The hydraulic pipes will reach cabin 3, where the HPWH and the preheating tank will be placed. The inertial tank will be positioned in a technical room inside building F83, while the dry cooler is already present and is located externally near cabin 2.

4.5.1 Design of the thermal section

The detailed layout of the thermohydraulic section of the experimental setup is reported in Figure 4.20. The sizing of the piping has been performed by evaluating the pressure drop and the maximum velocities inside it. Each component necessary to ensure the correct operation of the system and respect the safety conditions has been also sized.
The solar loop is of the closed type and uses a mixture of water and glycol as heat transfer fluid, allowing to transfer of the thermal energy produced by the PV/T collectors to the storage tank integrated inside the HPWH. In order to ensure a correct and safe operation of the solar plant in the return circuit will be included a filter, an expansion vessel, a circulator, a non-return valve, an automatic deaerator, an electric filling unit, a tap for draining the circuit, and the safety valve. In correspondence with the highest point of the supply branch, a pressure relief valve will be inserted, to eliminate the incoming air during the system start-up. Furthermore, several temperature sensors have to be installed in the connection pipes between PV/T collectors, in order to analyse the rise of temperature during the operation. Pt100 screw probes with connecting cable have been selected, characterised of a temperature range of operation from -50 up to + 200 °C. These temperatures value are also useful to test the thermal efficiency. In particular, according to UNI EN ISO 9806, the maximum permitted deviation of the measured parameters must be ± 0.1 K and of ± 0.4 K for the fluid temperature at each solar collector inlet and at solar colector outlet respectively. For measuring the surface temperatures of the collectors PT100 contact temperature probes have been chosen. A miniature-electromagnetic flowmeter by Profimess, characterised by a operation range of 0,2 ÷ 50 l/min, have to be located at the inlet of the first PV/T collector in order to ensure a stable mass flow through the collectors, with a permitted deviation of ±2% during the thermal efficiency tests. To assess the solar thermal energy gain a flow meter with a temperature probe will also be in the return circuit as well as a temperature sensor in the delivering branch. Through a three-way valves system, it is possible to ensure that the water does not circulate inside the HPWH, but instead passes through a heat exchanger inside a second tank. The latter solution is particularly necessary for the colder months when the maximum temperature reached on the delivery could be lower than that in the HP accumulation. If water is sent at a lower temperature, the opposite effect to the desired one would be obtained, i.e. the cooling of the accumulation same.
The cold water, before entering the HP for producing DHW, passes through a 500 L preheating tank, slightly raising its temperature in order to increase the efficiency of the system. The advantage of this last measure will be carefully verified within the laboratory.
Concerning the sizing, 1/2 " pipes in insulated copper were chosen and, since the modules will be hydraulically connected in series, a flow rate of 150 L/h was assumed. As setpoint temperatures, a temperature of 85 °C was assumed for the supply pipe and 30 ° C for the return pipe.

The volume of the expansion vessel, on the other hand, must have a volume greater than 5.015 L, immediately checked with those envisaged with a nominal volume of 30 L while the safety valve must have a steam discharge flow rate greater than 9.04 kg / h.
Concerning the HPWH circuit consists, besides the heat pump itself, of the inertial storage tank and a dry cooler. During performance tests, the water withdrawal will be simulated by using a 2000 liters tank of uninsulated polyethylene. From the lower side of the tank will be taken the cold water, while the DHW produced will be put inside it from the upper side. The dry-cooler is inserted considering the case where the thermal capacity results not enough to dissipate the thermal energy produced.
The delivery circuit presents a two-way motorised valve to allow reproducing the load profile, while the return circuit includes a filter, a pump, an expansion vessel, and a non-return valve. As for the PVTs loop, a thermal energy meter is previewed between HPWH intake and outlet. Furthermore, a temperature probe before the cold water inlet of the HPWH to assess the temperature rising if the pre-heating storage tank was used.
The sizing of the heat pump circuit was performed by considering a DHW flow rate of 2000 L/h and a XL tapping profile according to (*COMMISSION REGULATION (EU) No 814/2013 of 2 August 2013-Implementing Directive 2009/125/EC of the European Parliament and of the Council with regard to ecodesign requirements for water heaters and hot water storage tanks*, 2013), while for the piping a multilayer pipe with a nominal diameter of 1”. A centrifugal pump characterised by a rated power of 0.550 kW was selected.

4.5.2 Design of the electrical section

The PV system includes the following components:

- a hybrid inverter that allows the injection of electricity into the network;
- a string of 7 PV/T collectors;
- electrochemical lithium-ion storage with a capacity of 4.8 kWh.

By considering the technical features of inverter and PV/T hybrid modules, it was chosen to connect the latter in series constituting a single string, therefore, the related calculations were made to verify the compatibility of the string with the inverter.
The related results are shown in Table 4.11:

Table 4.11. Sizing results of the PV/T string.

PV/T string	
Peak power	2100 Wp
Voltage V_{MPP}	226.81 V
Min. Voltage V_{MMP} (70°C)	197.20 V
Max. Voltage V_{MPP} (-10°C)	249.82 V
Open Circuit voltage V_{OC}	277.20 V

Max. open circuit voltage V_{OC} (-10°C)	305.33 V
Current I_{MPP}	9.26 A
Short-circuit current I_{SC}	9.39 A
Max. short-circuit current I_{SC} (70°C)	9.61 A

After checking the section of the cables, the string sectioning panel has been dimensioned e drafted the single-line diagram of the PV system in question.
The PV system regulation and protection devices are present in three different electrical panels:

- The field panel, where there are the fuse holder disconnectors of the string, the switch - disconnector that allows separating the string from the rest of the system and the voltage discharger for atmospheric overvoltages;

- The Q3 panel, which is the panel relating to laboratory in question, where the generator device will be installed which will allow the inverter to be separated from the power supply of the HPWH and any other load;

-The Q1 panel, as described above, the panel of this laboratory will be powered downstream of the main panel in the cabin where the inverter and electrical storage will be installed. Since the PPE related to an existing PV system is already present in this, the PPE will also be used for the system in question since it is not expected that the two PV systems will operate simultaneously. By adopting this solution with regard to PPE, the HPWH is also enabled to operate on an island.

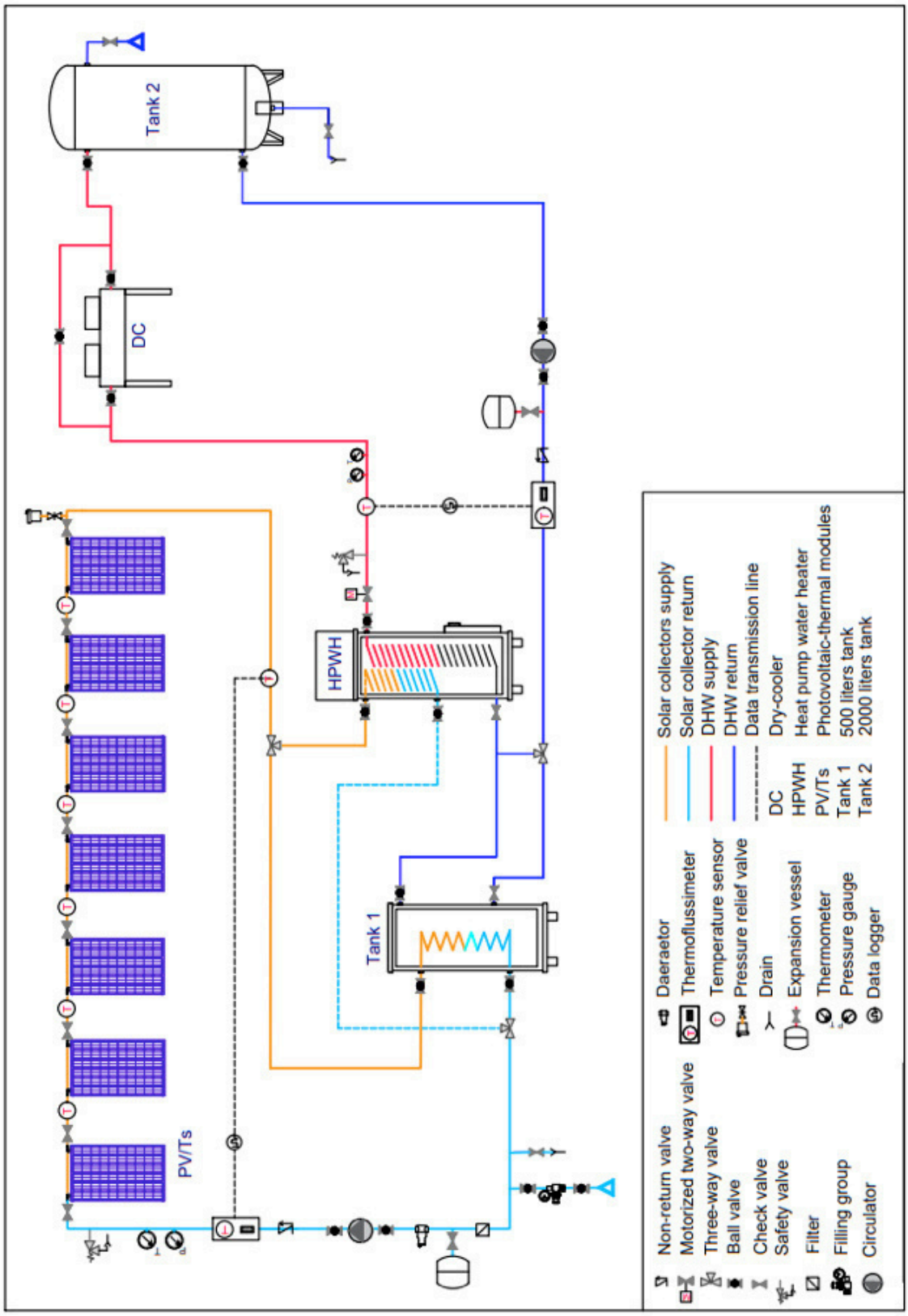

Figure 4.20. Thermal section of the experimental setup.

References

Aste, N., Leonforte, F. and Pero, C. Del (2015) 'Design, modeling and performance monitoring of a photovoltaic – thermal (PVT) water collector', 112, pp. 85–99. doi: 10.1016/j.solener.2014.11.025.

Beccali, M. *et al.* (2020) 'Solar and Heat Pump Systems for Domestic Hot Water Production on a Small Island: The Case Study of Lampedusa', *Applied Sciences*, 10(17). doi: 10.3390/app10175968.

Brottier, L. and Bennacer, R. (2020) 'Thermal performance analysis of 28 PVT solar domestic hot water installations in Western Europe', *Renewable Energy*, 160, pp. 196–210. doi: 10.1016/j.renene.2020.06.072.

COMMISSION REGULATION (EU) No 814/2013 of 2 August 2013-Implementing Directive 2009/125/EC of the European Parliament and of the Council with regard to ecodesign requirements for water heaters and hot water storage tanks (2013).

Duffie, J. A. and Beckman, W. A. (2013) *Solar engineering of thermal processes*. Fourth Edi. John Wiley & Sons. doi: 10.1016/0142-694x(82)90016-3.

Florschuetz, L. W. (1979) 'Extension of the Hottel-Whillier model to the analysis of combined photovoltaic/thermal flat plate collectors', *Solar Energy*, 22(4), pp. 361–366. doi: 10.1016/0038-092X(79)90190-7.

Guarracino, I. (2017) *Hybrid photovoltaic and solar thermal (PVT) systems for solar combined heat and power*. Imperial College London.

Leonforte, F. (Politecnico di M. (2014) *MESSA A PUNTO E ANALISI PRESTAZIONALE DI UN COLLETTORE IBRIDO FOTOVOLTAICO TERMICO A FLUIDO TERMOVETTORE ACQUA. Dottoratodi tecnologia e progetto per l'ambiente costruito*.

Report ENEA (2020) *RdS/PTR2020/140*.

Rizzini, M. (2015) 'Analisi sperimentale di pannelli fotovoltaici termici innovativi presso il SolarTech Lab', p. 101.

Ruoping, Y. *et al.* (2020) 'Study of operation performance for a solar photovoltaic system assisted cooling by ground heat exchangers in arid climate, China', *Renewable Energy*, 155, pp. 102–110. doi: https://doi.org/10.1016/j.renene.2020.03.109.

Specialists, T. – T. E. S. (2017) 'TESSLibs 17 HVAC - Component Libraries for the TRNSYS Simulation Environment - Electrical Library Mathematical Reference TESS'. Madison, Wisconsin, USA, pp. 1–40.

TRNSYS website. http://www.trnsys.com/tess-libraries/TESSLibs17_General_Descriptions.pdf, Accessed: 04/01/2021.

UNI EN 16147 (2017) *Pompe di calore con compressore elettrico - Prove, valutazione delle prestazioni e requisiti per la marcatura delle apparecchiature per acqua calda sanitaria*.

UNI EN ISO 9806 (2017a) *Energia solare - Collettori solari termici - Metodi di prova*.

Zenhäusern, D. *et al.* (2017) 'PVT Wrap-Up: Energy systems with photovoltaic-thermal solar collectors - Technology, market, experiences', *ISES Solar World Congress 2017 - IEA SHC International Conference on Solar Heating and Cooling for Buildings and Industry 2017, Proceedings*, pp. 1133–1144. doi: 10.18086/swc.2017.18.12.

5. Analysis of Results of numerical simulations

This chapter reports the results of simulations performed with the TRNSYS software described in chapter 4.

The innovative systems hereby investigated include a heat pump water heater (HPWH) integrated into a solar plant which can have different configurations in terms of the number of photovoltaic and thermal (PV/T), photovoltaic (PV), and solar thermal (ST) panels.

At a preliminary stage, the dynamic modelling and simulations are aimed at optimising the size of system components for better supporting a power-to-heat approach.

A comparison between these solar technologies was performed by varying also the number of panels in order to determine the best one for DHW production. PV systems were sized to meet just the consumption of the heat pump with the aim of maximizing self-consumption through the use of thermal and/or electrical storage systems.

Results were used in order to identify the best configuration in terms of energy-saving, to well understand the effectiveness of the solar collectors (PV/T, PV, or ST) under different load demands. Several indices are defined and calculated to guide toward correct sizing, to check users' satisfaction, and to assess primary energy savings. To quantify the thermal and electrical contributions of the solar plants to cover the thermal and electrical energy needs of the overall DHW plant, the solar fractions (thermal and electric) were calculated. Furthermore, through primary energy analysis, the degree of interaction with the electricity grid was assessed and opportunities to support demand-response actions for grid electricity management were investigated.

The results show how the energy consumption from the analysed systems is mainly influenced by the amount and structure of domestic hot water demand per day. Also, according to the chosen plant layouts, it is shown that the thermal contribution of PV/T slightly influences the system performances. Better results in terms of less non-renewable primary energy consumption are recorded for the PV-based plant. Solar thermal collectors, even if sized for high solar fractions, do not properly support the daily heat pump operation, especially in winter, and present a certain electricity consumption for auxiliaries which results to be penalizing.

Starting from these results an alternative plant layout was analysed based on the introduction of a preheating water tank between the HPWH and the PV/T system. The main objective was to reduce the thermal consumption of the system by exploiting solar production, consequently reducing the electricity consumption of the HP and at the same time ensuring coverage of the latter using the electricity production of the PV/T system. Several simulations have been hypothesized and simulated to analyse the performance of the proposed configuration plant for DHW production. Results showed better exploitation of the thermal energy supplied by the PV/T collectors and a sensible reduction of the HPWH electricity consumption.

5.1 Heat pump electricity consumption

In order to obtain an overview of the thermal and electrical behaviour of the HPWH for the proposed tapping profiles, some of the scenarios were simulated without any solar plant integration. It resulted that, for a given daily DHW demand (720 litres/day at 40 °C), no remarkable differences are recorded while changing the tapping profiles. The electricity consumption is about 1080 kWh/year for all the cases. A slight difference could be noticed by applying the tapping profile #7 to the others (1056 kWh per year, -2% with respect to the previous result).
Figure 5.1 shows average daily data every month for heat delivered by the HP condenser to the storage compared with the heat demand for DHW production. Once again it can be noted that similar results are obtained for tapping #1 and tapping #7. Indeed, the daily hot water demand did not change varying the hourly request.
Therefore, looking at Figure 5.1, it is possible to note that similar results were recorded for the delivered energy by the HP condenser for two samples tapping profiles.

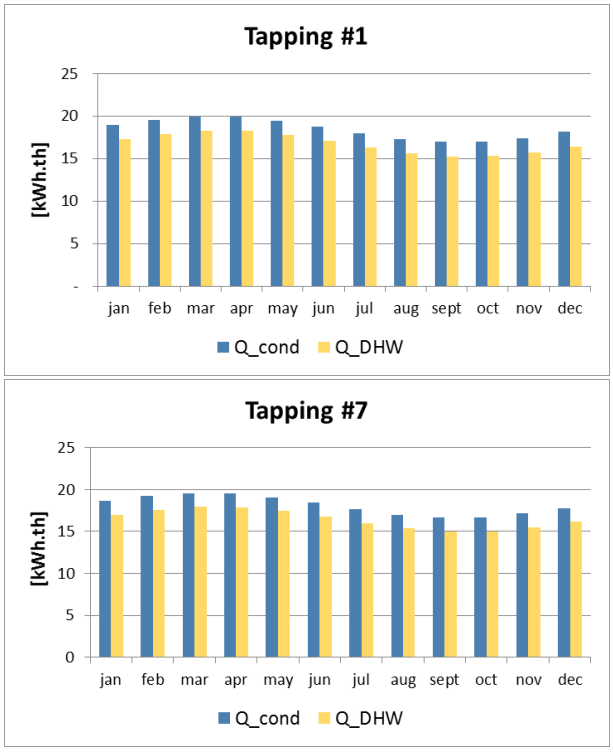

Figure 5.1. Average daily data on a monthly basis of heat delivered by the HPWH (Q_cond) and heat demand for DHW (Q_DHW).

On the other hand, differences can be noticed in the time distribution of HPWH on/off cycles (Figure 5.2) for the different tapping profiles. In this case, in a typical day, all the European Regulation profiles (tapping #1 to #6) cause similar behaviours. HPWH switches on mainly in the early morning and in the evening. When tapping #7 is applied

the HPWH ON/OFF cycle is more distributed all day long, with "ON" events about every three hours.

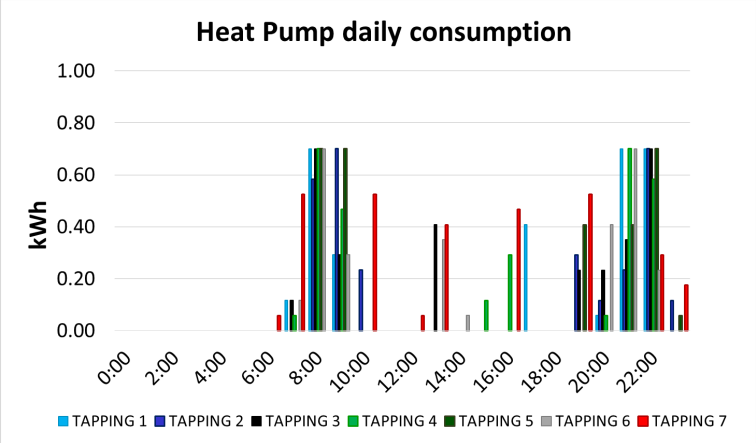

Figure 5.2. Hourly HPWH electricity consumption during a typical day.

Starting from these considerations, for the sake of simplicity, the next sections present and discuss energy indices calculated for the case of tapping #1 while, concerning the time-dependent operational indices, tapping #1 and #7 figures are compared.

5.2 Indices of Performance

As previously introduced a set of energy and operational indices was calculated and analysed. They were used in order to identify the best configuration in terms of energy-saving, to well understand the effectiveness of the solar collectors (PVT, PV, or ST) under different load demands, to consider thermal and electrical contributions through primary energy analysis, to assess the degree of interaction with the electricity grid and evaluate the way the system could interact in an advanced Demand-Response scenario.
The overall energy demand of the DHW plant can be split into electrical and thermal demand. The electricity demand E_{tot} is written as it follows:

$$E_{tot} = E_{HPWH} + E_{pump-ST} = E_{PV} + E_{grid} - E_{loss} \tag{5.1}$$

The total consumed electricity E_{tot} is made by two contributions: the heat pump consumption (E_{HPWH}) and the one of the solar thermal pump ($E_{pump\text{-}ST}$). Considering the electricity balance of the system, the terms on the right side of Eq. (5.1) represents, respectively, the electric energy supplied by the PV system including electric storage (E_{PV}), the energy supplied by the grid (E_{grid}) net of the energy losses due to inverter efficiency and charge/discharge battery efficiencies (E_{loss}).
The thermal energy balance is written as follows:

$$Q_{DHW} = mc_p(T_{hot} - T_{cold}) = Q_{HPWH} + Q_{ST/PV} - Q_{loss} \tag{5.2}$$

where the required thermal output (Q_{DHW}) is defined as the product among the DHW mass flow (m) entering/exiting the heat exchanger in the tank, the water-specific heat content (c_p), and the temperature difference between DHW heat exchanger inlet/outlet. This product has to be equal to the input provided by the plant including both thermal energy from the heat pump cycle (Q_{HPWH}) and the solar plant loop ($Q_{ST/\ PVT}$), net of thermal losses (Q_{loss}). Specifically, the mass flow (m) of water exiting from the tank heat exchanger at the temperature (T_{hot}) was calculated as the one required to fulfil the desired tapping event with water delivered to the user at 40 ◦C after its mixing with the cold-water stream from the aqueduct. Fig. 5.3 represents schematically the energy balance of the system.

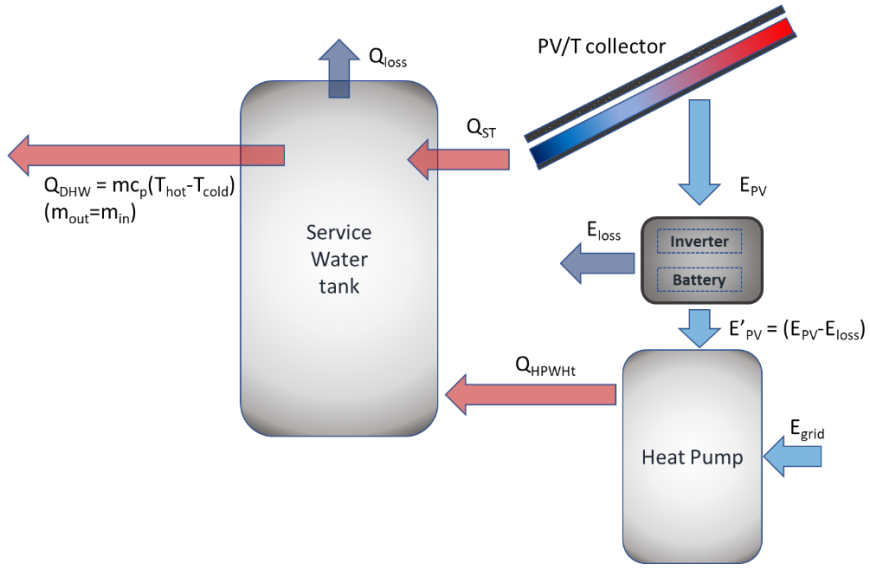

Figure 5.3. Electrical and thermal balance.

Starting from Eqs. (5.1) and (5.2), a set of indices was introduced for the assessment of the plants' performances. For a first comparison among the systems, the Electric Energy Saving (*EES*) was introduced as the ratio between the energy consumed from the grid by a conventional HPWH (E_{HPWH}^{Std}) and the energy consumed from the grid by the RES-based plants (E_{HPWH}^{RES}), including consumption by auxiliaries in the system (e.g. solar pumps):

$$EES = 1 - \frac{E_{HPWH}^{Std}}{E_{HPWH}^{RES}} \tag{5.3}$$

In addition, some indices accounting for both heat and electric renewable contributions to the system (Neyer and Köll, 2017) were calculated to assess the overall effect of the solar collectors (PV/T, PV, or ST) in the DHW system for different load demands. To do that and to evaluate the contribution of the hybrid collectors on the overall DHW

plant, solar fractions were introduced for first considering separately the thermal (SF_{th}) and electric (SF_{el}) balance:

$$SF_{th} = \frac{Q_{\mathrm{ST/PVT}}}{Q_{\mathrm{ST/PVT}} + Q_{HPWH}} \tag{5.4}$$

$$SF_{el} = \frac{E_{\mathrm{PV/PVT}}}{E_{\mathrm{PV/PVT}} + E_{grid}} \tag{5.5}$$

where $Q_{ST/PVT}$ and $E_{PV/PVT}$ represent the thermal and the electrical energy contribution from the RES plants, respectively. Moreover, if both thermal and electrical contributions were considered at the same time, the energy balances must be expressed in terms of primary energy. As a first step, it is necessary to introduce a primary energy factor for electricity, ε. In this context, it is calculated considering as useful energy the electricity produced by Italian power plants and supplied through the National Power Grid to final users (E_{grid}). Therefore, the primary energy use is related to the fuel consumption from non-renewable sources ($EP_{i,\ NREN}$) of the power plants. It can be calculated as follows:

$$\varepsilon_{NREN,\mathrm{grid}} = \frac{\sum_{i=1}^{n} EP_{i,NREN}}{E_{grid}} \tag{5.6}$$

According to Eurostat energy statistics and energy balances (Esser and Sensfuss, 2016), the values of primary energy conversion factors (ε) are nominally fixed by the Energy authority at the national level. The Italian Regulatory Authority for Energy, Networks, and Environment (ARERA) set the current value to $\varepsilon_{NREN,grid}$ = 1.95. Furthermore, for each energy conversion process, i.e. a process using several energy carriers for producing heat (hot water), it is possible to calculate a non-renewable Primary Energy Ratio, which is defined as the ratio of the useful energy output (Q_{DHW}) to the non-renewable primary energy input. As the electricity in our case is the only possible energy carrier, which can be generated by external power plants (E_{grid}), such a ratio is calculated as follows:

$$PER_{NREN,\mathrm{el}} = \frac{Q_{DHW}}{E_{grid}\varepsilon_{NREN,grid}} = \frac{mc_p(T_{hot} - T_{cold})}{E_{grid}\varepsilon_{NREN,grid}} \tag{5.7}$$

The higher the PER_{NREN} (Neyer and Köll, 2017) value, the lower the non-renewable primary energy consumption and the higher the renewable sources' support. Finally, to evaluate the impact of RES on DHW production, a reference scenario was introduced where an Electrical Storage Water Heater (ESWH) produces DHW. The Primary Energy Ratio for this reference system ($PER_{NREN.ref}$) was calculated assuming its electricity-to-heat efficiency η_{ref} equal to 0.9 (due to fouling and heat losses):

$$PER_{NREN,\mathrm{ref}} = \frac{Q_{DHW}}{E_{grid,ref}\varepsilon_{NREN,grid}} = \frac{mc_p(T_{hot} - T_{cold})}{E_{grid,ref}\varepsilon_{NREN,grid}} \quad (5.8)$$

Hence, the non-renewable energy-saving factor ($f_{sav.NREN}$), with respect to the reference system, is then introduced as it follows:

$$f_{sav.NREN} = \left(1 - \frac{PER_{NREN,\mathrm{ref}}}{PER_{NREN,grid}}\right) \cdot 100 \quad (5.9)$$

Eq. (5.9) suggests that the higher the value of the non-renewable energy-saving factor, the higher the primary energy saving compared to the benchmark system. Finally, to evaluate how the systems can interact with hypothetical grid aggregators in Demand Response (DR) scenarios, three other indices were introduced. In particular, they measure how the system's electricity consumption is distributed along the day in one year, how much it is fulfilled by the PV without and with the support of the storage. They are defined as follows:

$$\tau_a = \frac{\sum_{i=1}^{365}\sum_{n=1}^{5}\sum_{h=14:00}^{20:00} E_{HPWH,h,n,i}}{E_{HPWH-grid}} \quad (5.10)$$

$$\tau_b = \frac{\sum_{i=1}^{365} E_{HPWH\_PV,i}}{E_{HPWH}} \quad (5.11)$$

$$\tau_c = \frac{\sum_{i=1}^{365} E_{HPWH\_PV.b,i}}{E_{HPWH}} \quad (5.12)$$

where:

- h is the hour in the day, n the day in a week, i the day in the year;
- E_{HPWH_PV} is the energy directly delivered to the load by the inverter from the PV string;
- $E_{HPWH\_PV.b}$ is E_{HPWH_PV} plus energy taken from the electric storage;
- $E_{HWPH,\,h,\,n,\,i}$ is the hourly energy consumption of the heat pump throughout the year;
- E_{HWPH} is the yearly electrical consumption of the heat pump;
- $E_{HWPH\text{-}grid}$ is the yearly electrical consumption of the heat pump from the grid.

According to this definition, τ_a is the ratio between the yearly electricity consumption of the HPWH from the grid occurring between 2 p.m. and 8 p.m. from Monday to Friday (DR time slot in the following) and the total yearly electricity consumption from the grid. The time slot considered in this index is based on the current Italian experimentation on DR from aggregated active end-users for providing reserve services in the ancillary service market. In particular, the considered time slot corresponds to the

hours of the day having the highest probability that DR actions will be requested, according to the ARERA resolution n. 422/2018 (ARERA, 2018) concerning the Mixed Enabled Virtual Units (UVAM in Italian). According to Eq. (5.10), τ_a provides a measure of the energy availability of the device for participation in DR programs. The greater τ_a, the higher the capacity of decreasing the energy consumption in the selected time slot for solving grid congestions. According to the other experiences in DR programs, values above 30% indicate a good capacity of participating in DR programs.
τ_b evaluates the contemporaneity between the photovoltaic production and the HPWH electricity consumption considering real operating conditions. Regarding the possibility of participating in DR programs, τ_b gives a precious indication regarding the residual load from the grid of the HPWH (that is the total load net of the PV contribution).
Indeed, the greater τ_b, the lower is the residual load and the capacity of reducing the power demand to solve grid congestions. With respect to τ_a, τ_b has a wider significance since it does not refer to a specific time slot but the whole day.
τ_c takes into account the fraction of the electric load covered by the photovoltaic plant including the battery. τ_c has the same significance as τ_b in the presence of battery energy storage systems. The difference between τ_c and τ_b provides a measure of the capacity of the battery system of injecting power into the grid for solving grid congestions.
The three indices are defined in a way that considers the possibility that the HPWH could participate in DR programs in time intervals where it requires electricity to the grid, preserving, in this way, self-consumption. All the indices are evaluated on a yearly basis but can be assessed also month by month.

5.3 Results for system configuration A

Simulations of three different solar plants for DHW production that can be integrated with the selected HPWH were performed for the climate of Palermo (Italy). For each solar plant configuration, different solar collectors/panels sizes are tested. Furthermore, different DHW tapping profiles are assumed in simulations (Table 4.1).
The results show how the energy consumption from the analysed systems is mainly influenced by the amount and structure of domestic hot water demand per day. Also, according to the chosen plant layouts, it is shown that the thermal contribution of PV/T slightly influences the system performances. Better results in terms of less non-renewable primary energy consumption are recorded for the PV-based plant. Solar thermal collectors, even if sized for high solar fractions, do not properly support the daily heat pump operation, especially in winter, and present a certain electricity consumption for auxiliaries which results to be penalizing.
The energy indices were evaluated for all the PV, PV/T, and ST -assisted plants for tapping #1, in the three possible configurations conf_1 conf_2, and conf_3 with four, six, and eight panels/collectors respectively.
Operational indices and energy fluxes that hour by hour characterise the overall system operation, are analysed considering the two days with the maximum and minimum

irradiation over the typical year, 07th February (604 Wh/m^2 per day) and 08th July (8761 Wh/m^2 per day).

5.3.1 Energy indices comparison

The energy indices were evaluated for all the solar-assisted plants (PV, PV/T, and ST), for tapping #1, in the three possible configurations: conf_1 with four panels/collectors, conf_2 with six panels/collectors, and conf_3 with eight panels/collectors.
Very similar annual values of the electrical solar fraction (Figure 5.4) were obtained for PV and PV/T plants achieving nearly 100% of HPWH electrical demand covered when 8 panels are installed.

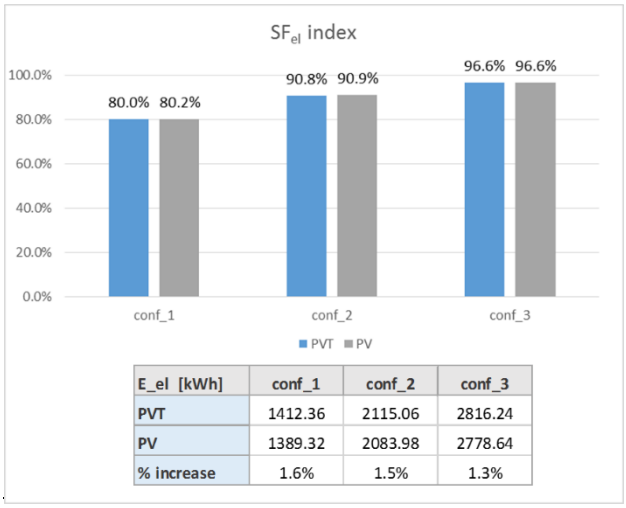

E_el [kWh]	conf_1	conf_2	conf_3
PVT	1412.36	2115.06	2816.24
PV	1389.32	2083.98	2778.64
% increase	1.6%	1.5%	1.3%

Figure 5.4. Yearly basis electrical solar fractions and power production for PV and PV/T for tapping 1 and three possible configurations.

It is necessary to underline that few differences were reported between PV and PV/T plants. To better understand this behaviour, electrical production of the PV/T was calculated with the following assumptions excerpted from EN ISO 9806 (EN ISO 9806), IEC/EN 61215-2005 (IEC/EN 61215-2005), and IEC/EN 61730-2005 (IEC/EN 61730-2005):
- case 1, PV/T collector with no heat removal ($m_{ST} = 0$);
- case 2, PV/T collector with heat removal ($m_{ST} = 0.03$ kg/m^2 s, $T_{in} = 20$ °C).

In both cases, according to the above-mentioned EN standards, steady-state conditions were simulated: solar irradiation is set to 1000 W/m^2 and temperature of outdoor air to 25 °C. Simulations in standard steady-state conditions gave an increase in electricity production of about 9% in case 2 (with heat removal) compared to case 1. Considering that the corresponding difference between the PV cells' temperatures in the two different operating conditions is about 18 °C, there is a specific increase in the

efficiency of 0.5%/°C. The latter value is in agreement with the manufacturer's technical datasheet.
Nonetheless, by comparing under real operation conditions, as for the PV and PV/T electrical production, slight differences were noticed. In particular, during the winter months, the useful solar heat by the PV/T system was null because the difference between the outlet temperature from collectors and the temperature at the top of the storage was always negative. An appreciable increase in electricity production (maximum gain of the efficiency equal to 4%) and useful heat delivered to the storage occurred only in the summer months. Indeed, in this period, PV/T collectors are effectively cooled by the water drawn from the middle/bottom of the storage during hot and sunny days. Solar contribution is positive, leading to increased electricity production, up to 10 kWh per month (Figure 5.5 and Figure 5.6).

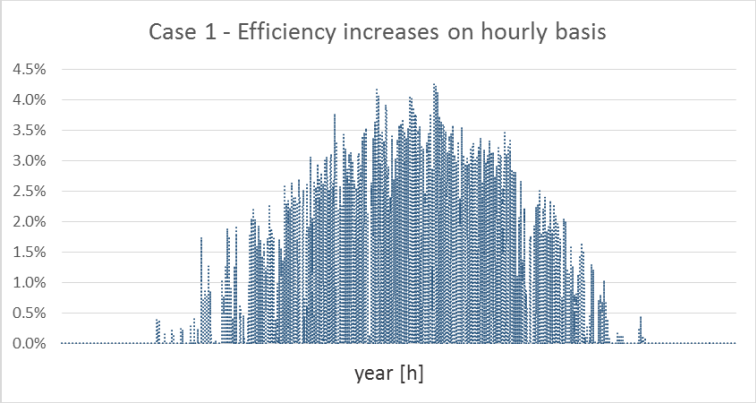

Figure 5.5. Efficiency increases in PV/T configurations to PV.

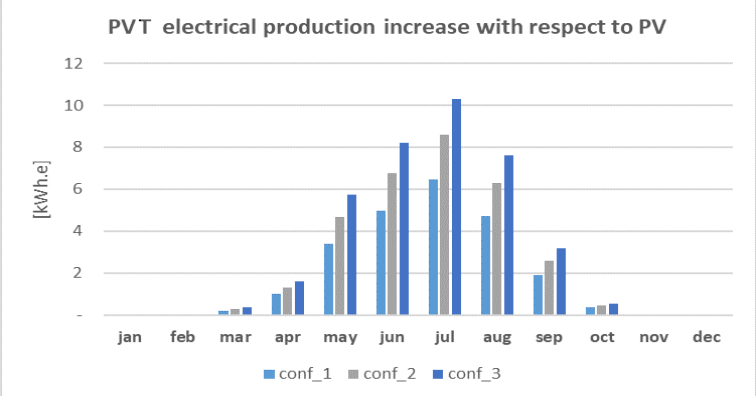

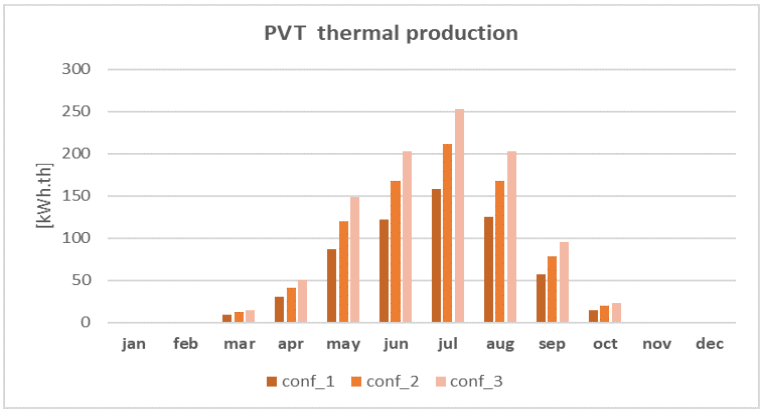

Figure 5.6. PV/T electrical and thermal production for the three configurations.

As concerns the heat balance for solar thermal and hybrid plants, it can be noted that the above-described behaviour can be confirmed. Solar thermal fraction for ST collectors was always higher than 75%, while it did not achieve the 15% for PV/T modules. It means that a traditional solar thermal collector can more efficiently cover the heat demand. For the sake of completeness, Figure 5.7 shows the solar fractions and the useful heat delivered by the two typologies of systems month by month in conf_2.

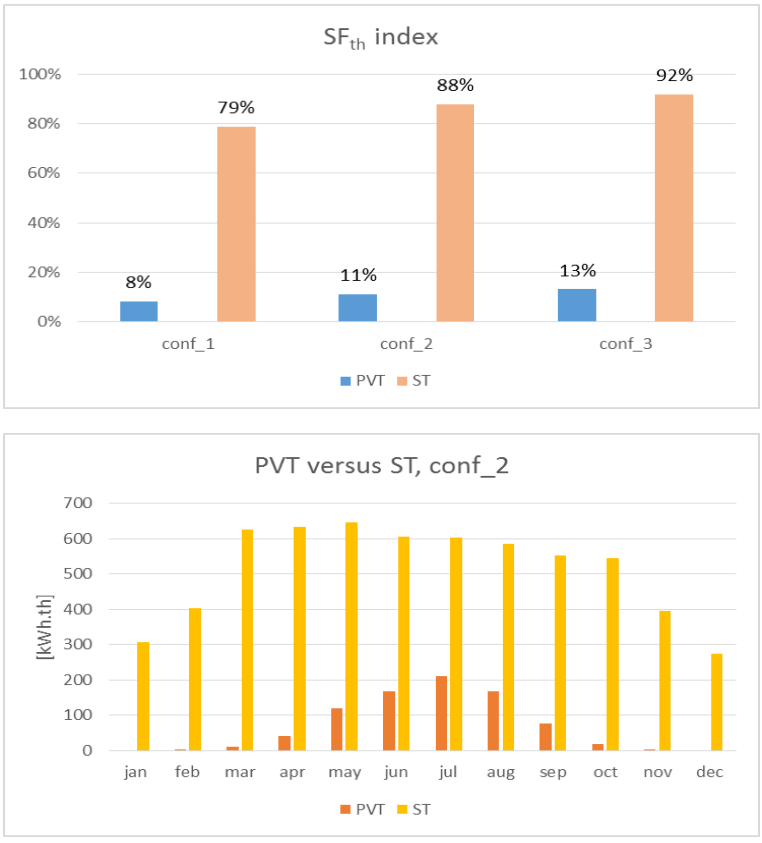

Figure 5.7. Solar Thermal Fraction of PVT and ST and monthly useful heat yield by the collectors.

Also, in relation to the useful heat produced month by month, a significantly lower thermal performance is confirmed for PVT than for ST collectors. Even in the summer months the PVTs fail to reach even half of the thermal production of the solar thermal collectors. This huge difference can be explained by considering that the thermal potential of a PV/T collector is limited by the need to ensure the robustness of the PV cells which, at temperatures that are too high, would suffer a decrease in their electrical performance. In addition to this, it should be considered that the PV/T under analysis is an unglazed collector and the absence of the glass cover can affect the thermal performance of the collector.

PER_{NREN} was calculated to compare ST, PV, and PVT systems (Figure 5.8). Stated that DHW thermal demand was the same in all analysed systems, some differences could be noticed among solar plants typologies. On a yearly basis, plants equipped with PV and PVT were characterized by very similar figures. In particular, PER_{NREN} values grew up linearly by increasing the number of panels in the system. The higher the available and exploited energy for the DHW production purpose, the higher the PER_{NREN}. On the other hand, PER_{NREN} values related to ST plants are lower. It has to be reminded that solar thermal collector plants were designed to meet the thermal demand for 79% until 90% of the load. Nevertheless, a residual electrical consumption due to solar pump is distributed all year long. Higher electrical consumption from the grid was recorded during winter months with respect to PV-assisted plants that were mainly driven by self-produced energy (Figure 5.6, above). It causes the different behaviour of the ST plants, which has a negative influence on PER_{NREN} figures.

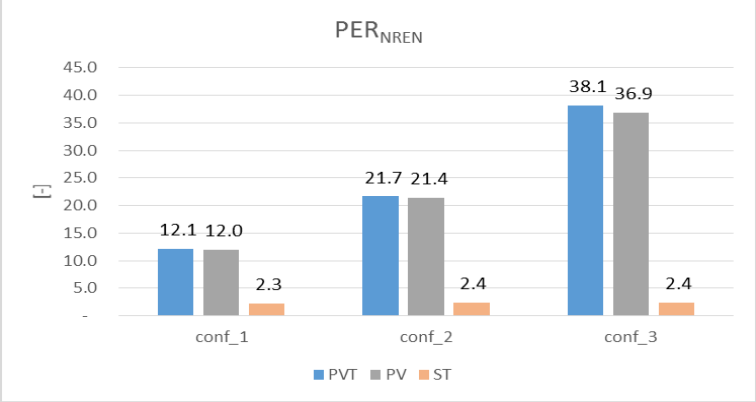

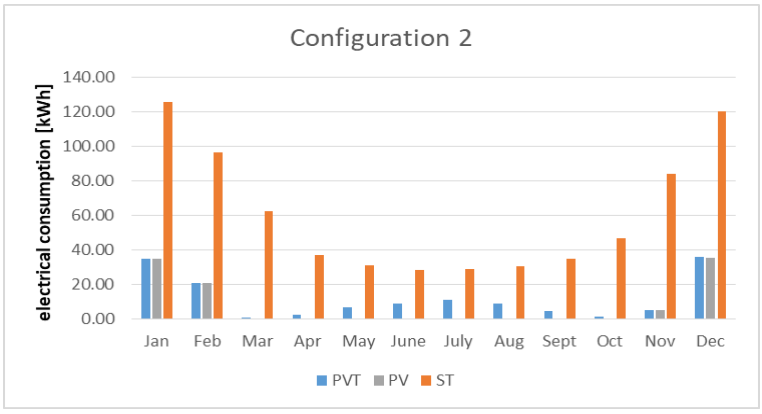

Figure 5.8. Primary energy ratio comparison among plants in different configurations (above); monthly HPWH grid electricity consumption in configuration 2 (below).

As a confirmation, EES indices show higher values for PV-based system that reach 97% for configuration 3. ST systems do not achieve values higher than 54% (Figure 5.9).

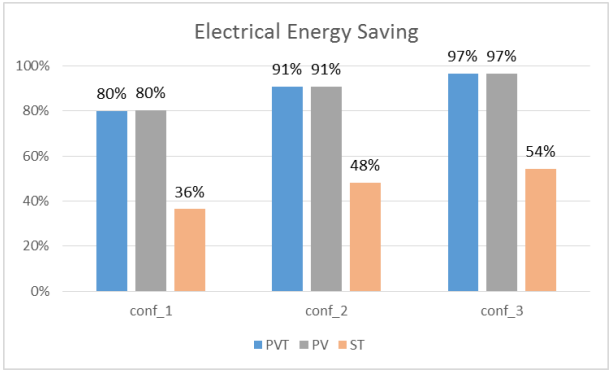

Figure 5.9. Electric energy-saving index (EES) comparison.

All the proposed solar systems were hereby compared to grid-electricity-driven DHW technologies by the calculation of the non-renewable energy-saving factor ($f_{sav.NREN}$). As declared in the method section, a typical ESWH was chosen as a benchmark. $f_{sav.NREN}$ ranges from 96 to 99% when increasing the number of panels respectively for PV or PV/T. Due to previous considerations concerning electricity consumption of auxiliary equipment, ST-based systems achieved lower values (about 80%) (Figure 5.10).

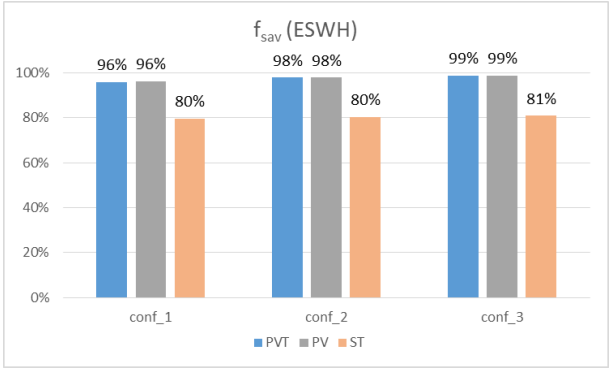

Figure 5.10. Non-renewable energy-saving factor calculated for the investigated systems.

5.3.2 Energy fluxes analysis and operational indices

As an example of the energy fluxes that hour by hour characterise the overall system operation, it is worth analysing the two days with the maximum and minimum irradiation over the typical year, 07th February (604 Wh/m^2 per day) and 08th July (8761 Wh/m^2 per day). Average ambient temperatures are 11.9 °C and 26.3 °C.
Figures 5.11 report the trends of the main energy items for PV/T configuration 2 when tapping #1 and tapping #7 are considered. In particular, the following physical quantities are represented in an hourly time step:

- E_PVT (string), the electricity produced by PV/T string;
- E_HPWH, the energy demand by the heat pump;
- E_to/from_battery, the energy flux entering to the battery from the PV/T string (positive value) or exiting from the battery to feed the load (negative value);
- E_to/from_grid, the surplus energy produced by the PV/T string that is delivered to the grid (positive value) or the incoming energy from the grid that is delivered to the load (negative value);
- Q_ST, the thermal energy produced by the PV/T string;
- FSOC, the fractional state of charge of the battery;
- m_DHW, the domestic hot water demand.

It is worth noting that, regardless of the tapping profile:

- On the winter reference day, HPWH is mainly driven by electricity taken from the grid. The electricity produced during midday is used for battery charging even if the FSOC lies under 10%. The battery is able to support HPWH operation from late afternoon until early evening. Moreover, solar thermal production, on this particular day, is negligible in both cases.
- On the summer reference day, HPWH consumption is totally covered by the PV system. Indeed, electrical production exceeds the HPWH demand and it is useful for battery charging and ensuring the maximum allowed FSOC, which ensures electricity for the evening and morning. In both cases, surplus energy is sent to the grid during the midday with slight differences between the two cases (5719 Wh for tapping #1 and 5913 Wh for tapping #7).

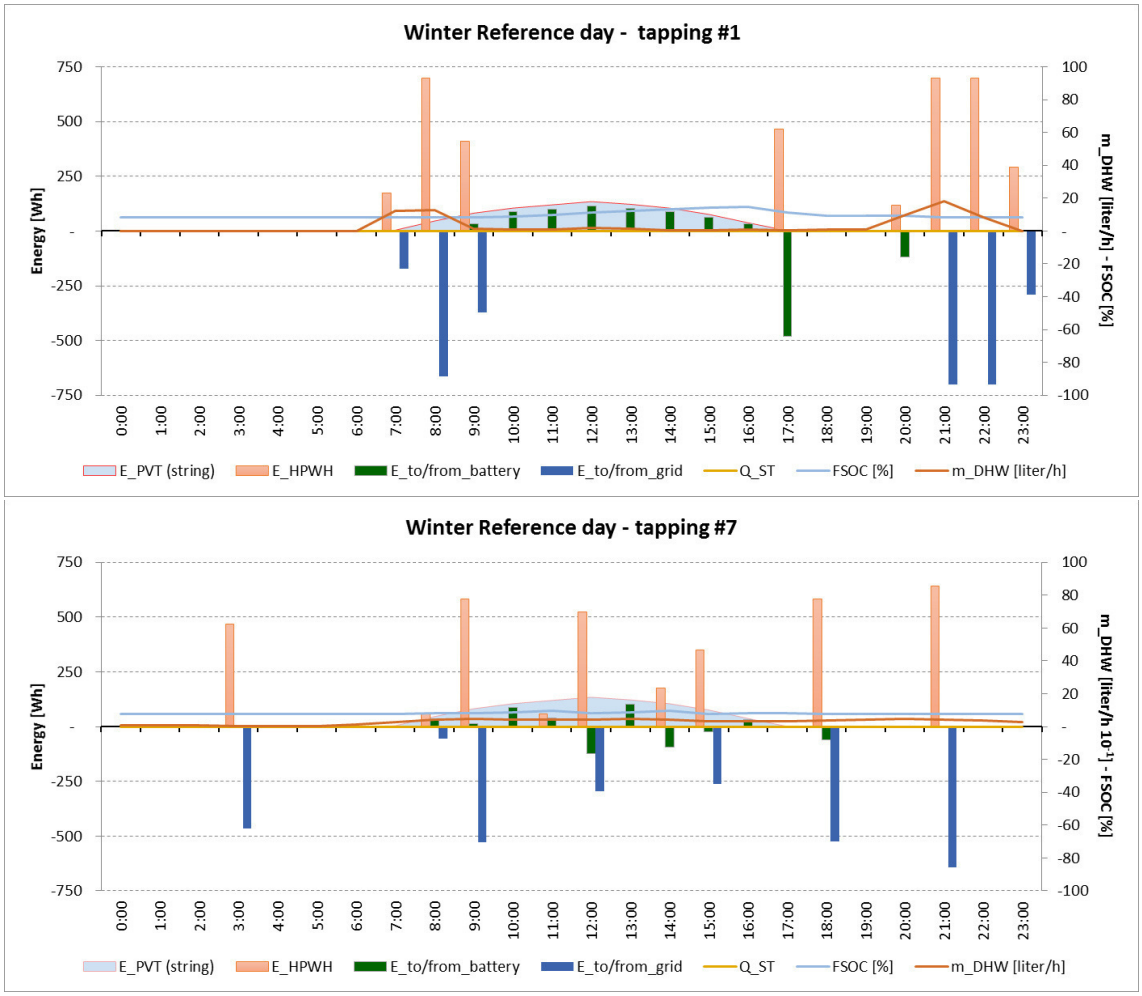

Figure 5.11. Hourly energy fluxes and DHW demand on the 8th of July for tapping #1 and #7 (PV/T configuration 2).

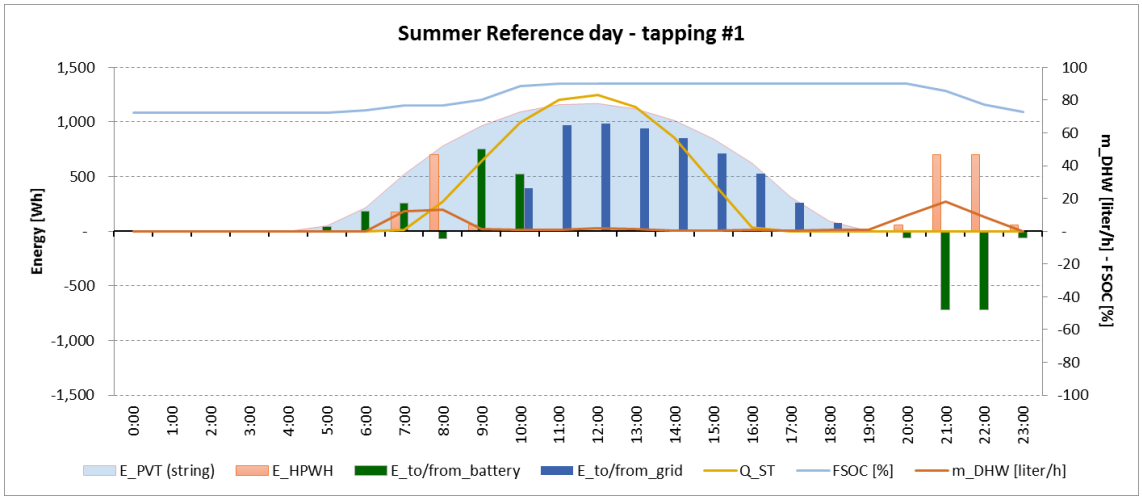

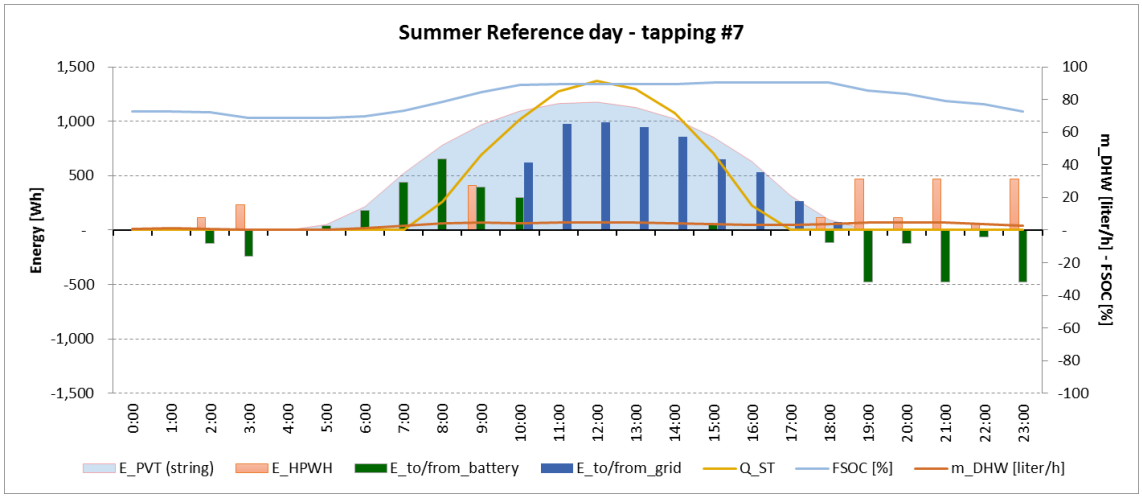

Figure 5.12. Hourly energy fluxes and DHW demand on the 7th of February for tapping #1 and #7 (PV/T configuration 2).

As introduced in the method section, three operational indices were considered to analyse the distribution of the hourly electrical exchanged with the grid and the fraction of heat pump consumption covered by self-production all year long: τ_a, τ_b, and τ_c.
It is worth noting that, considering the solely HPWH system without any solar plant integration, a different magnitude of τ_a was recorded according to the adopted tapping.
Figure 5.13 shows the monthly values of E_{HPWH} in the DR time slot used for assessing τ_a calculated for tapping #1 and tapping #7 for the solely HPWH without any solar plant integration. The two profiles completely differ from each other's in terms of hourly distribution of water uses so, the DHW withdrawal in the analysed time slot is about 6% of the daily volume for tapping #1 and 37% for tapping #7. This fact leads to having, for tapping #1, null values all year long of τ_a for all the solar plants regardless of the solar technology and configuration. On the other hand (figure 5.10), for tapping #7, some consumption in the DR time slot on yearly basis was recorded (mainly in winter months). Small differences were noticed between PV and PVT configurations. ST systems have higher values of electricity consumption taken from the grid compared to the others.

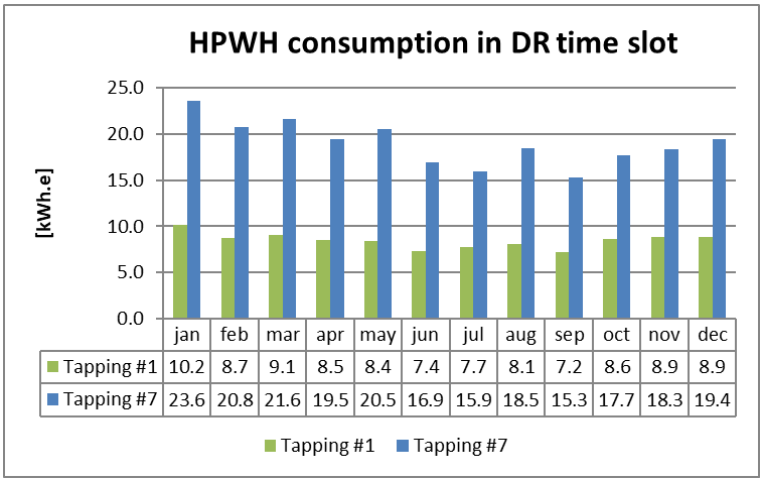

Figure 5.13. HPWH consumption in DR time slot without solar integration.

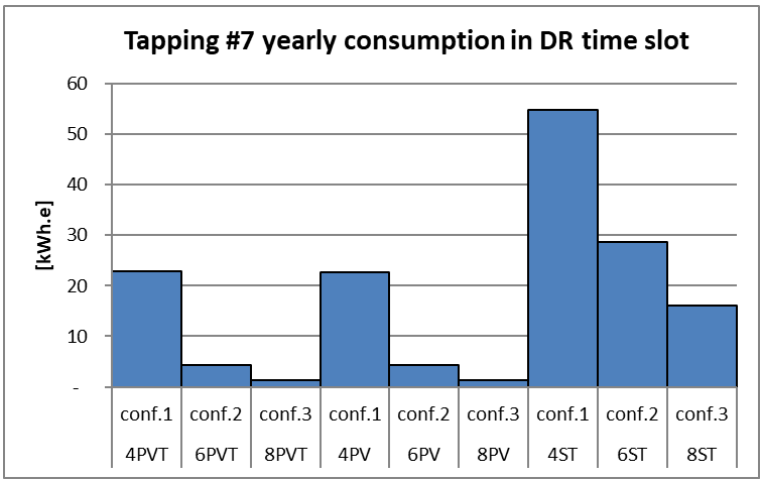

Figure 5.14. Yearly consumption of the HPWH in DR time slot for tapping #7 for all the solar configurations.

Concerning the calculation of the τ_b index, some differences were noticed among the analysed configurations. Generally, the higher the number of PV or PV/T panels, the higher the produced power, the higher the possibility that self-production could match the power required to drive the HPWH. As well, in this case, differences belonging to different tapping profiles arise according to their specific hourly distribution. During the summer months, when the maximum thermal contribution by PV/T occurs, the electricity demand is lowered. Figures 5.15 to 5.17 show that self-consumption is higher in the case of the PV system to the configuration with PV/T system both for tapping #1 and tapping #7. Moreover, when tapping #7 is adopted, self-consumption from the solar plant increases to the case of tapping #1.

By including battery-electric energy storage in the system, similar results are found for both tapping profiles. Nonetheless, some differences were outlined by increasing the number of panels in the string. On a yearly basis, self-consumption grows by about 19%

in configuration 2 and 29% in configuration 3 with respect to configuration 1. Figure 5.18 shows the results for Configuration 2.

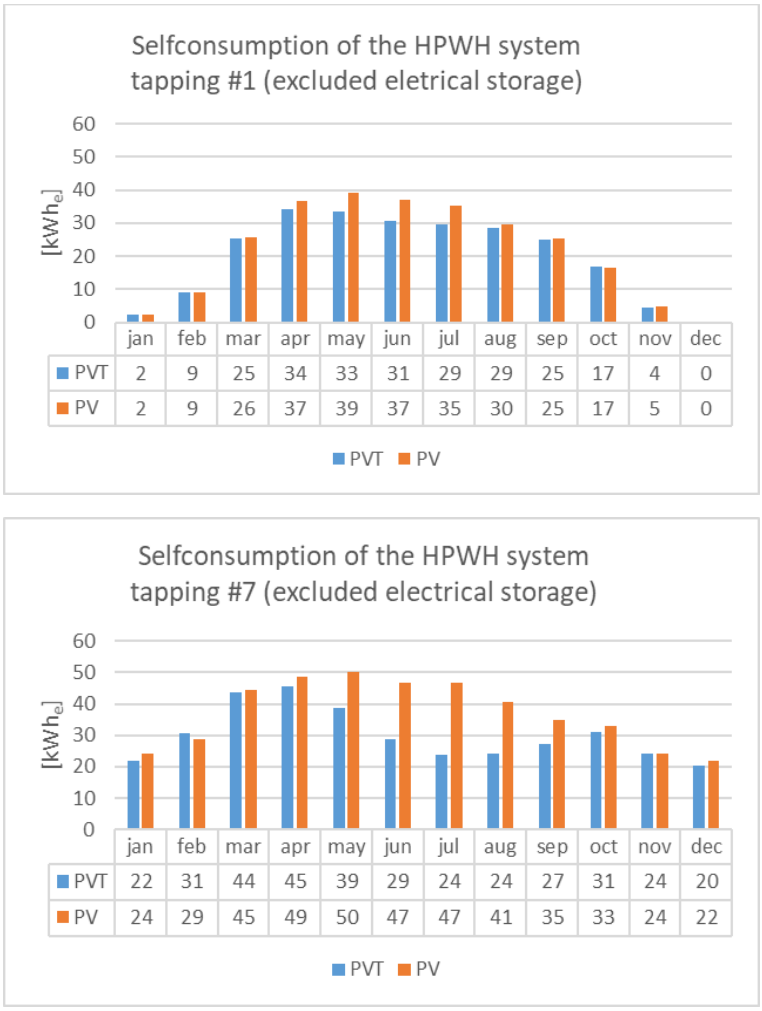

Figure 5.15. Electricity provided to the HPWH by the PV system for each month for configuration 1 and tapping #1 and tapping #7.

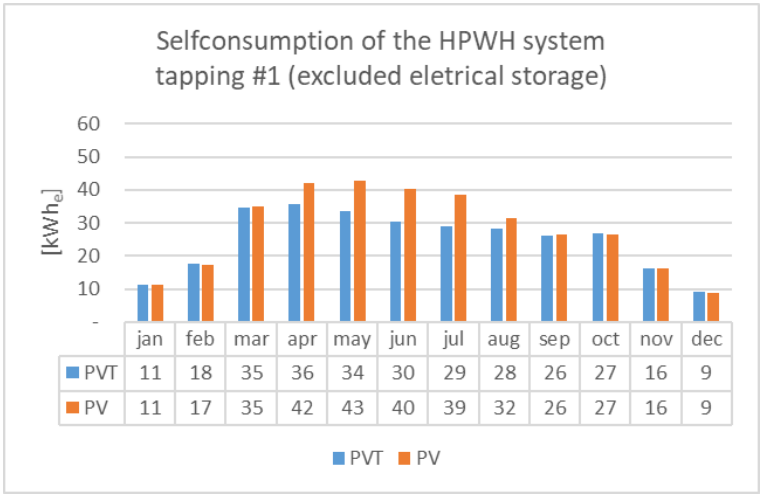

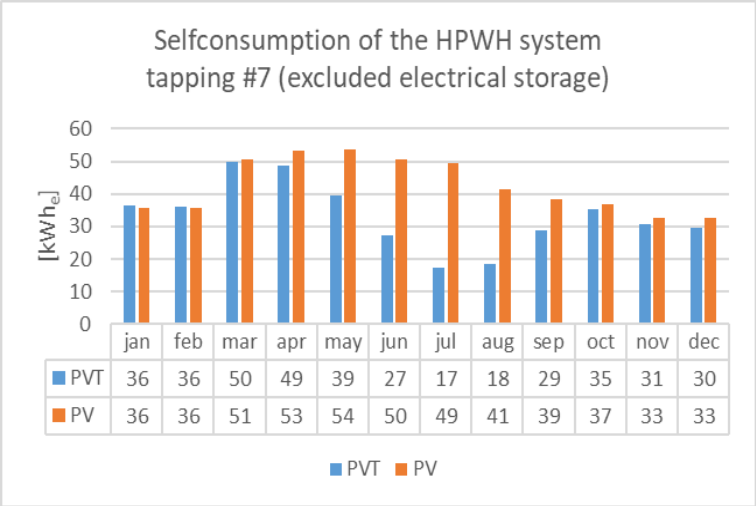

Figure 5.16. Electricity provided to the HPWH by the PV system for each month for configuration 2 and tapping #1 and tapping #7.

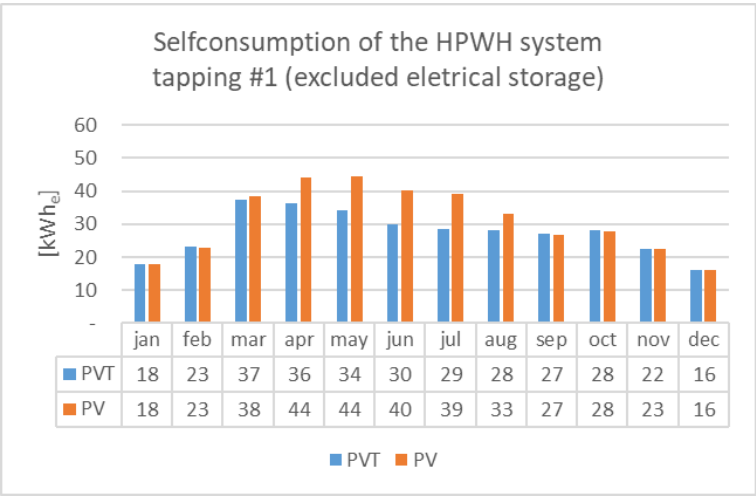

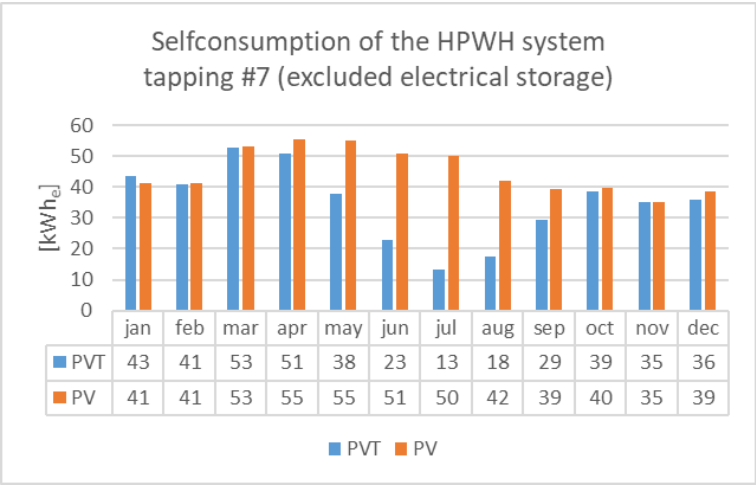

Figure 5.17. Electricity provided to the HPWH by the PV system for each month for configuration 3 and tapping #1 and tapping #7.

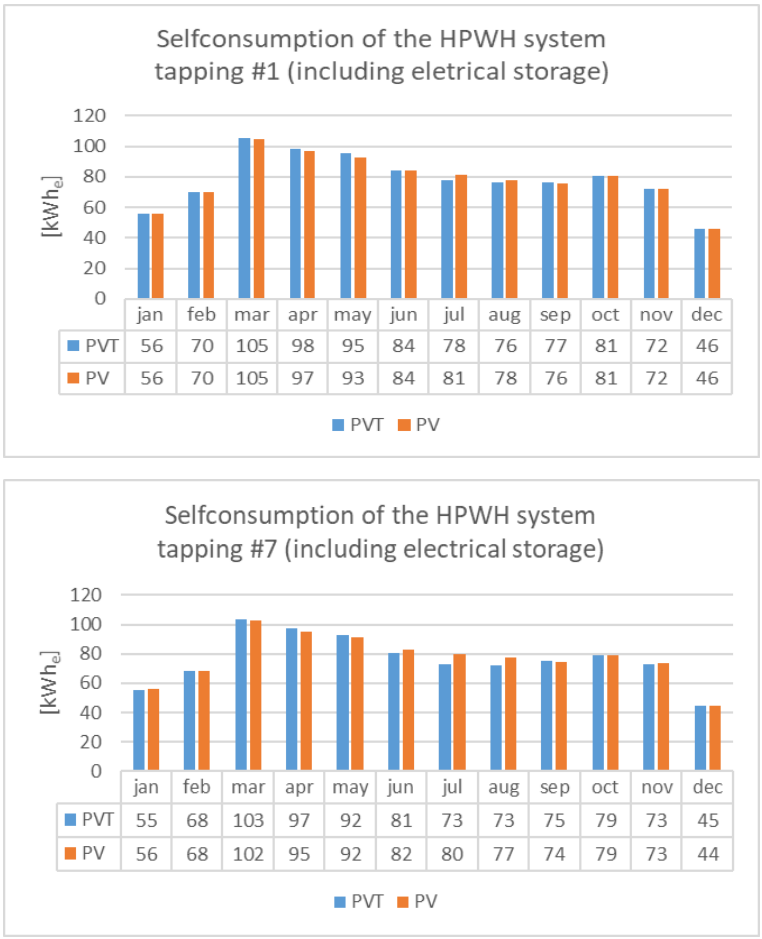

Figure 5.18. Electricity provided to the HPWH by the PV system with batteries for each month for configuration 3 and tapping #1 and tapping #7.

Table 5.1 and Table 5.2 show the detailed results for τ_a, τ_b, and τ_c indices on a yearly basis.

τ_a assumes extremely low values in all the analysed configurations. This means that, the power consumption of the HPWH is totally or quasi-totally covered by the PV production in the established DR time slot and that the device is not able to support an aggregator for DR programs.

Looking at τ_b results, some differences between the two tapping profiles can be observed. Contrariwise, τ_c results are identical for both profiles thanks to the availability of electricity from the whole PV/PVT system (including battery).

τ_b is between 24% and 35% considering tapping #1 and between 34% and 51% considering tapping #7. These results confirm that the HPWH does not present a good contemporaneity between consumption and production and that the residual load is, in general, enough significant for being used in DR programs, even if the results obtained for τ_a demonstrate that the residual load is mainly outside the DR time slot where it is higher the probability that grid congestion occurs. At the same time, it is worth noting how the tapping profile can influence the index. Tapping profiles like #1 reduce the

self-consumption quota generating higher residual loads while tapping #7 allows a better coincidence between consumption and generation but reduce the residual load usable for DR programs. The same effect is visible on τ_c.

The difference between τ_c and τ_b is between 31% and 54% for tapping #1 and between 49% and 64% for tapping #7. These values provide a measure of the energy availability from storage for supporting DR programs to the detriment of self-consumption maximization. Indeed, the energy stored in the batteries and used for increasing the self-consumption quota of the system, in particular situations, if economically advantageous for the owner of the system, can be used for solving grid congestions.

Table 5.1. Values for τ_a, τ_b, and τ_c indices (tapping #1).

	HPWH	HPWH+PVT			HPWH+PV		
		conf.1	conf.2	conf.3	conf.1	conf.2	conf.3
τ_a	9.4%	0.0%	0.0%	0.0%	0.0%	0.0%	0.0%
τ_b	-	22%	28%	30%	24%	31%	35%
τ_c	-	73%	87%	94%	73%	87%	94%
Yearly HPWH consumption [kWh]	1080	1080	1080	1080	1080	1080	1080
Yearly HPWH consumption from grid [kWh]	1080	227	107	46	227	107	46

Table 5.2. Values for τ_a, τ_b, and τ_c indices (tapping #7).

	HPWH	HPWH+PVT			HPWH+PV		
		conf.1	conf.2	conf.3	conf.1	conf.2	conf.3
τ_a	21.6%	11%	4%	4%	11%	4%	4%
τ_b	-	34%	38%	40%	42%	48%	51%
τ_c	-	73%	87%	94%	73%	87%	95%
Yearly HPWH consumption [kWh]	1057	1057	1057	1057	1057	1057	1057
Yearly HPWH consumption from grid [kWh]	1057	210	96	35	210	96	35

5.4 Results for system configuration B

For the purpose of the study of configuration B, 3 main scenarios were analysed:

- Basic scenario SC.0 (equivalent to configuration A with 6 PV/T collectors): the system without a pre-heating tank;
- Pre-heating scenario: the system with 500-liter pre-heating tank on the solar thermal side:

- SC.A1 pre-heating setpoint temperature T_{solar} = 35 ± 2 ° C;
- SC.A2 pre-heating setpoint temperature T_{solar} = 55 ± 2 ° C.

In both cases SC.A1 and SC.A2, according to the HPWH operating limits, the heat pump tank set-point temperature is assumed equal to 45 ± 2° C. It results in the fact that with Scenario A.1, the operation in pre-heating mode during 24h is the most probable mode. On the other hand, given the higher temperatures available in the pre-heating stage in Scenario A.2, both "standard" and "pre-heating mode" are to be investigated.
Regarding the thermal and electrical producibility of the PVT string in Scenarios A.1 and A.2 compared to SC.0, as expected, the pre-heating system has allowed greater yearly useful heat production (up to 4 times in SC.A1, and 5.6 in SC.A2 greater than the basic system). The increase in useful heat production allows a decrease in the temperature of the photovoltaic cells. It provides an increase in photovoltaic production of about 3% on an annual basis, without substantial differences between SC.A1 and SC.A2. The increase in solar production in both Scenarios A has also allowed a reduction in the electricity consumption of HPWH (Figure 5.19).

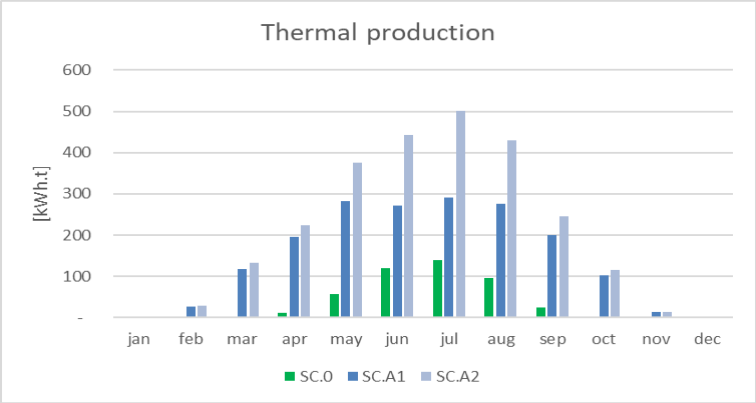

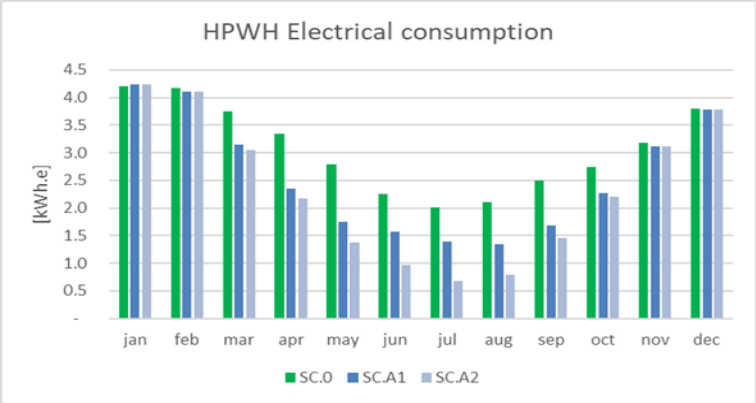

Figure 5.19. Comparison of baseline scenario and SC.A1 e SC.A2 scenarios.

As shown in figure 5.19, the electrical and thermal consumption profiles were analysed for a typical day of the month with an irradiation value close to the median of the monthly values (3.7 kW / m^2day, March). It is a useful analysis being a hybrid PVT system. For the SC.0 scenario, there is zero solar thermal production; while in the case of Scenarios A, there is a solar thermal production equal to 3.0 and 3.3 kWt, respectively for the SC.A1 and SC.A2 Scenarios (Figure 5.20).

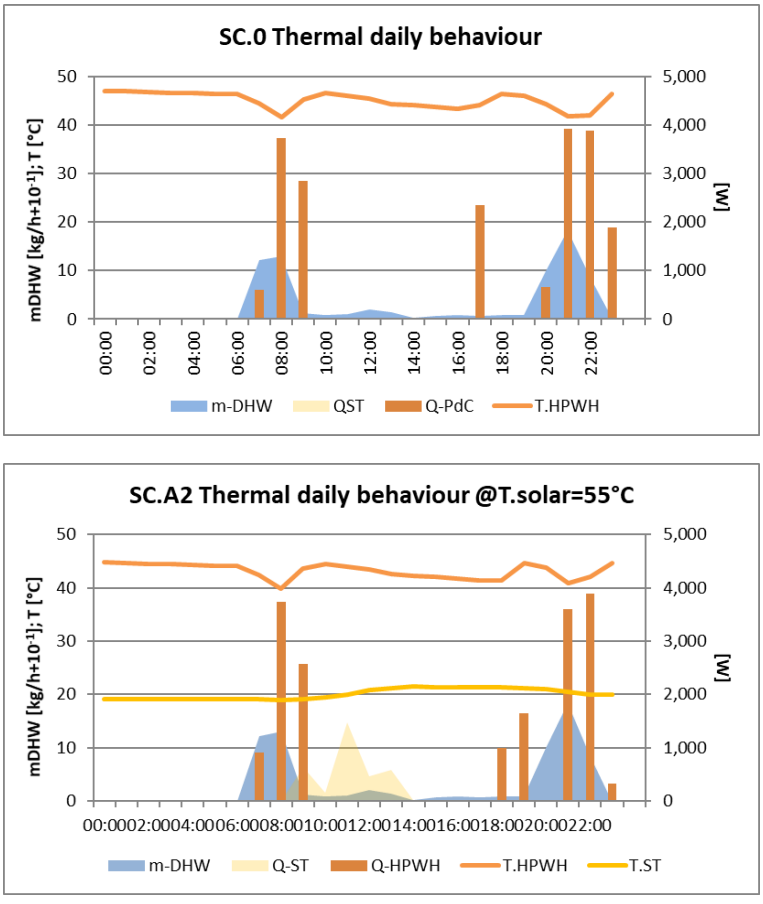

Figure 5.20. Analysis of the system's electricity consumption on a typical day in intermediate seasons.

On the chosen day, Scenario SC.0 and SC.A are different as well from an electrical point of view. It should be noted that the state of charge of the battery (SOC) in the SC.0 is insufficient to cover the electricity requirement during the first hours of the day. Consequently, some consumption from the grid is recorded in SC.0.
Indeed, even if some thermal production in SC.A is recorded during January and February, it is not still enough to influence the thermal behaviour of the whole system. Consequently, the electricity consumption by the heat pump is actually the same both in SC.0 and SC.A (Figure 5.21). On the other hand, during these months the available energy from the PV system does not ensure the energy self-sufficiency for the HPWH even including the electrical storage effect: the SOC of the battery generally drops down close to the minimum allowed charge in the evening (720 Wh).
So that, in the chosen day and the SC.0 Scenario, the initial state of charge is still insufficient to match the electricity demand in the early hours of the day (in the absence of sufficient PV production). Consequently, it should be necessary to draw electrical energy from the grid. From April the two main scenarios (SC.0 and SC.A) allow energy self-sufficiency.

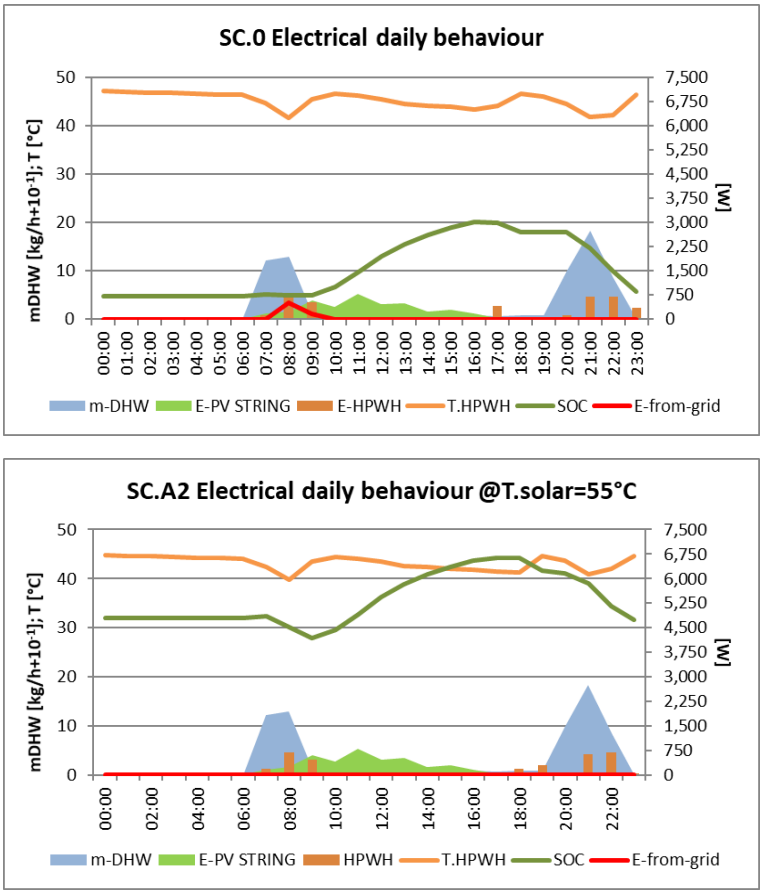

Figure 5.21. Analysis of electricity consumption of the system on a typical day in the winter seasons.

Finally, it is useful to highlight the influence of the set-point temperature assumed for the pre-heating storage management. An analysis has been performed for a typical day in the month of the greatest solar irradiation for the location under study (200 kWh / m^2 July). If there are no significant DHW withdrawals, the thermal energy produced during the day continues to be stored in the solar tank and used during the evening. On a typical day and for the chosen withdrawal time profile, the daily electricity consumption of the HPWH increased by 38% (Figure 5.21) by limiting the temperature of the pre-storage tank to 35° C. In all scenarios, electricity consumption is in any case covered by the PV/battery system.

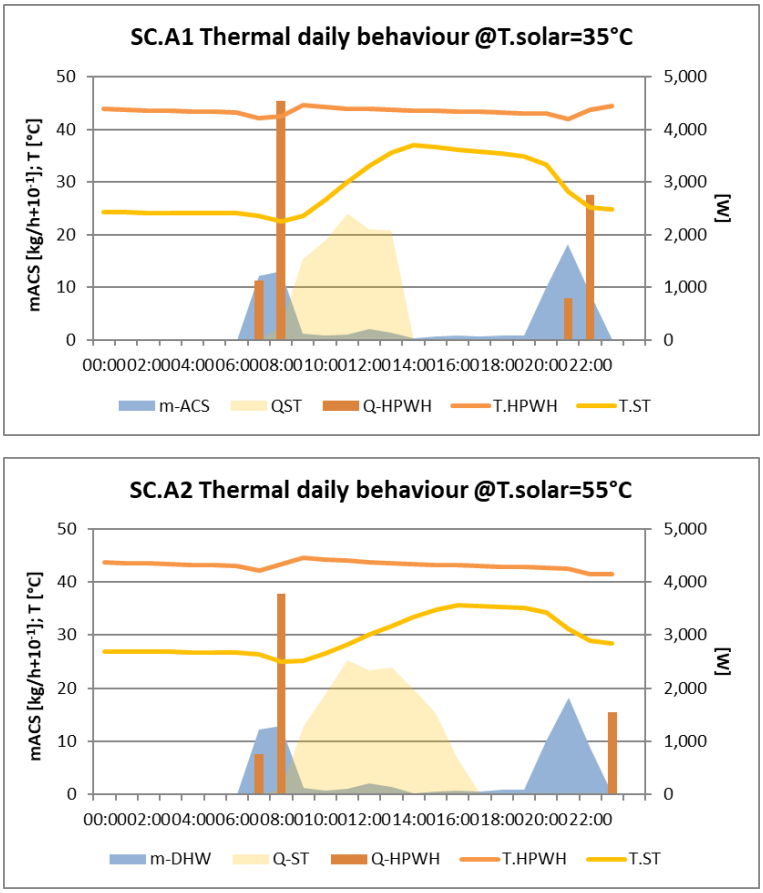

Figure 5.22. Analysis of the thermal consumption of the system in the typical summer day.

Finally, the reduction of the heat is to be provided by HPWH. It was assessed according to the temperature of the water entering the heat exchanger (T_{in}=$T_{aqueduct}$ in the case SC.0 and T_{in}=T_{ST} in the case of SC.A). Consequently, a decrease in electricity consumption (Figure 5.22) has been calculated. With the same heat demand for DHW, there was a reduction in heat demand between Scenarios SC. A and SC.0 equal to about 35% and a consequent reduction in electricity consumption equal to an average of 21%, in the presence of the pre-heating storage.

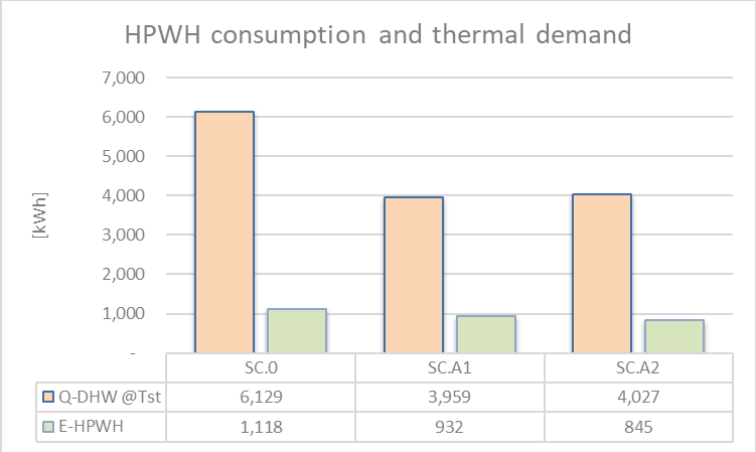

Figure 5.23. HPWH consumption and thermal demand.

As reported in Figure 5.23, the lower the heat demand of the HP, the higher the SF_{th} index. It is expressed as the ratio between the production of the ST system and the demand for DHW at 40° C. This latter was evaluated considering the lower temperature of the water. In particular, the SF_{th} calculated for the two scenarios SC.A1 and SC.A2 are higher than the SF_{th} calculated for SC.0 respectively of the 14% and the 20%.
Finally, the SF_{el} index and the EES index for each scenario show how the photovoltaic system is able to meet the electricity consumption of the HP regardless of the system chosen (always greater than 70%). As shown in Figure 5.24, it is possible to note that there are slight differences between the values obtained individually in each scenario due to the different reference points (consumption of the HP).
It should be noted that the consumption (in absolute value) from the grid decreased from 283 kWh for the SC.0 scenario to 256 for both the SC. A scenario (-10%). As already highlighted in Figure 5.21, the photovoltaic production is almost the same (approximately 1670 kWh per year). On the other hand, the energy fed into the grid (without accounting for the amount stored) is reduced from 820 kWh for the SC.A2 Scenario to 510 kWh for the SC.0 Scenario.

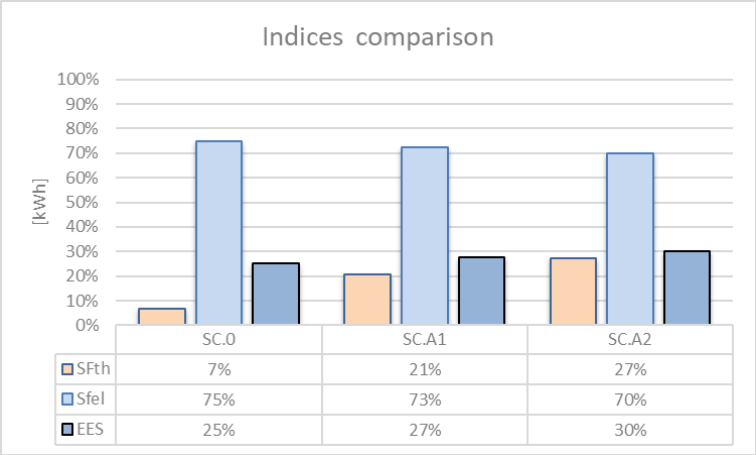

Figure 5.24. Indices comparison between the analysed scenarios.

So, in summary, as concern configuration A, PV and PV/T plants showed very similar annual values of the electrical solar fraction, whereas solar thermal fraction for ST collectors was always quite higher than for PV/T modules, meaning that traditional solar thermal collectors can more efficiently cover the heat demand. *PERNREN* results stated that DHW thermal demand was the same in all analysed systems; PV and PVT were characterized by very similar linear growing of the values with increasing the number of panels in the system. PER_{NREN} values related to ST plants were lower because of the residual electrical consumption due to solar pump. The non-renewable energy-saving factor ($f_{sav.NREN}$) showed similar results, with values for PV or PV/T ranging from 96 to 99% respectively when increasing the number of panels and lower values for ST-based systems caused by electricity consumption of auxiliary equipment. Hour by hour energy fluxes on the winter reference day, highlighted that HPWH is mainly driven by electricity taken from the grid ad solar thermal production is negligible. On the summer reference day, HPWH consumption is totally covered by the PV system ensuring the maximum allowed FSOC. τ_a, τ_b, and τ_c operational indices were considered. By analysing τ_a no significant differences were noticed between PV and PVT configurations, wheras ST systems have higher values of electricity consumption taken from the grid. τ_b index showed an higher self-consumption in the case of the PV system compared to the configuration with PV/T system both for tapping #1 and tapping #7. Similar results are found by including battery-electric energy storage in the system. These results confirmed that the HPWH does not present a good contemporaneity between consumption and production. Configuration B, which was analysed by considering two different, preheating setpoint temperatures (SC.A1 and SC.A2), was compared to configuration A. The pre-heating system allowed up to 4 times yearly useful heat production in SC.A1, and 5.6 in SC.A2 greater than the basic system and a contemporary increase in photovoltaic production of about 3%. The solar thermal production, which was zero without pre-heating, reached 3.0 and 3.3 kWt, respectively for the SC.A1 and SC.A2 Scenarios. SF_{th} showed an increase of the 14%

and the 20% for the two scenarios SC.A1 and SC.A2 respectively and a reduced consumption from the grid by 10%.

References

Esser, A. and Sensfuss, F. (2016) *Final report Evaluation of primary energy factor calculation options for electricity*. Karlsruhe.

Neyer, D. and Köll, R. (2017) 'Sensitivity analysis on the technical and economic performance of thermal and PV driven solar heating and cooling systems', *ISES Solar World Congress 2017 - IEA SHC International Conference on Solar Heating and Cooling for Buildings and Industry 2017, Proceedings*, pp. 1796–1807. doi: 10.18086/swc.2017.28.15.

6. A relevant case study: retrofit solutions for Mediterranean small islands

An analysis was carried out in order to test the application of several RES-based systems for producing DHW, including solar plants which were described in chapter 4, on the energy system of the Mediterranean minor islands as a relevant case study. As reported also in the study of G. Mutani et al. (ENEA website, 2020) the energy system of most small islands in the world is predominately based on fossil fuels, with inefficient and expensive energy production. In fact, the physical separation that occurs on the islands determines separate management of the networks from the national ones, favouring monopolies for the production and distribution of energy, with the associated economic and environmental disadvantages. The small islands can therefore be defined as "isolated energy communities", becoming an ideal laboratory to face the most urgent and important environmental challenges (ENEA website, 2020).
Many studies are available on the use of renewable energy sources on islands. For example, Chen et al. (Chen *et al.*, 2020) studied a pathway for small islands to replace fossil fuels by renewable sources, applied to a case study in Jamaica. They found that renewable energy can be achieved in such a manner as to satisfy and be in line with the Intergovernmental Panel on Climate Change guidelines for limiting temperature rise to 1.5 ◦C. The aim of the study of Alves et al. (Alves, Segurado and Costa, 2020) was to analyse the impact of the interconnection of two Azores small islands in the path to 100% RES for the whole energy system. Bertheau (Bertheau, 2020) focused his attention on Cobrador Island in the Philippines to study the impact of providing more affordable, reliable, and sustainable access to energy on consumption patterns, appliance uptake, and overall socio-economic development. To do this, similarly to this study, a survey was conducted to assess the impact of providing a continuous renewable-based power supply on local development and the sustainable development goals. Meschede et al. (Meschede *et al.*, 2016) proposed a general method to classify global islands about RES installation potentiality, employing cluster analysis based on climatic, physical, and socio-economic parameters. The possibility to convert the existing thermal-power plant into combined heat and power (CHP), i.e., a cogeneration system, including the construction of district heating/cooling networks, was investigated by Beccali et al. (Beccali, Ciulla, *et al.*, 2017). Nevertheless, this study conducted on six Italian small islands demonstrated that CHP technology is only moderately economically attractive when public support mechanisms are included in the analysis. Better results are achieved if hybrid renewable poly-generation systems are considered; however, once again, huge investments are needed. Indeed, the economic attractiveness of such systems is related to the linear density of the energy demand and to the fact that the majority of the energy available for heating and cooling purposes is currently used. Calise et al. (Calise *et al.*, 2016) studied an innovative poly-generation system powered by solar and geothermal sources on Pantelleria Island. The described plant is able to

cover the electricity and the heat demands of a small community, as well as to simultaneously cover the freshwater demand of the island. In another work, Calise et al. (Calise *et al.*, 2017) investigated the possibility of integrating energy and water supply systems so that excess wind power production could be used in desalination units to supply the freshwater demand on Cape Verde Island. The main idea was to use desalinated water in a pumped hydro system to store the extra produced power from wind and to fulfil the gap between intermittent RES production and the island energy demand.

In most cases renewable resources such as sun, wind, biomass, are available which can be exploited, representing an opportunity for more sustainable development of the current energy scenario. In this regard, Ciriminna et al. (Ciriminna *et al.*, 2016) identified some critical barriers against a significant penetration of renewable energy on Sicilian islands, which are mainly related to local regulations and landscape management that usually forbid RES large-scale plant installations. It was also observed that an interactive strengths, weaknesses, opportunities, and threats (SWOT) analysis on the energy system could contribute to a collective and social learning process facing institutional, organizational, or common problems that usually inhibit the application of sustainable strategies on small islands (Möller *et al.*, 2012). Even though RES large-scale plants could undergo economic and administrative barriers, retrofit actions at the building level could, in turn, be diffusively proposed. Indeed, it was largely proven that they could lead to a substantial reduction in the energy demand toward a Net Zero Energy Building target (Ferrari and Beccali, 2017). Moreover, the extensive use of renewable energy sources could strongly influence the load curve of the community, as demonstrated by Ilkan et al. (Ilkan, Erdil and Egelioglu, 2005) for the island of Northern Cyprus where the use of solar thermal water heaters was intensely encouraged by the local government, leading to a maximum yearly saving about 72 GWh (Zizzo *et al.*, 2017). Indeed, solar thermal technologies can be a very good solution to decrease the electricity demand by domestic hot water (Artur *et al.*, 2020), because a great amount of energy consumption also takes place during the operational period, in order to satisfy the demand for domestic hot water (DHW) (Picallo Perez, Sala and Hernández, 2020). Moreover, the use of active and smart systems at the building level, enabling the possibility of implementing demand-side management (DSM) policies, could be easily applied in a typical building on Lampedusa Island (Italy), controlling the effect of flexible electrical loads on the load curve of the island.

Grid flexibility has become a central theme in the technical and scientific community. Briefly, grid flexibility represents the grid's ability to quickly respond to any unexpected changes in loads or production. As the load is an unpredictable variable, the matching condition between production and consumption has always been respected by managing the power plants to always match the load, especially the one with the shorter response times. The advent of renewables, defined as non-programmable sources, has transferred part of the system’s unpredictability from consumption to production. Consequently, as

stated by Garcia D.A. et al (ENEA website, 2020), it was decided to also shift flexibility services to production creating the demand response concepts.

The exploitation of renewable energy sources (RES) in the islands, especially in the Italian ones, is less diffuse than on the mainland and is characterized by various issues. In this regard, it was considered interesting to analyse the application of solar plant solutions for DHW production in this context with higher uses of non-renewable energy for electricity generation.

The studies carried out relies on energy-retrofit strategies on Lampedusa Island (Italy, 35◦3005600 north (N) 12◦3402300 east (E), 568 degree-days). Lampedusa is one of the Italian small islands not connected to the mainland electric grid, for which the Italian Government established financial support to avoid a local inhabitant fee for extra costs in electricity production, according to a social equity principle. In 2017, the government introduced a legislative decree aimed at financing different energy-retrofit strategies, including the installation of solar thermal plants or heat pumps for domestic hot water (DHW) production. The general goal for Lampedusa Island by 2030 is to reduce the yearly electricity consumption by up to 37,660.0 MWh via installing photovoltaic plants with overall 2140.0-kW peak power and via installing 2370 m^2 of solar thermal collectors. It is necessary to carefully investigate the best integration patterns for having an optimal system implementation together with suitable operation strategies (Majidi, Mohammadi-Ivatloo and Anvari-Moghaddam, 2019) and to compare alternative systems for the optimization of plants (Beccali *et al.*, 2014) both in economic and environmental terms (Vega and Cuevas, 2020). Several authors, such as , Guarracino et al. (Guarracino *et al.*, 2016), highlighted the importance of using real input data at high resolution for a correct estimation of the yearly and monthly performance of the system, as opposed to averaged data. This could be very important, especially if a novel control strategy that can adjust the system's outputs in response to varying demands has to be designed.

Among flexible loads, the one most influencing the peak and the energy consumption of a typical house in Lampedusa is the electrical storage water heater (ESWH).

It is then reasonable to suppose that better results could be achieved if both strategies (use of RES source with high efficiency of water heater and demand response strategies) were applied.

According to this legislative panorama and the state of art, the impact of the substitution of existing electric storage water heaters (ESWH) with dedicated HPWH, eventually coupled to a photovoltaic (PV) plant, a solar thermal plant (ST), or a solely ST system was analysed. The goal is to evaluate how thermal and electrical storage could interact with each other while exploiting renewable energy sources and guaranteeing DHW supply at a proper water temperature and to evaluate the technical and economic performances of these alternative systems exploiting renewable energy for domestic hot water production.

Furthermore, an alternative scenario was examined where the existing ESWH is substituted with the DHW production system described in chapter 4, considering, in

particular, the configuration_2 where the HPWH is coupled to a 6 PV/T panels system. The effectiveness of this retrofit solution is analysed by using the energy and operational indices introduced in chapter 5 appropriately adjusted for the context of the minor island of Lampedusa (Sicily, Italy).
The chapter is organized as follows: Section 6.1 shows the methods applied to conduct the work, describes the simulated systems and the models, and defines the domestic hot water tapping profiles; Section 6.2 presents the results and, in particular, the performances of the heat pump, the conventional electric heater, and the photovoltaic-assisted systems, along with a description of the solar thermal-assisted water heaters and an economic analysis.

6.1. Methods

TRNSYS simulations have been performed based on an hourly weather database from Meteonorm software and on the DHW demand input inferred by a monitoring campaign on some residential consumer units (users) in Lampedusa. Two users in Lampedusa were chosen as representatives with respect to statistical data. They are both families made up of two components living in a typical residential home on the island (120 m^2). The experimental campaign, as well as data processing, was carried out by researchers from the University of Palermo and the National Agency for New Technologies, Energy and Sustainable Economic Development (ENEA) involved in the project. Data were acquired with a 10-min time-step. To obtain reliable data via simulation, a 10-min time-step was chosen, and results were then processed on hourly, daily, and monthly basis. In this study, the operation and the efficiency of a set of systems for DHW production were determined through dynamic simulation models using the TRNSYS 17 platform (‘TRNsys Simulation Software’, 2019). In order to appreciate the interactions with electrical grids and to test time-shifting actions that can be implemented, an analysis on a short time scale (minutes) was conducted. A preliminary task was to correctly identify the typical DHW consumption hourly profile (tapping) and the volume of the daily-consumed DHW via a representative final user on Lampedusa Island. These values (hourly tapping profile and DHW demand per day) depend on the number of persons in the consumer unit and on their habits. Moreover, the use of hot water is influenced by seasonal fluctuations due to climatic conditions. The method is based on data extracted from the observations of a representative consumer unit during an experimental campaign. In addition, statistical data on population and housing in Lampedusa and the results of previous studies (ENEA—Italian Minister of Economic Development, 2016) (ENEA—Italian Minister of Economic Development, 2017) were considered. According to the last population census, most families in Lampedusa are formed of two or three people (about 42%). Through a survey, presented in previous studies (Beccali, Bonomolo, *et al.*, 2017), it was verified that the most widespread DHW production plant is an 80-L ESWH equipped with a 1200-W electric resistance. Moreover, due to

the touristic vocation of the island, the number of people living in apartment units varies from two in the winter to three in the summer. In order to identify the average daily DHW consumption, the monitored data of energy consumption in the most critical seasons (EDHW) were compared with those calculated using a TRNSYS model of the heater. Indeed, simulations were conducted by varying the hot water volume demand per day until energy consumption matched the averaged recorded data in the critical months. Maximum ($V_{DHW,max}$) and minimum DHW demand values ($V_{DHW,min}$) were respectively calculated in the winter and summer as follows:

$$V_{DHW,i} = f_{m,i} V_{DHW,\max} \ (L) \tag{6.1}$$

$$f_{m,i} = -\frac{n_i - n_{\max}}{n_{\max} - n_{\min}} (V_{DHW,\max} - V_{DHW,\min}) + V_{DHW,\max} \ (L) \tag{6.2}$$

where i is the generic number of the month in the year, n_{max} and n_{min} are respectively the months in which $V_{DHW,max}$ and $V_{DHW,min}$ values were recorded from the experimental campaign, and $f_{m,i}$ is a monthly correction factor. A linear trend was then used to extrapolate the daily DHW volume for the other months. In order to generalize results, hot water consumption per person per day was calculated. Similarly, the hourly frequency of on/off ESWH cycles was calculated from monitored data to build the hourly tapping profile as follows:

$$x_h = \frac{f_h}{f_{MAX}} \ (\%) \tag{6.3}$$

where x_h is an hourly factor for the $V_{DHW,i}$, f_h is the operation time of the ESWH, and f_{MAX} is the maximum frequency value in the day. Yearly energy consumption and temperature trends in the water storage were used to run the simulation models of possible retrofit options. Based on the actual DHW demand, remarks on plant sizing and service modes were made using simulations in real operating conditions. In order to evaluate the role of thermal storage for the best exploitation of solar energy while ensuring comfort conditions, we introduced three indices.
They were utilized for a first sizing of the proposed plants and can be calculated as follows:

$$DI = 1 - \sum_{i=1}^{h} \frac{n.hour_{T\_DHW\,40}}{n.hour_{tot\_1}} \ (\%) \tag{6.4}$$

$$PDI = \sum_{i=1}^{h} \frac{n.hour_{T\_DHW\,40}}{n.hour_{tot\_2}} \ (\%) \tag{6.5}$$

$$SPI = \sum_{i=1}^{h} \frac{n.hour : (T_{DHW} < T_{set})}{n.hour} \ (\%) \tag{6.6}$$

where T_{DHW} is the outlet tank temperature, $n.hour_{T\_DHW40}$ is the number of hours when the outlet tank temperature is 40 ◦C, $n.hour_{tot\_1}$. is the number of hours for which $m_{DHW} > 0$, and T_{set} is the setpoint temperature. Additionally, the discomfort index (DI) and the potential discomfort index (PDI) (Beccali *et al.*, 2019) were introduced in order to check how many hours in a given period (month, year) the outlet tank temperature (T_{DHW}) dropped to a minimum comfort temperature (T_{DHW}.-comfort = 40 ◦C) during tapping events (number of hours, $n.hour_{tot\_1}$, for which $m_{DHW} > 0$) and no-tapping events (number of hours, $n.hour_{tot\_2}$, for which $m_{DHW} = 0$). The setpoint index (SPI) allows quantifying how many times in a detected period ($n.hour$) the tank temperature goes below the desired setpoint value (T_{set}). Furthermore, three additional indices (Dakkak *et al.*, 2003), (Sigarchian, Malmquist and Fransson, 2014) were calculated to measure the electric storage and evaluate its behavior. In particular, the average fractional state of charge (F_{SOCav}) is equal to the ratio between the mean values of charge in a defined period ($E_{battery.av}$) and its nominal capacity ($E_{battery.max}$). The electric storage index (ESI) quantifies how many times in a detected period that the charge in the battery (SOC) drops to a minimum value (SOC_{min}) or overcomes a maximum threshold. The first was set equal to the HPWH daily consumption (BI_{min}), while the second was assumed to be equal to its nominal capacity. They can be calculated using the following formulas:

$$FSOC_{av} = \frac{E_{battery,av}}{E_{battery,\max}} \ (\%) \tag{6.7}$$

$$ESI_{\min} = \sum_{i=1}^{h} \frac{n.hour : (SOC_h < SOC_{\min})}{n.hour} \ (\%) \tag{6.8}$$

$$ESI_{MAX} = \sum_{i=1}^{h} \frac{n.hour : (SOC_h < SOC_{MAX})}{n.hour} \ (\%) \tag{6.9}$$

where $E_{battery.av}$ is the mean value of charge in a defined period, $E_{battery.max}$ is the nominal capacity, SOC is the state of charge in the battery, SOC_{min} is the minimum allowed value of the state of charge in the battery, SOC_{MAX} is the maximum value of the state of charge in the battery, and SOC_h is the calculated state of charge in the battery in a specified time-step.

Finally, two financial indices were further introduced and calculated for the studied systems. They are the net present value (NPV) and the simple payback time (SPT)

$$NPV = -C_0 + \sum_{z=1}^{T_{eq}} \frac{R_z - M_z}{(1+i)^z} \ (€) \tag{6.10}$$

$$SPT = \frac{C_0}{R} \ (\text{year}) \tag{6.11}$$

where Co is the initial cost, including purchase and installation costs, T_{eq} is the equivalent time, R_z is the economic saving concerning the current DHW production

system, and M_z is the maintenance cost of the retrofit plant. The above-described methodology is represented in Figure 6.1.

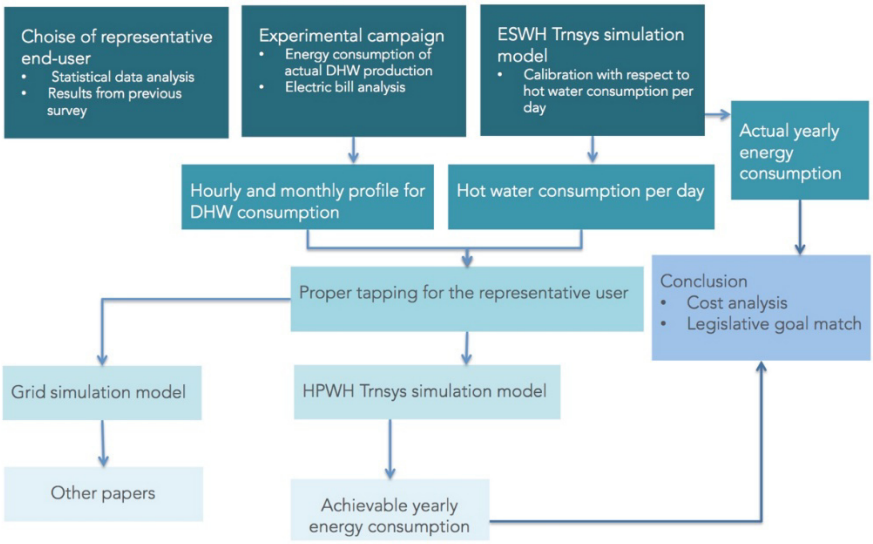

Figure 6.1. Workflow of the presented work.

6.1.1 Simulated Systems

Four different combinations of plants for DHW production were considered as alternatives to the standard ESWH (Figure 6.2). The following categories of technologies, currently available on the marketplace, were selected:

• System 1, heat pump water heater connected to the grid;

• System 2, heat pump water heater coupled with PV plant;

• System 3, heat pump water heater coupled with ST collector;

• System 4, solar thermal plant.

Moreover, to further investigate the performance of PV-assisted HPWHs, two different sizes of System 2, operating in stand-alone mode, were simulated. In particular, the so-called system 2.1 was characterized by a peak power of 720 Wp, while system 2.2 was characterized by a power of 1200 Wp. Solutions 2.1a and 2.2a, as well as 2.1b and 2.2b, share the same battery set-up, i.e., 2400 and 4800 Wh, respectively. The stand-alone plants were analyzed in order to verify how the electrical storage size influences the overall system performance while ensuring comfort conditions and the energy-saving goal. The electrical storage was sized based on the worst working conditions for the overall plant, i.e., the day with the highest daily consumption and lowest solar irradiation. In addition, electrical consumption of 1200 Wh for the HPWH was assumed. Electrical storage was supposed to be able to ensure two and four days of autonomy (N_{aut}). The two selected solutions (2400 and 4800 Wh) were applied to both

stand-alone configurations. They were named system 2.1a, system 2.1b, system 2.2a, and system 2.2b. Additionally, a grid-connected plant (system 2.5) was investigated. System 2.5 was sized in order to meet the yearly consumption of the HPWH without accounting for contemporaneity issues between load and production. In that way, the overall yearly energy balance between produced and consumed energy was set to zero. Furthermore, the HPWH could be considered to virtually consume only the renewable energy generated by the PV, using the electrical grid as virtual electric storage.

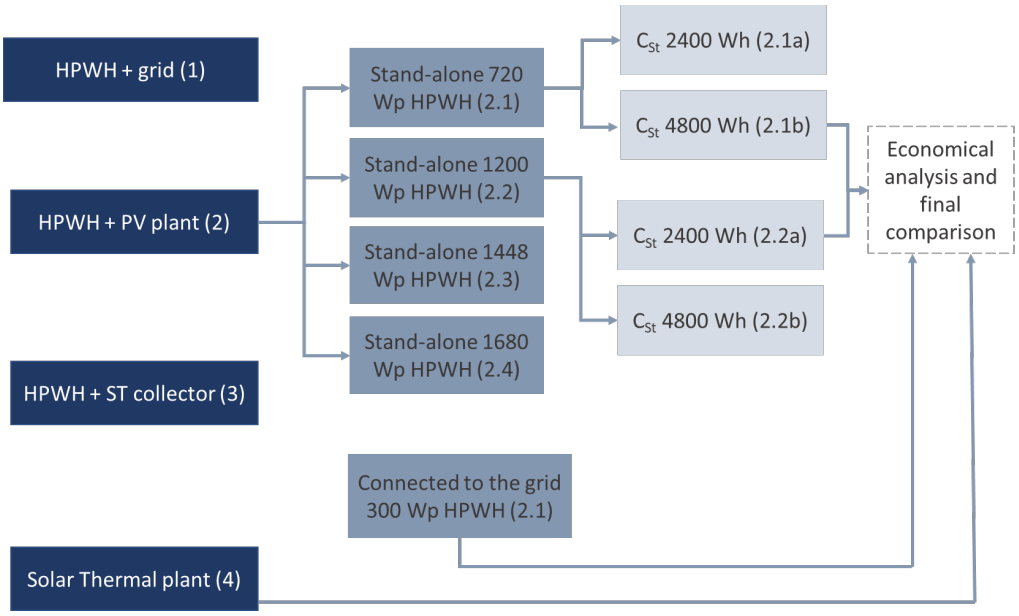

Figure 6.2. Scheme of the simulated plants.

6.1.2 Simulation Models

The HPWH considered for systems 1, 2, and 3 was an all-in-one air-to-water device. This kind of system uses its DHW tank as a hot sink and includes two wrap-around heat exchangers. The first one is used as a condenser in the heat pump cycle, while the other is suitable for connecting additional heat sources. The main features of the HPWH are listed in Table 6.1. These data refer to the standard UNI EN 16147:2011 (UNI EN 16147, 2017) that introduced two testing cycles. Both tests rely on a heating cycle aimed at warming water from 10 °C to 55 °C. In the first test, inlet air temperature and humidity were fixed at 7 °C and 89%, respectively (cycle A7/W10-55), while the second test relied on inlet air temperature at 15 °C and relative humidity at 74% (cycle A15/W10-55). The HPWH model was run in stationary conditions with an input according to EN 16147:2011.

For simulating the described HPWH, a specific model based on the combined use of two available types 938 and 1237 was developed. In particular, type 938 (Amirirad *et al.*, 2018) was used for performing the air-to-water heat pump cycle obtaining the heat delivered to the water sink (Q-to-water) at a given time step (15 min). Q-to-water was

used as input in type 1237 (Panagiotidou, Aye and Rismanchi, 2020) to evaluate the water tank temperature at the specific tapping condition. The water temperature was used as input in type 938 with the tank as the heat sink of the HP. The refrigerant flow rate was evaluated as a function of Q-to-water, forcing a temperature difference between the inlet/outlet of the fluid equal to 5 ◦C in each time-step. The proposed model was run at the nominal condition described in EN-16147:2011 (A15/W10-55 and A7/W10-55 cycles). It was validated through the comparison of figures of energy consumption, coefficient of performance (COP), and warm-up time reported in the technical data sheet, obtaining relative errors below 10%. Figure 6.3 shows the simulation model scheme.

Table 6.1. Heat pump water heater (HPWH) features from the technical datasheet. DHW—domestic hot water.

Features		
Heating with heat pump, maximum temperature	65	°C
Warm-up time at chosen cycle A15/W10-55(*)	5:17	h:min
Warm-up time at chosen cycle A7/W10-55(*)	6:10	h:min
Energy consumption by chosen cycle A15/W10-55	3.95	kWh
Energy consumption by chosen cycle A7/W10-55	4.05	kWh
COPDHW A15/W10-55	3.07	-
COPDHW A7/W10-55	3.00	-
Maximum power consumption with heat pump	490	W
Back-up electric resistance heater power	2000	W
Nominal air-flow rate	480	m^3h^{-1}
Volume	200	litres
Maximum tank temperature with electric resistance	90	°C
U-Value of the DHW tank shell	0.9	$W(m^2K)^{-1}$

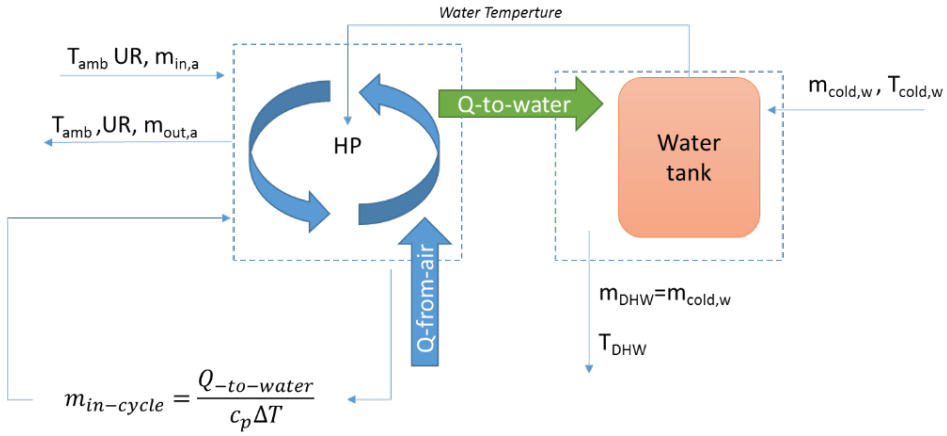

Figure 6.3. HPWH simulation model.

As previously mentioned, System 2 was modeled to test how thermal and electrical storage could interact with each other for achieving the maximum energy (electricity) saving target by ensuring comfort conditions and by exploiting the solar radiation source as much as possible. For this reason, three different PV plants were supposedly based on the results of the HPWH simulation: two stand-alone (SA) systems, characterized by two different rated peak powers, and a grid-connected system. The PV panel component system characteristics are presented in more detail in the next paragraph, while component features are listed in tables 6.2 and 6.3.

Table 6.2. Photovoltaic (PV) panel features by the technical datasheet. GC—grid-connected; SA—stand-alone.

PV plant	PV	η	Pmp (W)	Vmp (V)	Imp (A)	A (m^2)
GC	Mono-crystalline	15.4%	300	37.6	8	1.9
SA	Mono-crystalline	15.4%	240	30.8	8	1.6

For the systems based on combination with solar thermal collectors (3 and 4), different configurations were supposed. First of all, the main solar thermal component consisted of a flat-plate collector with highly selective surface properties (efficiency parameters are listed in Table 6.3). Furthermore, we considered a forced circulation water loop scheme, driven by a 50-W pump. System 4 is a solar thermal plant with a conventional electric heater as backup. System 3 includes a solar thermal system coupled with an HPWH. In the latter case, the ST system was connected with a second wrap-around heat exchanger present in the HPWH tank.

Table 6.3. PV panel and solar thermal plant (ST) collector features by the technical datasheet.

PV-Technology	η	Pmp (W)	Vmp (V)	Imp (A)	A (m^2)
Mono-crystalline	15.4%	300	37.6	8	1.9
Mono-crystalline	15.4%	240	30.8	8	1.6
ST technology	**η**	**a1 ($W(m^2K)^{-1}$)**	**a2 ($W(mK)^{-2}$)**	**A (m^2)**	**-**
Flat plate collector	0.76	3.48	0.016	2.2	-

In order to compare the analysed systems, the same tapping profile and thermal storage characteristics (200 L DHW tanks equipped with a 2000 W backup electric heater) were adopted for all case studies. The DHW tank was simulated using the Trnsys type 1237 (‘TRNsys Simulation Software’, 2019). Such storage is suitable to be connected with different energy sources and includes a wrap-around HX calculation algorithm, appropriate for different alternative generation sources (Figure 6.4). Furthermore, the same components and types were used for all the simulated models. Daily and monthly schedules were applied for determining the hourly tapping input as inferred from the monitored data. As mentioned before, to assess the seasonal fluctuation of DHW thermal energy demand due to climate conditions, the calculated water temperature in the tank was set as input for the thermostat cut-off. Inlet water temperature from the

public water network was set equal to the ground temperature at 2 m depth by using type 77 ('TRNsys Simulation Software', 2019). In systems 1, 2, and 3, the boiler setpoint temperature was based only on HPWH constraints (Table 6.1) and was fixed at 63 ± 2 ◦C. On the other hand, in system 4, whenever a useful solar contribution was available from the collector loop, the temperature in the boiler was allowed to rise to the maximum value (see Table 6.1) (88 ± 2 ◦C); otherwise, it was set according to the HPWH limits. The aim was to exploit the water tank as much as possible for the storage of the available solar thermal source. The overall logical scheme of simulations is depicted in Figure 6.4.

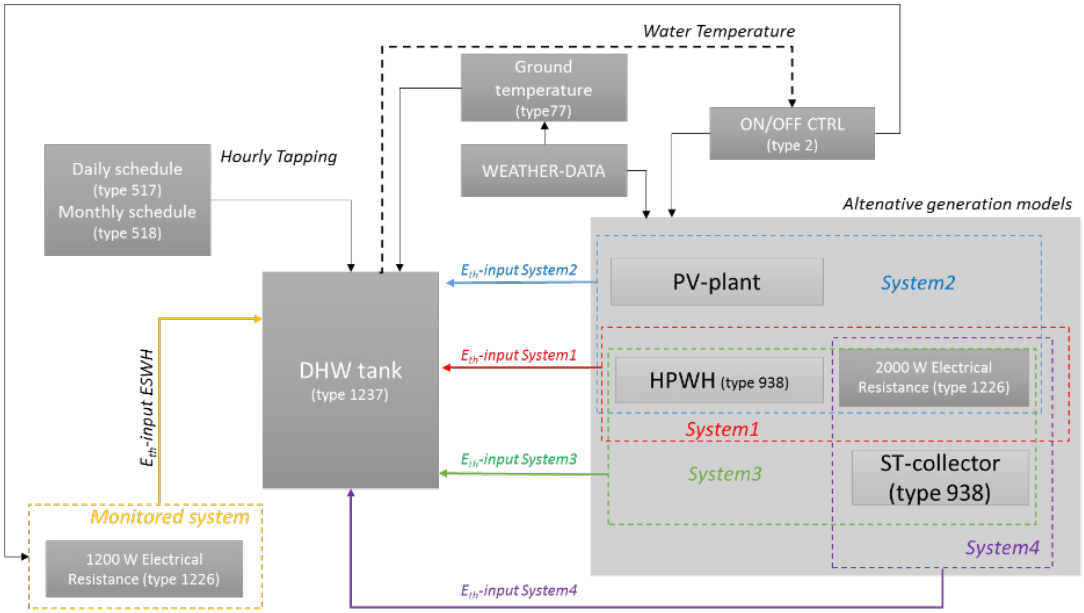

Figure 6.4. TRNSYS model scheme.

Analyses were performed on yearly and monthly basis and for a typical day per month, which was selected according to the median daily irradiation values on a horizontal surface (Figure 6.5). In fact, all the solar collectors were considered with a horizontal tilt angle to fulfil building integration and landscape protection constraints.

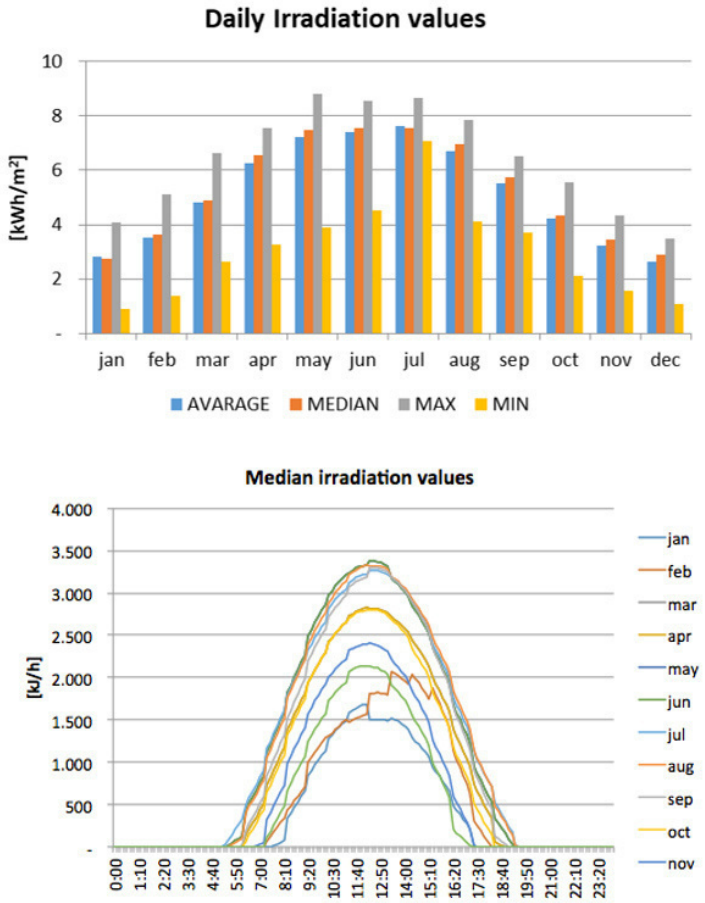

Figure 6.5. Analysis of specific horizontal irradiation values on Lampedusa Island, Italy (35°30′56″ north (N)).

6.1.3. Empirical Definition of Domestic Hot Water Tapping Profiles

Figure 6.6 shows the average daily energy consumption month by month calculated from monitored data for two users equipped with a conventional ESWH system. It is worth noting that, even if different magnitudes of values were observed, monthly data regarding the two detected users had similar decreasing trends from February until July/August. Furthermore, data for September are probably affected by the presence of a larger number of persons in the residential units.

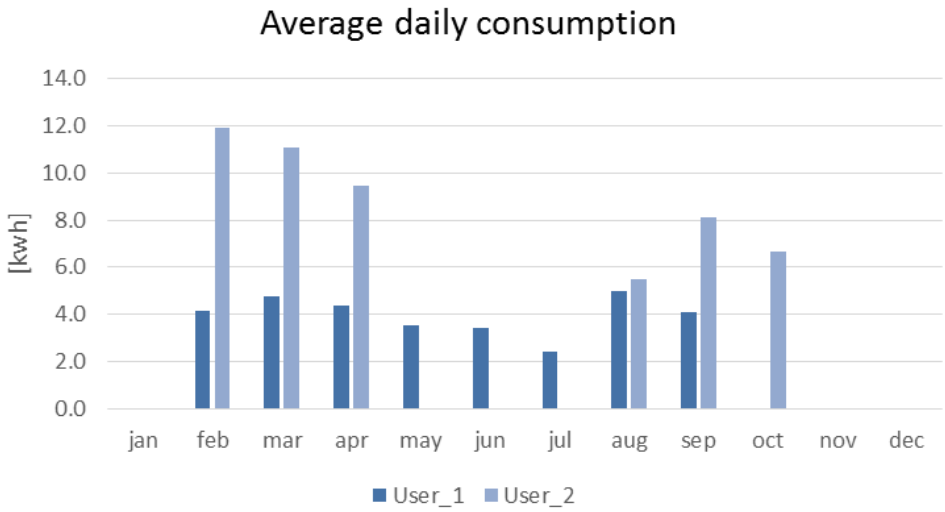

Figure 6.6. Monitored data.

Data were processed for determining the frequency of operation of the ESWH system during a typical tapping event. Moreover, to obtain the most consistent tapping profile, hourly frequencies when the power values were below the daily median were excluded. Figure 6.7 shows results in terms of percentage by hour the ESWH was "switched on" with respect to monitored data and the introduced constraints (Figure 6.7).

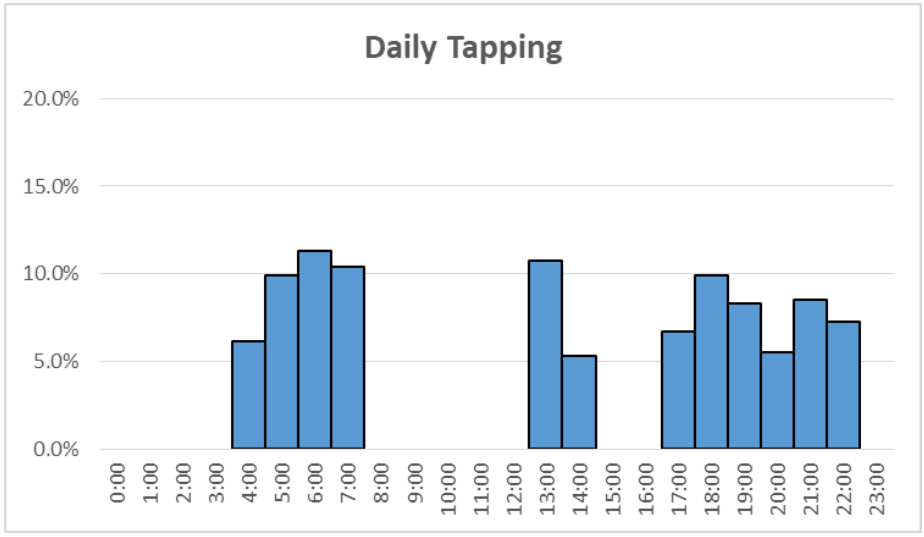

Figure 6.7. Daily tapping profile.

A TRNSYS calibration routine was carried out to fit the experimental data with calculations. The model was run, introducing the tapping profile as hourly input. Daily water consumption at 40 ◦C (input) was varied until the simulated monthly energy consumption (output) matched the recorded figures with a relative error below 5%. The hot water consumption for the monitored consumer units varied from 90 L per day in February to 45 L per day in July (user 1) and from 180 L per day in February to 120 L

per day in September (user 2). Average values between users were successively applied for determining a common linear monthly trend. This was calculated according to Equation (2) in order to obtain the monthly correction factor ($f_{m,i}$) (Figure 6.8).

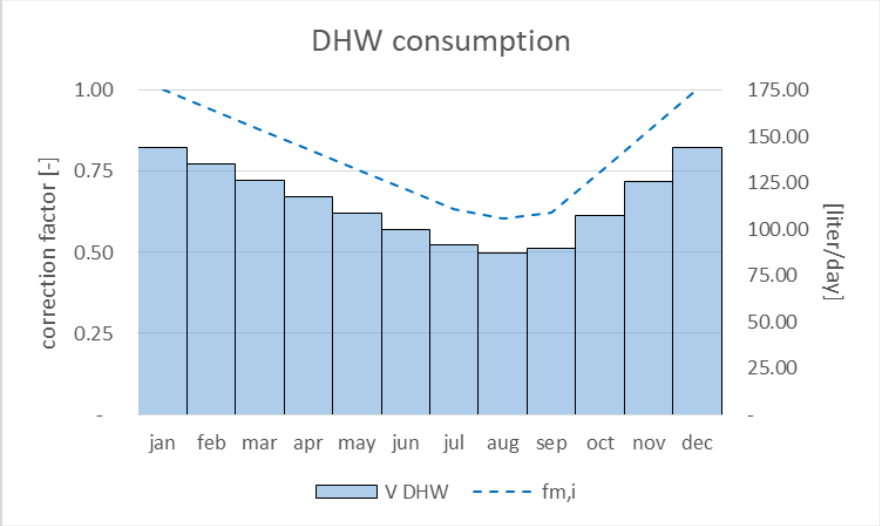

Figure 6.8. DHW consumption per day at 40 °C for analysed consumer residential unit.

6.2 Results

6.2.1 Analysis of Heat Pump Water Heater Performance

Comparing the simulation results and reference values of the technical datasheet, the relative error below 5% were obtained. COP was calculated according to international standard procedures. As suggested by EN 16147:2017 (UNI EN 16147, 2017), an error below 10% for the energy consumption in both warming-up cycles was obtained. These results demonstrated a good accuracy of the model. As described in Section 6.2, before analysing the proposed systems, an ordinary ESWH was also simulated to obtain electricity consumption reference values of 1137 kWh per year with monthly values varying from 125 kWh in August for the tapping profile adopted. The simulated results for system 1 were compared with those of ESWH (Figure 6.9).

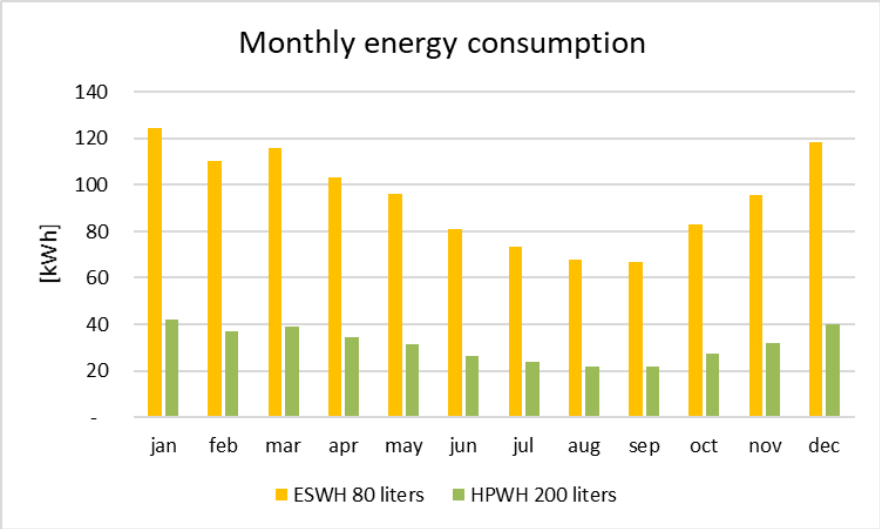

Figure 6.9. Comparison between electrical storage water heater (ESWH) and HPWH energy consumption.

It is worth noting that, through the replacement of the conventional system with a heat pump, an average electrical energy saving equal to 65% could be achieved. This is consistent with the rated COP and the higher available storage capacity due to the higher DHW tank volume of the heat pump system. In particular, yearly energy consumption was reduced from 1137 to 375 kWh, avoiding 761 kWh electricity withdrawals from the local grid. It is worth noting that, according to the technical datasheet, the considered HPWH was able to match the thermal demand of the so-called "L" tapping profile (EN 12831-3, 2017). Therefore, it could deliver up to 11.66 kWh of thermal energy per day (Istat website, 2020). Results from simulations presented in previous works (Beccali, Bonomolo, *et al.*, 2017), (ENEA—Italian Minister of Economic Development, 2016), (ENEA—Italian Minister of Economic Development, 2017) show that, in the worst case (which corresponds to January), the average thermal demand can be about 4.1 kWh of thermal energy per day.

6.2.2. Analysis of Stand-Alone Photovoltaic Systems

According to the present work purposes, four stand-alone configurations (HPWH (2.1), (2.2), (2.3), and (2.4)) were considered to outline electrical storage behaviour. Preliminary simulations were useful for determining PV plant features to be tested. Looking at the results of simulations, January and December appear as the most critical months with average daily electrical consumption equal to 1.4 kWh per day (Figure 6.10).

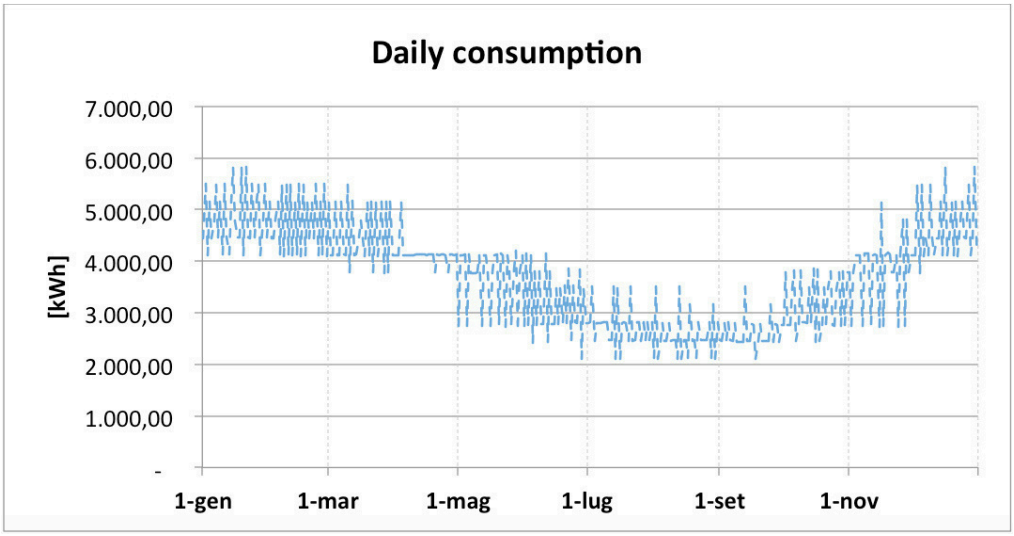

Figure 6.10 - Daily energy consumption for the system.

Moreover, the HPWH was switched on mainly in conjunction with tapping events in the early morning and the evening. As mentioned above, the median value of irradiation was calculated. Based on these data, a day for each month characterized by irradiation figures closest to the median was selected. For these 12 days (one per month), the daily frequency of on and off operation of the heat pump in the selected time range was evaluated. Figure 6.11 shows the percentage of time that the HPWH was "on" in an hour during the year for the adopted tapping profile.

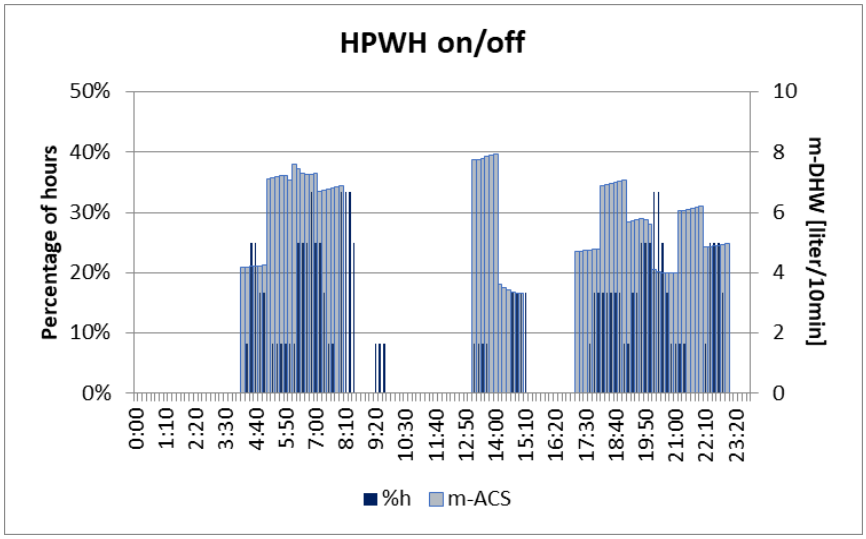

Figure 6.11. Percentage of time that the HPWH was "on" in an hour during the year with respect to the adopted tapping profile.

To check the thermal storage behaviour in operating conditions, further simulations were run. In this case, the energy produced by the PV plant was exclusively considered to drive the HP, without any electrical storage support. Whenever the temperature tank dropped to the setpoint value and, simultaneously, whenever the power from the PV

string was suitable to drive the cycle without relating to the electrical grid or battery, the model allowed the switching on of the HPWH. As described above, four different PV plant sizes were considered: 720 Wp, 1200 Wp, 1440 Wp, and 1680 Wp. They correspond to three, five, six, and seven PV panels, respectively. Table 6.4 shows the plant configuration with respect to the following features: number of days of autonomy (N_{aut}) for stand-alone (SA) plants, inverter (P_{Inv}) and plant power (PPV), battery capacity (C_{St}), and number of PV panels, for which characteristics could be inferred from Tables 6.2 and 6.3. It can be noted that systems 2.3 and 2.4 were definitively oversized in order to use them as comparison terms with respect to system 2.1 and system 2.2 considering that no battery storage is available. In Table 6.4, the characteristics of the four selected PV plants (systems 2.1, 2.2, 2.3. and 2.4) are listed. The last two plants were definitely oversized to use them as comparison terms.

Table 6.4. PV plant features.

PV plant	Type; Naut	Pinv (W)	PPV (Wp)	CSt (Wh)	No. of panels	Ppanel (Wp)
System 2.1	SA; 2-4	1500	720	2400(a)/4800(b)	3	240
System 2.2	SA; 2-4	750	1200	2400(a)/4800(b)	5	240
System 2.3	SA; 0	1500	1440	0	6	240
System 2.4	SA;0	2000	1680	0	7	240
System 2.5	GC	750	300	0	1	300

It is possible to see in Figure 6.12 that all plant configurations could match the summer DHW demand (from May until October) without discomfort events (monthly DI and PDI equal to 0%); moreover, as seen by looking at the irradiance value (Figure 6.5 in Section 6.2) and the adopted tapping profile (Figures 6.7 and 6.8 in Section 6.1), winter months appeared the most critical. The next step was to calculate the discomfort indices DI and PDI (Figure 6.12).

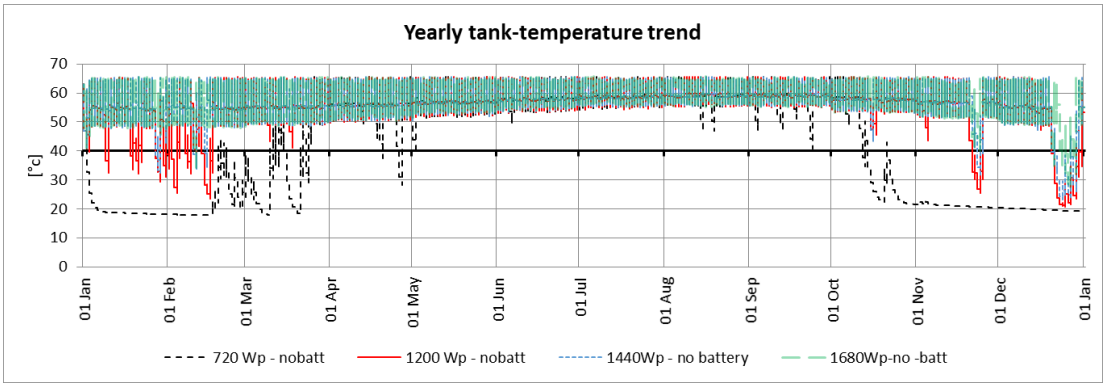

Figure 6.12. Temperature trend with reference to comfort limit.

As in this case, the most critical results were recorded in December for the 720-Wp plant (system 2.1) because of the small size of PV generator compared to the HP

nominal power and to the low values of irradiation. A higher PV plant power obviously leads to better results (Figure 6.13).

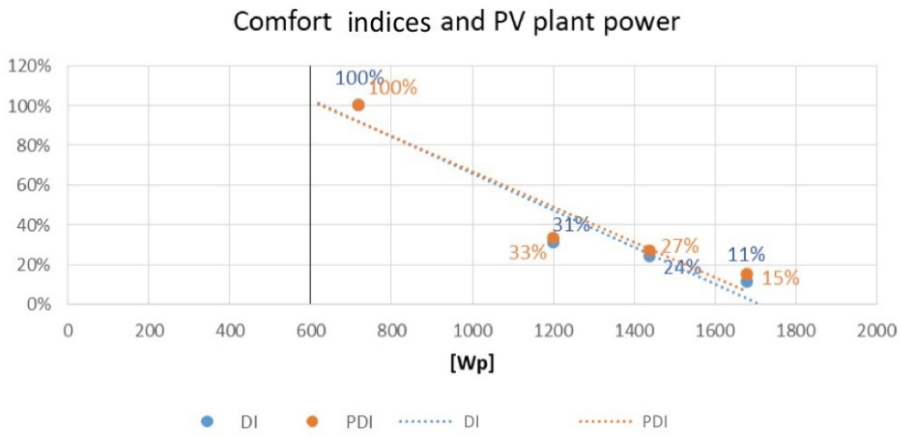

Figure 6.13. Yearly comfort indices for the tested PV plants.

Nevertheless, an auxiliary electrical load would be necessary to avoid oversizing of the PV respect to the HPWH nominal power. In any case, using the plant characterized by a power of 1200 Wp (system 2.2), the contemporaneity between the energy needed for DHW production and PV useful production reached values higher than 90% (Figure 6.14).

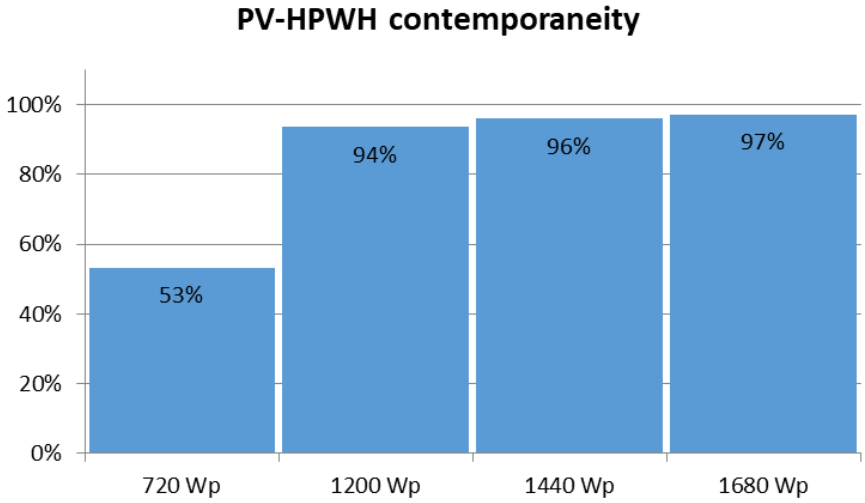

Figure 6.14. Contemporaneity between DHW production load and PV useful production.

Figure 6.15 shows the results obtained for discomfort and storage indices in the most critical month (December) for the SA systems.

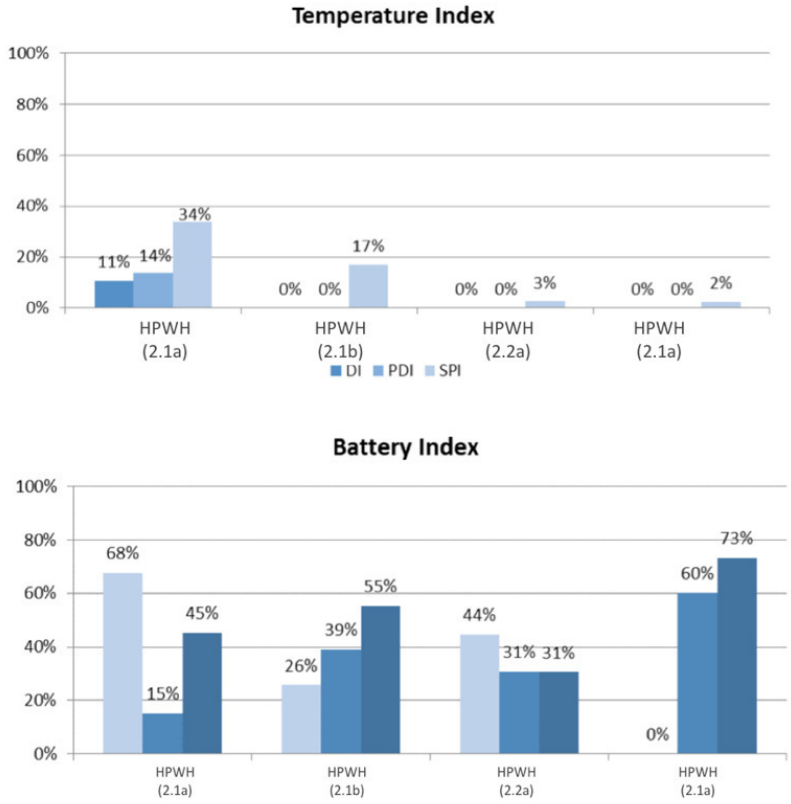

Figure 6.15. Temperature and battery indices.

It is worth noting that, except for the HPWH + ST (2.1a) systems, all other SA systems with PV plants allowed satisfying comfort conditions, with PDI and DI indices equal to 0%. This means that tank temperature never dropped below the 40 ◦C comfort limits. On the other hand, only the 1200-Wp plants were almost suitable to preserve the temperature as close as possible to the setpoint one. Finally, focusing on the storage indices, some differences among analysed systems could be underlined (Figure 6.16).

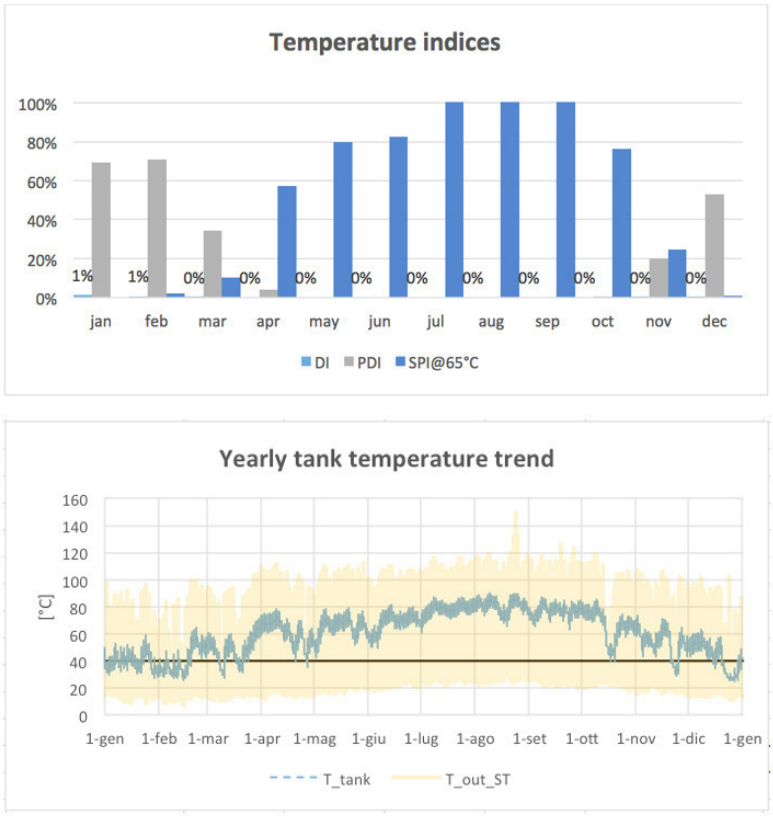

Figure 6.16. Temperature indices and storage temperatures for solar thermal systems without electric backup.

Remembering that the BI_{min} index was introduced to evaluate critical situations in which the state of charge drops to the minimum value (HPWH daily consumption), it can be noted that it varied from 68% for the HPWH + ST (2.2a) plant to 0% for the HPWH + ST (2.1b) one. Intermediate values, almost acceptable, were calculated for the HPWH + ST (2.1b) and HPWH + ST (2.2a) systems, with 26% and 44%, respectively. On the other hand, the BIMAX and $FSOC_{av}$ indicate how electric storage was exploited in the critical month. In this way, some oversizing conditions were highlighted for the HPWH + ST (2.2b) configuration (73%). Actually, a higher BI_{MAX} denotes a higher time when the state of charge is close to the battery nominal capacity, indicating that it was not properly used in the system. Summarizing from the present analysis, the HPWH + ST (2.2a) system had the worst performance because it weakly matched comfort requirements. On the other hand, the HPWH + ST (2.1b) system resulted to be oversized with respect to DHW load demand fulfilled by the HPWH. Finally, the GC (2.5) system accounted for a 300-Wp panel. The simulation results show that system 2.5 can annul the yearly consumption of non-renewable primary energy since the PV plant entirely produces the electricity required by the HPWH. Nonetheless, despite the peak power of the system is less than the power required by HPWH, all the produced energy is sold back to the utility. Economic consequences are investigated in Section 6.4.

6.2.3. Analysis of Solar Thermal System Assisted Water Heaters

As for the PV plant investigation, a preliminary check concerning the temperature indices related to the solar thermal systems was carried out without considering any backup. It is worth noting that, also in this case, during tapping events, the comfort conditions were generally ensured all year long (Figure 6.15), while potential discomfort conditions were recorded only in winter months. On the other hand, considering a setpoint temperature of 65 ◦C, it has to be noted that the SPI index had average yearly values of 53% while it reached 0% in the winter months. This means that the solar thermal system was not able to continuously ensure the setpoint temperature in the tank (Figure 6.15). Two alternative backup electrical-based systems were consequently introduced. Firstly, a typical 2-kW electrical resistance was provided in the tank (ST (4) system). Moreover, the previously studied heat pump water heater was coupled with a solar thermal loop (HPWH + ST (3)). Figure 6.17 shows the comparison between the electrical consumption results of the simple HPWH and the results for the ST (4) and HPWH + ST (3) systems. Taking as a reference the HPWH results, the ST (4) system led to an extra 4% energy consumption from the grid, while the HPWH + ST (3) system allowed 58% electrical saving. Regardless of the choice of electrical backup, the adoption of solar thermal collectors led to achieving tank temperatures generally included between 65 and 80 ◦C (SPI index in Figure 6.17 with yearly average figures of 70% and 11%).

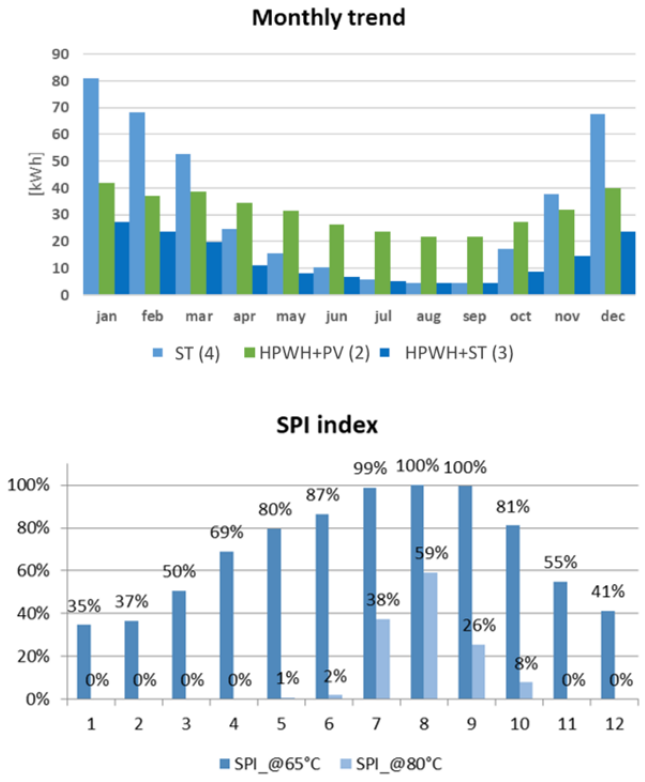

Figure 6.17. Top: electrical consumption of the systems; bottom: monthly setpoint index (SPI).

6.2.4. Economic Analysis and Comparison between Systems

The previous results demonstrated in which ways the selected plants could ensure comfort conditions while exploiting the thermal and/or electrical storage capacity of the systems. For the sake of clarity, the following systems were analysed:

• System (1), HPWH + grid: heat pump water heater without any RES plant assistance;

• System (2.1a), HPWH + PV, heat pump water heater with a PV plant having 2400 Wh storage capacity and 720 Wp

• System (2.2b), HPWH + PV, heat pump water heater with a PV plant having 2400 Wh storage capacity and 1200 Wp

• System (2.5), HPWH + GC PV, heat pump water heater with a 300-Wp PV plant directly connected to the grid;

• System (3), HPWH + ST: heat pump water heater coupled with a solar thermal plant

• System (4), ST plant: commercial solar thermal plant relying on a solar thermal collector with an electrical resistance back-up and DHW tank

Systems HPWH (2.1b) and HPWH (2.2a) were "discarded" because the sizing was not proper. From the energy-saving point of view, taking as a reference an ordinary ESWH system (with 1137 kWh electrical consumption per year), all plants achieved energy savings in a range from 100% for the PV plants to 86% for the HPWH + ST (3) system, with an average of 66.5% for the HPWH and ST (4) system (Figure 6.18).

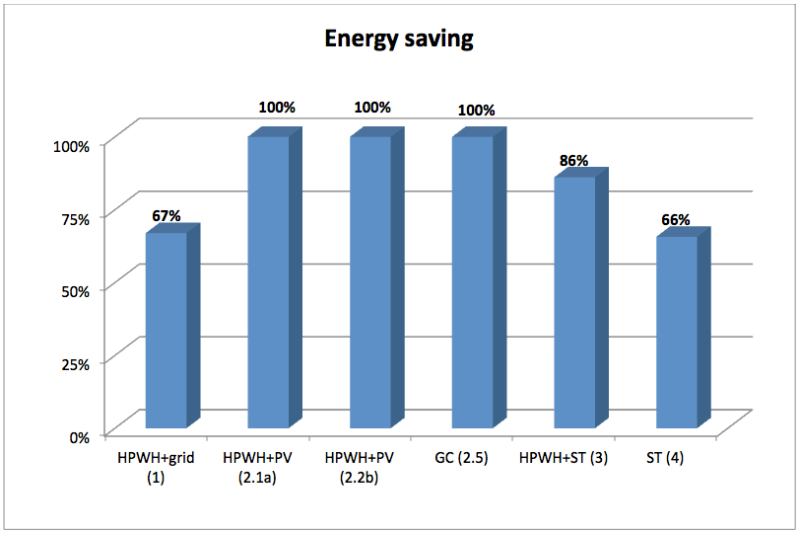

Figure 6.18. Comparison of the DHW energy saving.

Differences could be noted when looking at economic indices. In Figure 6.19 and Table 6.5, the calculated net present value and the payback time (PBT) for the proposed

systems are reported. System initial costs were estimated via an analysis of the Italian market (Minambiente website, 2016), (pti regione Sicilia Website, 2020). The average electricity cost from a user's bill was considered in the calculation (0.23 €/kWh), while the selling price for the produced electricity for the grid-connected PV plant was considered equal to 0.10 €/kWh. Furthermore an interest rate of 3% was assumed.

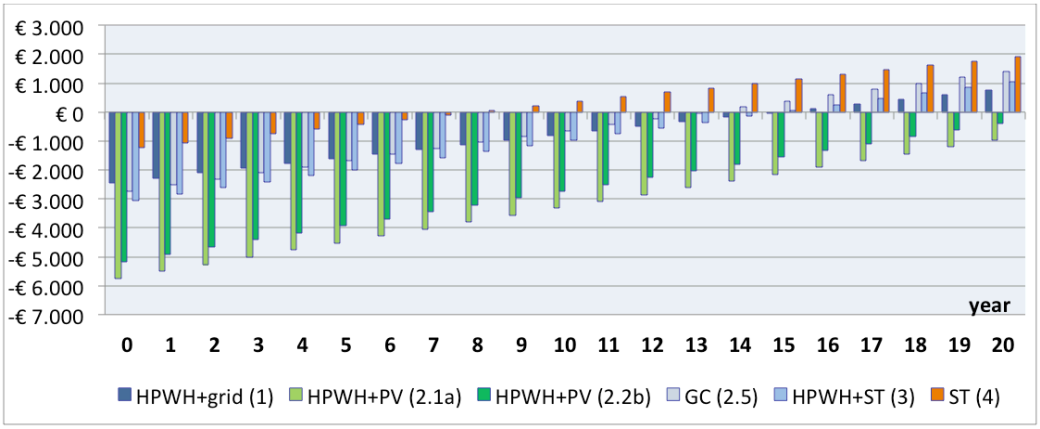

Figure 6.19. Cash flow and the net present value of selected solutions (without national incentive).

A 20-year useful lifetime was assumed for all the plants. First of all, it can be noted that, if no public subsidy is considered, stand-alone PV plants show a negative cash-flow rate, with a consequently negative NPV (Figure 6.19). At the same time, these systems present the worst payback time, higher than 21 years. On the other hand, all other systems present positive NPV varying from 760 € for the HPWH system to 1902 € for the solar thermal plant with electric back-up. ST (4) and HPWH + grid (1) systems, despite similar energy-saving values, strongly differ in NPV and PBT, with the latter having the lowest value, i.e., half of the first. Finally, low differences could be noted in all figures between the GC (2.5) and ST (4) plants.

Table 6.5 Payback time and net present value (without national incentive).

	HPWH + grid	**HPWH (2.1a)**	**HPWH (2.1b)**	**GC (2.5)**	**HPWH (3)**	**ST (4)**
PBT (years)	15.2	24.1	21.6	13.1	14.7	7.6
NPV (€)	769	-974	-384	1.405	1065	1902

The Italian incentive mechanism for such a system allows for some reduction in the purchase price for plant components to be distributed in 10 yearly payments. Incentive values vary from 50% to 65% for PV components and ST and HPWH components, respectively. Under such circumstances, all systems have a positive net present value estimated at 20 years (Figure 6.20).

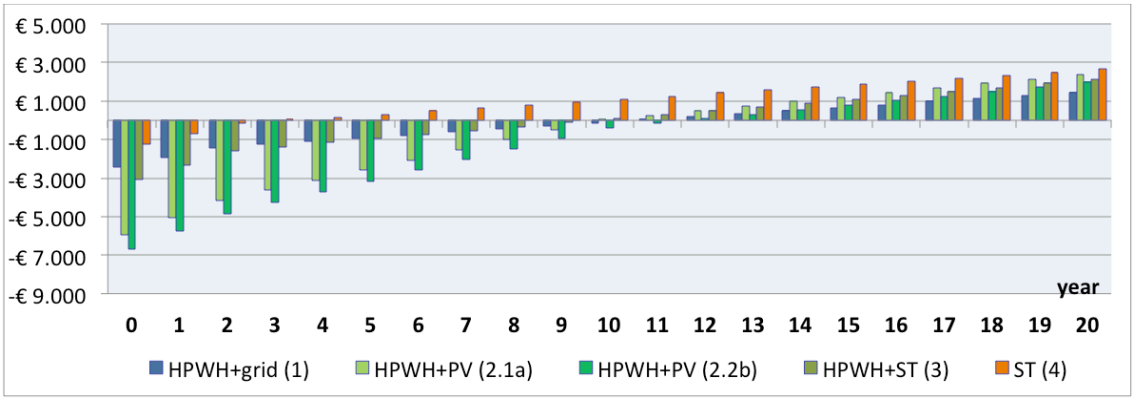

Figure 6.20. Cash flow and the net present value of selected solutions (with national incentive).

The best NPV is associated with the HP coupled with a stand-alone PV system and a small battery (system HPWH (2.1b)) and the solar thermal-assisted HP (system HPWH + ST (3)). The shortest payback time was calculated for the solar thermal system (Table 6.6).

Table 6.6**.** Payback time and net present value (national incentive).

	HPWH + grid	**HPWH (2.1a)**	**HPWH (2.1b)**	**GC (2.5)**	**HPWH (3)**	**ST (4)**
PBT (years)	6.9	11.9	9.5	12.1	6.7	3.6
NPV (€)	2357.02	2280.30	3015.43	1620.35	3061.53	2719.03

6.2.5 Energy fluxes analysis and operational indices

In the previous chapter, energy, and operational indices were calculated assuming Italian national data for what concerns the primary energy conversion factor and the time-slot choices. To assess what happens in a small island context, different values for these parameters have to be applied. This is due to the different local energy mix for electricity generation and different time distribution of consumption, as outlined in (Beccali et al., 2017).
In order to assess a reliable primary energy conversion factor for the specific island energy context, considering that electricity is today produced exclusively by diesel generators, yearly electricity production data were considered and processed as follow:

$$\varepsilon_{NREN} = \frac{\sum_{n=1}^{12} E_p \cdot \eta_d}{\sum_{n=1}^{12} C_d LHV} \tag{6.12}$$

where E_p and C_d are, respectively, the electricity and the related diesel fuel consumed by the local distribution company every month, η_d is the distribution efficiency of the grid (supposed to be 0.75), while LHV is the lower heating value of the fuel (11.86 kWh/kg). The result is an ε_{NREN} equal to 3.43.

The PER indices and $f_{sav.NREN}$ were calculated considering data for the Pantelleria Island. Similarly, different timeslots for assessing τ_a operational index (called τ_d index for the island) were assumed: from 17:00 until 24:00 during weekdays (when the island load profile shows a peak demand that can be compensated by DR action). Table 6.7 and 6.8 report all the values of the energy and operational indices which change under the above-mentioned hypotheses for tapping #1 and tapping #7 respectively, while Figure 6.21 shows the self-consumption for configuration 2 for the two tapping profiles.

Table 6.7. Energy and operational indices results for tapping #1.

	HPWH+PVT			HPWH+PV			HPWH+ST		
	conf.1	conf.2	conf.3	conf.1	conf.2	conf.3	conf.1	conf.2	conf.3
PER_{NREN}	6.6	12	20.9	6.4	11.3	18.6	2.1	2.3	2.5
$f_{saveNREN}$	96%	98%	99%	96%	98%	99%	82%	84%	85%
τ_d	8%	3%	1%	8%	3%	1%	38%	33%	30%

Table 6.8. Energy and operational indices results for tapping #7.

	HPWH+PVT			HPWH+PV			HPWH+ST		
	conf.1	conf.2	conf.3	conf.1	conf.2	conf.3	conf.1	conf.2	conf.3
PER_{NREN}	9.6	17.2	30.3	9.5	17	29.3	3.7	4.5	5.1
SF_{el}	80%	91%	97%	80%	91%	97%	-	-	-
$f_{saveNREN}$	96%	98%	99%	96%	98%	99%	90%	92%	93%
τ_d	9%	4%	1%	10%	4%	1%	45%	40%	34%

Tables 6.7 and 6.8 do not report τ_b and τ_c because they remain the same since they are not affected by the hypotheses made to assess the island context.

In comparison with the results obtained for Palermo, since ε_{NREN} factor increases from 1.92 to 3.43, PER_{NREN} decreases for all the plants, due to the higher non-renewable contribution of the grid electricity consumption. Solar thermal systems present higher figures of potential primary energy saving ($f_{sav.NREN}$) in comparison to values referred to their operation when connected to the national grid.

As for Palermo results, in the case of small islands, τ_d, like τ_a, assumes extremely low values for all configurations with PV and PVT panels, and this confirms that the HPWH is not able to adequately support an aggregator for DR programs during the selected DR time slot (from 17:00 to 24:00) without detriment of the self-consumption of the system. Nevertheless, the situation changes in the case of HPWH with ST panels, since the same index is, for both tapping #1 and tapping #7 above 30%. Anyway, similar results can be found also for HPWH with ST on the mainland, therefore, it can conclude that, in general, configurations devoted to maximise self-consumption are not suitable for DR programs.

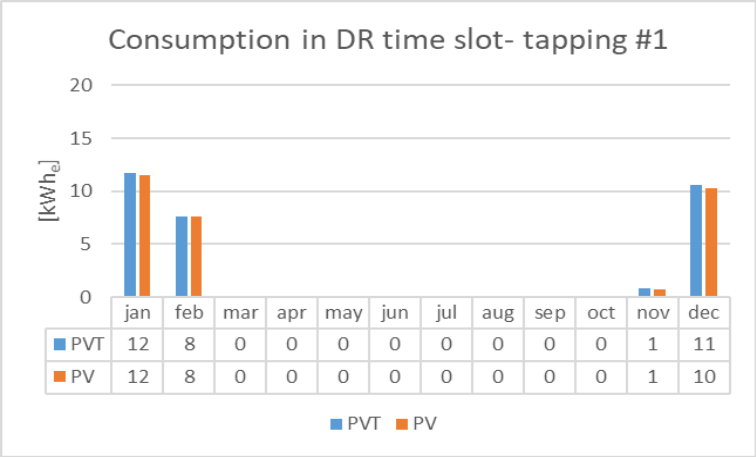

Figure 6.21. Monthly consumptions in the DR time slot for islands for configuration 2 and tapping #1.

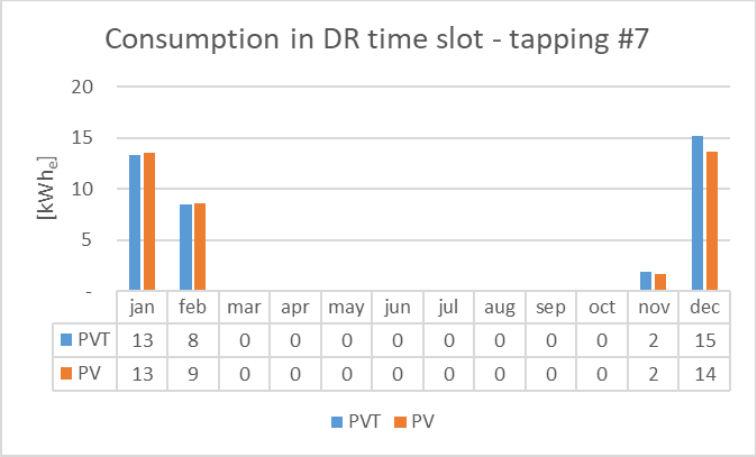

Figure 6.22. Monthly consumptions in the DR time slot for islands for configuration 2 and tapping #7.

References

Alves, M., Segurado, R. and Costa, M. (2020) 'On the road to 100% renewable energy systems in isolated islands', *Energy*, 198, p. 117321. doi: 10.1016/j.energy.2020.117321.

Amirirad, A. *et al.* (2018) 'Experimental and Simulation Studies on Air Source Heat Pump Water Heater for Year-round Applications in Canada', *Energy and Buildings*, 165. doi: 10.1016/j.enbuild.2018.01.052.

Artur, C. *et al.* (2020) 'Domestic hot water technology transition for solar thermal systems: An assessment for the urban areas of Maputo city, Mozambique', *Journal of Cleaner Production*, 260, p. 121043. doi: https://doi.org/10.1016/j.jclepro.2020.121043.

Beccali, M. *et al.* (2014) 'Life cycle performance assessment of small solar thermal cooling systems and conventional plants assisted with photovoltaics', *Solar Energy*, 104, pp. 93–102. doi: https://doi.org/10.1016/j.solener.2013.10.016.

Beccali, M., Ciulla, G., *et al.* (2017) 'Assessing the feasibility of cogeneration retrofit and district heating/cooling networks in small Italian islands', *Energy*, 141, pp. 2572–2586. doi: 10.1016/j.energy.2017.07.011.

Beccali, M., Bonomolo, M., *et al.* (2017) 'Characterization of a small Mediterranean island end-users' electricity consumption: The case of Lampedusa', *Sustainable Cities and Society*, 35(July), pp. 1–12. doi: 10.1016/j.scs.2017.07.015.

Beccali, M. *et al.* (2019) 'Alternative Energy Storage Options for Heat Pump Water Heater Coupled with Photovoltaic Plant for Domestic Hot Water Production', in, pp. 1–11. doi: 10.18086/swc.2019.24.01.

Bertheau, P. (2020) 'Assessing the impact of renewable energy on local development and the Sustainable Development Goals: Insights from a small Philippine island', *Technological Forecasting and Social Change*, 153, p. 119919. doi: https://doi.org/10.1016/j.techfore.2020.119919.

Calise, F. *et al.* (2016) 'A novel solar-geothermal trigeneration system integrating water desalination: Design, dynamic simulation and economic assessment', *Energy*, 115, pp. 1533–1547. doi: https://doi.org/10.1016/j.energy.2016.07.103.

Calise, F. *et al.* (2017) 'A novel hybrid polygeneration system supplying energy and desalinated water by renewable sources in Pantelleria Island', *Energy*, 137, pp. 1086–1106. doi: https://doi.org/10.1016/j.energy.2017.03.165.

Chen, A. A. *et al.* (2020) 'Pathways to climate change mitigation and stable energy by 100% renewable for a small island: Jamaica as an example', *Renewable and Sustainable Energy Reviews*, 121, p. 109671. doi: https://doi.org/10.1016/j.rser.2019.109671.

Ciriminna, R. *et al.* (2016) 'Solar Energy for Sicily's Remote Islands: On the Route from Fossil to Renewable Energy', *International Journal of Sustainable Built Environment*, 5. doi: 10.1016/j.ijsbe.2016.04.003.

Dakkak, M. *et al.* (2003) 'Operation strategy of residential centralized photovoltaic system in remote areas', *Renewable Energy*, 28, pp. 997–1012. doi: 10.1016/S0960-1481(02)00222-7.

EN 12831-3 (2017) *Energy Performance of Buildings-Method for Calculation of the Design Heat Load-Part 3: Domestic hot water systems heat load and characterisation of needs, Module M8-2, M8-3*. Available at: https://standards.iteh.ai/catalog/standards/cen/aa713aa5-cf93-41ca-a2c1-d6b367310a1b/en-12831-3-2017 .

ENEA—Italian Minister of Economic Development (2016) *Electrical System Research Program Agreement, Annual Implementation Plan 2016, Project D.1. Technologies for Building Buildings of the Future, Activities in Agreement with UNIPA: Simulation and Comparison of Technologies for Air Conditioning and Domestic* .

ENEA—Italian Minister of Economic Development (2017) 'Electrical System Research Program Agreement, 2017 Annual Implementation Plan, Experimental and Numerical Analysis of Solar Driven Technologies for Air Conditioning and the Production of DHW and ICT Systems for Control and Reduction of Electrical Loads in'.

ENEA website (2020) *No Title*. Available at: https://www.enea.it/en/publications/volume-pdf/the-minor-islands-between-sun-sea-and-wind.pdf.

Ferrari, S. and Beccali, M. (2017) 'Energy-environmental and cost assessment of a set of strategies for retrofitting a public building toward nearly zero-energy building target', *Sustainable Cities and Society*, 32. doi: 10.1016/j.scs.2017.03.010.

Guarracino, I. *et al.* (2016) 'Dynamic coupled thermal-and-electrical modelling of sheet-and-tube hybrid photovoltaic/thermal (PVT) collectors', *Applied Thermal Engineering*, 101, pp. 778–795. doi: https://doi.org/10.1016/j.applthermaleng.2016.02.056.

Ilkan, M., Erdil, E. and Egelioglu, F. (2005) 'Renewable energy resources as an alternative to modify the load curve in Northern Cyprus', *Energy*, 30(5), pp. 555–572. doi: https://doi.org/10.1016/j.energy.2004.04.059.

Istat website (2020) *Istituto Nazionale di Statistica. Population Housing Census.* Available at: http://dati-censimentopopolazione.istat.it/Index.aspx?lang=en.

Majidi, M., Mohammadi-Ivatloo, B. and Anvari-Moghaddam, A. (2019) 'Optimal robust operation of combined heat and power systems with demand response programs', *Applied Thermal Engineering*, 149, pp. 1359–1369. doi: https://doi.org/10.1016/j.applthermaleng.2018.12.088.

Meschede, H. *et al.* (2016) 'Classification of global island regarding the opportunity of using RES', *Applied Energy*, 175, pp. 251–258. doi: https://doi.org/10.1016/j.apenergy.2016.05.018.

Minambiente website (2016) *43. LINEE GUIDA. Alla Presentazione dei Progetti per il Programma per la Riqualificazione Energetica Degli Edifici della Pubblica Amministrazione Centrale PREPAC (D.M. 16 Settembre 2016).* Available at: https://www.minambiente.it/sites/default/files/archivio/notizie/linee_guida_PREPAC_maggio2017.pdf.

Möller, B. *et al.* (2012) 'Creating consciousness about the opportunities to integrate sustainable energy on islands', *Energy*, 48(1), pp. 339–345. doi: https://doi.org/10.1016/j.energy.2012.04.008.

Panagiotidou, M., Aye, L. and Rismanchi, B. (2020) 'Solar driven water heating systems for medium-rise residential buildings in urban mediterranean areas', *Renewable Energy*, 147, pp. 556–569. doi: https://doi.org/10.1016/j.renene.2019.09.020.

Picallo Perez, A., Sala, J. M. and Hernández, A. (2020) 'Application of Thermoeconomics in HVAC Systems', *Applied Sciences*, 10, p. 4163. doi: 10.3390/app10124163.

pti regione Sicilia Website (2020) 'Sicilian Official Price List.' Available at: http://pti.regione.sicilia.it/portal/page/portal/PIR_PORTALE/PIR_LaStrutturaRegionale/PIR_AssInfrastruttureMobilita/PIR_Diptecnico/PIR_Areetematiche/PIR_CRLLPP.

Sigarchian, S. G., Malmquist, A. and Fransson, T. (2014) 'Modeling and Control Strategy of a

Hybrid PV/Wind/Engine/Battery System to Provide Electricity and Drinkable Water for Remote Applications', *Energy Procedia*, 57, pp. 1401–1410. doi: https://doi.org/10.1016/j.egypro.2014.10.087.

'TRNsys Simulation Software' (2019). Available at: http://www.trnsys.com.

UNI EN 16147 (2017) *Pompe di calore con compressore elettrico - Prove, valutazione delle prestazioni e requisiti per la marcatura delle apparecchiature per acqua calda sanitaria*.

Vega, J. and Cuevas, C. (2020) 'Parallel vs series configurations in combined solar and heat pump systems: A control system analysis', *Applied Thermal Engineering*, 166, p. 114650. doi: https://doi.org/10.1016/j.applthermaleng.2019.114650.

Zizzo, G. *et al.* (2017) 'A feasibility study of some DSM enabling solutions in small islands: The case of Lampedusa', *Energy*, 140, pp. 1030–1046. doi: https://doi.org/10.1016/j.energy.2017.09.069.

Conclusions

The present thesis proposed a study about the energy performances and potential of the DHW production system based on the use of an HPWH exclusively dedicated to this purpose, assisted by solar energy and, in particular, by hybrid PV/T collectors. After having carried out a state-of-the-art study of these technologies, a detailed analysis of the thermal and electrical characteristics was provided both for PVT collectors and HPWH systems.

Three main solar technologies were analysed: PV, ST and, PV/T collectors. For each technology, three different sizes of solar generators were considered. Different hourly load profiles were analysed maintaining a fixed daily DHW volume consumption, to ensure the production of DHW for a micro-energy community in a low housing density context. Furthermore, two systems' configurations were hypothesized. In the first one, the solar thermal circuit was directly connected to the heat exchanger placed inside the technical water storage of the HPWH itself (configuration A); in the second one, the same circuit was connected to a DHW pre-heating tank (configuration B).

In order to evaluate system performances, a TRNSYS model was specifically built and the sensible components in the plant (hybrid collector and instantaneous HPWH) were validated considering the information from datasheets. Several simulations were carried out, on a yearly basis, considering the weather data for the city of Palermo (Italy). It was stated that regardless of the hourly tapping profile, the daily electrical consumption of the solely HPWH did not vary from system to system (1080 kWh per year). On the other hand, even if a 500 L water tank was adopted and a daily demand of 720 L was assumed, differences were noticed in the on/off cycles when hourly tapping profile changes and this fact can influence self-consumption of energy generated by PV or PV/T.

To better investigate these aspects, energy and operational indices were introduced and assessed. Energy indices refer to electricity energy saving as well as to solar fractions and non-renewable primary energy consumption. Slight differences can be noticed when PV and PV/T electrical production were compared month by month. PV/T heat delivery to the system was generally low and mainly concentrated in the summer months, according to the chosen plant layout. Comparable results are found out for PV and PV/T electric fractions, which differ by less than 1%, while remarkable differences, can be noticed between PV/T and ST thermal fraction (over 70% for all three configurations). On the other hand, looking at the PER_{NREN} indices, higher values are recorded for PV-based systems (12.1, 21.7, and 38.1 for conf_1, conf_2, and conf_3 respectively). This is because most of the electrical consumption by the HPWH was covered by the renewable energy self-produced all year long. On the other hand, some residual consumption of electricity by the grid was generally recorded for ST systems. Looking at the energy indicators, it can be said that the PV-assisted systems were the ones with the best performances. PV/T does not allow any remarkable advantages in the

overall balances (electricity and heat) while requires additional components and devices. The main reason is that the average temperatures in the tank are quite high, to better fulfil the DHW demand, and the cooling effect of the cells in the water loop is negligible. This implies low solar useful heat and an increase in cells efficiencies. In comparison with PV and PV/T, solar thermal systems do not efficiently handle the whole energy demand, and results are penalised by the residual electricity consumption of the pump that is entirely fed by the grid. Moreover, in a context such as a small island, where power production is entirely made with fossil fuels, PER_{NREN} decreases for all the plants. Solar thermal systems present higher figures of potential primary energy saving ($f_{sav.NREN}$) in comparison to values referred to their operation when connected to the national grid. Operational indices were introduced to analyse the electrical loads' distribution during specified timeslots that are considered suitable for the application of DR strategies. A certain difference in magnitude was noticed when changing the tapping profile. In particular, tapping #7 allows a better coincidence between solar production and consumption. It results that the HPWH system coupled with PV and PV/T panels are not suitable for supporting DR programs while maximizing self-consumption and that this conclusion is the same both on the mainland and in small islands. Nevertheless, the battery storage system, sized for increasing the quota of self-consumed energy, can be used as a power booster if required by the aggregator and if this usage is economically convenient for the HPWH owner.

Furthermore, by focusing analyses on the use of the thermal energy produced by the solar thermal collectors within the entire plant, an alternative system configuration was examined (configuration B). The latter provides the introduction of a preheating water tank between the HPWH and the PV/T system in order to reduce the thermal consumption of the system by exploiting solar production, consequently reducing the electricity consumption of the HP and at the same time ensuring coverage of the latter using the electricity production of the PV/T system. The improved energy performances of this latter were analysed by making comparisons with configuration A. It has been found that the introduction of a thermal pre-storage tank and correct management of it, has allowed a better operation in terms of useful heat production compared to a direct connection of the solar circuit with the heat pump tank. This thermal contribution allows to reduce the energy demand required by the heat pump (-35% compared to the base scenario) and to consequently reduce its consumption (-20% on average). The increase in solar thermal production has also increased electrical producibility by about 3% thanks to the reduction in the temperature of the cells due to the operation of the PV/T itself. In general, photovoltaic production proved to be sufficient to cover over 70% of the annual consumption of HP in all the cases analysed.

These studies have been finalized to the realization of a real-scale experimental setup aimed at characterizing the operation of the systems under study, in the context of a collaboration project with ENEA (Report RdS / PTR2019 "Feasibility study of solutions for the energy efficiency of the Minor Islands"). The goal of the project is to create an

experimental setup that allows monitoring and verifying, on the one hand, the thermal and electrical performance of the PV/T collectors as the environmental and operating conditions vary, and on the other to monitor the performance of heat pumps electrically powered by the solar system for different user profiles. The experimental set-up was designed and sized according to the indications of the regulations currently in force in the area.
Considering that there is currently no "ad hoc" regulation for PVT hybrid solar collectors to refer to for quality and performance tests, the regulations relating to solar thermal collectors and photovoltaic panels are used.
Following the indications of these regulations, the layout of the hydraulic and electrical circuits of the system have been defined. After having dimensioned the main components, the experimental apparatus necessary for the realization of the experimental set-up of the manifold and to be able to carry out the necessary measurements for the various tests required by the regulations was identified.
After a phase of managing the purchases of all the necessary components, the experimental analyses to be performed on the system in an external environment were defined. The plant is currently being assembled at the dedicated site, identified at the Casaccia ENEA Research Center in Rome (Italy). After commissioning and testing the main components, it will be possible to proceed with the planned experimental analyzes and the data collection and analysis campaign.

Finally, in this thesis, the relevant case study of the energy system of the Mediterranean minor islands was investigated. Several RES-based systems for producing DHW, including solar plants which have already been extensively discussed, were analysed. In particular, the use of heat and electricity storage, as well as solar thermal and photovoltaic panels to be coupled to a heat pump, was investigated. To do this, four technologies from the marketplace were chosen, simulated, and analysed: a heat pump water heater connected to the grid, a heat pump water heater coupled with a photovoltaic plant, a heat pump water heater coupled with a solar thermal collector, and a typical solar thermal plant. First of all, the electricity consumption of an ordinary ESWH for a family on Lampedusa Island was calculated through simulation (yearly 1137 kWh, varying from 125 kWh in January to 67 kWh in August). This value was used as a reference to calculate the energy savings achievable with the other systems. It was found that the replacement of the reference system with an electric heat pump could provide an average energy saving equal to 65%. Indeed, in this case, the yearly energy consumption can be reduced from 1137 to 375 kWh, avoiding 761 kWh of electricity withdrawal from the local grid. Regarding the heat pump water heater coupled with a PV plant, four further stand-alone and one grid-connected photovoltaic plants were considered. Moreover, two solar thermal-based systems were introduced: one coupled with an electrical backup resistance (called ST (4)) and the other with the heat pump itself (called HPWH + ST (3)). Firstly, all proposed solar-assisted plants were run without accounting for electrical storage (photovoltaic plants) or a backup system (solar

thermal plant) to check for their performance using a set of comfort indices. Based on the comfort conditions, the most suitable size for a stand-alone PV-plant was detected. Some comfort issues were detected for the systems with 720 Wp. while a peak power of 1200 Wp could dramatically mitigate such a problem. Then, two alternative electric storages were evaluated through a calculation of values for the "battery indices". The following PV-based plants were then selected: a system characterized by a power of 1200 Wp and a storage capacity of 2400 Wh (called HPWH (2.1a)) and a system characterized by a power of 720 Wp and a storage capacity of 4800 Wh (called HPWH (2.2b)). Similarly, the ST plant was firstly evaluated using comfort indices. The results showed that, if backup systems are not included in the systems, setpoint temperature could only not be maintained in the tank during winter months and some potential discomfort events could be detected. By using the system characterized by 1200 Wp, the contemporaneity between the energy needed for domestic hot water production and PV useful yield achieved values higher than 90%. Looking at the comparison between the electrical consumption of the electricity-driven pump water heater and those driven by the solar thermal (called ST (4)) and the pump water heater coupled with solar thermal systems (called HPWH + ST (3)), the solar thermal (called ST (4)) one achieved an extra 4% of energy taken from the grid. By comparing the pump water heater consumption with that of the pump water heater coupled with solar thermal systems (called HPWH + ST (3)), a 58% reduction was evaluated. In general, from an energy-saving point of view, all plants achieved energy savings concerning the traditional electric storage water heater in use, varying from 100% for the selected photovoltaic plants to 86% for the pump water heater coupled with solar thermal systems (called HPWH + ST (3)), with an average 66.5% for the solely pump water heater and solar thermal systems (ST (4)). For all of them, a economic analysis was performed in order to select the most affordable in economic terms. Net present value and payback time for the proposed systems were evaluated. When not considering the national economic incentives, the stand-alone photovoltaic plants showed a negative cash-flow rate with a consequently negative net present value. Contrariwise, the other analysed domestic hot water plant plants led to positive net present values varying from 760 € for the solely pump water heater (payback time = 15.1) to 1902 € for the solar thermal plant with an electrical heater back-up (payback time = 7.6). If Italian incentives are considered, the net present value is strongly reduced and the values are positive for all analysed plants. From an energy-saving point of view, the most promising plants include the use of the pump water heater coupled with a proper photovoltaic (100% energy saving) or solar thermal plant (86% energy saving). This fact is verified even if the photovoltaic plant needs incentive support to be economically attractive. Similarly, the PBT calculated for the pump water heater-based plant shows a value close to the estimated useful life for the plant (14.7 vs. 20 years), if national incentives are not considered. On the other hand, the electric storage water heater with a solar plant, ensuring 66% of energy saving, should have the highest economic

advantages in terms of net present value and payback time, even if no incentives are taken into account.

Finally, an alternative scenario was also examined where the existing ESWH is substituted with the DHW production system described in chapter 4, considering, in particular, the configuration_2 where the HPWH is coupled to a 6 PV/T panels system. The effectiveness of this retrofit solution is analysed by using energy and operational indices, such as PER and $f_{sav.NREN}$, which have been introduced in chapter 5. Considering that in context such a small island, where power production is entirely made with fossil fuels, PER_{NREN} decreases for all the plants. Solar thermal systems present higher figures of potential primary energy saving ($f_{sav.NREN}$) in comparison to values referred to their operation when connected to the national grid. Furthermore, it results that HPWH system coupled with PV and PV/T panels are not suitable for supporting DR programs while maximizing self-consumption.

APPENDIX A

SYSTEM			
Installation in a prefabricated structure of an experimental plant with a 500-liter heat pump system for DHW production - electrical and thermal storage			
Supply and installation of hydraulic components			
Item	Description	Model	Amount
NP1	Supply and installation, within corrugated walls, of 1/2 "insulated multilayer pipe - hydraulic connection between solar field, 500 lt boiler and Daikin heat pump installed in Cabin 3, including fittings		50
NP2	Supply and wall installation of 1 "non-insulated multilayer pipe - water heater connection 500 lt Daikin heat pump - 2000 liter buffer tank including fittings		20
NP3	Safety valve opening 6 bar including T for tube 1/2 multilayer	Compact diaphram safety valve type GIACOMINI R140C - R140CY009	1
NP4	Exposed discharge funnel for safety valve	Exposed drain funnel, for use with safety valves R140 - type GIACOMINI R141 or equivalent	1
NP5	Analog pressure gauge for 1/2" multilayer pipe complete with connection (for solar circuit)		3
NP6	Expansion vessel 1/2 ”- 50 liters, per circuit 1/2 "multilayer solar panel, including fittings	Welded expansion vessel for solar systems of 50 liters type CALEFFI or similar	1
NP7	Automatic filling group for multilayer pipe 1/2 "solar circuit including circuit fittings solar and hot water circuit	Automatic pre-adjustable anti-limescale filling unit, inspectable by CALEFFI or equivalent	1
NP8	1/2 "multilayer pipe filter for solar circuit	Inspectable filter with magnet type GIACOMINI R74M or equivalent	1

NP9	Deaerator for multi-layer solar circuit piping 1/2 "	DISCAL CALEFFI 1/2" disaerator for systems solar or equivalent	1
NP10	Check valve for multilayer circuit piping solar 1/2 "		1
NP11	Manual three-way valve for solar circuit 1/2 "		2
NP12	T-fitting with pocket for PT temperature sensor 500 (already supplied) in the 1/2 "solar circuit		5
NP13	Ball shut-off valve for solar circuit - 1/2 "copper pipe, nominal temperature 100 ° C		6
NP14	Ball shut-off valve for 1 "multilayer piping, heat pump circuit - 2000 liter storage tank, nominal temperature 100 ° C, including fittings		6
NP15	Supply and installation of a 2000 liter polyethylene water mains tank to be installed in a prefabricated structure, water temperature max 65 ° C including: - tank float with overflow valve, - 5 m polyethylene pipe for connection to the water pipe - emptying tap - construction of connection to the delivery pipe and the return pipe from the heat pump (1 ")		1
NP16	Close coupled centrifugal pump 1 "threaded connection	Calpeda type NM 2 / A / B o equivalent	1
NP17	Two-way automatic valve with by-pass actuator (open closed) powered at 24 V for installation in 1 "multilayer piping (connection between the heat pump and the 2000 liter buffer tank)		1
NP18	Timer for activating the automatic two-way 24 V bypass valve		
NP19	1 ”welded 30 liter expansion tank for heat pump hydraulic circuit - 2000 liter buffer tank		1
NP20	ball shut-off valve with lever for user hot water circuit temp. nominal 70 ° C in multilayer pipe 1 "		8
NP21	manual three-way valve for cylinder bypass 500 liters circuit - heat pump, for 1 "multilayer piping including fittings		1
NP22	T-fitting for bypass circuit between 500 liter storage tank and cold side heat pump 1 "pipe		1
NP23	check valve for multilayer piping 1 "heat pump circuit - 2000 liter buffer tank		1
NP24	Supply and installation in Cabin 3 of circulator for solar circuit type wilo TOP-STG 25/13 EM or equivalent including fittings for assembly with 1/2 "multilayer piping		1

Only installation of hydraulic components			
NP25	Installation, including electrical wiring and thermal connection, of 7 thermo-photovoltaic modules of the 320 Wp Fototherm type (to be supplied with 2 m of 1/2 "insulated copper piping and fittings to connect the solar collectors in series) in aluminum bearing structure already prepared, including supply of: screws, supports, fittings and anything else needed to give the finished work and rule of art		7
NP26	Installation in Cabin 3 of heat pump for DHW Daikin ECOH2O: outdoor unit ERWQ02AV3 + indoor unit 500 liters (EKHHP500A2V3) including wiring from QE4 panel		1
NP27	Installation in Cabin 3 BSV-type vitrified boiler with fixed exchanger for the production of domestic hot water 500 lt ELBI, complete with fittings		1
NP28	IFX M4 isoil heat meter 1 "M threaded connection in 1" multilayer pipe on cold side and thermocouple in 1 "multilayer pipe on hot side		1
NP29	Isoil IFX M4 heat meter 3/4 "M threaded connection in 1/2" multilayer pipe on cold side and thermocouple in 1/2 "multilayer pipe on hot side		1
NP30	Installation of PT 500 temperature sensors between the inlet / outlet of the thermal solar collectors with the pocket already prepared in 1/2 "copper pipe including connection to the multipolar signal cable already prepared		5
Supply and installation of electrical components			
Item	Description	Model	Amount
NP31	Supply and installation of a support structure for 7 photovoltaic modules made of hot-dip galvanized sheet metal profiles or raw extruded aluminum of the triangle type with fixed inclination at 30 ° (of the ATL 100.30 type by Alusistemi or equivalent) complete with side member profile in raw extruded aluminum or in galvanized sheet with bolts and central and final clamps necessary for fixing the individual components and photovoltaic modules. The anchoring of the structure to the ground is carried out by means of concrete ballast compatible with the aforementioned triangular support profile, including any burial to ensure a level installation of the structure		

NP32	Supply and installation of solar cable type H1Z2Z2-K (Uo / U: 1000/1000 V ac 1500/1500 V dc) within a DN 40 PE corrugated tube for the connection of the thermo-electric PV system (7 modules) to the string disconnection (QFV-T) and from this to the Azzurro inverter located in Cabin 3. Including multicontact connectors for connection to the string terminal and to the disconnection panel		
NP33	Supply and installation of flexible PE corrugated pipe DN 40 for the passage of the solar cable from the string terminal to the string sectioning panel located in the cabin 3		30 m
NP34	Supply and installation of FG16OR16 - 0.6 / 1 kV cable for power supply from QE4 electrical components in Cabin 3: 3G4 sqmm to power the heat pump m 15 3G4 mmq to power the blue inverter 15 m 3G2.5 mmq for 15 m hydraulic pump power supply 3G2.5 sqmm for 20 m solate circulator power supply 3G2.5 sqmm for powering thermal measuring instruments Isoli FX M4		m 15 m 15 m 15 m 20 m20
NP35	Supply and installation within corrugated PE DN 40 di 12-pole signal cable type FS18OR18 for connecting the PT 500 temperature probes 5 to a datalogger already present in Cabin 3 including a watertight box for connection of PT 500 terminals		m 25
Only installation of electrical components			
NP36	Installation in Cabin 3 of a 3 kW Azzurro hybrid inverter for PV including QE4 panel cabling, to the field panel and to the battery pack		1
NP37	Installation in 5 kWh lithium storage cabin 3 including wiring (5 m) from Azzurro inverter with 10 mmq H1Z2Z2-K unipolar cable		1
NP38	Installation of a pre-wired field switchboard (QFV-T) in Cabin 3 for disconnecting the thermo-electric PV string (7 modules) and dc power supply of the Azzurro inverter		1
NP39	Installation of 76 pre-wired module switchboard (QE-4) in Cabin 3 for powering the heat pump, inverter, hydraulic pump and instrumentation included		1

NP40	Single-phase multimeter with indirect insertion - RS485 ModBus in AC including TA (supplied by customer)		2
NP41	Installation in QFV string sectioning panel DC multimeter for PV string monitoring		1

List of figures

List of tables